2-5-2016 12:00 AM

Stable Isotope Paleolimnology of Barry Lake, Ontario, Canada Since AD - 1268

Zijun Liu
The University of Western Ontario

Supervisor
Dr. Fred Longstaffe
The University of Western Ontario

Graduate Program in Geology
A thesis submitted in partial fulfillment of the requirements for the degree in Master of Science

Abstract

The paleolimnology of Barry Lake, SE Ontario, Canada is described using mineralogy, magnetic susceptibility, carbon:nitrogen ratio, mass accumulation rates, grain-size, $\delta^{18}O$ and $\delta^{13}C$ of authigenic calcite and mollusc aragonite, $\delta^{13}C$ and $\delta^{15}N$ of organic matter, and archival records. These sediments span the Medieval Warm Period (MWP), Little Ice Age (LIA), and human settlement. *Interval I* proxies (AD 1268-1350, MWP) indicate warmer and drier conditions and elevated lacustrine production. *Interval II* (AD 1350-1615) was cooler and wetter, with lower lacustrine production and low-oxygen conditions causing loss of shelly fauna. *Interval III* (AD 1615-1850, LIA) was colder, with lower lacustrine production beginning at AD 1720, coincident with European activity beginning at AD 1830. *Interval IV* (AD 1850-2011) is marked by rising temperature and lacustrine production, declining human impact, and since AD ~1950, new nitrogen input (fertilizer?). These data provide a baseline for future change in climatic and anthropogenic factors affecting Barry Lake.

Keywords

Paleolimnology, stable isotopes, climate, AD ~1300-2011, Barry Lake, Ontario

Acknowledgments

First and foremost, I would like to express my sincere gratitude to my supervisor Dr. Fred Longstaffe, who has been a supportive, encouraging and patient mentor throughout this project. Fred, I am very appreciative to everything you have done, from stable isotope courses to field trips to monetary support. I am deeply honoured to have this opportunity to work with you on this interesting project. I will always remember your words that help me through my hard times. I wish you all the best in the future.

I am grateful to my committee member Dr. Katrina Moser, who has provided great paleolimnology course and advice to this project. I also thank the examination committee (Drs. Steve Hicock, Lisa Hodgetts and Katrina Moser) for their helpful and thoughtful revisions and technical questions during my defence.

Next, I would like to thank a number of people that without whom this project would never exist. First, I would like to express my great appreciation to the owner of Barry Lake, George Archer. George, thank you for allowing us to take gravity cores and water samples from Barry Lake, and also thank you for your generosity for allowing us borrow your boat during our field trip in November 2014. Next, I would like to thank Dr. Fred Longstaffe, Dr. Avner Ayalon and Dr. Ryan Hladyniuk for collecting the two gravity cores and water measurements in November 2011 on such a cold day. Ryan, I would never paddle to the lake centre without your muscles; thank you for assisting me with my three field trips, and thanks for all your advice and suggestions throughout this project.

I am indebted to the hard-working staff at the Laboratory for Stable Isotope Science (LSIS): Li Huang, Kim Law and Grace Yau for their expertise and guidance during the analytical measurements required in this project. I would like to thank Linda Kimpe at the University of Ottawa's Laboratory for the Analysis of Natural and Synthetic Environmental Toxins (LANSET) and Ron Hatfield at the BETA Analytic Inc. for their help and patience in analyzing and explaining the ^{210}Pb and AMS ^{14}C dating results, respectively. I would also like to extend my appreciation to Erika Hill at the Lakes and Reservoirs Systems Research Facility (LARS), Dr. Desmond Moser and Ivan Barker at the Zircon and Accessory Phase Laboratory (ZAPLab) and Dr. Hossein Kazemian at the Control and Crystallization of

Pharmaceuticals Laboratory (CCPL) at Western for their help and supervision conducting the magnetic susceptibility, scanning electron microscope and grain size measurements, respectively. I would also like to thank my colleagues, ‘Lake Podders’ and friends that have provided helpful advice and assistance on my experiments and have brought so much fun in my life: Rohan Aranha, Gila Binyamini, Laura Colgrove, Luqi Cui, Nadia Dildar, Xi Lu, Mengmeng Qu, Roshni Patel, Tessa Plint, Jacob Walker, Jane Wilson, Shuo Sun, Alex Smofsky, Farnoush Tahmasebi, Tian Zhao, and Xiaoming Zhang.

This project was also made possible by funding. Operating funds were provided by the Natural Sciences and Engineering Research Council of Canada Discovery Grant (FJL), the Canada Research Chairs Program (FJL), the Canada Foundation for Innovation (FJL) and the Ontario Research Fund (FJL).

Last but not least, I would like to thank my family. I thank my parents Shuli Cao and Quanwen Liu for their infinite love and support throughout my life. Special thanks to my husband Dong, I thank you for your love, care and company. You are always there when I need you, thank you.

Table of Contents

List of Tables

List of Figures

List of Appendices

Chapter 1

1 Introduction

1.1 Overview

Southern Ontario is the most heavily populated and economically important region in Canada, and its climate is profoundly affected by the Laurentian Great Lakes (Government of Canada and USA, 1995). Kling et al. (2003) suggested that future climate around the Great Lakes will become warmer and drier. To better predict the future, we can extend our knowledge on historical climatic data by studying geologic proxies such as those derived from lake sediments. Lakes provide a basin to accumulate sediments with archives of ecosystem history, and those sediments provide sufficient information about the lake history because proxies in sediments can be preserved for a longer time than the lake itself (Cohen, 2003).

There are a number of Holocene (last 10000 years) paleoclimatic studies of lake sediments around Ontario (e.g. Fritz et al., 1975; Lewis et al., 1994; McFadden et al., 2004; Laird et al., 2012) that provide millennial–scale observations but offer only low resolution of changes that have occurred on the multi–century or multi–decadal scale. Paleoecological studies (e.g. McAndrews and Boyko–Diakonow, 1989; Fuller, 1997; St. Jacques et al., 2008; Paquette and Gajewski, 2013; Lafontaine–Boyer and Gajewski, 2014; Keizer et al., 2015) focus on changes in vegetation composition in eastern North America during the late Holocene, which included climatic events such as the Medieval Warm Period (MWP) (AD 1000–1300) (Anno Domini: the number of years since the birth of Jesus Christ) and the Little Ice Age (LIA) (AD 1450–1850). These authors examine the multi-decadal climatic and vegetation variations during the last 1000 years using fossil pollen records. Similarly, Campbell and McAndrews (1991) applied cluster analysis of pollen records to study the late Holocene climate variations in Ontario. Other than pollen studies, Buhay and Edwards (1995) used stable isotopic measurements in wood cellulose to determine the climate between AD 1610 and 1885 in southwestern Ontario.

The previous pollen studies provide a high-resolution record of vegetation changes during the last 1000 years in Ontario, Canada. Vegetation, however, responds to many variables from climatic (temperature, precipitation, soil moisture) to non-climatic (human activities, insect infestations, fire), and it remains difficult to separate these factors (Bennett and Willis, 2001). Stable isotope analysis of lake sediments is gaining increasing usage in paleolimnological investigations to overcome some of the limitations of pollen analysis (Wolfe et al., 2001). Materials used for stable isotope measurements include carbonates minerals of authigenic and biogenic origin, and organic matter, all of which are commonly preserved and easily accessible in lake sediments (Wolfe et al., 2001).

In this thesis, I investigate climate variations in southern Ontario since AD 1268 through stable isotope analyses of lake sediments. The sediments were collected from Barry Lake (surface area 0.16 km^2, maximum water depth 8 m), a kettle lake located 40 km north of central Lake Ontario shoreline and 32 km east of Peterborough, Ontario, Canada (Figs. 1.1a, b). Satellite images (Fig. 1.1b) and field observations show that the catchment of Barry Lake consists of drumlins and farmlands with low residential occupation. The principal objective of the thesis is to reconstruct the century-scale climatic changes and human disturbances in southern Ontario as revealed by stable isotopic data. Together with the climatic references from recent pollen studies (e.g. Bernabo, 1981; Paquette and Gajewski, 2013; Lafontaine-Boyer and Gajewski, 2014; Keizer et al., 2015), the results obtained in this thesis help to test the usefulness of stable isotopes in paleoclimatic reconstructions and provide another century-scale climatic record for southern Ontario.

a)

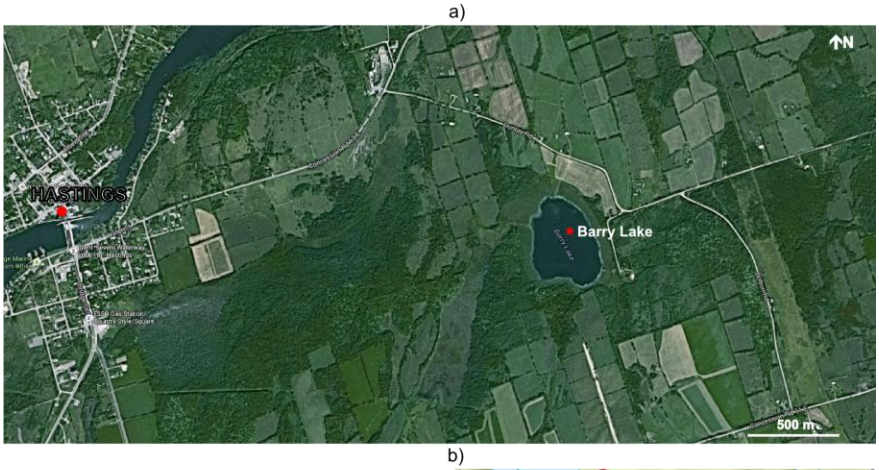

b)

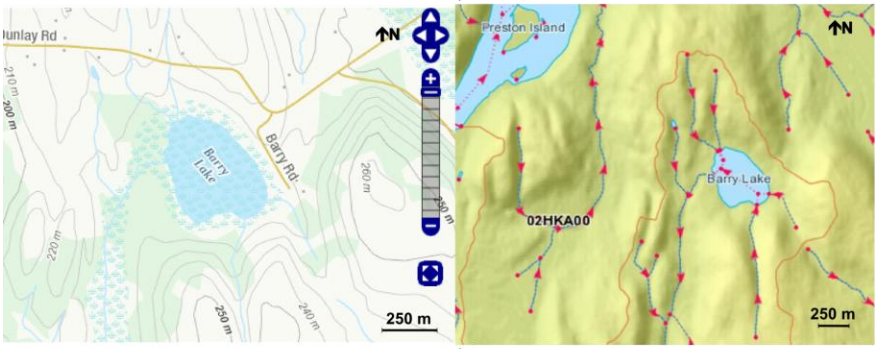

c)

Figure 1.1 (a) Locations of Barry Lake, Rice Lake, Crawford Lake relative to Lake Ontario (Google Map, 2015). (b) Satellite image of Barry Lake (44 °18'28"N, 77 °55'17"W) in southeastern Ontario, Canada (Google Earth, 2015). (c) Inflows and outflows to/from Barry Lake (GeoGratis, 2015).

1.2 Thesis Objectives

This thesis employs a multiproxy approach to evaluate paleoclimatic variations, lake productivity changes, and impacts from human activities at Barry Lake, Ontario, Canada since AD 1268. The proxies used include mineralogy, magnetic susceptibility (MS), total organic carbon (TOC) content, total nitrogen (TN) content, atomic carbon to nitrogen ratio (C/N), organic carbon and nitrogen mass accumulation rates (C-MARs; N-MARs), grain-size distribution, $\delta^{18}O$ and $\delta^{13}C$ of carbonates and $\delta^{13}C$ and $\delta^{15}N$ of bulk organic matter (OM). The climate information is mainly recovered from the stable isotopic compositions of authigenic calcite and mollusc shells. The productivity proxies involve measurements of bulk organic matter (OM) chemical and isotopic compositions. In addition, archival monthly air temperature and precipitation data since AD 1866 is available through Environment Canada (EC), which is used as a climate reference for the last 150 years for comparison with results obtained using the proxies described above.

Pollen studies show that vegetation in Ontario and Quebec is affected by the MWP and the LIA. To assess whether these events were recorded at Barry Lake is my first research question:

(1) Are the cooling event “Little Ice Age” (LIA) (AD 1450 to 1850) and warming event "Medieval Warming Period" (MWP) (AD 1000–1300) manifested in the sediments of Barry Lake?

To answer this question, an age-depth model is first constructed to determine the depths in the sediments associated with the time of these climatic events. Second, measurements of modern water and modern mollusc shells are obtained to establish a modern baseline for the stable isotopic compositions of the isotopic proxies used in the study. Third, past moisture supply and temperature changes are qualitatively examined by interpreting lake water $\delta^{18}O$ reconstructed from the $\delta^{18}O$ of ancient mollusc shells and authigenic calcite from Barry Lake sediments.

This thesis also aims to determine the sources of OM and historical changes in the lacustrine productivity of Barry Lake, which is addressed by the second research question:

(2) How does the $\delta^{13}C$ of dissolved inorganic carbon (DIC) and OM vary since AD 1268, and do those variations record changes in carbon/OM sources and lacustrine production?

The $\delta^{13}C$ variations of DIC are reconstructed using the $\delta^{13}C$ of ancient mollusc shells and authigenic calcite. Values of $\delta^{13}C_{DIC}$ are a useful tracer of climate-determined processes and provide a reflection of the isotopic compositions of inflow water, CO_2 exchange between atmosphere and lake water and photosynthesis/respiration of aquatic plants within the lake (Leng and Marshall, 2004). The changes in OM sources and lacustrine production are also evaluated using traditional proxies that include TOC, TN, C/N ratios, C- and N-MARs and isotopic compositions of OM.

Diatom and pollen studies of lake sediments from highly populated locations in southern Ontario suggest human disturbances beginning at 1 ka Before Present (BP, where present is 1950) (e.g. Ekdahl et al., 2007; Sonnenburg et al., 2013; Watchorn et al., 2013). While the diatom proxy is not available for the present study, assessment of possible human disturbances is also possible using other proxies, which leads to the third research question:

(3) Are there any impacts of historical human activities evident in sediments from Barry Lake using proxies such as MS, MARs and the isotopic composition of OM?

Human activities such as land clearance and agriculture can alter watershed conditions. As a result, land erosion rates can increase, and lake productivity may change (Meyers and Teranes, 2001; McFadden et al., 2004; Routh et al., 2007, 2009). Changes in erosion rates can be reflected by shifts in sediment magnetic susceptibility (MS) (Kirby et al., 2004). Changes in lacustrine productivity can be indicated by changes in OM isotopic compositions and MARs (Leng and Henderson, 2013). The age-depth model for the Barry Lake sediments is examined for such changes at times most likely to be associated with human impacts, as previously inferred from archaeological and historical records available for the region.

1.3 Thesis Structure

The objectives of this thesis and a review of relevant literature are presented in Chapter 1. The review covers local history, currently available climate information for the last 1000 years and regional geology.

Chapter 2 describes the rationale for investigating climatic and in-lake productivity changes using stable isotopes.

Chapter 3 describes the methodology used in this study including two main categories: sample collection and laboratory analyses. Samples are sediments collected in two gravity cores, modern water, and modern snails. The isotopic compositions of modern water and modern snails have been used to establish a modern isotopic baseline for the locality, whereas the isotopic compositions ($\delta^{13}C$, $\delta^{18}O$) of authigenic calcite and mollusc shells from the sediments have been used to infer historical climate change. In-lake primary productivity is evaluated using the TOC, TN, C/N ratios, C-MARs, N-MARs, $\delta^{13}C$, and $\delta^{15}N$ of OM. Other measurements such as MS, grain-size distribution, and mineral abundances have also been made to assist with interpretation.

Chapter 4 presents the results of field work and laboratory analyses of the various samples collected from Barry Lake and its sediments.

Chapter 5 provides a discussion and interpretation of the results beginning with the establishment of an age-depth model. Modern Barry Lake conditions are then discussed including water physical and chemical properties (temperature, dissolved oxygen, specific conductivity and pH) and isotopic compositions of water, authigenic calcite and mollusc shells. A century-scale history of climatic changes and human disturbances affecting Barry Lake since AD 1268 is presented based on the data collected from the proxy records preserved in the sediment cores and available from weather and other historical archives.

Chapter 6 summarizes the major findings of this thesis and provides suggestions for future work.

1.4 Study Area

Barry Lake (44°18'28"N, 77°55'17"W) is a kettle lake located in southeastern Ontario, Canada, 32 km east of Peterborough, Ontario, and 40 km north of Lake Ontario (Figs. 1.1a, b). The main water body is surrounded by bog and wetland plants. Four water inflows, two to the northwest and two to south/southeast, and one outflow to west are shown in the GeoGratis-Canada Base Map (Fig. 1.1c) (GeoGratis, 2015). However, no visible inflows and outflows were observed during field trips to the lake in AD 2014. The inflows likely represent groundwater input, and the bog to west likely hides the outlet.

The only previously published study of Barry Lake is a pollen diagram (Fig. 1.2) by McAndrews (1984). He defined four pollen zones and noted the beginning of European settlement around AD 1820, as demarcated by the rise in ragweed *Ambrosia* and grass *Gramineae* pollen. This pollen diagram led to the birth of this thesis investigation. To the best of our knowledge, there are no other studies of Barry Lake until this thesis.

1.5 Historical Climatic Events

During the past millennium, a warm period (MWP) and a cold period (LIA) were documented widely between AD 1000–1300 and 1450–1850, respectively, although their timing and extent vary among regions (PAGES 2k Consortium, 2013). There is controversy concerning climatic conditions during the MWP with some studies reporting droughts in southern Ontario, and other sites were considered to have experienced relatively wet conditions (Campbell and McAndrews, 1991; Lafontaine-Boyer and Gajewski, 2014). Palynological investigations from eastern Ontario (Keizer et al., 2015), southwestern Quebec (Paquette and Gjewski, 2013), Michigan (Booth et al., 2012) and diatom assemblages from northwestern Ontario (Laird et al., 2012) suggest warm conditions spanning from AD 950 to 1500, corresponding to the onset of MWP.

The impact of the LIA in southern Ontario has been documented in several studies on forest composition (Campbell and McAndrews, 1991; Buhay and Edward, 1995; Keizer et al., 2015). Most pollen production diagrams suggest a decrease during the LIA, presumably as a result of lower vegetative productivity during the period of climate

deterioration (Paquette and Gajewski, 2013). The timing and extent of the LIA also vary from site to site. Lafontaine-Boyer and Gajewski (2014) proposed the coldest period as AD 1600–1700 in southwestern Quebec, while Keizer et al. (2015) reported it to be AD 1725–1870 in eastern Ontario. Results from high-latitude ice melt records in southern Greenland and pollen data from Minnesota suggest that the coldest periods occurred in the early and late 1500s, and AD 1700±20 and 1840±15 (Koerner, 1977; Gajewski, 1988; Koerner and Fisher, 1990; Bradley and Jonest, 1993). Tree-ring width data in the western United States imply that the late nineteenth and early twentieth centuries were cold with slightly warmer periods in AD 1750–1760 and 1830–1850, while density networks of tree-rings in the western United States indicate that the coldest conditions occurred in the early 1600s and early 1800s (Fritts, 1991; Schweingruber et al., 1991; Briffa et al., 1992; Bradley and Jonest, 1993). Warm conditions during AD 1650–1660, 1800, 1860 and 1930 have also been inferred from tree-ring width data (Fritts and Shao, 1992).

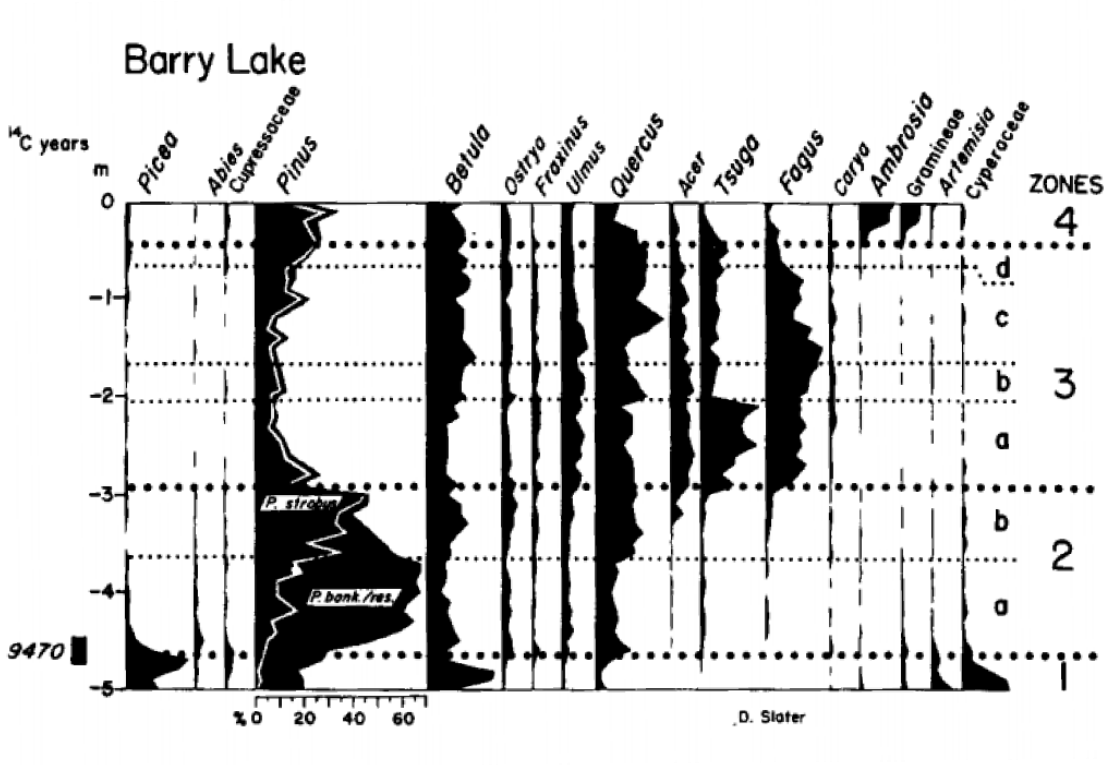

Figure 1.2 Standard pollen diagram from Barry Lake. Minor taxa are not shown. The radiocarbon date of 9470±210 (I-9501) was obtained from material at 445–465 cm. Analysis by D. Slater (McAndrews, 1984).

Historical climate data including monthly temperatures and precipitation are available from Environment Canada (Environment Canada, 2015). Seven stations (Fig. 1.3; Table 1.1) around Barry Lake were selected for this study, among which stations Peterborough and Peterborough STP share the same location but report records for different time periods. Figures 1.4a, b and 1.5a, b depict the variations in mean summer (June to August) temperature, total summer precipitation amounts, mean annual temperatures and annual precipitation amounts since AD 1866, respectively. The archival temperature records are used later in this thesis to assist with calculation of the variations in historical lake water $\delta^{18}O$.

1.6 Previous Investigations

McAndrews (1984) published a pollen diagram (Fig. 1.2) for Barry Lake sediments. The core was collected in AD 1976 with 5 m in length, and one radiocarbon date of 9470 ±210 BP was obtained at 445–465 cm. Four pollen zones have been identified. *Zone 1* (9470 BP) represents a spruce-dominated boreal woodland marked by the appearance of spruce, wormwood and sedge *(Picea, Artemisia* and *Cyperaceae*, respectively*). Zone 2* represents a boreal forest condition during warming conditions. *Subzone 2a* is marked by jack pine *(Pinus banksiana)*, and *subzone 2b* by white pine *(P. strobus). Subzone 3* (5000 BP) is identified based on fluctuations in hemlock *(Tsuga*) and white pine *(Pinus). Zone 4* (130 BP) is defined by the rise of ragweed *(Ambrosia)* and grass *(Gramineae)*, indicating the beginning of modern European agriculture. *Zones 3* and *4* cover the time range of the sediments examined in this thesis, and the pollen results are used in this thesis in support of interpretations based on other proxies.

Table 1.1 Coordinates of Environment Canada stations around Barry Lake.

Stations	Coordinates*
Peterborough and Peterborough STP	44 °17'00"N 78 °19'00"W
Peterborough Airport	44 °14'00"N 78 °22'00"W
Peterborough Dobbin TS	44 °19'00"N 78 °22'00"W
Trent University	44 °22'00"N 78 °18'00"W
Campbellford	44 °18'00"N 77 °48'00"W
Stirling	44 °19'00"N 77 °38'00"W

*Coordinates information obtained from Environment Canada: http://climate.weather.gc.ca/index_e.html#access

Figure 1.3 Locations of six selected climate data recording stations in southeastern Ontario, Canada (Google Map, 2015).

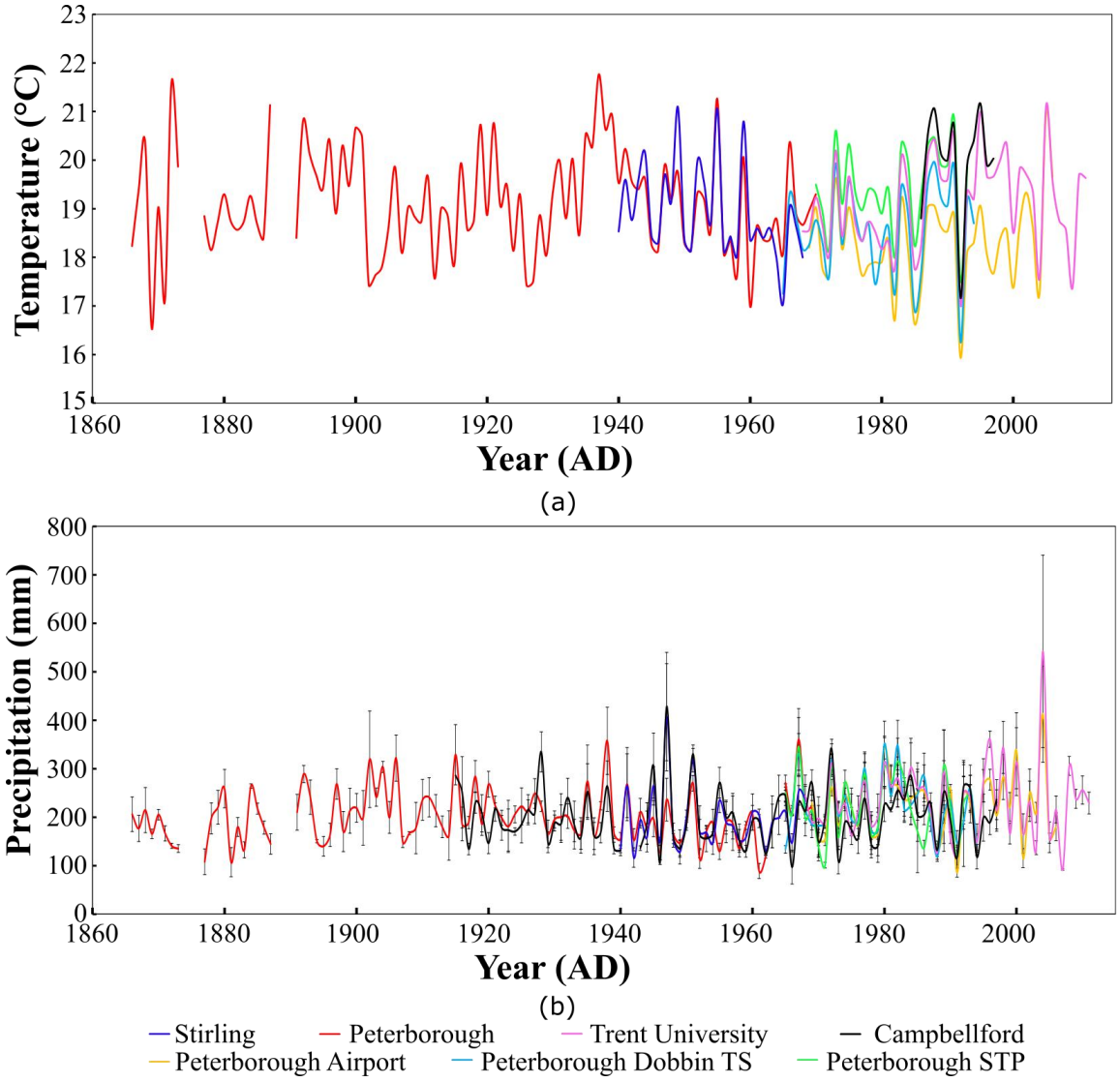

Figure 1.4 (a) Mean summer (June to August) temperature records between AD 1866 and 2011 recorded at seven stations in southeastern Ontario, Canada. (b) Total summer (June to August) precipitation amounts since AD 1866 recorded in seven stations in southeastern Ontario, Canada.

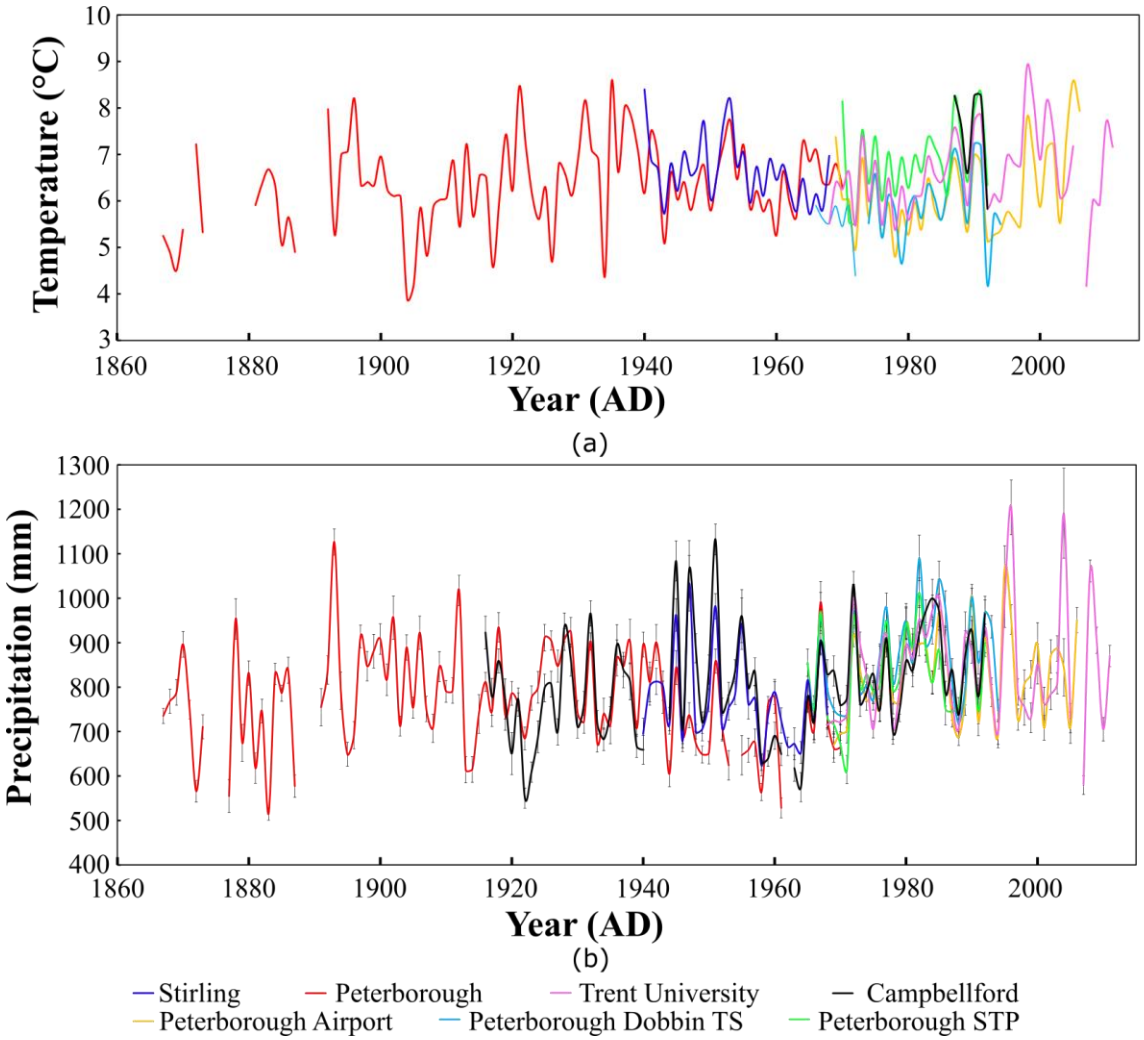

Figure 1.5 (a) Mean annual temperature records between AD 1866 and 2011 recorded at seven stations in southeastern Ontario, Canada. (b) Annual precipitation amounts since AD 1866 recorded in seven stations in southeastern Ontario, Canada.

1.7 Regional Geology

Paleozoic sedimentary rocks in Barry Lake and surrounding areas are composed of Middle Ordovician carbonates (Barnett et al., 1991). Liberty (1969) and Armstrong and Dodge (2007) reported that the Middle Ordovician carbonates of south-central Ontario comprise the Simcoe Group, which includes five formations in ascending order: Shadow Lake, Gull River, Bobcaygeon, Verulam and Lindsay; the Simcoe Group is equivalent to the Black River Group and the overlying Trenton Group of southwestern Ontario (Armstrong and Carter, 2006; Frizzell et al., 2011).

Most landforms in the Barry Lake area were created by the fluctuations in the position of the Laurentide Ice Sheet (LIS), which led to formation of drumlins and tills. Barnett et al. (1991) showed that the tills underlying Barry Lake consist of a sandy silt to silt matrix and have high total matrix carbonate content. Barry Lake lies in the Peterborough Drumlin Field (PDF). The PDF contains more than 3000 drumlins (Boyce and Eyles, 1991; Maclachlan and Eyles, 2013), extending from undrumlinized glacial deposits near Lake Simcoe to a drumlinized field having a northeast-southwest orientation near Trenton (Crozier, 1975). Several mechanisms for formation of the PDF have been offered including: erosion by ice (Gravenor, 1953; Eyles and Westgate, 1987); erosion by meltwater (Shaw and Sharpe, 1987); moulding by subglacial processes (Crozier, 1975; Eyles and Westgate, 1987), and deposition in subglacial cavities (Sharpe, 1987; Shaw and Sharpe, 1987).

Kettle holes are common enclosed topographic depressions formed during phases of ice-recession, when blocks of ice calving from a glacier become partially to wholly buried by glacial outwash. Ice-blocks eventually thaw and depressions form, when average air temperature is above 0 ℃ (Grabau, 1920; Russell and Knudsen, 1999; Stankowski et al., 2002). When these holes filled with water as local hydrological conditions permit, kettle lakes are formed. Generally, these lakes are shallow, and they provide important habitats for numerous plants, fishes and amphibians (Kantrud et al., 1989; Kalettka and Rudat, 2006; Werner et al., 2007).

Kettle lakes offer good conditions for the accumulation of organic matter (Filion and Begin, 1998; Corti et al., 2012). These lakes are commonly colonized by micro- and macrophytes, and vegetation often develops from swamp to bog communities (Filion and Begin, 1998). Late-Quaternary and Holocene vegetation and climate conditions can be reconstructed from pollen, plant remains, and diatom assemblages deposited in lacustrine and peat sediments in kettle lakes (Cwynar, 1988).

Chapter 2

2 Stable Isotope Geochemistry

An atom's nucleus is composed of a specific number of protons and neutrons, and atoms with the same number of protons but a different number of neutrons are called isotopes (Faure and Mensing, 2005). Among the >3300 known nuclides, ~250 nuclides are stable (i.e. do not spontaneously undergo radioactive decay). The stable isotopes examined in this study are ^{1}H, ^{2}H; ^{12}C, ^{13}C; ^{14}N, ^{15}N and ^{16}O, ^{18}O. The stable isotope ratio between the isotopes of the same element can be expressed as:

$$R = \frac{R_a}{R_b} \qquad \text{Equation 2.1}$$

where R_a and R_b are the abundances of the heavy isotope and the light isotope, respectively.

These isotope ratios are most commonly measured by mass spectrometry and are expressed as δ-values in parts per thousand (‰) relative to Vienna Standard Mean Ocean Water (VSMOW) for H and O; Vienna Pee Dee Belemnite (VPDB) for C and sometimes O, and AIR for N. An example for oxygen is:

$$\delta^{18}\mathrm{O} = \left[\frac{(^{18}\mathrm{O}/^{16}\mathrm{O})_{\mathrm{spl}}}{(^{18}\mathrm{O}/^{16}\mathrm{O})_{\mathrm{std}}} - 1\right] \qquad \text{Equation 2.2}$$

where $(^{18}\mathrm{O}/^{16}\mathrm{O})_{\mathrm{spl}}$ and $(^{18}\mathrm{O}/^{16}\mathrm{O})_{\mathrm{std}}$ are the $R(^{18}\mathrm{O})$ of sample and standard, respectively.

Isotopic fractionation occurs during a change in state (i.e. liquid water to water vapour) (Faure and Mensing, 2005), and it is expressed by the isotope fractionation factor α:

$$\alpha_v^l = \frac{R_l}{R_v} \qquad \text{Equation 2.3}$$

where R_l and R_v are the isotopic ratios of the liquid and vapour in equilibrium at a constant temperature. At equilibrium, fractionation factors for light stable isotopes decrease with increasing temperature (Faure and Mensing, 2005).

2.1 Water

Water is composed of H and O, and its lightest molecule, or isotopologue ($^{1}H_2{}^{16}O$), evaporates preferentially to its heavier molecules (i.e. $^{2}H_2{}^{18}O$) (Gat, 1984; Faure and Mensing, 2005). Craig (1961) demonstrated that the $\delta^{2}H$ and $\delta^{18}O$ of precipitation around the world form the Global Meteoric Water Line (GMWL), the equation of which is expressed by Rozanski et al. (1993) as:

$$\delta^{2}H = (8.2 \pm 0.07) \times \delta^{18}O + (11.27 \pm 0.65) \qquad \text{Equation 2.4}$$

Precipitation in a given region experiences somewhat different conditions than the global average. As such, local precipitation isotopic compositions are expressed by a Local Meteoric Water Line (LMWL), which typically has a different slope and intercept than the GMWL (Ingraham, 1998; Jonsson et al., 2009). Longstaffe et al. (2014) described the Great Lakes Meteoric Water Line (GLMWL) by averaging $\delta^{2}H$ and $\delta^{18}O$ of monthly precipitation measured from 1996 to 2011 for 10 Canadian sites located close to the shoreline of the Great Lakes as:

$$\delta^{2}H = 7.1 \times \delta^{18}O + 1.0 \qquad \text{Equation 2.5}$$

Several factors including latitude, altitude, temperature, evaporation, continentality and precipitation amount affect the hydrogen and oxygen isotopic compositions of precipitation and lake water. As mentioned earlier, evaporation moves the light isotopes into the vapour phase, leaving the remaining water enriched in the heavy isotopes. In mid and high latitude areas, snow melt during early spring preferentially adds light isotopes to lake water (Rozanski et al., 1993; Jonsson et al., 2009). Pronounced seasonal differences in water isotope compositions can also occur in a given locality in association with: (i) seasonal changes in local temperature, (ii) seasonal differences in the source of air masses (from tropical to arctic) and/or different storm trajectories, and (iii) seasonally variable evapotranspiration fluxes (Rozanski et al., 1993).

2.2 Biogenic Carbonate

Aquatic molluscs are widely distributed in marine and freshwater environments, from tropical to arctic regions (Keith and Weber, 1964). The shells of most molluscs are composed of aragonite (Leng and Marshall, 2004). Shells of snails are typically formed in spring and consolidated in warmer seasons, while clams such as *Pisidium* form their shells more or less continuously throughout their lifetime (Holopainen, 1980; von Grafenstein et al., 1999; Apolinarska, 2009).

Some organisms deposit their carbonate shells out of carbon or oxygen (or both) isotopic equilibrium with ambient water, resulting in the 'vital effect' (VE) (Abell, 1985; Sharp, 2007). Kinetic and metabolic processes drive the VE (McConnaughey, 1989a,b). Kinetic effects during the hydration and hydroxylation of CO_2 lead to linearly correlated and more negative $\delta^{18}O$ and $\delta^{13}C$ for biogenic carbonates than expected for equilibrium because light isotopes (both O and C) diffuse faster than heavy isotopes and react faster with other substances (McConnaughey, 1989b). Organisms displaying kinetic effects precipitate their carbonate shells almost immediately after these reactions, thus inhibiting oxygen isotope re-equilibration between HCO_3^- and H_2O (Sharp, 2007). Several studies (Fritz and Poplawski, 1974; Leng and Marshall, 2004) showed that most molluscs precipitate their shells in or near oxygen isotopic equilibrium with ambient water, and kinetic effects are not considered further in this study.

Metabolic effects on the $\delta^{13}C$ of biogenic carbonates are mainly caused by photosynthesis and respiration (McConnaughey, 1989a), as light CO_2 is preferentially removed by photosynthesis and added back into the pool by respired CO_2. Respired CO_2 can be a component of the internal carbon pool in some organisms, but its influence on the $\delta^{13}C$ of mollusc shells has been questioned (Fritz and Paplawski, 1974; McConnaughey et al., 1997; Adkins et al., 2003). Metabolic carbon, originating from ingested food and respired carbon, has $\delta^{13}C$ typically much lower than dissolved inorganic carbon (DIC). It is commonly cited as a likely source of ^{13}C-depleted carbon when explaining $\delta^{13}C$ of mollusc shells that is lower than predicted for equilibrium (McConnaughey et al., 1997; Dettman et al., 1999). McConnaughey et al. (1997) claimed that mollusc shells contain <10 % metabolic carbon and >90 % carbon from DIC. Shannahan et al. (2005) reported

that shells of lung-breathing gastropods contain a significant amount of metabolic carbon, thus resulting in lower $\delta^{13}C$ of carbonate shells than predicted for equilibrium. In order to reliably interpret the isotopic compositions of mollusc shells, any vital effects involved in shaping those compositions need to be understood.

The $\delta^{18}O$ of freshwater molluscs is mainly controlled by ambient water $\delta^{18}O$ and temperature during shell formation under equilibrium conditions (Fritz and Poplawski, 1974; Abell and Williams, 1989; Escobar et al. 2010; Macdonald, 2012). Böhm et al. (2000) used data for molluscs, foraminifera and sponges to determine the following expression for the oxygen-isotope fractionation between aragonite and water from 3 to 28 ℃:

$$1000\times\ln\alpha_{\text{aragonite-water}}=\frac{18.45\times10^3}{T\ (K)}-\ 32.54 \qquad \text{Equation 2.6}$$

where

$$\alpha_{\text{aragonite-water}}=\frac{1000+\delta^{18}O_{aragonite}}{1000+\delta^{18}O_{water}} \qquad \text{Equation 2.7}$$

This geothermometer is applied in this study to calculate paleotemperature and paleo lake water $\delta^{18}O$ for biogenic aragonite from shells.

Fontes and Gonfiantini (1968) and Covich and Stuiver (1974) described how hydrologic input (precipitation, P) *versus* output (evaporation, E) (P/E) alter the isotopic compositions of water and associated biogenic and authigenic carbonates. During dry periods (low P/E), lake water and consequently precipitating carbonates become enriched in ^{18}O because of evaporation, whereas during periods of higher P/E, the amount of enrichment is smaller.

The $\delta^{13}C$ of freshwater molluscs is mainly controlled by the carbon isotopic composition of DIC (Abell and Williams, 1989). Several factors affect DIC carbon isotopic compositions: (1) $\delta^{13}C$ of inflow waters (Leng et al., 1999); (2) CO_2 exchange between the lake and the atmosphere (Talbot and Kelts, 1986; Ricketts and Johnson, 1996); (3) photosynthesis-respiration of aquatic plants; and (4) calcium carbonate precipitation

(McKenzie and Hollander, 1993). Unlike the oxygen isotopic composition, the effects of temperature on carbon isotopic compositions are small (Cespuglio et al., 1999). Emrich et al. (1970) found a decrease of 0.035 ‰ per 1 ℃ increase for inorganic aragonite-calcite mixtures; Grossman and Ku (1986) reported an increase of 0.11 ‰ per 1 ℃ increase in temperature for biogenic aragonite. Under isotopic equilibrium with atmospheric CO_2 (e.g. $\delta^{13}C$=–8.4 ‰ in 2014; Scripps CO_2 program, 2015), DIC can have $\delta^{13}C$ varying from –0.5 to +1.8 ‰ over the temperature range 5 to 25 ℃. The shells of freshwater molluscs can provide a measure of seasonal and inter-annual changes in lake water $\delta^{13}C_{DIC}$ during shell formation, and DIC of lake water can be determined directly if the shell has precipitated in equilibrium with DIC (Yoshimura et al., 2015).

Romanek et al. (1992) have reported the enrichment of ^{13}C in aragonite formed under equilibrium with source bicarbonate (HCO_3^-) to be:

$$\varepsilon_{\text{aragonite}-HCO_3^-} = 2.7 \pm 0.6\ ‰ \qquad \text{Equation 2.8}$$

where $\varepsilon_{\text{aragonite}-HCO_3^-} = \alpha_{\text{aragonite}-HCO_3^-} - 1$. Macdonald (2012) confirmed the calibration of this equation over the temperature range 10–40 ℃.

2.3 Calcite

Calcite in this study refers to the calcium carbonate (excluding mollusc shells) precipitated mainly in epilimnetic waters in freshwater systems either as the result of (i) changes in water temperature, ion activities and pH related to seasonal climatic changes (Brunskill, 1969; Strong and Eadie, 1978) and/or (ii) bioinduced precipitation (e.g. from phytoplankton) caused by removal of CO_2 by photosynthesis (Otsuki and Wetzel, 1974; Strong, 1978; Effler et al., 1981, 1982; Effler, 1984), leading to the so-called ‘whiting events’. Calcite precipitates mainly during warmer periods, when nutrient availability and increased light contribute to enhanced algal productivity (Reynolds, 1984).

Briefly, this calcite’s oxygen isotopic composition is determined by temperature and $\delta^{18}O$ of lake water during mineral precipitation (Leng and Marshall, 2004). Experiments show that the oxygen isotopic composition of calcite precipitated by phytoplankton such as

cyanobacteria form in equilibrium with the ambient water (Stabel, 1986; Merz, 1992). The temperature of calcite formation can be calculated using Leng and Marshall's (2004) expression of Kim and O'Neil's (1997) equation:

$$T(℃)=13.8 - 4.58\times(\delta c - \delta w)+0.08\times(\delta c - \delta w)^2 \qquad \text{Equation 2.9}$$

where δc is the oxygen isotopic composition of calcite reported relative to VPDB and δw is the oxygen isotopic composition of water reported relative to VSMOW.

Several studies (Benson et al., 1991, 1996, 1998, 2002; Li and Ku, 1997; Li et al., 2000; Seltzer et al., 2000) have used the $\delta^{18}O_{calcite}$ as a proxy for climate-forced relative lake level change. Generally, the precipitation (inflow) *versus* evaporation (outflow) (P/E ratio) is used to infer relative changes in climatic conditions (Benson et al., 1991; Johnson et al., 1991; Lister et al., 1991; Li et al., 2000; Seltzer et al., 2000; Benson and Paillet, 2002; Benson et al., 2002). During dry conditions (lower lake level; P/E<1.0), $\delta^{18}O_{calcite}$ will increase as evaporation preferentially removes ^{16}O from lake water; conversely $\delta^{18}O_{calcite}$ will typically decrease under wetter conditions, which are typically accompanied by higher lake levels.

The $\delta^{13}C_{calcite}$, as is the case for mollusc shells, is mainly derived from DIC in lake waters (Talbot, 1990; Li and Ku, 1997; Leng and Marshall, 2004; Lamb et al., 2007). Romanek et al. (1992) described the equilibrium enrichment of ^{13}C in calcite relative to source bicarbonate (HCO_3^-) to be:

$$\varepsilon_{calcite-HCO_3^-} = 1.0 \pm 0.2\ ‰ \qquad \text{Equation 2.10}$$

where $\varepsilon_{calcite-HCO_3^-} = \alpha_{calcite-HCO_3^-} - 1$.

Unlike the equilibrium precipitation conditions noted for oxygen isotopes, cyanobacteria-induced calcite precipitation produces a 2 ‰ enrichment in ^{13}C relative to DIC (Merz, 1992). This enrichment results from preferential uptake of ^{12}C during cyanobacteria photosynthesis, which leaves the surrounding water enriched in ^{13}C. Merz (1992) also reported that no respiratory carbon is involved in the calcite precipitation; enrichment of ^{13}C in calcite indicates extracellular sources for its carbon.

2.4 Organic Matter

Organic matter (OM) is a mixture of lipids, carbohydrates, proteins and other biochemical compounds produced by organisms living in and around the lake (Meyers and Ishiwatari, 1993; Meyers and Lallier-Vergès, 1999; Meyers, 2003). Two main sources of OM to most lakes are terrestrial higher plants and aquatic algae (Meyers and Lallier-Vergès, 1999). Based on their biochemical compositions, plants can be divided into two groups: (1) nonvascular plants that lack carbon-rich cellulose and lignin, such as algae; and (2) vascular plants, typically terrestrial, which are rich in fibrous tissues. Atomic C/N ratios are commonly considered to provide a way to distinguish the two categories. C/N ratio is normally calculated as an atomic ratio:

$$C/N = \frac{\%\mathbf{TOC}/\mathbf{12.01}}{\%\mathbf{TN}/\mathbf{14.01}} \qquad \text{Equation 2.11}$$

The C/N ratio of unaltered aquatic algae lies between 4 and 10, as they are protein-rich and cellulose-poor. Unaltered OM originating from terrestrial plants typically has a C/N ratio greater than 20.

2.4.1 Isotopic Compositions

OM produced by terrestrial plants using C_3 and C_4 pathways from atmospheric CO_2 has average $\delta^{13}C$ of –27 ‰ and –13 ‰, respectively (O'Leary, 1988). The $\delta^{13}C$ of OM derived from phytoplankton using dissolved CO_2 is often indistinguishable from organic matter derived from C_3 terrestrial plants (Meyers and Lallier-Vergès, 1999). Overall, OM produced by aquatic plants using the C_3 pathway is ~20 ‰ lighter than its DIC source (O'Leary, 1988; Wolfe et al., 2001). Formation and sedimentation of algal OM removes ^{12}C from the surface-water DIC pool, leaving the remaining DIC enriched in ^{13}C, which in turn causes an increase in the $\delta^{13}C$ of subsequently formed OM (Meyers, 2003). Lakes with increasing productivity therefore may be characterized by an increase in $\delta^{13}C$ of OM.

In some cases, algal OM can have $\delta^{13}C$ as low as –32 ‰, as a result of a large input of isotopically light soil ($\delta^{13}C$ =–12 ‰) into a lake; under other circumstances, the $\delta^{13}C$ of algal OM can be as high as –9 ‰, caused by a carbon source change from dissolved

atmospheric CO_2 to dissolved HCO_3^- ($\delta^{13}C$ =+1 ‰) (Meyers, 2003). The concentration of dissolved atmospheric CO_2 can become insufficient during periods of high lake productivity, thus driving aquatic plants to utilize dissolved HCO_3^- (Hollander and MacKenzie, 1991; Keeley and Sandquist, 1992; Bernasconi et al., 1997) and in high pH waters where HCO_3^- is dominant (Hassan et al., 1997).

The 'Suess effect' describes the change in the $\delta^{13}C$ of atmospheric CO_2 resulting from fossil fuel combustion (Keeling et al., 1979) and needs to be considered when comparing modern and pre-industrial $\delta^{13}C_{OM}$ and atmospheric contributions to DIC. Verburg (2007) estimated atmospheric CO_2 $\delta^{13}C$ for any post-industrial date based on a best fit of the $\delta^{13}C$ of atmospheric CO_2 (n=160) between 1692 and 2000 (Friedli et al., 1986; Francey et al., 1999; Keeling et al., 2001; Langenfelds et al., 2002):

$$\delta^{13}C_{atm}=7.7738118\times10^{-16}\times Y^6 - 1.2222044\times10^{-11}\times Y^5+7.1612441\times10^{-8}\times Y^4 - 2.1017147$$

$$\times10^{-4}\times Y^3+3.3316112\times10^{-1}\times Y^2 - 273.71502\times Y +91703.261 \qquad \text{Equation 2.12}$$

where Y is the calendar year. This equation produces values identical to those measured $\delta^{13}C_{CO_2}$ by Cuntz (2011) and the Scripps CO_2 program except for the years after AD 2000, for which the estimations are 0.1 to 0.2 ‰ lower than the actual measurements. The small discrepancies may reflect human interventions such as Kyoto Protocol, which may have slowed the rate of increase in emission of CO_2. Since there was only 0.21 ‰ decrease in $\delta^{13}C_{atm}$ between 1692 and 1850, which is likely within the sample measurement error of most isotope laboratories (Verburg, 2007), the Suess correction factor used in the present study has been calculated by subtracting the calculated $\delta^{13}C$ of atmospheric CO_2 for a specific year from the average $\delta^{13}C$ of pre-industrial atmospheric CO_2 (–6.5 ‰) for each sample after AD 1850.

The two most important nitrogenous sources utilized by most plants are nitrate (NO_3^-) and ammonium (NH_4^+) (Szpak et al., 2013). Nitrate commonly is the most abundant nitrogen source for plants, but ammonium can predominate under waterlogged or acidic soil conditions (Yoneyama et al., 2003; Pilbeam, 2010). Atmospheric molecular nitrogen is another nitrogen source for some plants (Meyers and Lallier-Verg ès, 1999; Szpak et al.,

2013). Yakir (2011) stated that NH_4^+ becomes the dominant nitrogen source in nutrient-poor (oligotrophic) lakes, whereas eutrophic systems (nutrient-rich) will depend more on NO_3^-. As such, plants in eutrophic systems are typically more enriched in ^{15}N than in oligotrophic systems. On average, plants that utilize atmospheric N_2 have $\delta^{15}N$ ~0 ‰, and those incorporating NO_3^- and NH_4^+ tend to have $\delta^{15}N>0$ ‰ (Szpak et al., 2013); $\delta^{15}N$ of aquatic algae typically range from +2 to +13 ‰, and about –5 to +3 ‰ for most terrestrial plants (Meyers, 2003). The presence of N_2-fixing phytoplankton (e.g. cyanobacteria) can lead to low $\delta^{15}N$ of OM (e.g. to –2 ‰) (Talbot and Laerdal, 2000; Meyers, 2003). Variations in $\delta^{15}N_{TN}$ typically reflect: (i) a change in lake trophic state (Brenner et al., 1999), (ii) denitrification through microbial decomposition of OM (Talbot, 2001, Woszczyk et al., 2014), and (iii) a change in nitrogen sources (e.g. soil erosion and nutrients from agricultural activities can contribute to an increase in $\delta^{15}N_{TN}$) (Ahlgren et al., 1994; Meyers and Teranes, 2001; Routh et al., 2007, 2009).

Microbial decomposition of OM can alter the isotopic compositions of OM (Meyers and Lallier-Vergès, 1999). For nitrogen isotopes, microbial decomposition of OM in the lake via denitrification or the delivery of soil-derived N from arable land can produce higher $\delta^{15}N$ (Talbot, 2001). The latter process can shift the $\delta^{15}N$ in residual OM to ~30 ‰ more positive than in the OM (Lu et al., 2010). During denitrification, the product N_2 typically has $\delta^{15}N$ ~20 ‰ lower than the reactant NO_3^- (Talbot, 2001), thus increasing the ^{15}N concentrations in the residual nitrate (and OM that utilizes it). Bratton et al. (2003) reported that denitrification causes an increase in $\delta^{15}N$ of sediments in Chesapeake Bay from +5 to +10 ‰ within a few centuries.

For carbon, decomposition under oxic conditions would produce increasing $\delta^{13}C$ (Talbot and Livingstone, 1989; Li et al., 2008). Under subaerial oxidation, Schelske and Hodell (1991) and Sifeddine et al. (2011) found no significant changes in both $\delta^{13}C$ and $\delta^{15}N$. Under anoxic conditions, OM is selectively decomposed, mainly N-containing and ^{15}N and ^{13}C-enriched compounds, leading to ^{15}N and ^{13}C depletion in bulk OM (Bernasconi et al., 1997; Li et al., 2008; Torres et al., 2012). Methanotrophy and/or methane oxidation of OM in water column can deliver ^{12}C-enriched C to the DIC pool and produce more negative $\delta^{13}C$ in OM that subsequently incorporates this DIC (Woszczyk et al., 2014).

2.4.2 Chemical Properties

The concentration of total organic carbon (TOC) is a fundamental proxy to describe the abundance of organic matter in sediments (Meyers and Teranes, 2001; Meyers, 2003). Typical organic matter contains ~50 % carbon, so the concentration of organic matter is about twice the amount of TOC (Meyers, 2003). The origin, delivery routes, depositional processes and extent of alteration and degradation are also reflected in the abundance and composition of OM accumulated in lake sediments (Meyers, 2003). TOC can be diluted by addition of inorganic sediment and concentrated by dissolution of carbonate minerals in sediment (Dean, 1999), and TOC commonly increases when sediment grain size decreases (Thompson and Eglinton, 1978). OM can be easily decomposed under aerobic conditions but produce different results (Woszczyk et al., 2014). For highly weathered OM, Talbot and Livingstone (1989) reported that decomposition under oxic conditions leads to decreasing TOC amount and increasing $\delta^{13}C_{OM}$. Filey et al. (2001) found that post-sedimentary decomposition of OM in alternating (oxic/anoxic) conditions in a diagenetic environment in rooted zone can result in a lowering of C/N ratio. Mass accumulation rates for organic carbon (C-MARs) provide more useful measures of the delivery and preservation of OM than TOC because the former compensate for changes in bulk sedimentation rates and for sediment compaction (Meyers and Lallier-Vergès, 1999; Meyers, 2003).

Except at very low concentrations of OM, TN also largely reflects the abundance of organic matter in sediments (Meyers, 2003; Hyodo and Longstaffe, 2011). Degradation can greatly affect TN content; Li et al. (2008) and Choudhary et al. (2009a, b), for example, reported that microbial degradation of N-bearing compounds in OM can lead to a decrease in TN content, producing high C/N ratio in residual OM. Mass accumulation rates for total nitrogen (N-MARs), similar to C-MARs, provide a better representation of OM than TN for measuring changes in organic matter accumulation (Meyers, 2003). Following Yu et al. (2007), C-MARs and N-MARs can be calculated:

$$\text{(C or N)-MARs} = [\text{wt.\% (C or N)}] \times [\text{LSR}] \times [\text{DBD}] \times 1000 \qquad \text{Equation 2.13}$$

where LSR is the linear sedimentation rate and DBD is the dry bulk density of the sediment.

C/N ratios are sometimes useful in distinguishing sources of OM found in aquatic systems, having values of 4 to 10 for unaltered algae and >20 for terrestrial plants (Meyers and Lallier-Vergès, 1999). Aquatic algae growing under nitrogen deficient conditions, however, can have C/N ratios in the range of 13 to 20 (Hecky et al., 1993; Talbot and Laerdal, 2000). Some studies (Bernasconi et al., 1997; Li et al., 2008; Torres et al., 2012) showed that anaerobic decomposition results in higher C/N ratio, as N-containing phases are selectively removed. In contrast, Meyers and Lallier-Vergès (1999) reported that CO_2 and CH_4 produced by decomposition of OM under anaerobic conditions can escape from sediments, leading to lower TOC contents in the residual materials, but NH_4^+ produced from nitrogeneous OM, is absorbed by clay minerals and therefore retained in the sediments, causing a decrease in the measured C/N ratio. Under aerobic conditions, degradation is more effective, and several studies have documented the decreasing C/N ratio are resulted from highly weathered OM (e.g. Talbot and Livingstone, 1989; Meyers and Lallier-Vergès, 1999; Zhao et al., 2015). Hladyniuk and Longstaffe (2015a) have also noted that highly degraded OM with low C/N can be retained on soil clays transported to the lacustrine environment, further complicating interpretation of C/N results obtained for bulk sediment OM samples. Accordingly, C/N ratios should be interpreted with caution in lacustrine systems.

Chapter 3

3 Methodology

3.1 Sample Collections

3.1.1 Gravity Cores

Two Glew gravity corers (Glew et al., 2001): BL–G11–01 (01) and BL–G11–02 (02) were collected at Station 2 (ST2) (water depth: 7.5 m) on November 6th, 2011 at Barry Lake (Fig. 3.1) by Dr. Fred Longstaffe, Dr. Ryan Hladyniuk (The University of Western Ontario) and Dr. Avner Ayalon (Geological Survey of Israel). Cores were extruded onshore using a vertical-type extruder at 0.5 cm interval. A total of 83 and 82 samples were acquired and individually sealed in Whirl-Pak bags for cores 01 and 02, respectively. Samples from core 01 were stored at the Laboratory for Stable Isotope Science (LSIS) at 4 ℃ and used as required for physical, chemical and isotopic multiproxy analyses. Samples from core 02 were stored frozen at LSIS until required for dating and chronology reconstruction. Water properties including temperature, salinity and specific conductivities and Secchi depth were measured at Station 1 (ST1) at one-meter intervals using a YSI measurement device.

3.1.2 Water Sample Collection

Water samples were collected during expeditions to Barry Lake on May 12th, July 14th and November 3rd, 2014. Twenty water samples (ten for δ^2H_{water} and $\delta^{18}O_{water}$, and ten for $\delta^{13}C_{DIC}$) were collected each time at four stations (Figs. 3.2a-c). One station was located close to the shore (S1 in May, July and November), from which shallow water samples were taken. At the other stations, water samples were collected from the surface (0.5 m), middle (3–3.5 m) and bottom (6–7 m) of the lake using a vertical point water sampler.

Chemical and physical parameters (temperature, specific conductivity, dissolved oxygen (DO) and pH) of the lake water were measured using a YSI Professional Plus® handheld multiparameter instrument. Water pH was not measured in July 2014 because the pH probe malfunctioned. Three probes (temperature/conductivity, DO and pH) were

calibrated at least one day before the field trips. A thermometer, distilled water and a standard conductivity solution were used for the calibration of the temperature/conductivity probe. Standard pH 4 and pH 7 solutions were used for calibration of the pH probe. A moisturized sponge was used for the calibration of the DO probe (a demonstration of the calibration processes for this YSI instrument can be found at https://www.youtube.com/watch?v=6lz7BQxCaSM). Lake water depth was measured using a depth finder. Secchi depth was measured using a Secchi disk deployed from the sunny side of the boat.

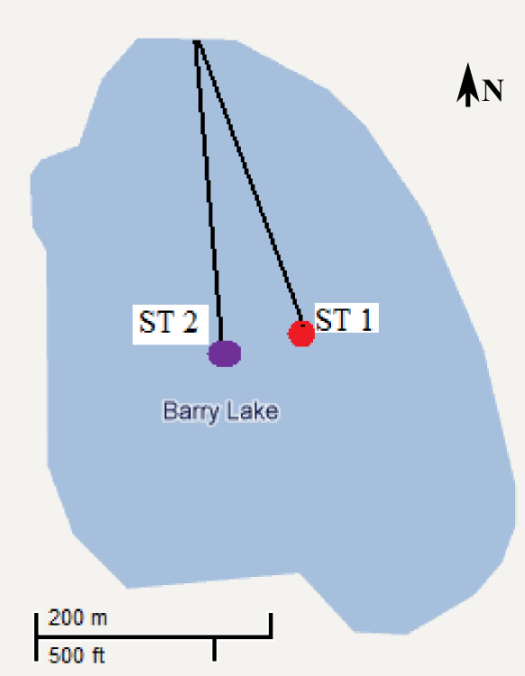

Figure 3.1 Locations of the two gravity cores collected in 2011 from Barry Lake.

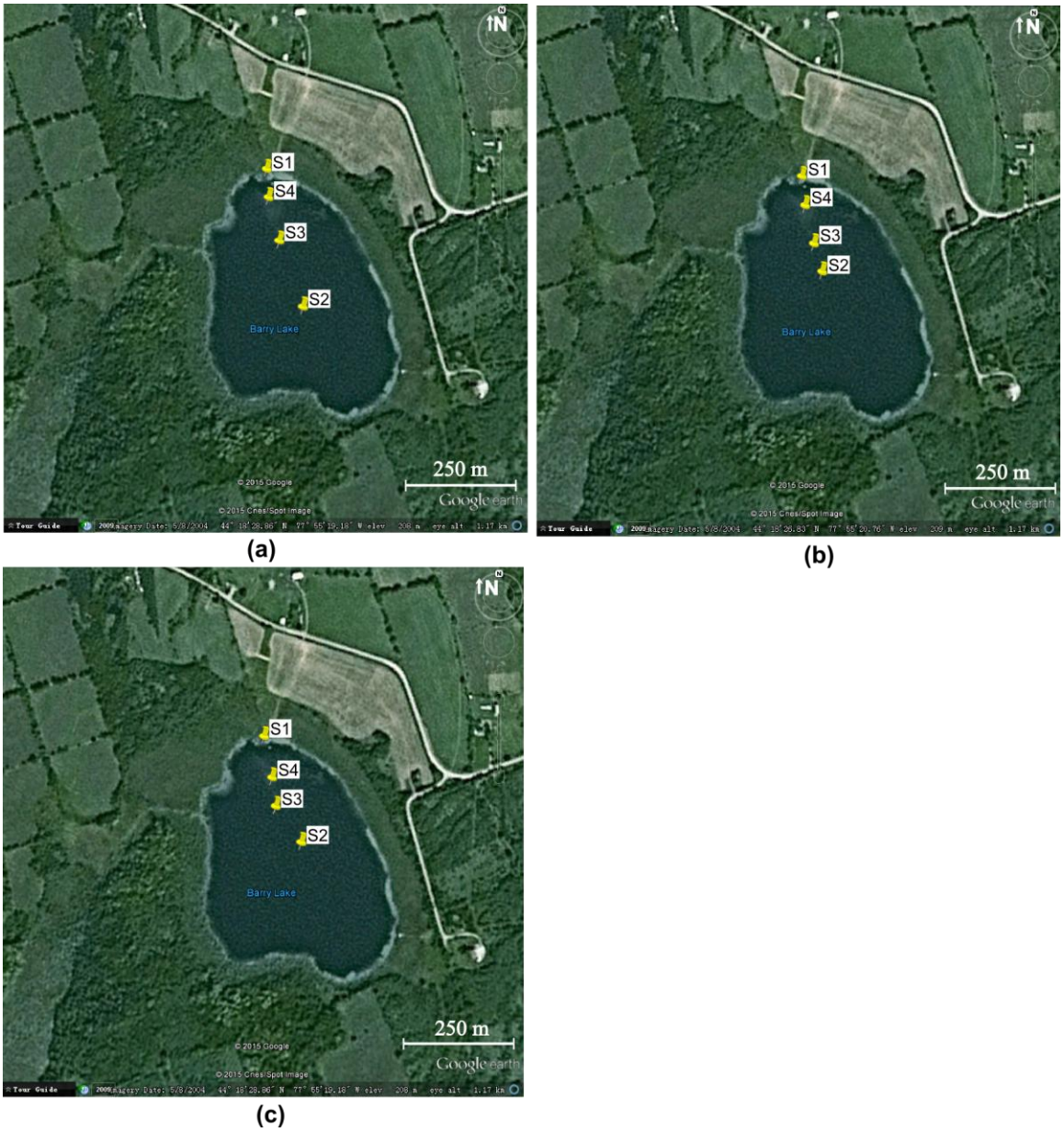

Figure 3.2 Locations of the four stations during three field trips to Barry Lake in 2014. (a) May, 12, 2014. (b) July 14, 2014. (c) November 3, 2014.

3.2 Analytical Methods

3.2.1 ^{210}Pb Dating

^{210}Pb is a natural radionuclide (half life: 22.26 years) produced by ^{226}Ra decay (Appleby, 2001; Ruiz-Fernández and Hillaire-Marcel, 2009) (Fig. 3.3), and ^{210}Pb is divided into "unsupported" and "supported" ^{210}Pb. The "unsupported" $^{210}Pb_u$ is derived primarily from

atmospheric fallout (Turekian et al., 1983), and the "supported" $^{210}Pb_s$ is produced by radioactive decay of ^{226}Ra located within the sediment of the catchment (Norton et al., 1985; Benoit and Hemond, 1987) (Fig. 3.4). Limited by its half-life, the ^{210}Pb dating method is only applicable for the most recent 150 years (Binford et al., 1993; O'Reilly et al., 2011).

$$^{238}U \xrightarrow{4.51\times10^{9}\ y} {}^{226}Ra \xrightarrow{1602\ y} {}^{222}Rn \xrightarrow{3.82\ d} {}^{210}Pb \xrightarrow{22.26\ y} {}^{210}Po \xrightarrow{138.4\ d} {}^{206}Pb$$

Figure 3.3 ^{238}U decay series, showing the principal radionuclides concerned with the production of ^{210}Pb, and their half-lives (Appleby, 2001).

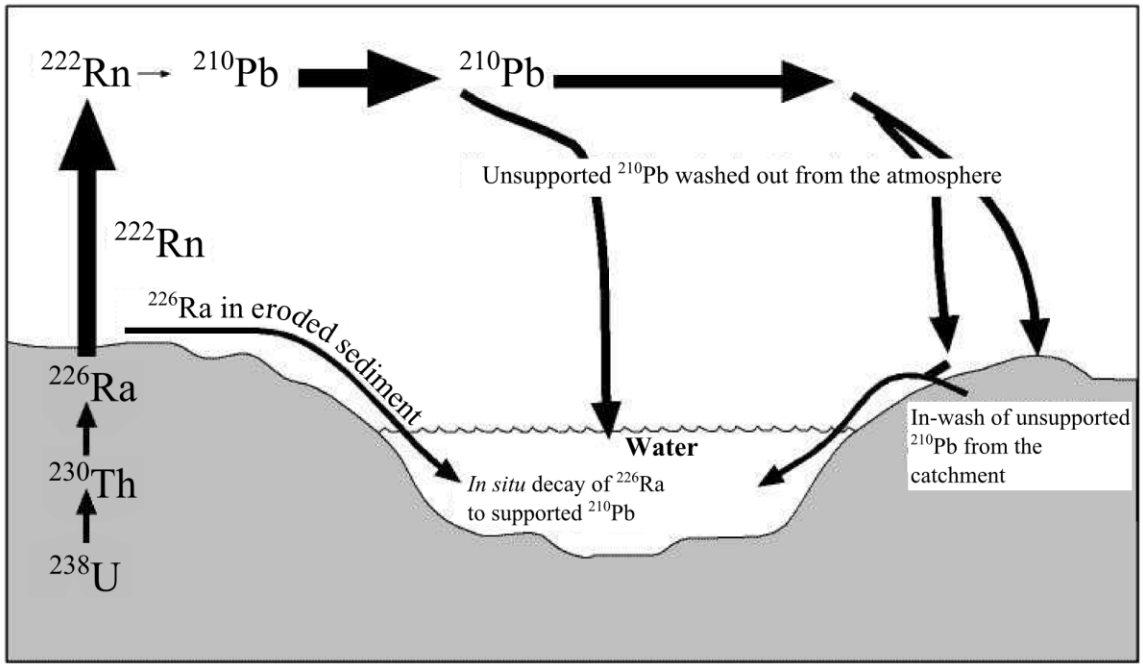

Figure 3.4 Pathways by which ^{210}Pb reaches aquatic sediments (after Oldfield and Appleby, 1984).

^{137}Cs is an artificial radionuclide (half life: 30.14 years), and the profiles of ^{137}Cs fallout from nuclear weapons tests into the environment are used to validate chronologies produced by ^{210}Pb dating (Pennington et al., 1973; Ritchle et al., 1973; Gelen et al., 2003; O'Reilly et al., 2011). Atmospheric nuclear testing started in the early 1950s and reached a maximum in AD 1963 (Pennington et al., 1973; Davies et al., 1984). The Chernobyl reactor accident in AD 1986 resulted in another upward spike in ^{137}Cs deposition (Dörr

and Münnich, 1991). The radioisotope ^{241}Am was also present in nuclear weapons fallout but was undetectable in the Chernobyl accident at locations distant from the reactor site (Appleby et al., 1991; O'Reilly et al., 2011). Like the ^{137}Cs profile, the ^{241}Am profile can be used to validate ^{210}Pb chronology of sediments (Davis et al., 1984; Appleby et al., 1991; Blais et al., 1995).

Two models: (i) Constant Rate of Supply (CRS) and (ii) Constant Initial Concentration (CIC) are commonly used in ^{210}Pb dating. In general, the CRS model is most widely applied because it considers variations in sediment accumulation rates, and the accumulation rates in most natural sediment systems fluctuate (Appleby, 2001, 2008; MacKenzie et al., 2011). The CIC model is only useful when the ^{210}Pb activities show a monotonic decline in sediments (Appleby and Oldfield, 1978; Blais et al., 1995). Physical and biological processes, however, can lead to variations in ^{210}Pb supply such that neither model produces reliable results (Appleby, 2001). Independent chronological evidence, particularly from ^{137}Cs and ^{241}Am, is commonly used to validate ^{210}Pb dating results (Appleby and Oldfield, 1978; Appleby, 2001, 2008).

Samples from gravity core BL–G11–02 were transported, still frozen, to the Laboratory for the Analysis of Natural and Synthetic Environmental Toxins (LANSET), at the University of Ottawa for ^{210}Pb dating. The ^{210}Pb and ^{137}Cs measurements were made using an Ortec® High Purity Germanium Gamma Spectrometer (Oak Ridge, TN, USA). Certified reference materials obtained from the International Atomic Energy Agency (IAEA) (Vienna, Austria) were used for efficiency corrections. The results were analyzed, and the ^{210}Pb dating profiles were produced using the software ScienTissiMe (Barry's Bay, ON, Canada; http://www.scientissime.net/).

3.2.2 AMS ^{14}C Dating

Accelerator mass spectrometry (AMS) radiocarbon (^{14}C) dating is commonly used to establish the sedimentary chronology beyond the ^{210}Pb dating horizon. Generally, terrestrial macrofossils such as seeds, leaves, needles and bracts are the best materials for providing reliable ^{14}C dates in lacustrine sedimentary sequences (Deevey et al., 1954; Olsson, 1983; Marcenko et al., 1989; Björck and Wohlfarth, 2001; Birks, 2002; Olsson,

2009; Grimm, 2011). In lake sediments, macrofossils of aquatic plants are also common. These plants can utilize dissolved inorganic carbon (DIC) as a carbon source in addition to, or instead of, atmospheric CO_2. As a result, radiocarbon dates obtained from such materials can be hundreds to thousands of years older than their real age (Barnekow et al., 1998; Oswald et al., 2005; Marty and Myrbo, 2014). This discrepancy results from the hard-water effect (HWE), which is caused by contribution of old carbon from sources such as the dissolution of allochthonous carbonates, thus producing lower ^{14}C activities (Deevey et al., 1954; Olsson, 1983; Marty and Myrbo, 2014). Terrestrial macrofossils, which utilize only atmospheric carbon dioxide, do not suffer from HWE. In contrast, submerged vegetation and aquatic mosses are sometimes characterized by radiocarbon dates that are spuriously old, which require correction for the HWE (Deevey et al., 1954; Hakansson, 1979; Olsson, 1983; Birks, 2002).

Samples (0.5 cm intervals) from core BL–G11–02 were freeze-dried following completion of ^{210}Pb dating; this process revealed a total of ~11 mg seeds of submerged aquatic macrofossil (*Najas flexilis*) and wood fragments (Fig. 3.3) at the 34.5–35 and 35–35.5 cm intervals. These samples were sent to Beta Analytic Radiocarbon Dating Laboratory (Laboratory number: Beta-408561) for AMS ^{14}C dating, where it was necessary to combine seeds and wood in both intervals to gather sufficient material for the procedure. For this analysis, the modern reference standard used was 95 % the ^{14}C activity of the National Institute of Standards and Technology (NIST) Oxalic Acid (SRM 4990C), and the date of the sample was calculated using the Libby half-time (5568 ± 30 years; Libby et al., 1949). The ^{14}C age was also corrected using the measured $^{13}C/^{12}C$ ratio for the combined sample. Correction for the HWE was also necessary and will be discussed in Section 5.1.

3.2.3 Magnetic Susceptibility

Magnetic susceptibility (MS) of the two Barry Lake gravity cores was determined at the Lakes and Reservoirs Systems Research Facility (LARS), the University of Western Ontario, using a Geotek® multi-sensor care logger (MSCL) equipped with a point sensor (MS2E). A standard was measured every 5 samples to ensure precision and accuracy of the measurements. MS was measured using wet sediment for BL–G11–01; wet BL–G11–

02 (except for 20 samples previously dried for radioisotope dating) and freeze-dried sediment for BL–G11–02.

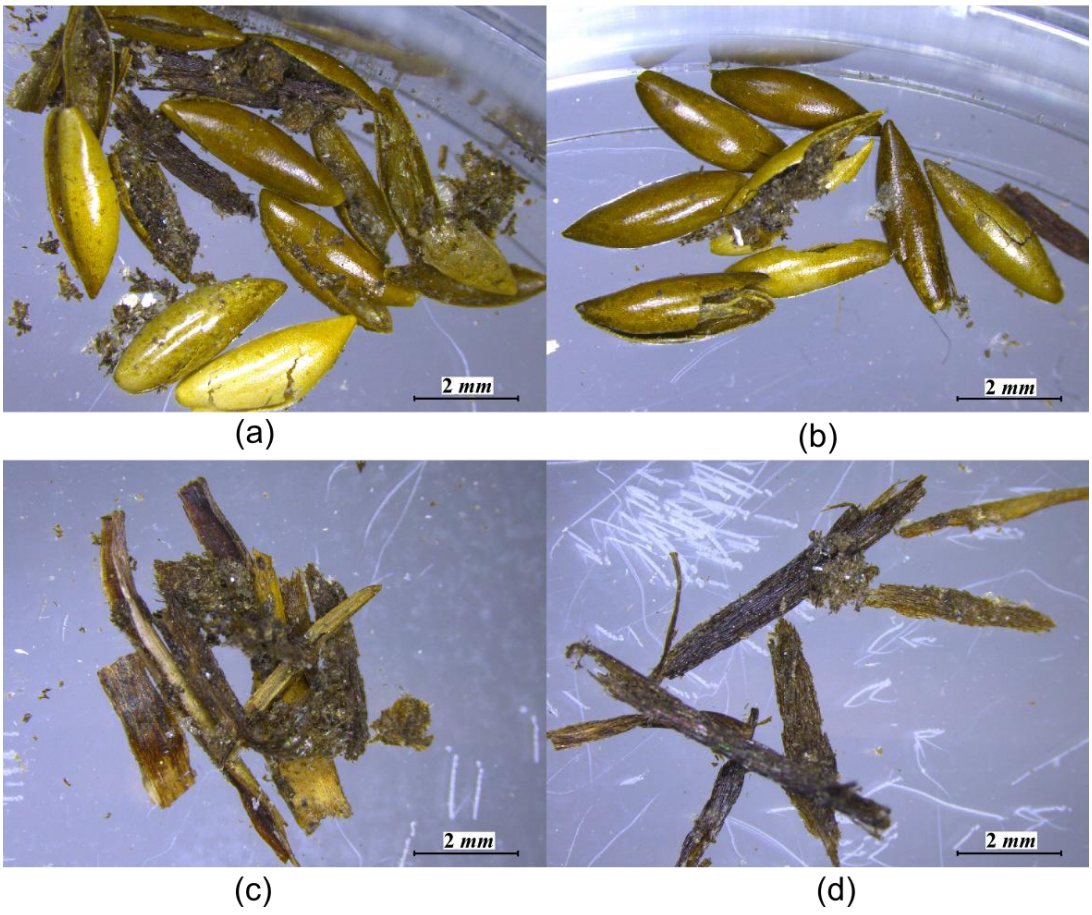

Figure 3.5 Organic matter used for ^{14}C dating: (a) *Najas flexilis* at 34.5-35 cm. (b) *Najas flexilis* at 35-35.5 cm. (c) Wood fragments at 34.5-35 cm. (d) Wood fragments at 35-35.5 cm.

3.2.4 Powder X-ray Diffraction and Scanning Electron Microscope

Powder X-ray diffraction (pXRD), which was used to characterize the mineralogy of the sediment in gravity core BL–G11–01 was performed at LSIS. Samples from gravity core BL–G11–01 were first freeze-dried, after which twenty to fifty milligrams of sediment was extracted and homogenized by grinding to a fine powder (<65 μm) using a rubber pestle and ceramic mortar (during freeze-drying, samples at 5–5.5 cm and 5.5–6 cm were mixed together by accident, reducing the number of intervals that could be analyzed). A representative sample (~30 mg) was then mounted in an Al-backpack holder or a glass-

frontpack holder (~10 mg sample) in preparation for pXRD. pXRD was performed using a high brilliance Rigaku RU-200BVH rotating anode X-ray diffractometer equipped with Co source and a graphite monochromater, and operated at 45 kV and 160 mA. The samples were scanned in step-scan mode from 2 °to 82 °2θ, using a step size of 0.02 °2θ and a scan rate of 10 °2θ/min. The abundance of each mineral was estimated using the background-subtracted peak height of its most intense diffraction, after counting for any peak overlaps with other minerals. These abundance estimates should be considered as representative of organic-free sediment, as organic matter (OM) is not detectable by pXRD. To obtain abundances for the whole sample (mineral plus OM), the amount of OM was estimated by twice the amount of TOC (Dean, 1974, 1999), and calcite abundances were determined directly during isotopic measurements. Since quartz, calcite and OM comprise most of the sediment (on a shell-free basis), these measures of OM and calcite content allowed quartz abundance to be estimated by difference.

Five sediment samples (7–7.5, 21.5–22, 36.5–37, 39.5–40 and 41–41.5 cm) were carbon-coated and then examined using a scanning electron microscope (SEM) at the Zircon and Accessory Phase Laboratory (ZAPLab), the University of Western Ontario, to qualitatively evaluate the sediment chemical composition and grain size using a backscattered electron detector (BSE) and energy-dispersive X-ray spectroscopy (EDS). BSEs are used for illustrating contrasts in composition of multiphase samples and for quickly distinguishing different phases. EDS is used to evaluate the chemical composition of the sediments. The SEM was operated in accelerating voltage at 15 kV and variable pressure of 40 Pa.

3.2.5 Grain Size Analyses

Grain-size analysis of samples from core BL–G11–01 was performed using a Malvern Mastersizer® 2000 laser grain-size analyzer housed in the Control and Crystallization of Pharmaceuticals Laboratory (CCPL), Faculty of Engineering, the University of Western Ontario. The Mastersizer® 2000 is capable of measuring grain size ranging from 0.02 to 2000 microns in diameter. The Masterizer® 2000 assumes that grains are perfect spheres; it uses the volume of a grain to measure its size and to calculate a diameter that is equivalent in volume using the technique of "equivalent spheres" (Xiao et al., 2009).

Tests before the measurements showed that an amount of 15 mg sediment was able to generate laser obscuration between 10 and 20 %, which is the optimum range for grain size analysis. About 15 mg of sediment from 21 freeze-dried samples were gently disaggregated into individual grains using a mortar and spatula scoop. Any shell fragments in the sample were then removed by hand picking. The samples were then treated with 15 ml of 0.3 % bleach at 65 ℃ for at least 24 hours to remove organic matter. The bleach was next removed from the sample by rinsing with distilled water at 16000 RPM (revolutions per minute) for 20 minutes. The rinsing-centrifugation process was repeated six times. Finally, to prepare for the laser grain-size analyses, 10 ml of 0.1 % sodium hexametaphosphate solution was added to ~10 to 15 mg of sample as a dispersing agent. The motor speed was set to 2100 RPM with a one-minute ultrasonic interval. The sample solution was added to 500 ml of distilled water when the system was ready, and then they were pumped through the system for analyses. The one-minute ultrasonic treatment was performed when instructed by the automated system. The Mastersizer® 2000 produces three measurements and one weighted average per sample. The sample is considered to have been dispersed completely if no major changes are observed in the replicate analytical curves.

3.2.6 Water Isotopic Analyses

The $\delta^{2}H_{water}$, $\delta^{18}O_{water}$ and $\delta^{13}C_{DIC}$ of lake water were measured at LSIS using a Thermo Finnigan GasBench® II connected to a Thermo Scientific Delta^{plus} XL continuous-flow isotope ratio mass spectrometer (CF-IRMS) and a heater block equipped with a CombiPal® autosampler, as described below.

3.2.6.1 Hydrogen Isotopes

The $\delta^{2}H_{water}$ was measured using the H_2-equilibration method described by Horita (1988). Briefly, one mL of water was pipetted into a glass vial using a micropipette. A reusable platinum catalyst stick was then added to each vial, such that half of the catalyst length was submerged in the water. The vial was then capped and sealed using a septum and flushed with 3 % H_2 in He for 5 minutes prior to isotopic analysis. Waters were

equilibrated with H_2 in He at 35 ℃ in the GasBench® heater block for at least 30 minutes. The gas was then automatically transported to the IRMS using an autosampler.

Four internal standards, which were previously calibrated to VSMOW (Coplen, 1994), were measured regularly throughout the analytical session including LSD (–161.8 ‰), MID (–108.1 ‰), EDT (–56.0 ‰) and Heaven (+88.7 ‰). LSD and Heaven were used to generate the calibration curve with VSMOW and had reproducibilities (reported throughout this thesis as standard deviation, SD) of ±4 ‰ (n=3) and ±3 ‰ (n=3), respectively. Accuracy and precision were evaluated using MID and EDT having average δ^2H of –107 ±2 ‰ (n=3) and –55 ±1 ‰ (n=6), respectively, which compares well with the accepted values for these standards. Duplicate samples were analyzed every 10 samples and had an average reproducibility of ±1 ‰ (n=6) (Appendix A).

3.2.6.2 Oxygen Isotopes

The $\delta^{18}O_{water}$ was measured using the CO_2-equilibration method (Epstein and Mayeda, 1953). One mL of water and standards was injected into septum-sealed glass vials and then flushed with 0.3 % CO_2 for 5 minutes. Samples were equilibrated at 35 ℃ for 24 hours in the GasBench® heater block prior to isotopic analysis. The gas was then automatically transferred to the IRMS using an autosampler.

The standards used for hydrogen isotope measurements were also used for oxygen isotopic calibration to the VSMOW scale following Coplen (1994): LSD (–22.57 ‰), MID (–13.08 ‰), EDT (–7.27 ‰) and Heaven (–0.27 ‰). LSD and Heaven were used to generate the calibration curve, and had average reproducibilities of ±0.05 ‰ (n=2) and ±0.08 ‰ (n=2), respectively. MID and EDT were used to evaluate the accuracy and precision of the calibration and had average values of –13.03 ±0.31 ‰ (n=2) and –7.43 ±0.24 ‰ (n=4), respectively, which compares well with accepted values. Duplicate samples were analyzed every 10 samples and had an average reproducibility of ±0.02 ‰ (n=6) (Appendix A).

3.2.6.3 Carbon Isotopic Compositions of Dissolved Inorganic Carbon (DIC)

Glass vials like those used for water isotope analyses were baked at 450 ℃ for 3 hours prior to use to eliminate potential organic contamination. For samples, five drops of 100 % concentrated orthophosphoric acid were added to the bottom of the glass vials, which were then septum-sealed and flushed with He for 5 minutes. One mL of water sample was then injected into the flushed vial using a one mL syringe. The vials were reacted in the GasBench® heater block at 35 ℃ overnight prior to isotopic measurements. The produced gas was then transported automatically to the IRMS using an autosampler.

Five solid carbonate internal standards were used for calibration of the samples to VPDB (Coplen et al., 2006), including international standards NBS–19 (+1.95 ‰), NBS–18 (–5.0 ‰) and LSVEC (–46.6 ‰), and laboratory standards Suprapur (–35.28 ‰) and WS–1 (+0.76 ‰). For each standard, 0.25 mg was weighed into the bottom of a clean oven baked glass vial, and the vial was placed in a horizontal position. Concentrated orthophosphoric acid (100 %) was then added to the top of the vial such that the acid was separated from the standard powder. A septum cap was then attached to the vial and tightened, after which the vial was flushed with He for 5 minutes at room temperature. The vial was then turned upright, thus allowing the acid to react with the standard powder. The vial was then immediately placed in the GasBench® heater block overnight reacting at 35 ℃. Similar to samples, the evolved gas was then automatically transferred to the IRMS using an autosampler.

The standards were interspersed with the samples throughout the analytical session. LSVEC and NBS–19 were used for calibration of the isotopic results to VPDB (Coplen et al., 2006); their average reproducibilities were ±0.08 ‰ (n=5) and ±0.04 ‰ (n=5), respectively. NBS–18 and Suprapur were used to check the accuracy and precision of the measurements; their average $\delta^{13}C$ were –5.11±0.07 ‰ (n=5) and –35.55±0.03 ‰ (n=5), respectively, which compares well with their accepted values. Duplicate samples were analyzed every 5 samples with an average reproducibility of ±0.03 ‰ (n=12) (Appendix A).

3.2.7 Biogenic Carbonate Isotopic Analyses

Several species of molluscs were identified following Burch (1982) and Schueler and Karstad (2012) in the Barry Lake samples, and pXRD showed that aragonite was the shell-forming material. The aragonite $\delta^{13}C_{shell}$ and $\delta^{18}O_{shell}$ were analyzed at LSIS by reacting with orthophosphoric acid at 90 ℃ using a Micromass Multiprep® autosampling device coupled to a VG Optima® dual-inlet IRMS.

The shells were first placed in an ultrasonic bath and distilled water at low power for 5 minutes for cleaning, after which they were rinsed in distilled water and air-dried. Care was taken to ensure that any detritus adhering to the inside or outside of the shell was removed. Approximately 0.09 mg of the cleaned shell sample was then weighed into a reaction vessel, sealed with silicone septa and placed in a heated block maintained at 90 ℃. A double-bore needle was then pushed through the septa into the vial. The vial was then evacuated followed by the dispensing of orthophosphoric acid onto the sample. Samples and acid were reacted for 12 minutes. The evolved CO_2 was then passed through a trap to remove water and then cryogenically collected in an external cold finger, where the gas was then transferred to the IRMS for isotopic analysis.

Several standards were used to calibrate the results for samples to VSMOW (oxygen) and VPDB (carbon) and to evaluate accuracy and precision (Coplen et al., 2006). These included international standards: NBS–18 ($\delta^{13}C$= –5.0 ‰; $\delta^{18}O$= +7.2 ‰), NBS–19 ($\delta^{13}C$ = +1.95 ‰; $\delta^{18}O$ = +28.65 ‰) and LSVEC ($\delta^{13}C$= –46.6 ‰), and laboratory standards Suprapur ($\delta^{13}C$= –35.6 ‰; $\delta^{18}O$= +13.3 ‰) and WS–1 ($\delta^{13}C$ = +0.76 ‰; $\delta^{18}O$= +26.23 ‰). NBS–19 and LSVEC were used to generate the carbon isotope calibration curve (Coplen et al., 2006). Average reproducibilities were ±0.05‰ (n=22) and ±0.14‰ (n=18), for NBS‐19 and LSVEC, respectively. NBS–18 and NBS–19 were used to generate the oxygen isotope calibration curve. Average reproducibilities were ±0.07 ‰ (n=20) and ±0.04 ‰ (n=22) for NBS–18 and NBS–19, respectively (Appendix A).

NBS–18, WS–1 and Suprapur were used to assess the accuracy and precision of the carbon–isotope measurements and had average $\delta^{13}C$ of: –5.0±0.1 ‰ (n=11), +0.8±0.0 ‰ (n=2) and –35.7±0.1 ‰ (n=4), respectively, which compares well with accepted values.

WS–1 and Suprapur were also used to assess the accuracy and precision of the oxygen-isotope measurements and had average $\delta^{18}O$ of +26.24±0.09 ‰ (n=4) and +13.14±0.07 ‰ (n=6), respectively. Duplicates were analyzed every 11 samples with averaged reproducibility of ±0.23‰ (n=18) and ±0.39 ‰ (n=18) for carbon and oxygen, respectively (Appendix A).

3.2.8 Calcite Isotopic Analyses

The $\delta^{13}C_{calcite}$ and $\delta^{18}O_{calcite}$ of calcite were also measured at LSIS. At a first step, the samples were inspected for mollusc shells and shell fragments, which were removed by hand-picking prior to further processing. The remaining sediment was freeze-dried and then ground using a Wig-L-Bug® for 1.5 minutes. About 0.1 to 0.2 mg of sample was then weighed into a reaction vessel, with the exact weight determined as a function of calcite content of the sample, as estimated using pXRD. Analysis using the Micromass MultiPrep® device coupled to a VG Optima® dual-inlet mass spectrometer then proceeded as described earlier for the biogenic aragonite.

The same standards as for biogenic aragonite were used for calibration and evaluation of isotopic accuracy and precision (Coplen et al., 2006). Average $\delta^{13}C$ reproducibilities for NBS–19 and LSVEC were ±0.05 ‰ (n=9) and ±0.25 ‰ (n=7), respectively. Average $\delta^{18}O$ reproducibilities were ±0.08 ‰ (n=9) and ±0.04 ‰ (n=9) for NBS–18 and NBS–19, respectively. NBS–18, WS–1 and Suprapur had average $\delta^{13}C$ of –5.08±0.08 ‰ (n=20), +0.80±0.02 ‰ (n=2) and –35.62±0.05 ‰ (n=2), respectively, which compares well with accepted values. WS–1 and Suprapur had average $\delta^{18}O$ of +26.26±0.02 ‰ (n=4) and +13.16±0.01 ‰ (n=6), respectively, which also compares well with accepted values. Duplicates were analyzed every 11 samples and had an average reproducibility of ±0.06 ‰ (n=14) and ±0.04 ‰ (n=14) for carbon and oxygen, respectively (Appendix A).

3.2.9 Bulk Organic Matter Analyses

3.2.9.1 Total Organic Carbon, Total Nitrogen and C/N

TOC and TN were measured using a Carlo Erba Fisons® 1108 elemental analyzer at LSIS. Sediments were freeze-dried and then ground using a Wig-L-Bug® for 1.5 minutes. Prior

to analysis, carbonates were removed by acid fumigation (Harris et al., 2001). In this procedure, 2 mg of sample were weighed into silver capsules and placed into a sample tray. Three drops of water were then added to each capsule. About 300 mL of concentrated, 12N, hydrochloric acid (HCl) was added to the bottom reservoir of a glass dessicator. The sample tray was then placed in the dessicator on an elevated ceramic platform above the acid and the dessicator lid left partially open. The dessicator was then left overnight at room temperature in a fumehood. After 30 hours, one drop of 7.4N hydrochloric acid was added to each capsule to check for completion of the fumigation. No bubbles were observed after 30 hours. pXRD of test samples showed that the procedure was effective. The samples were then dried at 50 ℃ for 24 hours, after which the dried sediments in silver capsules were re-weighed, crimped and wrapped in tin capsules in order to maximize combustion in the elemental analyzer. The samples were dropped by a rotating autosampler into the combustion reactor set to 1020 ℃ and the reactor automatically fed a pulse of O_2. Combustible materials in capsules underwent flash combustion and were swept by He through the combustion reactor to ensure catalytic conversion of all carbon in the sample to CO_2 and all nitrogen to nitrogen oxides (NO_x). He carrier gas then swept the gases into the reduction reactor (650 ℃) where NO_x was reduced to N_2 gas over copper wire. Produced water was trapped using magnesium perchlorate, and the remaining gases then separated using a gas chromatographic (GC) column and detected using a thermal conductivity detector (TCD).

A separate aliquot of untreated sample (~5 mg) was used for nitrogen content (and isotopic) measurements, as acid treatment can alter original $\delta^{15}N$ by up to 8 ‰ (Teranes and Bernasconi, 2000; Harris et al., 2001). The atomic C/N ratio was then calculated based on TOC and TN results (Meyers, 1994) using Equation 2.11.

Two standards, Low Organic Content (LOC) soil (OC= 1.52 wt.%; TN= 0.13 wt.%) and High Organic Content (HOC) soil (OC= 6.10 wt.%; TN= 0.46 wt.%) were used to generate the calibration curves used for the total nitrogen content measurements and had average reproducibilities of ±0.09 % (n=13) and ±0.01 % (n=24) for LOC and HOC, respectively. Untreated HOC was used to generate the calibration for organic carbon content, as preliminary testing demonstrated that its organic carbon content was altered

by acid fumigation. The average reproducibility of untreated HOC for total organic carbon was ±0.11 %. The Peach Leaf standard (SRM number: 1547, TN=2.94 %) was also measured in each TOC and TN analytical session to evaluate accuracy and precision of nitrogen contents. The measured average value of 2.91±0.09 % (n=5) compares well with its accepted values. Duplicates were analyzed every 11 samples and had average reproducibilities of ±0.23 % (n=16) for OC and ±0.01 % (n=14) for TN (Appendix A).

3.2.9.2 Isotopic Compositions

The carbon and nitrogen isotopic compositions of OM were measured at LSIS. Sediments were first freeze-dried and then ground using a Wig-L-Bug® for 1.5 minutes. To remove carbonate from the samples, 7.4N hydrochloric acid was added to weighed sediments in beakers and reacted for 48 hours. After 48 hours, the samples were transferred to centrifuge tubes and washed with distilled water four times to remove the acid. The samples were then freeze-dried and weighed into tin capsules (0.4 to 1 mg) for isotopic measurements. About 1 to 2 mg of untreated sediments were weighted into tin capsules and used for nitrogen isotope analyses, as discussed earlier.

A Costech Elemental Combustion system coupled to a Thermo Scientific Delta^{plus} XL IRMS in continuous-flow (He) mode was used to determine the carbon and nitrogen isotopic compositions of organic matter. Values of $\delta^{13}C$ and $\delta^{15}N$ were measured in separate analytical sessions to generate reliable signal (amplitudes). The tin-encapsulated samples were delivered by a rotating autosampler to the combustion furnace held at 1020 ℃ together with a pulse of pure oxygen. All combustible materials were then converted into gases (CO_2 for carbon-bearing materials, and N_2 and/or NO_x for nitrogen-bearing materials). Similar to the procedure described above for elemental analysis of C and N, the produced gases were then swept by He carrier gases over catalysts and high purity copper to ensure that all carbon was present as CO_2 and all nitrogen as N_2. Water produced during these reactions was removed by a magnesium perchlorate trap, and when required for nitrogen isotopic analyses, CO_2 was first removed using Carbo-Sorb®. For simultaneous isotopic analyses, N_2 and CO_2 were separated using a GC column and swept by He carrier gas to the IRMS for isotopic measurements.

The carbon and nitrogen isotopic compositions of samples ($\delta^{13}C_{OM}$ and $\delta^{15}N_{TN}$) were calibrated to VPDB and AIR using USGS 40 ($\delta^{13}C$= –26.39 ‰; $\delta^{15}N$= –4.52 ‰) and USGS 41 ($\delta^{13}C$= +37.63 ‰; $\delta^{15}N$ +47.57 ‰) (Qi et al., 2003; Coplen et al., 2006), and had average reproducibilities of ±0.03 ‰ (n=11) and ±0.12 ‰ (n=10) for $\delta^{13}C$, respectively, and ±0.11 ‰ (n=15) and ±0.13 ‰ (n=13) for $\delta^{15}N$, respectively. Laboratory standard keratin (MP Biomedicals Inc., Cat. No. 90211, Lot No. 9966H; $\delta^{13}C$=+24.04 ‰; $\delta^{15}N$=+6.36 ‰) was used to evaluate the accuracy and precision of the analytical sessions, and yielded average values of –24.04 ±0.06 ‰ (n=15) for $\delta^{13}C$ and +6.39 ±0.1 ‰ (n=24) for $\delta^{15}N$, which compares well with its accepted values. Duplicates were analyzed every 10 samples and yielded average reproducibilities of ±0.07 ‰ (n=18) for $\delta^{13}C$ and ±0.06 ‰ (n=36) for $\delta^{15}N$ (Appendix A).

Chapter 4

4 Results

4.1 Core Details and Chronology

4.1.1 Core Description

Core photos were taken during the field trip in November 2011 (Figs. 4.1a, b). Overall, the wet sediment in both cores is darker in colour in the upper sections than the basal sections, where white shells and shelly fragments are present. The colour of the freeze-dried sediment varies from dark brown (2.5Y 5/4) to light brown (2.5Y 5/3) from the top to the bottom of the core. The sediments comprise fine-grained silt and clay, and the organic matter content in the bottom 10 cm of both cores is higher than its upper portions. Shell fragments appear at 29 cm, with whole shells being abundant and well-preserved in the bottom 9 cm (32 to 41 cm) of both cores.

4.1.2 Grain Size and Mineralogy

The mineral fraction of the sediment in Barry Lake gravity core BL–G11–01 is dominated by two phases: quartz and calcite, except for the shelly material, which is made of aragonite (Fig. 4.2a; Appendix B). The pXRD results, which are based on peak heights of the most intense diffractions of calcite and quartz, indicate that calcite is the most abundant inorganic phase varying from ~90 % of the inorganic fraction in the basal portions of the core to 20 % at 20 to 25 cm depth before increasing again to ~80 % near the top of the core (Fig. 4.2a); quartz abundance shows an antipathetic variation to calcite abundance.

Abundance measurements (wt. %) derived from data collected during isotopic measurements more closely approximate the actual calcite percentages in the sediments when the presence of organic matter and variations in calcite *versus* quartz pXRD crystallinity are considered (Fig. 4.2b). The pattern of variation in calcite abundance is similar to the pXRD results, with a maximum of 60 % calcite in basal sections of the core,

which then decreases to a minimum of ~5 % between 20 and 25 cm before rising again. As before, quartz abundance shows an antipathetic variation to the abundance of calcite.

The organic matter content below ~38 cm fluctuates widely from 30 to 45 % before steadily increasing to a maximum of ~70 % at 30 cm and 60 % at 25 cm. The organic matter content then declines to a relatively constant ~30% over the top 20 cm of the core.

Grain size curves (excluding shells and shell fragments removed by hand-picking) for core BL–G11–01 shown in Figure 4.2c. Curves are provided for 10 % (d0.1) and 90 % (d0.9) of the sediment that is finer than the indicated diameter, and for median grain size (d0.5) (Appendix C). Generally, sediment between 30 and 35 cm is coarser than sediment at other depths, with a maximum median size of 8.7 μm at 31 cm, and a minimum median size of 3.5 μm at 23.5, 27 and 37.5 cm. The presence of shell fragments that could not be removed by hand-picking and below 29.0 cm may have skewed the measured grain size to higher values.

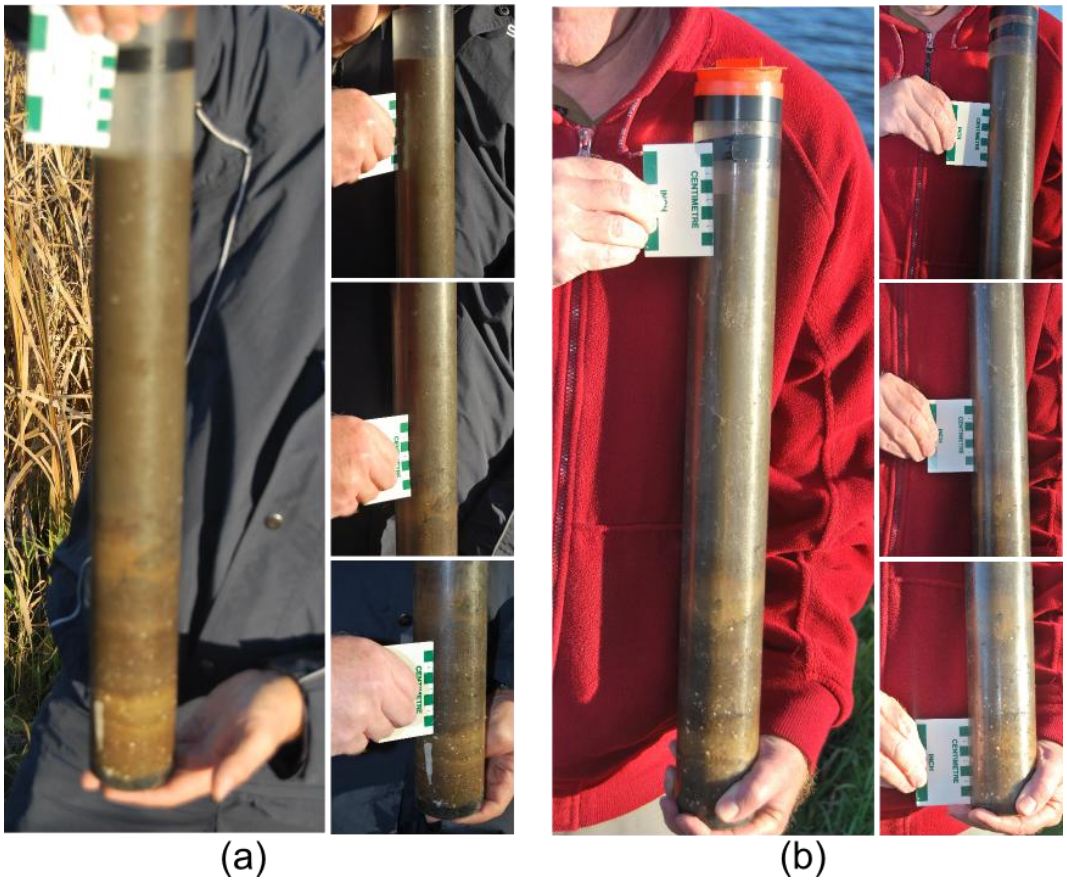

Figure 4.1 Field photographs of two gravity cores collected at Barry Lake in November, 2011: (a) Core BL–G11–01 (41.5 cm). (b) Core BL–G11–02 (41 cm). Photographs by F.J. Longstaffe.

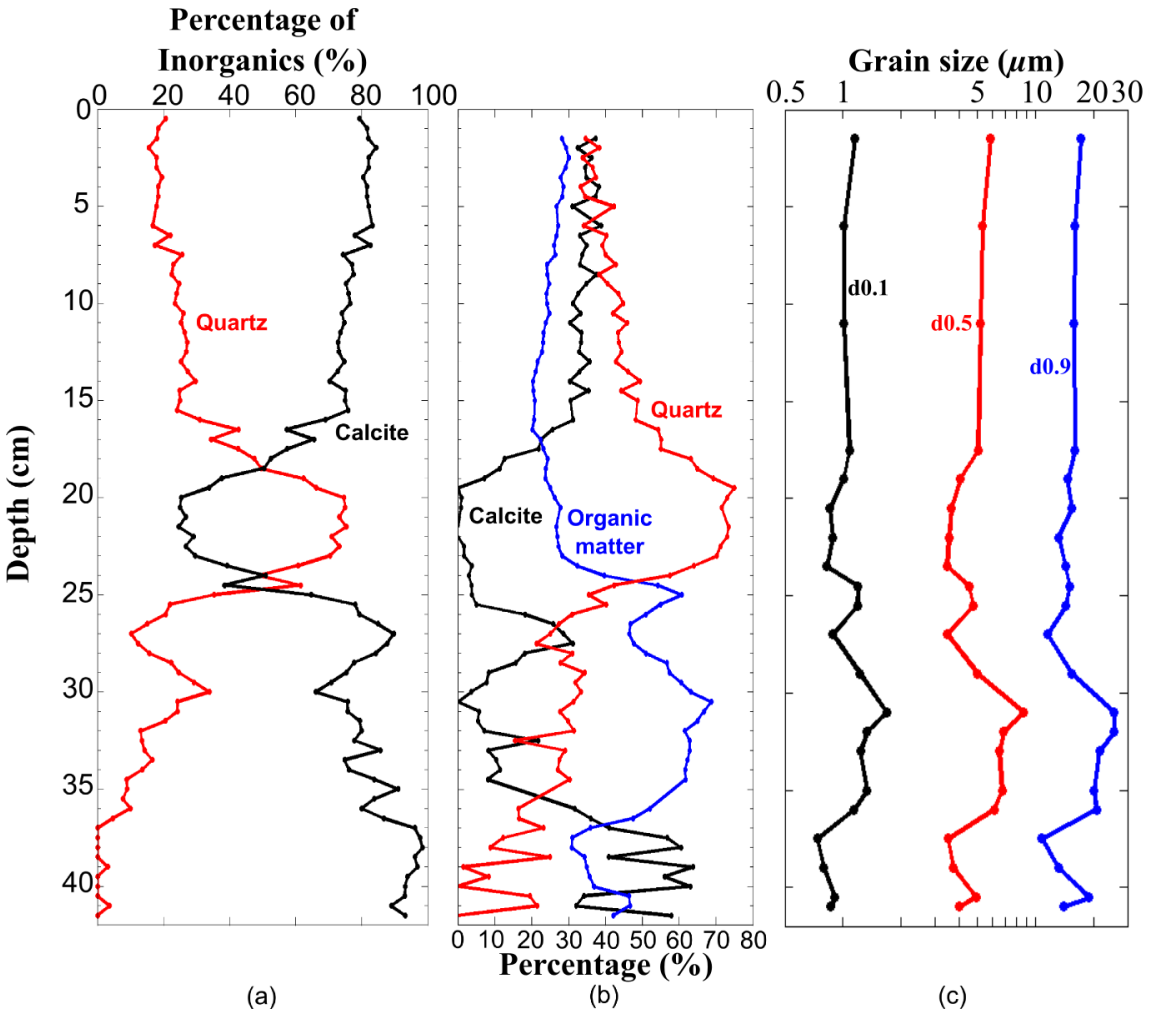

Figure 4.2 Mineral and organic matter abundances and grain-size information for core BL–G11–01. All results exclude shelly material (aragonite) removed by hand-picking. (a) Percentages (weighted peak heights of most intense diffraction) of quartz (red) and calcite (black) measured using pXRD. Some aragonite that could not be removed by hand-picking is present at and below 29.0 cm. (b) Percentages of quartz (red), calcite (black) and organic matter (blue). Calcite content (plus small amounts of aragonite at and below 29.0 cm) was estimated from data collected during isotopic analysis; organic matter content was estimated as 2× the total organic carbon content as determined by elemental analysis; quartz content was determined by difference. (c) Grain size distributions: d0.1, d0.5 and d0.9 indicate that 10 %, 50 % and 90 % of the sediment, respectively, is finer than the size (μm) indicated.

4.1.3 Magnetic Susceptibility

Overall, MS signals are relatively constant in core BL–G11–01 (analyzed wet) and core BL–G11–02 (analyzed dry) except for a large positive anomaly at ~21.5 cm in both cores (Figs. 4.3a, c) and a smaller positive anomaly at 19.5 cm in core BL–G11–02 (Fig. 4.3b; Appendix D). Dry samples yield lager MS signals than wet samples, but the relative variations in the MS signals are consistent among all of the analyses. For cores BL–G11–01 (analyzed wet), BL–G11–02 (a mixture of wet and dry samples) and BL–G11–02 (analyzed dry) (Figs. 4.3a-c), the maximum MS signals are +3, +11 and +13 at ~21.5 cm, respectively. For core BL–G11–02, the average MS value before the positive anomalies is 0 but increases to 2 after the anomalies.

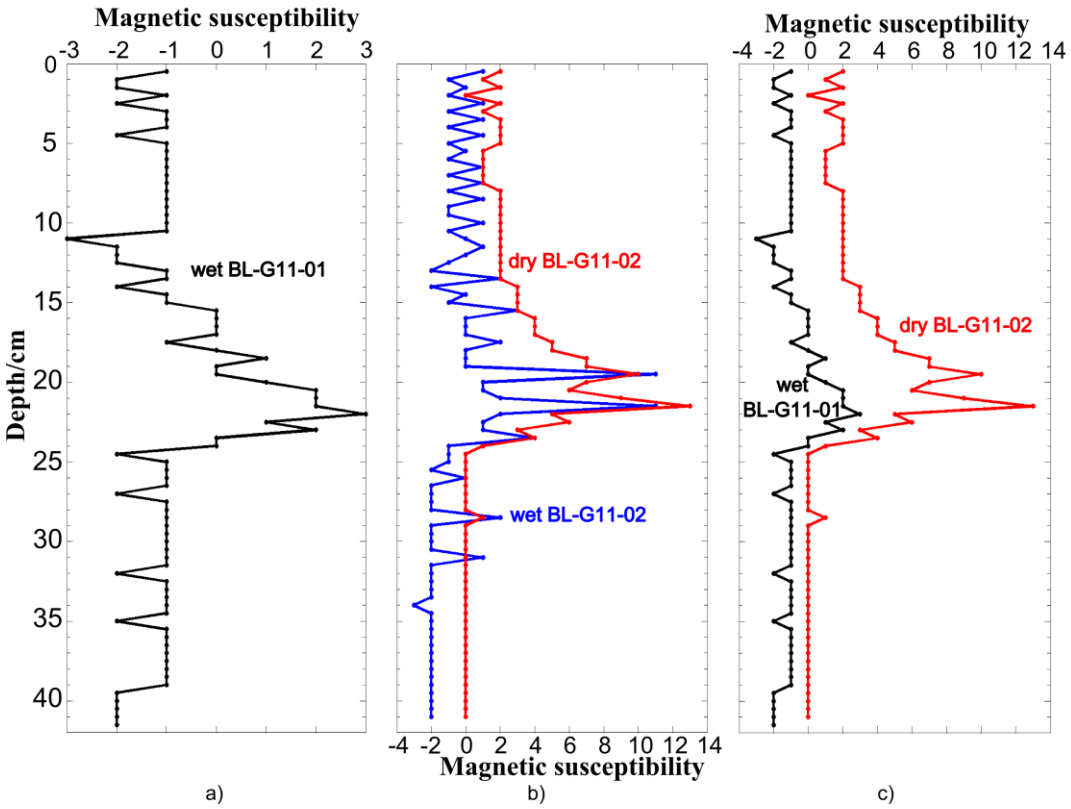

Figure 4.3 Magnetic susceptibility profiles. (a) Core BL–G11–01, black, analyzed wet. (b) Core BL–G11–02: blue, a mixture of wet and dry samples, and red, analyzed dry. (c) Core BL–G11–01: black, analyzed wet; core BL–G11–02: red, analyzed dry.

4.1.4 Chronology

Activities of $^{210}Pb_s$ and $^{210}Pb_u$ with depth are summarized in Table 4.1. Four models have been applied in the interpretation of these data (Fig. 4.4a; Table 4.2): constant flux and sedimentation (CF/CS), constant rate of supply (CRS), constant initial concentration (CIC) and ^{137}Cs (Cesium).

The CF/CS and ^{137}Cs models provide the longest dating records but have big differences in dates between them. The ^{137}Cs model is generated using only 2 points: the surface and the apex of the cesium profile; the remainder of the dates are produced by curve-fitting to these two points. The CF/CS model assumes a constant sedimentation rate, which is unrealistic in most natural systems. The CIC model is only reliable when the ^{210}Pb activities show a monotonic decline in the sediments (Appleby and Oldfield, 1978; Blais et al., 1995). Therefore, these three models are considered invalid.

The peak of ^{137}Cs (139.22 Bq/kg) and ^{241}Am (5.42 Bq/kg) activities occur at 11.25 cm (Fig. 4.4b; Table 4.3), and second-highest peaks are at 8.25 cm for ^{137}Cs (130.89 Bq/kg) and 7.25 cm for ^{241}Am (5.21 Bq/kg), respectively. The CRS model yields dates AD 1967 ± 0.4, 1980 ± 0.2, and 1985 ± 0.2 at depths of 11.25 cm, 8.25 cm and 7.25 cm, respectively, which corresponds well to the injection of these isotopes into the atmosphere by nuclear weapon tests in that peaked in 1963 (Pennington et al., 1976; Blais et al., 1995; Benoit and Rozan, 2001) and the Chernobyl reactor accident in 1986 (Bollhöfer et al., 1994; Korhola et al., 2002). The CRS model is considered the most reliable for this study, as it accounts for variations in sedimentation rates (Johnston et al., 2010) and correlates well with the independent evidence from ^{241}Am and ^{137}Cs activities.

The AMS ^{14}C dating result is 880 ± 30 BP (Table 4.4). This date requires a hardwater effect (HWE) correction before it can be used in the age-depth model. The age-depth model for the Barry Lake sediments is discussed in the next chapter.

Table 4.1 Activities of unsupported $^{210}Pb_u$ and supported $^{210}Pb_s$ with depth for core BL–G11–02.

Cumulative Drymass	Midpoint Depth	Unsupported $^{210}Pb_u$ Activity	Error ($^{210}Pb_u$ activity)	Supported $^{210}Pb_s$ Activity	Error ($^{210}Pb_s$ activity)
[g/cm^2]	[cm]	[Bq/kg]	[Bq/kg]	[Bq/kg]	[Bq/kg]
0	0	1136.6369	128.0722	20.8638	5.2118
0.0079	0.25	799.9516	65.9650	20.8638	5.2118
0.0539	1.25	984.6041	69.0504	20.8638	5.2118
0.1199	2.25	859.1148	56.8124	20.8638	5.2118
0.1908	3.25	912.5921	60.9267	20.8638	5.2118
0.2635	4.25	853.8798	61.8208	20.8638	5.2118
0.3405	5.25	838.5574	60.5732	20.8638	5.2118
0.4229	6.25	658.6894	53.0601	20.8638	5.2118
0.5084	7.25	501.2535	44.8835	20.8638	5.2118
0.5944	8.25	473.3332	41.3292	20.8638	5.2118
0.7258	9.75	374.1412	40.1396	20.8638	5.2118
0.8572	11.25	192.0747	35.9239	20.8638	5.2118
1.0430	13.25	216.8787	37.6120	20.8638	5.2118
1.2395	15.25	167.8673	37.0866	20.8638	5.2118
1.4132	17.25	363.0126	46.2826	20.8638	5.2118
1.5645	19.25	140.7915	27.0917	20.8638	5.2118
1.7136	21.25	101.2225	29.1261	20.8638	5.2118
1.8347	23.25	31.8836	39.5858	20.8638	5.2118
1.9376	25.75	0	60.2717	20.8638	5.2118
2.0248	28.25	58.5214	42.5567	20.8638	5.2118
2.1109	30.75	0	43.0798	20.8638	5.2118

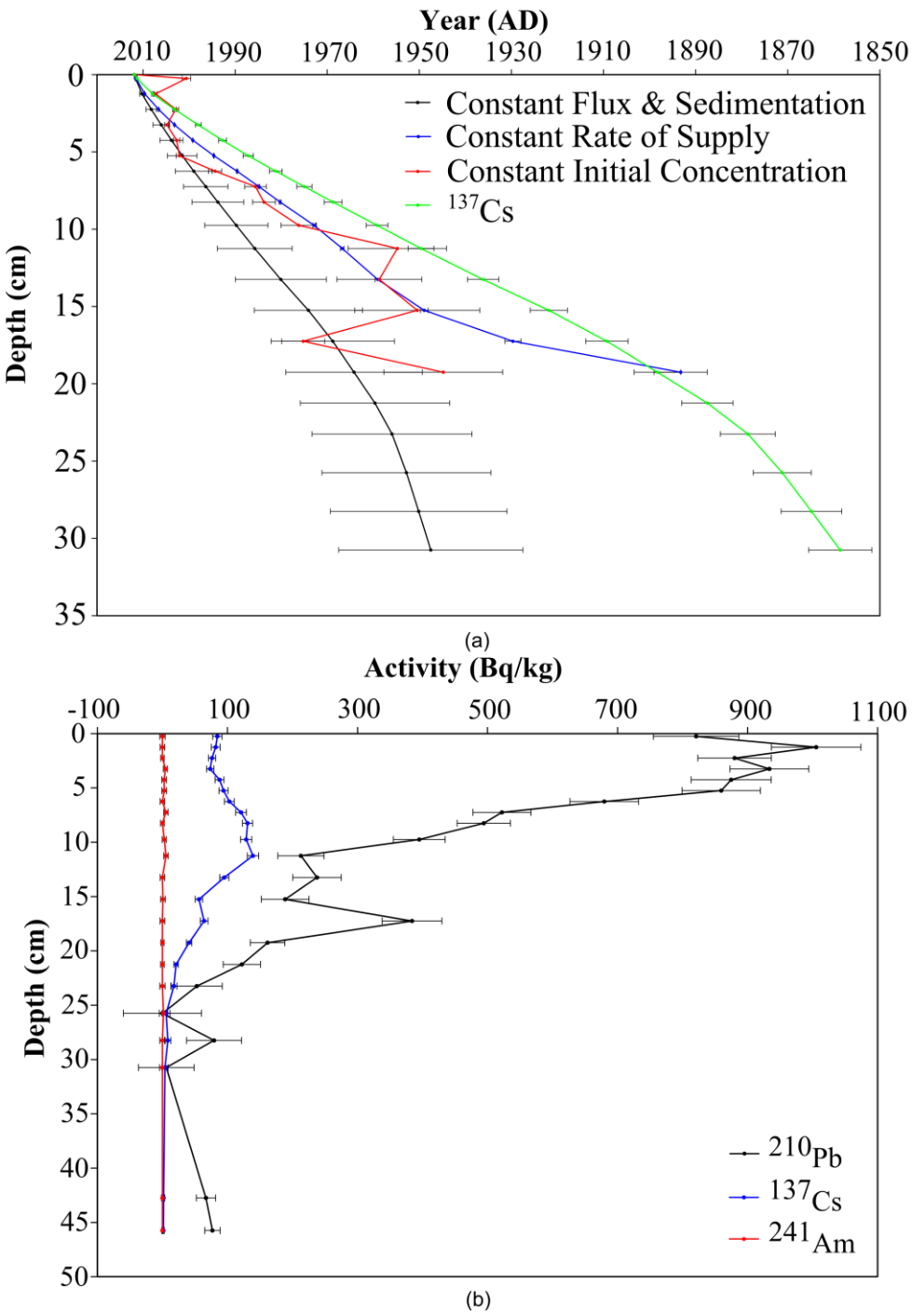

Figure 4.4 (a) Age-depth relationships for the four ^{210}Pb dating models. (b) Activities of ^{210}Pb, ^{137}Cs and ^{241}Am measured for core BL–G11–02.

Table 4.2 Summary table of the radioisotope dates obtained by CF/CS, CRS, CIC, and ^{137}Cs models by depth for core BL–G11–02.

Midpoint Depth	Constant Flux & Sedimentation			Constant Rate of Supply			Constant Initial Concentration			^{137}Cs		
[cm]	Age [y]	Year [y]	Error [y]	Age [y]	Year [y]	Error [y]	Age [y]	Year [y]	Error [y]	Age [y]	Year [y]	Error [y]
0	0	2011.87	0	0	2011.87	0	0	2011.87	0	0	2011.87	0
0.25	0.2404	2011.63	0.0747	0.3396	2011.53	0.0028	11.2806	2000.59	0.9302	0.5725	2011.30	0.0256
1.25	1.6425	2010.23	0.5103	2.2291	2009.64	0.0185	4.6111	2007.26	0.3234	3.9119	2007.96	0.1752
2.25	3.6541	2008.22	1.1353	5.2517	2006.62	0.0245	8.9893	2002.88	0.5945	8.7028	2003.17	0.3897
3.25	5.8176	2006.05	1.8074	8.7067	2003.16	0.0222	7.0501	2004.82	0.4707	13.8557	1998.01	0.6204
4.25	8.0338	2003.84	2.4960	12.6665	1999.20	0.0265	9.1856	2002.69	0.6650	19.1337	1992.74	0.8567
5.25	10.3794	2001.49	3.2247	17.2524	1994.62	0.0636	9.7671	2002.1	0.7055	24.7202	1987.15	1.1069
6.25	12.8929	1998.98	4.0056	22.3028	1989.57	0.1065	17.5201	1994.35	1.4113	30.7066	1981.16	1.3749
7.25	15.4994	1996.37	4.8154	27.0276	1984.84	0.1515	26.2915	1985.58	2.3542	36.9142	1974.96	1.6529
8.25	18.1200	1993.75	5.6296	31.6440	1980.23	0.2015	28.1320	1983.74	2.4564	43.1556	1968.71	1.9324
9.75	22.1265	1989.74	6.8743	39.0327	1972.84	0.2992	35.6839	1976.19	3.8283	52.6978	1959.17	2.3596
11.25	26.1337	1985.74	8.1193	45.1279	1966.74	0.3983	57.0952	1954.78	10.6786	62.2416	1949.63	2.7870
13.25	31.7970	1980.07	9.8788	52.8340	1959.04	0.5628	53.1950	1958.68	9.2253	75.7297	1936.14	3.3909
15.25	37.7885	1974.08	11.7402	62.9377	1948.93	0.8503	61.4212	1950.45	13.5696	89.9993	1921.87	4.0299
17.25	43.0838	1968.79	13.3854	82.1893	1929.68	1.7384	36.6536	1975.22	4.6732	102.6109	1909.26	4.5946
19.25	47.6940	1964.18	14.8177	118.6290	1893.24	5.7728	67.0696	1944.8	12.9058	113.5910	1898.28	5.0862
21.25	52.2417	1959.63	16.2306	N/A	N/A	N/A	N/A	N/A	N/A	124.4220	1887.45	5.5712
23.25	55.9337	1955.94	17.3777	N/A	N/A	N/A	N/A	N/A	N/A	133.2151	1878.66	5.9649
25.75	59.0697	1952.80	18.3520	N/A	N/A	N/A	N/A	N/A	N/A	140.6840	1871.19	6.2994
28.25	61.7290	1950.14	19.1782	N/A	N/A	N/A	N/A	N/A	N/A	147.0175	1864.85	6.5830
30.75	64.3529	1947.52	19.9934	N/A	N/A	N/A	N/A	N/A	N/A	153.2669	1858.60	6.8628

Table 4.3 Activities of ^{210}Pb, ^{137}Cs and ^{241}Am with depth for core BL–G11–02.

Cumulative Dry Mass	Midpoint Depth	^{210}Pb Activity	^{210}Pb (error)	^{137}Cs Activity	^{137}Cs (error)	^{241}Am Activity	^{241}Am (error)
[g/cm^2]	[cm]	[Bq/kg]	[Bq/kg]	[Bq/kg]	[Bq/kg]	[Bq/kg]	[Bq/kg]
0.0079	0.25	820.82	65.76	84.41	7.04	0	4.11
0.0539	1.25	1005.47	68.85	81.87	6.63	0	3.41
0.1199	2.25	879.98	56.57	76.25	5.63	0	2.68
0.1908	3.25	933.46	60.70	73.43	5.63	4.52	3.12
0.2635	4.25	874.74	61.60	87.82	6.74	2.60	3.53
0.3405	5.25	859.42	60.35	93.93	7.04	2.70	3.55
0.4229	6.25	679.55	52.80	102.80	7.56	0	3.41
0.5084	7.25	522.12	44.58	120.83	8.27	5.21	3.33
0.5944	8.25	494.20	41.00	130.89	7.78	0	2.87
0.7258	9.75	395.00	39.80	128.77	8.69	2.85	3.18
0.8572	11.25	212.94	35.54	139.22	8.70	5.42	3.44
1.0430	13.25	237.74	37.25	95.06	7.03	0	3.40
1.2395	15.25	188.73	36.72	56.09	5.71	0.82	3.54
1.4132	17.25	383.88	45.99	64.10	5.91	0	3.64
1.5645	19.25	161.66	26.59	40.98	4.04	0	2.49
1.7136	21.25	122.09	28.66	21.01	3.40	0	2.78
1.8347	23.25	52.75	39.24	17.66	4.69	0	4.04
1.9376	25.75	0	60.05	5.72	5.99	1.63	6.37
2.0248	28.25	79.39	42.24	8.21	4.82	0	4.11
2.1109	30.75	5.83	42.76	3.95	4.55	0	4.39
5.7012	42.75	66.91	14.84	1.71	1.71	0	1.45
6.4052	45.75	76.86	11.82	1.43	1.35	0	1.17

Table 4.4 AMS ^{14}C date for Barry Lake organic matter (*Najas Flexilis* and wood fragments) at 34.5 to 35.5 cm in core BL–G11–02.

Sample ID	Measured Radiocarbon Date	δ^{13}C	Conventional Radiocarbon Age*
Beta-408561	880 ±30 BP	–25.3‰	880 ±30 BP
	**Cal AD 1045 to 1095 (Cal BP 905 o 855) and Cal AD 1120 to 1220 (Cal BP 830 to 730)		

*Dates are reported as RCYBP (radiocarbon years before present, "present"= AD 1950). By international convention, the modern reference standard was 95 % the ^{14}C activity of the National Institute of Standards and Technology (NIST) Oxalic Acid (SRM 4990C) and calculated using the Libby ^{14}C half–life (5568 years). Quoted errors represent 1 relative standard deviation statistics (68 % probability) counting errors based on the combined measurements of the sample, background, and modern reference standards. Measured ^{13}C/^{12}C ratios (δ^{13}C) were calculated relative to the PDB-1 standard. The Conventional Radiocarbon Age represents the Measured Radiocarbon Age corrected for isotopic fractionation, calculated using the δ^{13}C.

** 2σ calibration

4.2 Modern Water Parameters and Isotopic Compositions

Modern water samples were collected in spring (May 12th), summer (July 14th) and fall (November 3rd) 2014, and all the results are summarized in Appendix E.

4.2.1 Temperature

The temperature of Barry Lake water in spring drops from 15.3 ℃ in the top 3 m to 7.3 ℃ at 7.5 m (lake bottom) (Fig. 4.5a). The summer water temperature drops from 24.0 ℃ in the top 3 m to 13 ℃ at 7 m (lake bottom). During the fall, the lake temperature is constant at ~9 ℃ from the surface to 6.5 m and then increases to 9.7 ℃ at 7.5 m (lake bottom).

4.2.2 Dissolved Oxygen

In spring, the dissolved oxygen (DO) increases from 10.28 mg/L at the surface to 14.40 mg/L at 4.5 m, and then decreases to 1.10 mg/L at 7.5 m (lake bottom) (Fig. 4.5b). During summer, DO decreases from 7.71 mg/L at 0 to 3.5 m to 0.6 mg/L from 4.5 m to 7 m (lake bottom). DO during the fall decreases from 10.79 mg/L in the top 6 m to 0.83 mg/L from 6.5 m to 7.5 m (lake bottom).

4.2.3 pH

The pH of Barry Lake water during spring and fall 2014 is all above 7 (Fig. 4.5c). In spring, pH increases from 8.10 to 8.38 from surface to 5 m depth and then decreases to 7.31 at 7.5 m (lake bottom). During the fall, pH decreases from 8.04 (0 to 6 m) to 7.36 at lakebed (7.5 m).

4.2.4 Specific Conductivity

The specific conductivity (SC) in spring decreases from 242.4 μS/cm in the top 3 m to 206.1 μS/cm at 5 m and then increases to 220.0 μS/cm at the lake bottom (7.5 m) (Fig. 4.5d). During summer, SC increases from 252.6 μS/cm at the surface to 280.9 μS/cm at lake floor (7 m). In the fall, SC is constant at 183.8 μS/cm in the top 6 m and then increases to 194.3 μS/cm at the lake bottom (7.5 m).

4.2.5 δ^2H and δ^{18}O of Lake Water

The average δ^2H of modern Barry Lake water is –62 ±1 ‰ (SD; n=10), –60 ±2 ‰ (SD; n=11), and –55 ±1 ‰ (SD; n=11) in spring, summer and fall, respectively. The average δ^{18}O of modern Barry Lake water is –8.4 ±0.1 ‰ (SD, n=10), –7.8 ±0.3 ‰ (SD; n=11) and –7.1 ±0.2 ‰ (SD; n=11) for the same sampling dates in spring, summer and fall, respectively (Fig. 4.6; Appendix F). During summer, the surface water δ^2H and δ^{18}O values are ~6 ‰ and ~0.6 ‰ higher than the bottom water, respectively, while during spring and fall, the lake water shows relatively uniform isotopic compositions with depth.

The Great Lakes Meteoric Water Line (GLMWL) (Longstaffe et al., 2014) is plotted together with the Barry Lake local surface water line (LSWL) in Figure 4.6. The slope of the Barry Lake LSWL (5.06) is shallower than the slope of the GLMWL (7.1).

4.2.6 $\delta^{13}C_{DIC}$ of Dissolved Inorganic Carbon

In spring and fall, the lakewater $\delta^{13}C_{DIC}$ remains relatively constant with depth and is –5.1 ‰ and –4.5 ‰, respectively. In summer, by comparison, the $\delta^{13}C_{DIC}$ decreases from –3.5 ‰ at the surface to ~4 m depth to –6.6 ‰ at the lake floor (6 m) (Fig. 4.7; Appendix F). The summer bottom water sample from station #2 was lost.

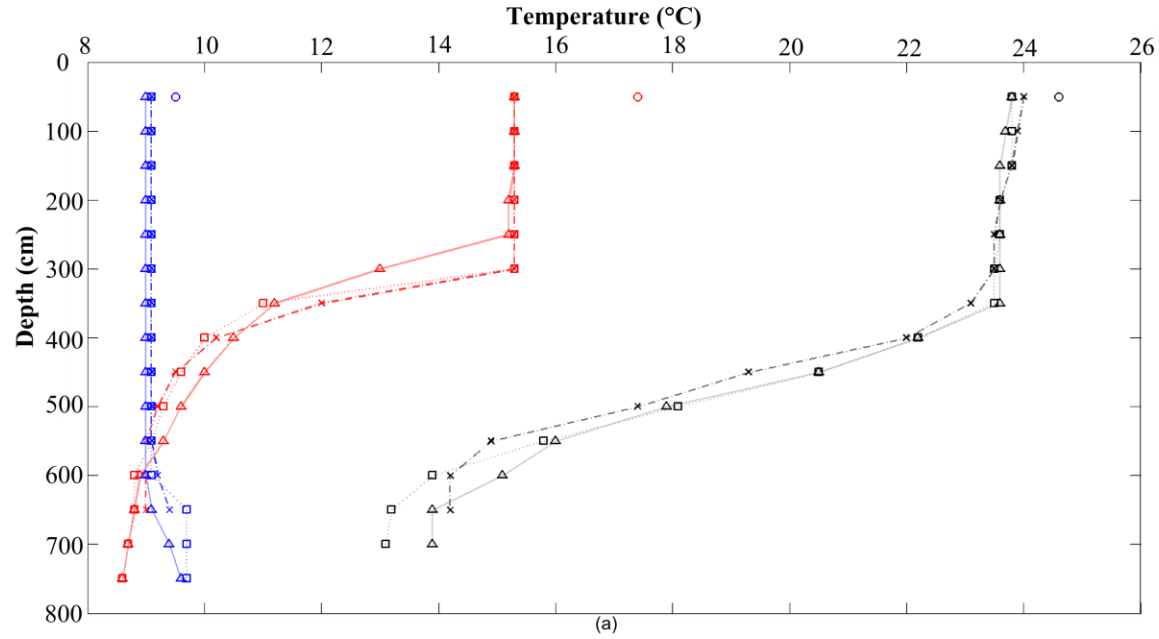
Temperature (°C)
8
10
12
14
16
18
20
22
24
26
Depth (cm)
0
100
200
300
400
500
600
700
800

(a)

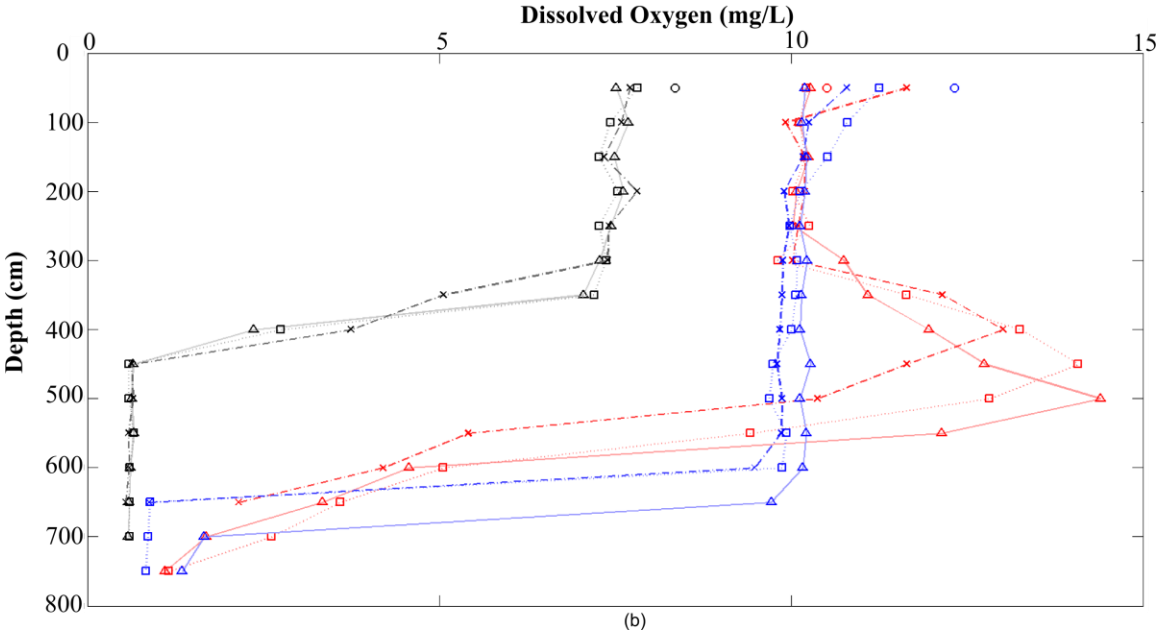
Dissolved Oxygen (mg/L)
0
5
10
15
Depth (cm)
0
100
200
300
400
500
600
700
800

(b)

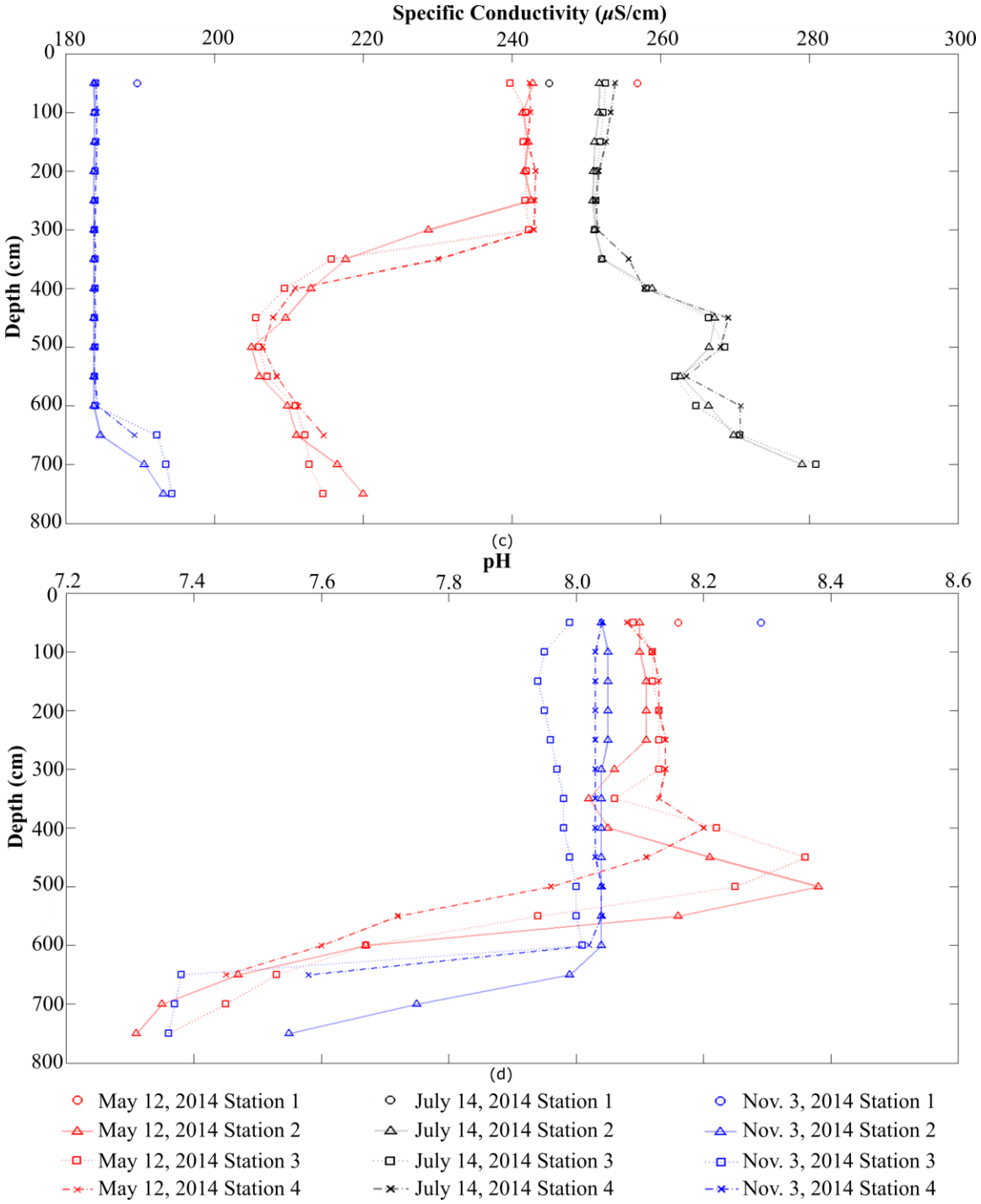

Figure 4.5 Physical property profiles for Barry Lake water: (a) Temperature. (b) Dissolved oxygen. (c) pH. (d) Specific conductivity (station locations in Fig. 3.2).

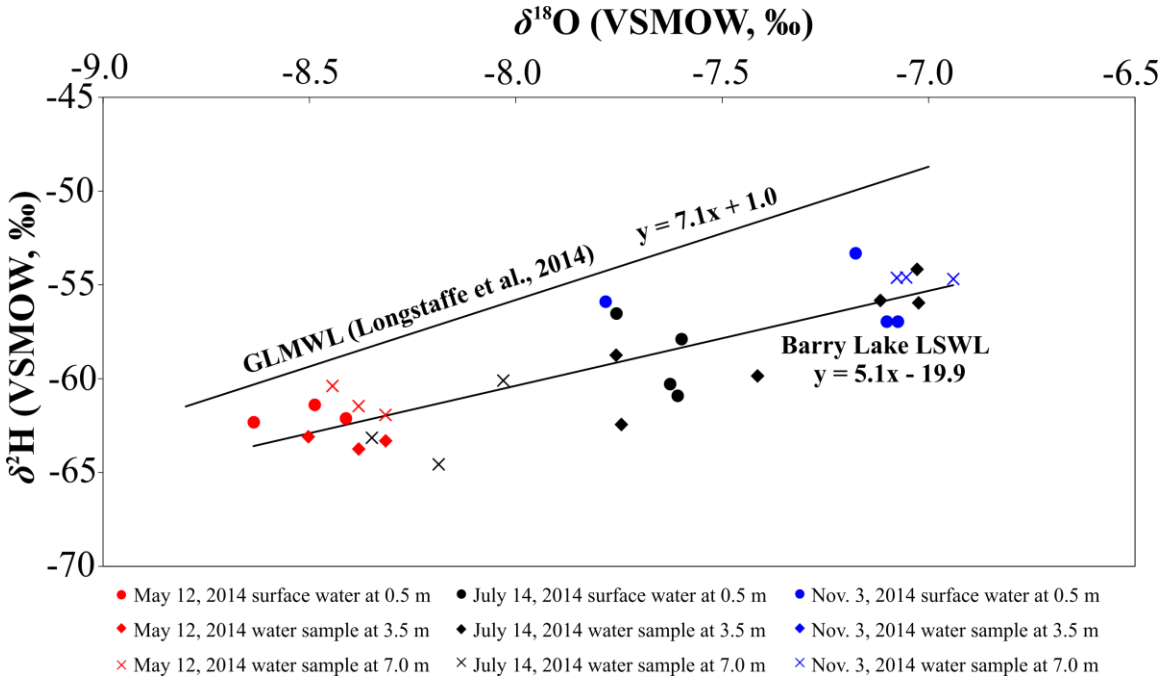

Figure 4.6 δ^2H and δ^{18}O of Barry Lake water during spring, summer and fall 2014, as sampled on May 12, July 14 and November 3, 2014, respectively. LSWL: Local Surface Water Line; GLMWL: Great Lake Meteoric Water Line (Longstaffe et al., 2014).

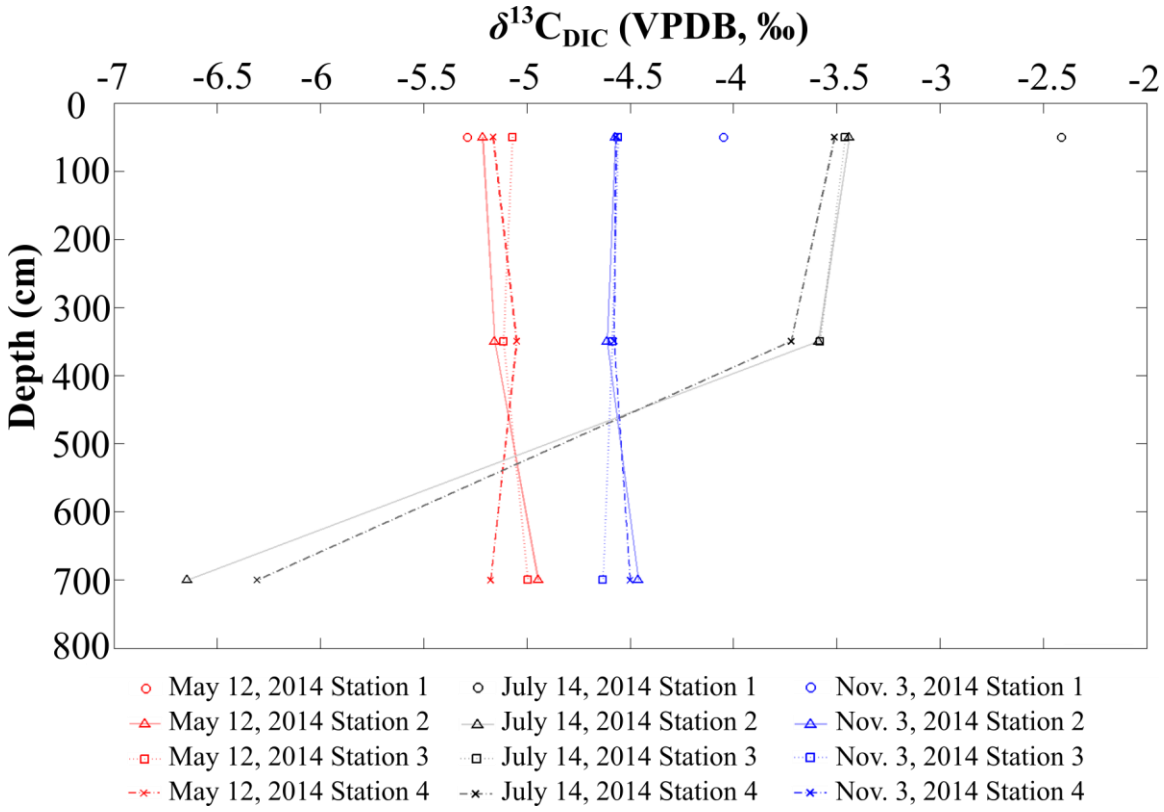

Figure 4.7 $\delta^{13}C_{DIC}$ in Barry Lake water during spring (May 12), summer (July 14), and fall (November 3) 2014 (station locations given in Fig. 3.2).

4.3 Scanning Electron Microscopy (SEM)

SEM photomicrographs and associated energy-dispersive spectra (EDS) also reveal that the sediment consists mostly of SiO_2 (quartz) and $CaCO_3$ (calcite/aragonite) with abundant diatoms present in the top 20 cm of core BL–G11–01 (Fig. 4.8). The spheroidal form of FeS_2 at the 7–7.5 cm interval in Figure 4.8a is a pyrite framboid, whose formation may be related to microbial processes (Rickard, 1970). In general, calcium carbonate crystals preserved in sediments have a rhombohedral/diamond shape (Figs. 4.8c, d, f), which is a typical calcite morphology. The calcite grains appear to be attached to other materials, which could be remnants of phytoplankton such as algae (Stabel, 1986) and/or cyanobacteria (Merz, 1992). Since aragonite shell fragments were removed by hand-picking prior to SEM analysis, the needle-shaped $CaCO_3$ in Figure 4.8e is likely needle-fiber calcite, formed by precipitation in the water column (Verrecchia and

Verrecchia, 1994). Quartz grains (SiO_2) (Fig. 4.8b) are rounded, typical of a detrital origin.

4.4 Biogenic Carbonate

4.4.1 Species Identification

Three modern lung-breathing gastropods have been identified at Barry Lake: *Helisoma anceps* (Fig. 4.9a), *Planorbella companulatum* (Fig. 4.9b), and *Lymnaea stagnalis* (Fig. 4.9c). Gastropod species identified in the gravity core sediments are: *H. anceps* (Fig. 4.10a), *P. companulatum* (Fig. 4.10b), *Hydrobiidae* (genus only) (Fig. 4.10c) and *Physidae* (genus only) (Fig. 4.10d). One bivalve genus, *Pisidium* (Fig 4.10e), has also been identified in the gravity core sediments.

Of the shelly fossils from the sediments, only *H. anceps* and *Pisidium* were analyzed for isotopic compositions because they are the two most abundant species throughout the core. *H. anceps*, which have a typical lifespan of one to two years, are periphyton and are mainly found attached to vegetation and rocks. Similar to other freshwater snails, *H. anceps* can migrate to deeper water during the fall to obtain food and return to the littoral zone in the spring (Wood et al., 2010). *Pisidium* (1-4 years lifespan) are infaunal or epifaunal filter feeders (Apolinarska and Hammarlund, 2009) and are active from late May to early November (Holopainen and Hanski, 1986; Kilgour and Mackie, 1991; Killeen et al., 2004).

4.4.2 Stable Isotopic Compositions of Shell Aragontie

4.4.2.1 Modern Shells

The average $\delta^{13}C$ of the modern gastropods is –3.5±0.5 ‰ (SD; n=5) for *H. anceps*, –4.3±0.6 ‰ (SD; n=4) for *P. campanulatum*, and –4.8±0.9 ‰ (SD; n=5) for *L. stagnalis* (Fig. 4.11; Appendix G). The average $\delta^{18}O$ of the modern gastropods is +23.1±0.6 ‰ (SD; n=5), +23.8±0.3 ‰ (SD; n=4) and +22.5±0.1 ‰ (SD; n=5) for *H. anceps*, *P. campanulatum* and *L. stagnalis*, respectively (Fig. 4.11; Appendix G).

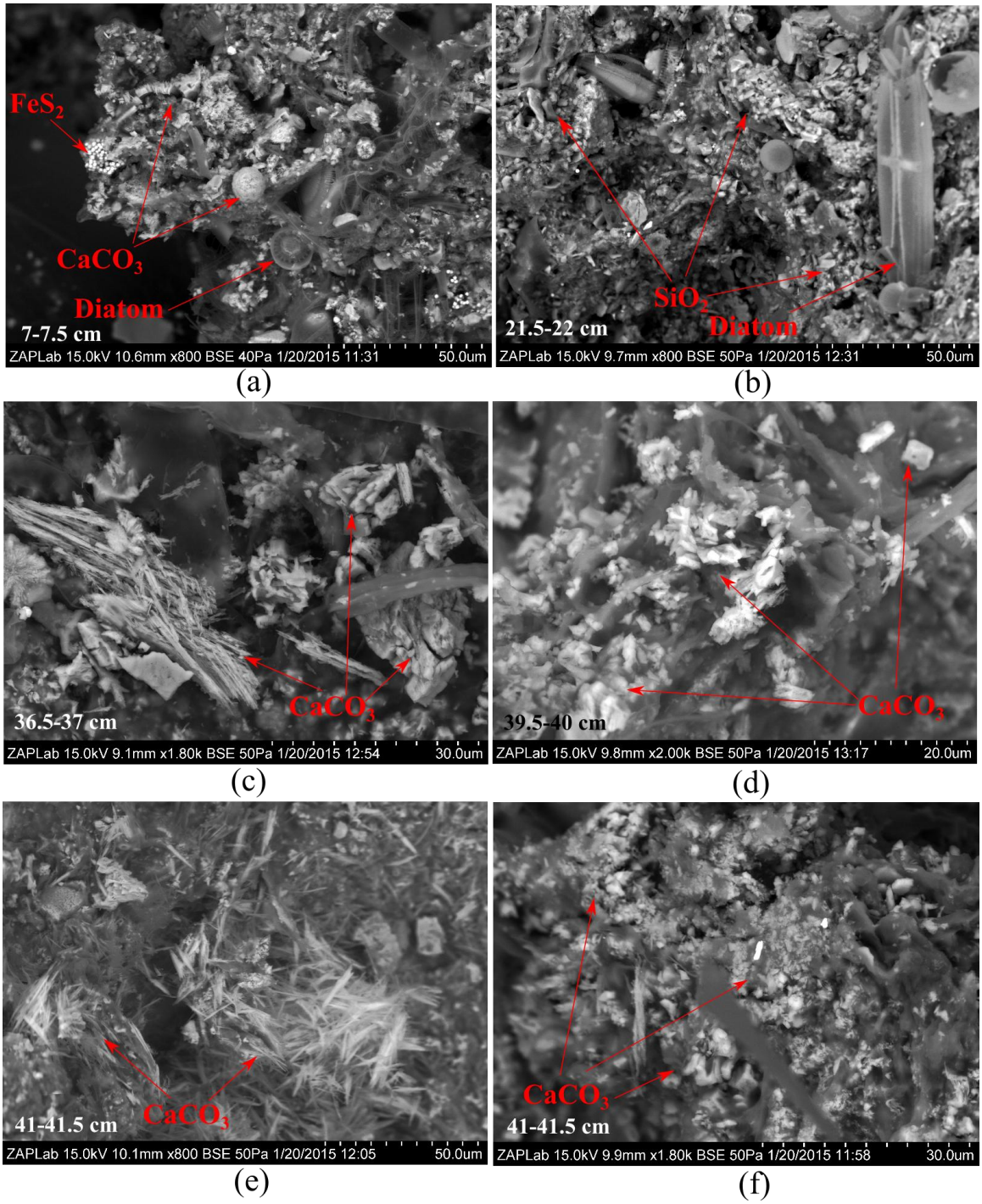

Figure 4.8 SEM Photomicrographs of Barry Lake sediment in core BL–G11–01: (a) 7–7.5 cm; note $CaCO_3$ (calcite), FeS_2 (pyrite framboid) and diatom. (b) 21.5–22 cm; note SiO_2 (quartz), (c) 36.5–37 cm; note $CaCO_3$ (calcite). (d) 19.5–40 cm; note $CaCO_3$ (calcite). (e) 41–41.5 cm; note needle–fiber shaped calcite ($CaCO_3$). (f) 41–41.5 cm; note $CaCO_3$ (calcite).

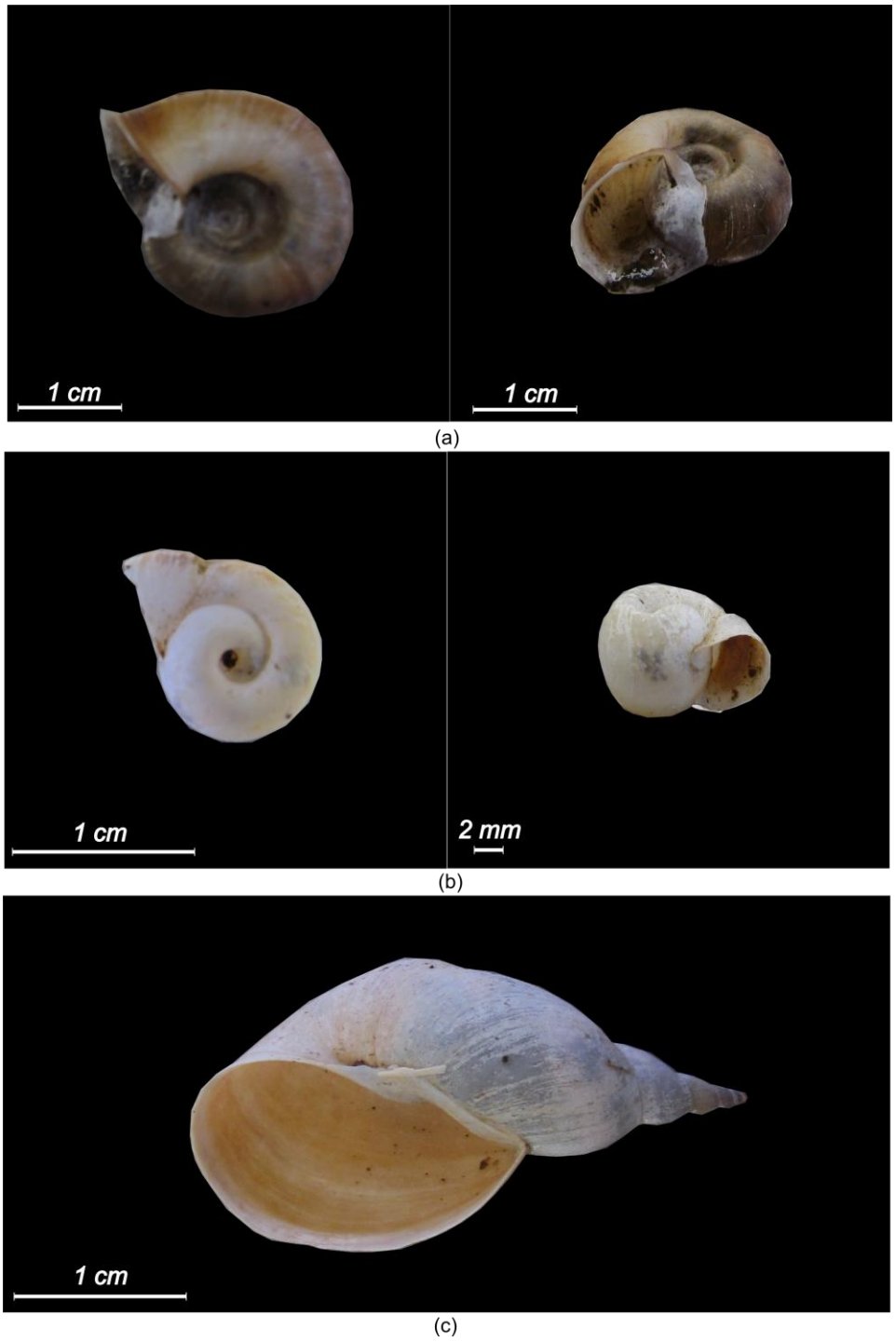

Figure 4.9 Modern gastropods species identified at Barry Lake: (a) *Helisoma anceps*. (b) *Planorbella companulatum*. (c) *Lymnaea stagnalis*.

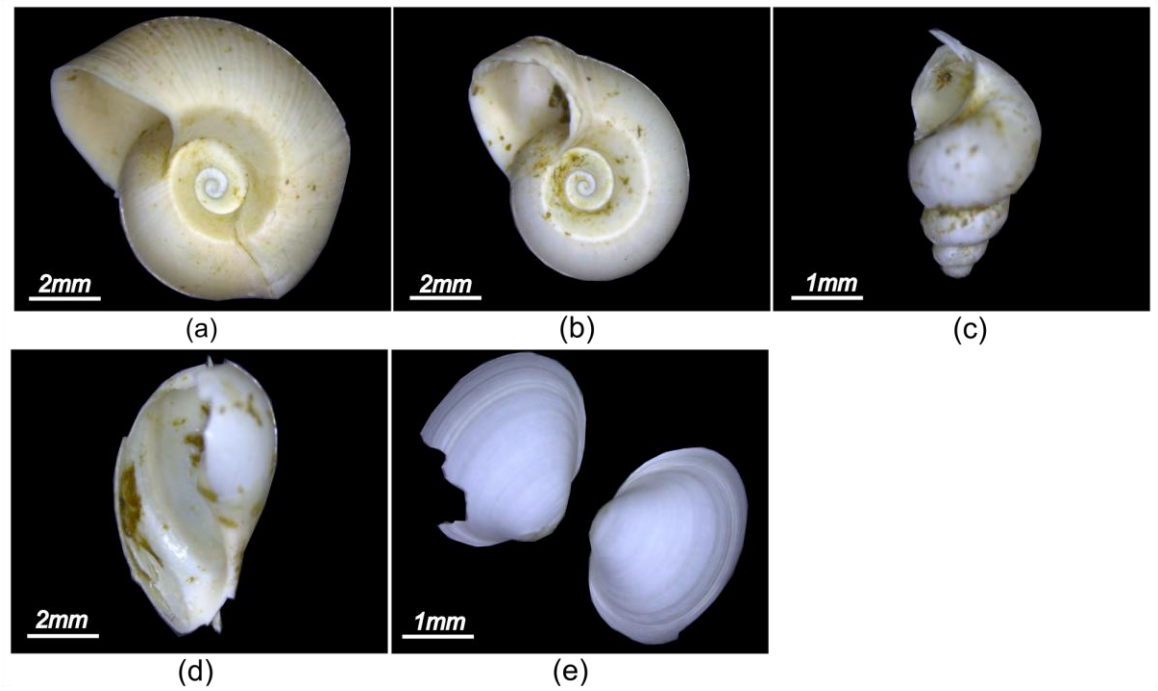

Figure 4.10 Ancient molluscs identified in Barry Lake sediment cores: (a) *Helisoma anceps*. (b) *Planorbella companulatum*. (c) *Hydrobiidae*. (d) *Physidae*. (e) *Pisidium*.

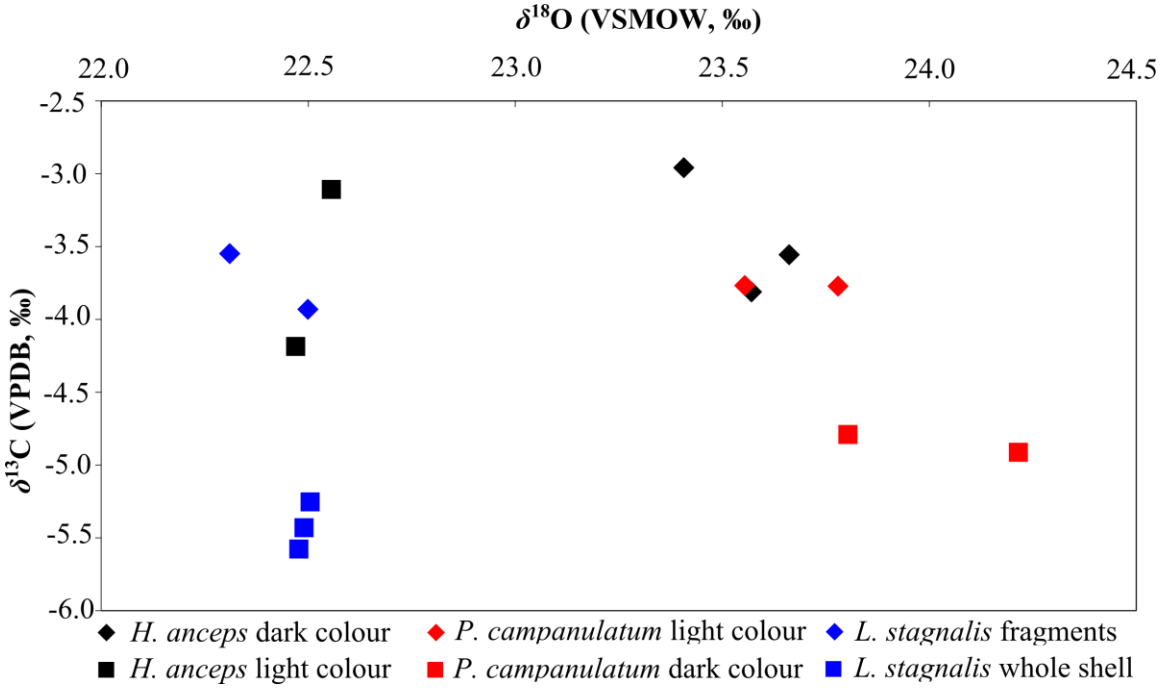

Figure 4.11 $\delta^{13}C$ and $\delta^{18}O$ of modern *Helisoma anceps* (black), *Planorbella campanulatum* (red) and *Lymnaea stagnalis* (blue). Dark colour means the colour of the shell overall is dark; light colour means the colour of the shell overall is light.

4.4.2.2 Ancient Shells

The preservation of aragonite in the ancient shells indicates that recrystallization to calcite has not occurred, and strongly suggests that these shells have retained their original isotopic compositions (Abell, 1985). The average $\delta^{13}C$ of shells sampled from core BL–G11–01 is –2.1 ±1.3 ‰ (SD; n=43) for *H. anceps* and –1.0 ±1.4 ‰ (SD; n=34) for *Pisidium* (Fig. 4.12a; Appendix H). The average $\delta^{18}O$ of *H. anceps* and *Pisidium* is +23.4 ±0.8 ‰ (SD; n=43) and +23.8 ±1.1 ‰ (SD; n=34), respectively. Error bars indicate the variation in $\delta^{13}C$ and $\delta^{18}O$ among different shells preserved in the same interval.

4.5 Isotopic Compositions of Calcite

In general, there is a strong positive covariance (R^2=0.71) between $\delta^{18}O_{calcite}$ and $\delta^{13}C_{calcite}$ throughout core BL–G11–01 (Figs. 4.13, 4.14; Appendix I). This behavior is common for closed-basin lakes in which the calcite is of authigenic rather than detrital origin (Talbot, 1990; Li and Ku, 1997).

Large fluctuations in $\delta^{13}C_{calcite}$ and $\delta^{18}O_{calcite}$ occur throughout the core (Figs. 4.13a, b). The $\delta^{13}C_{calcite}$ is constant around +2 ‰ from 41.5 to 38.5 cm followed by an increase to +3.5 ‰ at 37.5 cm. Around the same depth, the $\delta^{18}O_{calcite}$ shows a 1 ‰ increase from +23 to +24 ‰ from 38.5 to 37 cm. The $\delta^{13}C_{calcite}$ then decreases to +0.3 ‰ at 36 cm and keeps gradually decreasing to ~–0.1 ‰ at 30 cm before spiking to +4.1 ‰ at 27 cm. Similarly, the $\delta^{18}O_{calcite}$ keeps decreasing to ~+22 ‰ before reaching +23.6 ‰ at 28.5 cm. A ~2 ‰ decrease follows the $\delta^{13}C_{calcite}$ spike before reaching its maximum of +5.1 ‰ at 25 cm. Above 25 cm, the $\delta^{13}C_{calcite}$ sharply decreases to –1.0 ‰ and gradually increases to ~–0.2 ‰ to the top. The $\delta^{18}O_{calcite}$ sharply decreases to +20.5 ‰ at 21 cm and then gradually increases to +21.3 ‰ near the top of the core.

4.6 Bulk Organic Matter (OM)

4.6.1 Total Organic Carbon (TOC), Total Nitrogen (TN) and C/N ratio

The curves of TOC and TN show similar depth-dependent variations (Figs. 4.15a, b; Appendix J). Both show large fluctuations between 25 and 41.5 cm with particularly high values at 41, 30 and 25 cm, interspersed with declines to minima at 38 and 27 cm. Above

25 cm, both TOC and TN decrease sharply to minimal values at 15 cm and then gradually increase to the top of the core. C/N ratios vary between 7 and 11 throughout the core. In general, the C/N ratios gradually increase from both the bottom and top of the core to maxima of 11 and 10.3 at 30.5 and 25.5 cm, respectively (Fig. 4.15c; Appendix J).

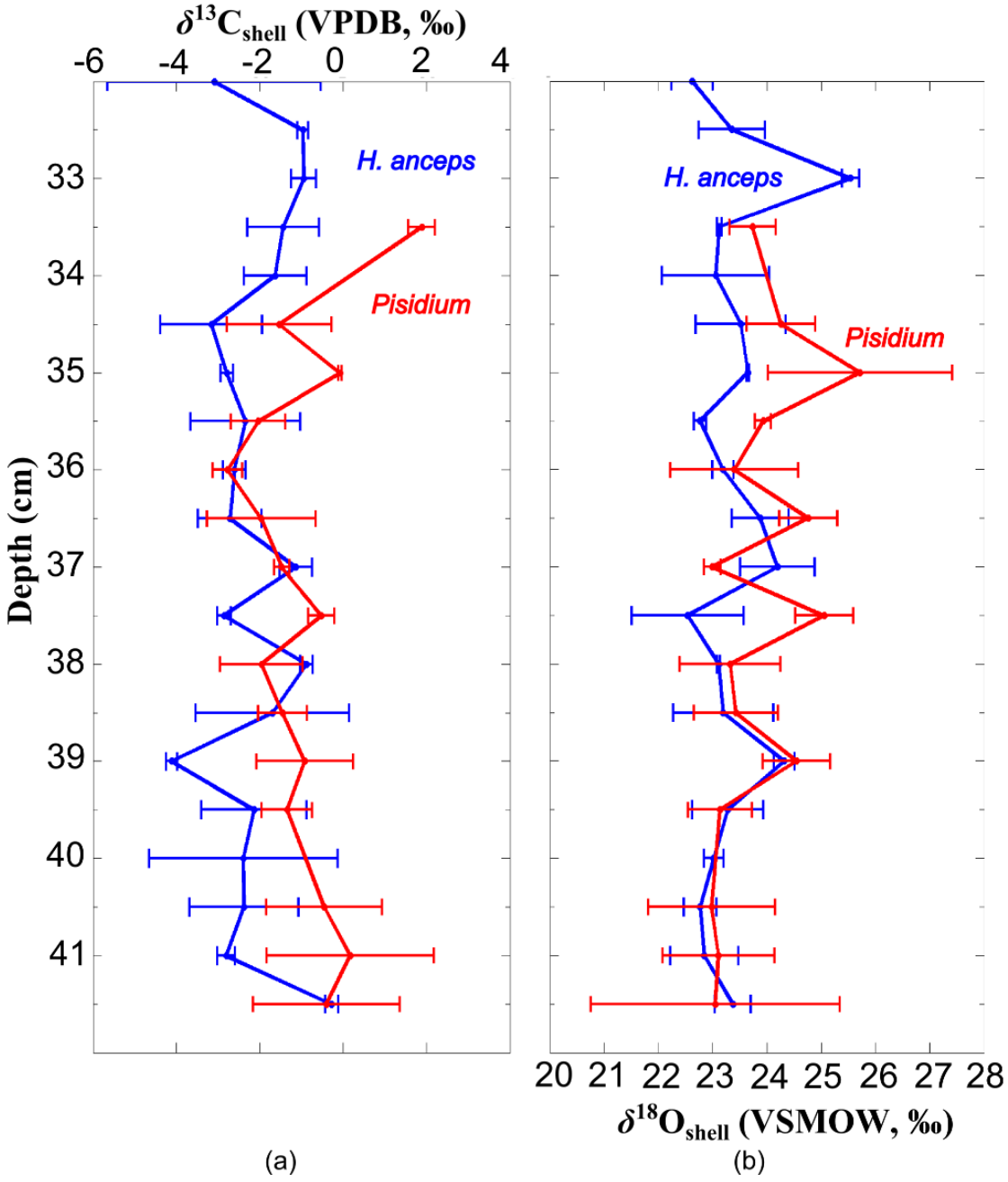

Figure 4.12 Depth versus stable isotopic composition of biogenic shell aragonite from core BL–G11–01: (a) δ^{13}C of ancient *H. anceps* (blue) and *Pisidium* (red). (b) δ^{18}O of *H.*

anceps (blue) and *Pisidium* (red). Error bars show the variations in isotopic compositions of multiple specimens from the same depth interval.

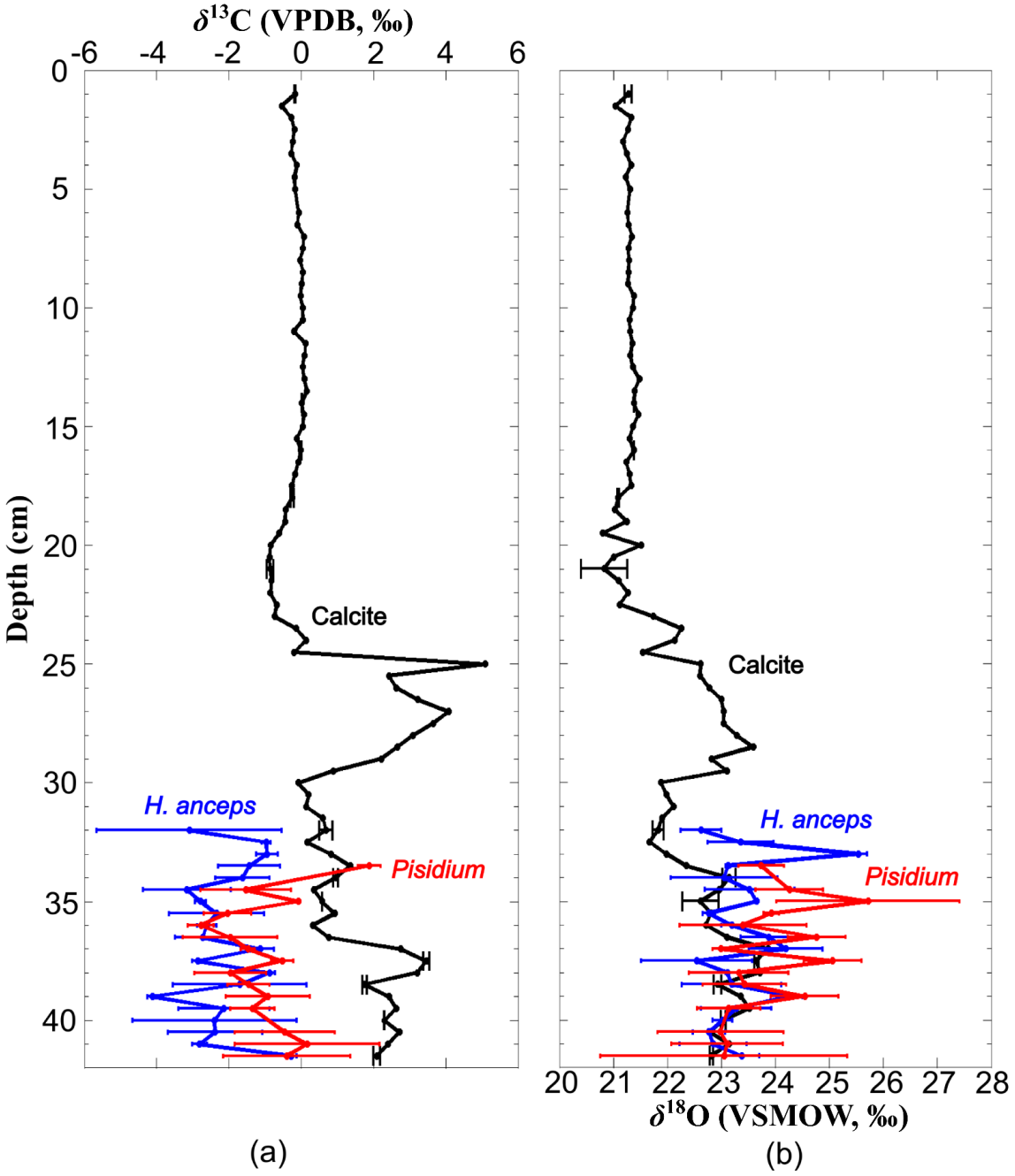

Figure 4.13 Depth (cm) versus: (a) $\delta^{13}C_{calcite}$ and $\delta^{13}C_{aragonite}$. (b) $\delta^{18}O_{calcite}$ and $\delta^{18}O_{aragonite}$ both for core BL–G11–01.

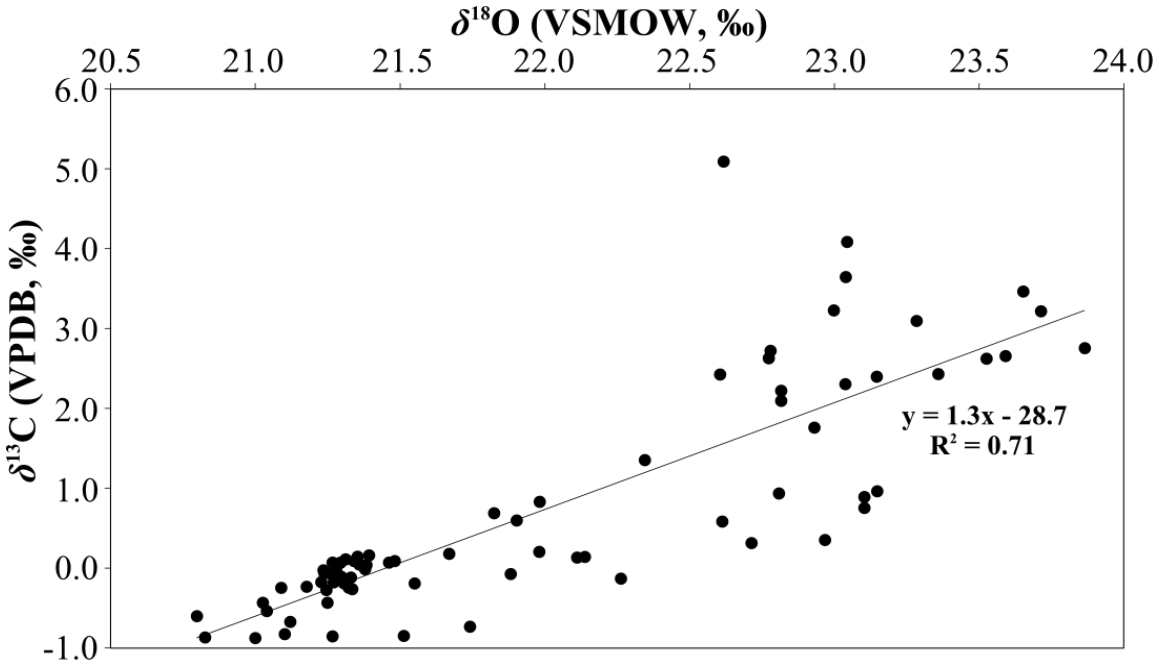

Figure 4.14 $\delta^{13}C_{calcite}$ versus $\delta^{18}O_{calcite}$ with R^2=0.71.

4.6.2 Organic Carbon and Nitrogen Mass Accumulation Rates

The C-MARs and N-MARs (Figs. 4.15d, e; Appendix J) show similar patterns to each other, as was the case for TOC and TN. The C-MARs and N-MARs display relatively constant low values ~2 and ~0.2 mg/cm^2/y, respectively in the bottom 20 cm. Both C-MARs and N-MARs increase sharply from 20 to 10 cm, having maxima of 9.95 and 1.41 mg/cm^2/y at 10.5 cm, respectively. Both of them then gradually decrease before reaching high values 9.71 and 1.31 mg/cm^2/y at 2 cm, respectively.

4.6.3 Isotopic Compositions of OM

The modern $\delta^{13}C_{OM}$ (after AD 1850) has been corrected for the Suess effect (gray curve in Fig. 4.15f), and the original $\delta^{13}C_{OM}$ is shown in black in Figure 4.15f. The correction was based on the dates provided by the CRS ^{210}Pb model (Table 4.2) and Equation 2.12.

At the bottom 15 cm of the core BL–G11–01, the $\delta^{13}C_{OM}$ generally remains at high values but shows at least four cycles of significant fluctuation from higher to lower to higher values. At 25 cm, the $\delta^{13}C_{OM}$ shows a sharp decrease from –26.4 to –31.0 ‰ at 22.5 cm. Values of Suess-corrected $\delta^{13}C_{OM}$ increase from –31.0 to –28.7 ‰ to the top of

core (Fig. 4.15f; Appendix J). The most distinct feature of the $\delta^{15}N_{TN}$ record is the sharp upward increase that begins at 24.5 cm (Fig. 4.15g; Appendix J). Below this depth, $\delta^{15}N_{TN}$ gradually increases from –1.9 ‰ to –1.4 ‰ from 41.5 to 24.5 cm (Fig. 4.15g). Above 24.5 cm, $\delta^{15}N_{TN}$ first increases to +1.5 ‰ at 15 cm and then gradually decreases to ~+0.5 ‰ at 4 cm (Fig. 4.15g).

4.7 Historical Climate Records

Temperature and precipitation records in the vicinity of Barry Lake show similar patterns and correlate well among the 7 stations surveyed (see Chapter 1, Fig. 1.3). Temperatures in the vicinity of Barry Lake, Ontario have been relatively stable since AD 1866. Average summer (June to August) and annual temperatures since AD 1866 are 19.1±1.0 ℃ and 6.4±0.9 ℃, respectively (Figs. 1.4a, 1.5a; 4.16a, b; Appendix K). The highest mean summer temperature 21.8 ℃ was recorded in AD 1937 at the Peterborough station, and the lowest mean summer temperature of 15.9 ℃ was recorded in AD 1992 at the Peterborough Airport station. The highest mean annual temperature was 8.9 ℃ recorded in AD 1998 at the Trent University station, and the lowest mean annual temperature was 3.9 ℃ recorded in AD 1904 at the Peterborough station.

Precipitation amounts in southeastern Ontario have not varied in a systematic fashion since AD 1866, but there has been a slight increase over the past 10 to 20 years (Figs. 1.4b, 1.5b, 4.16c, d; Appendix K). The average summer precipitation amount from AD 1866 to 2011 is 279±55 mm with Trent University station recording the highest summer precipitation amount (542 mm) in AD 2004, which accompanied the Great Flood in July 2004 that affected the City of Peterborough. The average amount of annual precipitation is 797±115 mm, with Trent University station recording the highest amount of 1062 mm in AD 2008 (Figs. 1.4b, 1.5b).

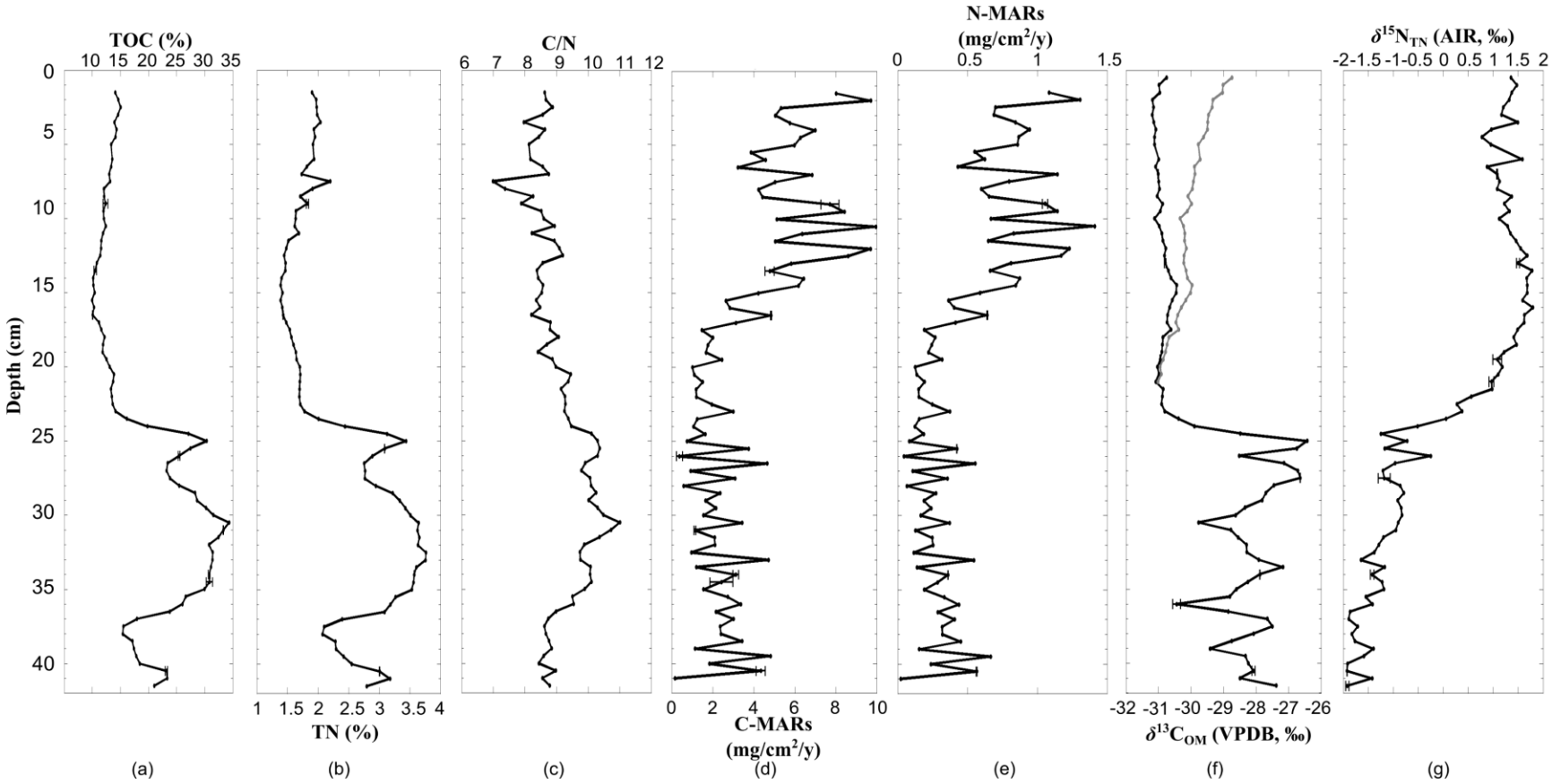

Figure 4.15 Depth versus: (a) Total organic carbon content. (b) Total nitrogen content. (c) C/N. (d) Organic carbon mass accumulation rate (C-MARs). (e) Nitrogen mass accumulation rate (N-MARs). (f) $\delta^{13}C_{OM}$. Measured $\delta^{13}C_{OM}$ is shown in black, and Suess-corrected $\delta^{13}C_{OM}$ (applied to years after 1850) is shown in gray. (g) $\delta^{15}N_{TN}$. All curves shown are for samples from core BL–G11–01.

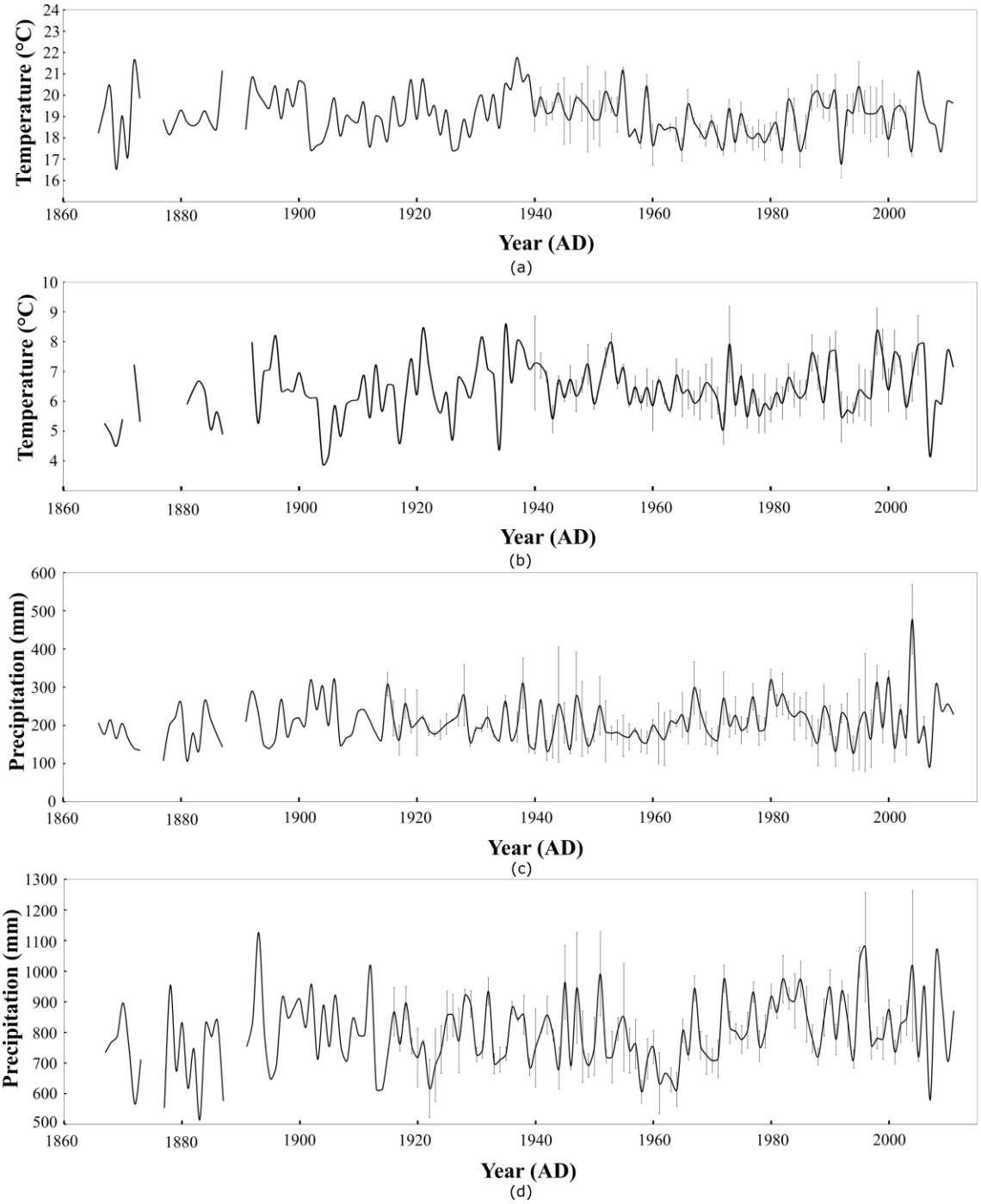

Figure 4.16 Average recorded temperature and precipitation of records (AD 1866 to 2011) for Environment Canada stations in the vicinity of Barry Lake (see Fig. 1.3 for station locations): (a) Average summer monthly (June to August) temperature. (b) Average annual temperature. (c) Total summer precipitation. (d) Total annual precipitation. Error bars indicate the range of variation in measurements recorded at the seven stations listed in Table 1.1.

Chapter 5

5 Discussion

In this chapter, the age-depth model used in this study is developed first, followed by discussion of modern Barry Lake conditions including the baseline for temperature, physical and chemical properties of lake water, as well as water and dissolved inorganic carbon (DIC) isotopic compositions of Barry Lake water. Next, the translations of stable isotopic compositions of shells and calcite to ancient lake water and DIC isotopic compositions are discussed. Finally, an interpretation is presented for climatic conditions, which combines all proxies used in this study including the stable isotopic compositions of calcite, shells, organic matter, ancient lake water and DIC, total organic matter (TOC) content, total nitrogen (TN) content, C/N ratios, organic carbon and nitrogen mass accumulation rates (C-MARs; N-MARs), magnetic susceptibility (MS), grain size and mineral abundances.

5.1 Age-depth Model

The two gravity cores (BL–G11–01 and BL–G11–02) are spatially close (likely within 1 m radius) (Fig. 3.1) and can be correlated on the basis of MS (Fig 4.2). An age-depth model for these cores (Fig. 5.1) has been established using the Bayesian age-depth modeling program Bacon (Blaauw and Christén, 2011) by combining fifteen ^{210}Pb dates, one calibrated ^{14}C date and one land clearance date. The oldest datable ^{210}Pb horizon is AD 1893 at 19 cm. Beyond this ^{210}Pb horizon, the age-depth model is constrained by the date of European land clearance (AD 1820; McAndrews, 1984). The maximum MS value at 21.5 cm (Fig. 4.2) in the cores is interpreted to indicate land clearance, which would have led to delivery of terrestrial magnetic minerals to the lake. The age-depth model is also constrained by a radiocarbon age (880±30 BP) at 35 cm. The radiocarbon date, however, is derived in part from the submerged aquatic plant *Najas flexilis*, and as such requires a hardwater effect (HWE) correction (Marty and Myrbo, 2014).

Several studies (Deevey et al., 1954; Hakansson, 1979; Olsson, 1983; Birks, 2002; Marty and Myrbo, 2014) document that radiocarbon dates derived from macrofossils of

submerged plants can be spuriously old, as these plants have the potential to have utilized DIC from old bedrock or surficial mineral matter, which can offset measured dates by hundreds or thousands of years. No HWE has been established previously for either Barry Lake or nearby lakes (e.g. Rice Lake), but there are HWE data for the Great Lakes (Table 5.1).

Table 5.1 Estimations of hardwater effect (HWE) for the Great Lakes.

Lakes	HWE (years)	References
Lake Michigan	250	Rea et al., (1994); Rea and Colman (1995); Moore et al., (1998)
Lake Nipissing	300	Terasmae (1979)
Georgian Bay	400	Rea et al., (1994); Rea and Colman (1995); Moore et al., (1998)
Lake Ontario	535±15	Anderson and Lewis (2012)
Lake Erie	825	Lewis et al., (2012)

As shown in Table 5.1, HWE ranges from 250 years in Lake Michigan to 825 years in Lake Erie. A HWE of 300 years, obtained from Terasmae (1979) has been applied in this study because (1) there should be a similar old carbon sources in Barry Lake and Lake Nipissing, given their identical underlying limestone bedrock and glacial till units (Ontario Geological Survey, 1991), and (2) there should be similar amount of old carbon in sediments derived from Paleozoic limestone and glacial deposits containing carbonate (Farrand and Miller, 1968; Terasmae, 1979).

All dates used in the age-depth model are summarized in Table 5.2. The Bacon software (Blaauw and Christén, 2011) was used to interpolate between dated horizons to assign ages to depths (Fig. 5.1).

Table 5.2 Age constraints and uncertainties for Barry Lake core BL–G11–02

Samples	Age (year before 1950)	Age (^{14}C year BP)	Error (y)	HWE (y)	Depth (cm)
surface	–62		1		0
lead1	–62		0.0028		0.25
lead2	–60		0.0185		1.25
lead3	–57		0.0245		2.25
lead4	–53		0.0222		3.25
lead5	–49		0.0265		4.25
lead6	–45		0.0636		5.25
lead7	–40		0.1065		6.25
lead8	–35		0.1515		7.25
lead9	–30		0.2015		8.25
lead10	–23		0.2992		9.75
lead11	–17		0.3983		11.25
lead12	–9		0.5628		13.25
lead13	1		0.8503		15.25
lead14	20		1.7384		17.25
lead15	57		5.7728		19.25
LandClear	130		5		21.5
radiocarbon		880	30	300	35

"lead(#)" are ^{210}Pb dates from the University of Ottawa; "LandClear" is the historical European settlement reported by McAndrews (1984), and "radiocarbon" is the radiocarbon date for *Najas flexilis* and wood fragments from Beta Analytic Inc. The radiocarbon date was calibrated using IntCal 13 (Reimer et al., 2013) and Bacon (for age-depth modeling). The errors reported for ^{210}Pb and radiocarbon dates are laboratory errors; the error on the land clearance date has been estimated. Additional Bacon settings include: t.a=33 for land clearance and 3 for others; t.b-34 for land clearance and 4 for others. All settings including t.a and t.b are described in Bacon 2.2 manual. Briefly, t.a and t.b are student-t parameters and set at 3 and 4 by default, respectively. More narrow error distributions (more closely resembling the normal distribution) can be assigned, for example, by setting t.a and t.b at 33 and 34, respectively.

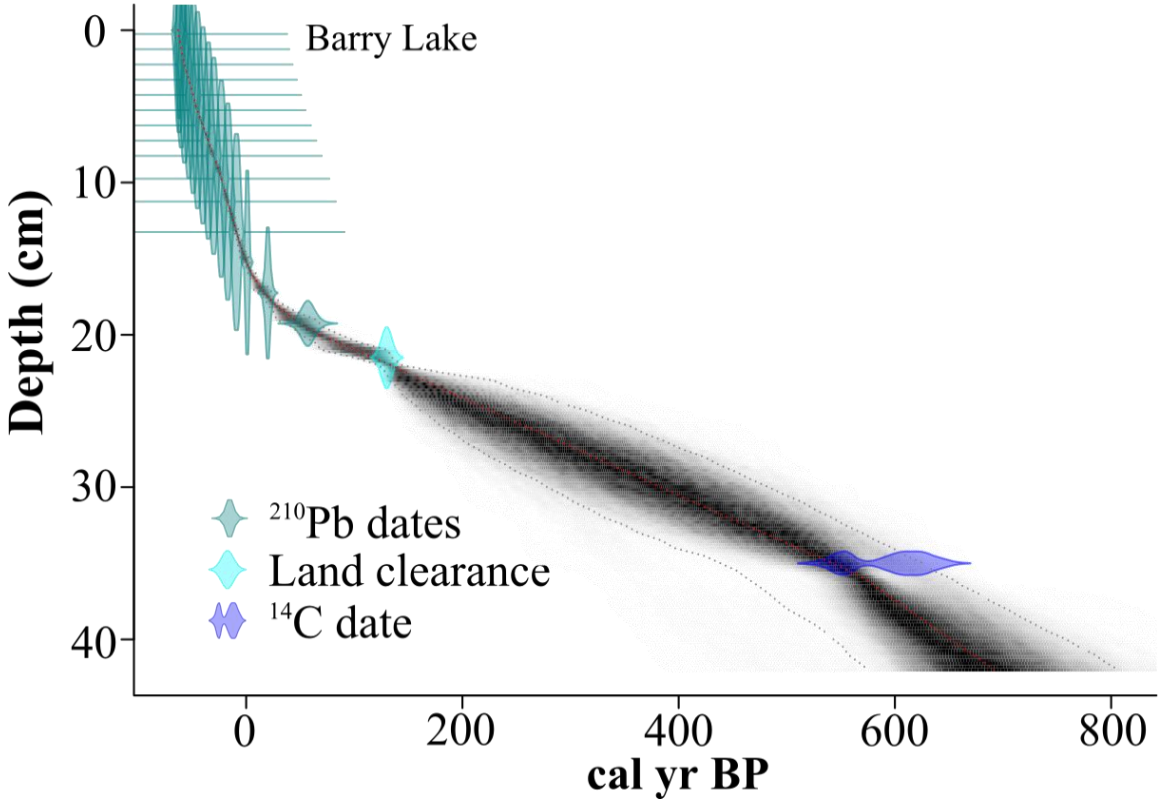

Figure 5.1 Bacon age-depth model (Blaauw and Christén, 2011) based on fifteen ^{210}Pb dates, one radiocarbon date, and one land clearance date. The 95 % confidence intervals are shown by gray dots and the possible distribution is shown in gray shading. The dense shading indicates the most likely age.

5.2 Modern Barry Lake

Modern Barry Lake is a clear (5 m Secchi depth) holomictic lake (i.e. completely mixes at least once during the year). During the period of our measurements, it was stratified from May to July 2014 (Fig. 4.5a). The epilimnion is represented by the top 3 m, where water temperature is uniformly warm; the metalimnion occurs between 3 and 6 m, where the temperature drops quickly, and the hypolimnion occurs in the bottom 6 to 7 m, where the temperature is stabilized near the lake bottom (Wetzel, 2001). Turnover of the lake had occurred by November 2014.

Modern Barry Lake is probably a mesotrophic-eutrophic lake as classified from its Secchi depth (5 m) and dissolved oxygen (DO) pattern (Wetzel, 2001). During the July 14th, 2014 sampling, the DO profile shows a clinograde profile, corresponding to a eutrophic lake DO pattern (Wetzel, 2001). The metalimnetic oxygen maxima was apparent during the spring 2014 sampling (May 12th, 2014) (Fig. 4.5b), where the oxygen concentrations in the metalimnion (3 to 6 m) exceeded 100 %, as a result of the photosynthetic activities of algae (Wetzel, 2001).

The δ^2H and δ^{18}O of modern Barry Lake water define a local surface water line (LSWL) (Fig. 4.6) as:

$$\delta^2H = 5.1 \times \delta^{18}O - 19.9$$

The slope of the LSWL (5.1) is lower than the Great Lakes Meteoric Water Line (GLMWL) (7.1) (Longstaffe et al., 2014). The slope of the GLMWL is controlled by air masses, precipitation amount and temperature, which vary regionally and seasonally (Longstaffe et al., 2014). In addition, Barry Lake water is affected by evaporation, which contributes to the lower slope of the LSWL relative to precipitation (i.e. GLMWL) (Gat and Dansgaard, 1972; Gibson et al., 1993; Kebede et al., 2009). Seasonal variations in lake water isotopic composition are apparent in Figure 4.6 and are consistent with the fact that winter precipitation (and therefore lake inflow, especially from spring melt) in general is more depleted of ^{18}O and ^{2}H than summer precipitation (Clark and Fritz, 1997; Jonsson et al., 2009). Evaporation in summer and fall further contributes to ^{18}O and to a

lesser extent in ^{2}H-enrichment of the lake water. The uniform δ^{2}H and δ^{18}O of Barry Lake with depth during spring and fall indicate substantial mixing of lake water, whereas evaporation is interpreted to be the reason for the 6 ‰ and ~0.6 ‰ increase in δ^{2}H and δ^{18}O, respectively in surface relative to deeper waters measured on July 14th, 2014. These isotopic results indicate that Barry Lake water is mixing in spring and fall, and stratified in summer.

Potential carbon sources of DIC to modern Barry Lake include (1) atmospheric CO_2 ($\delta^{13}C$ = –8.4 ‰), (2) CO_2 and DIC associated with Paleozoic carbonate bedrock and tills from the region ($\delta^{13}C$ = –1.6 to +1.5 ‰; Coniglio and Williams-Jones, 1992) carried in groundwater input (Leng and Marshall, 2004), and (3) biological activities such as photosynthesis and respiration of aquatic plants, and decomposition of organic matter (OM) (Leng and Marshall, 2004). In the latter case, photosynthesis preferentially utilizes ^{12}C, leaving the remaining DIC pool enriched in ^{13}C; respiration and decomposition release ^{12}C back into the DIC pool.

The $\delta^{13}C_{DIC}$ of Barry Lake water is uniform in spring and fall, 2014 at ~–5 and ~–4.5 ‰, respectively, while it is stratified in summer 2014, varying from –3.5 ‰ at surface to –6.5 ‰ at bottom (Fig. 4.7). If atmospheric CO_2 ($\delta^{13}C$ = –8.4 ‰) is the only carbon source in Barry Lake DIC, the $\delta^{13}C_{DIC}$ should have values ranging from –0.5 to +1.8 ‰ from 5 to 25 ℃ (fractionation factor from Mook et al., 1974). Such hypothetical compositions are 4 to 5 ‰ enriched in ^{13}C than Barry Lake DIC, indicating that other sources contribute DIC in addition to atmospheric CO_2. The biological activities of algal plants during summer 2014 almost certainly are responsible for the ~3 ‰ enrichment in ^{13}C of surface water relative to bottom water (Fig. 4.7). Photosynthetic of algal plants in the pelagic zone of the lake preferentially utilize ^{12}C, while root respiration of benthic macrophytes, as well as the decomposition of organic matter release ^{12}C-rich CO_2 to the benthic DIC pool causing depletion of ^{13}C at the lake floor (Baresić et al., 2011; Apolinarska, 2013). In spring and fall, photosynthesis is less active, and respiration and decomposition substantially lower $\delta^{13}C_{DIC}$. There may also be some contribution from Paleozoic carbonate bedrock, but it may not be significantly affecting $\delta^{13}C_{DIC}$. Here, it is considered that the carbon sources of Barry Lake DIC are a mixture of atmospheric CO_2

and CO_2 produced by biological activities of aquatic plants, plus a minor contribution from Paleozoic bedrock and tills. Biological activities dominate the measured changes in $\delta^{13}C_{DIC}$ during summer.

5.3 Stable Isotopic Compositions of Carbonates

5.3.1 Stable Isotopic Compositions of Shell Aragonite

Fritz and Poplawski (1974) indicated that aquatic gastropods including *Helisoma anceps* grown under different $\delta^{13}C_{DIC}$ conditions precipitate their shells in close to carbon isotopic equilibrium with DIC. McConnaughey et al. (1997), however, concluded that the carbon sources utilized by freshwater gastropods include both metabolic carbon (<10 %) and DIC (>90 %), and therefore may exhibit isotopic vital effects (VE). Metabolic carbon in freshwater gastropods originates from food and respired carbon and has much lower $\delta^{13}C$ than DIC (McConnaughey et al., 1997; Shanahan et al., 2005). The three modern gastropods species (*H. anceps, Planorbella companulatum* and *Lymnaea stagnalis*) analyzed in the present study are also lung-breathers. Shannahan et al. (2005) have reported shells of lung-breathing gastropods contain a high amount of metabolic carbon, which leads to lower $\delta^{13}C_{shell}$ than would be predicted for equilibrium precipitating from DIC alone.

The calculated $\delta^{13}C_{shell}$, assuming equilibrium with modern Barry Lake water DIC (–5.3 to –2.4 ‰) (Equation 2.8: $\varepsilon_{aragonite\text{-}HCO_3^-} = 2.7 \pm 0.6$ ‰), ranges from –2.6 to +0.3 ‰, much higher than the measured $\delta^{13}C_{shell}$ (–5.5 to –3.0 ‰) (Appendix G). VE is interpreted to be the cause of this offset and the carbon sources for the modern gastropod shells in this study are therefore interpreted as a mixture of DIC and metabolic carbon.

There are no published VE for *H. anceps*, *P. campanulatum* and *L. stagnalis*. Therefore, in order to evaluate historical lake water $\delta^{13}C_{DIC}$ variations, an estimation of VE for each species has been made: +2.4 ±0.5 ‰ for *H. anceps*, +3.2 ±0.6 ‰ for *P. campanulatum* and +3.6 ±0.9 ‰ for *L. stagnalis*. These VEs were estimated by averaging the differences between the expected equilibrium $\delta^{13}C_{shelll}$ (–2.6 to +0.3 ‰) and the actual measured $\delta^{13}C_{shell}$ for each species. The spring and summer surface water $\delta^{13}C_{DIC}$ range (–5.3 to –2.4 ‰) was used to calculate the expected equilibrium range of $\delta^{13}C_{shell}$, as these modern

species live in the littoral zone and precipitate their shells in spring and summer (von Grafenstein et al., 1999; Wood et al., 2010). The estimated VEs are about the same for a range of gastropod species, which may be helpful in other historical records where similar species are found. For *Pisidium*, its VE is –0.2 ‰, as reported by von Grafenstein et al. (1999). Using the VE-corrected $\delta^{13}C_{shell}$, changes in historical water $\delta^{13}C_{DIC}$ can then be estimated (Figs. 5.2a, 5.3n).

Modern gastropods in this study are considered to precipitate their shells in oxygen-equilibrium with ambient water. Mollusc shell growth is rapid during spring and summer (von Grafenstein et al., 1999). By assuming equilibrium oxygen isotopic precipitation of modern gastropod shells (*H. anceps*, *P. companulatum* and *L. stagnalis*) from Barry Lake spring and summer surface water (–8.6 to –7.6 ‰), shell formation temperatures can be calculated using Equation 2.6 ($1000 \times \ln\alpha_{aragonite\text{-}water} = \frac{18.45 \times 10^3}{T\ (K)} - 32.54$), and range from 17 to 20 ℃ (Appendix G). This average shell growth temperature (17 ± 3 ℃) (Appendix G) for modern *H. anceps* is identical within error to the measured spring surface lake water temperature (17 ± 2 ℃), consistent with the facts that *H. anceps* lives in the littoral zone and precipitates its shells during spring and summer (von Grafenstein et al., 1999; Wood et al., 2010).

H. anceps is the only Barry Lake species for which isotopic compositions were analyzed for both modern and ancient time periods, and less attention is paid here to the other two modern species. Briefly, the average calculated shell growth temperatures for *P. companulatum* and *L. stagnalis* are 14 ± 1 and 20 ± 0 ℃, respectively, more or less similar within error to the measured spring surface water temperature (17 ± 2 ℃). Therefore, in the discussion that follows, the historical lake water $\delta^{18}O_{water}$ has been reconstructed by assuming a constant *H. anceps* shell formation temperature of 17 ℃ (Figs. 5.2b, 5.3o).

No modern *Pisidium* samples were observed at Barry Lake, likely because *Pisidium* is an infaunal or epifaunal species (Apolinarska and Hammarlund, 2009). To utilize data from ancient *Pisidium*, the average modern bottom water $\delta^{18}O$ (–7.9 ± 0.6 ‰) was used to estimate its shell formation temperature. The result obtained from these calculations is 15 ± 5 ℃, which is higher than the average measured lake bottom water (depth from 6 to

7.5 m; from May to November) temperature (11 ± 2 ℃) but more or less close to average summer bottom water temperature (14 ± 1 ℃). This shell formation temperature is similar to that measured (~17 ℃) for *Pisidium* living near the shoreline of southeastern Lake Huron (Pinery Provincial Park) (Macdonald, 2012). For the purposes of reconstructing historical lake water $\delta^{18}O$, a constant shell formation temperature of 15 ℃ has been assumed for ancient *Pisidium* samples.

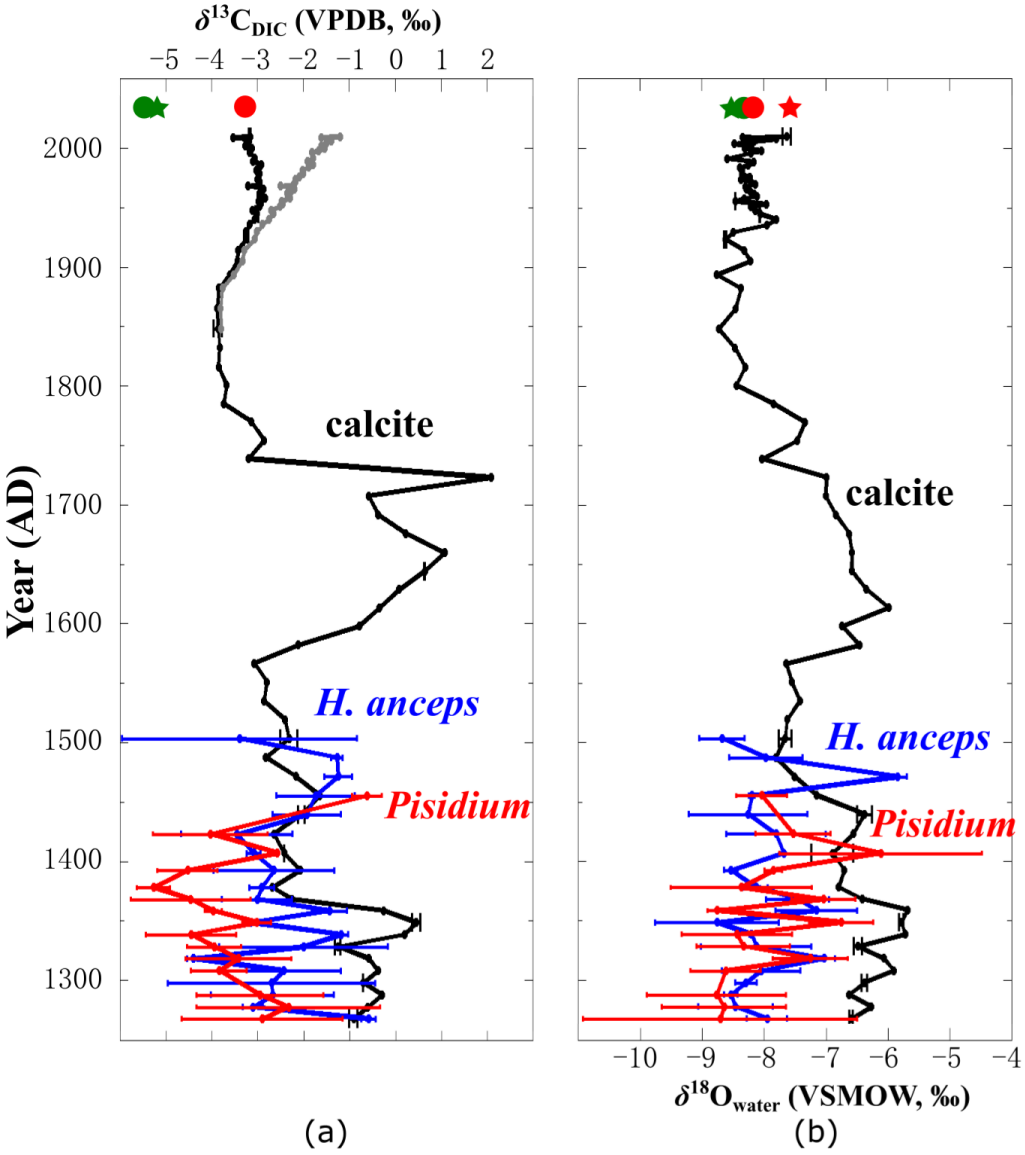

Figure 5.2 Calculated Barry Lake water isotopic compositions: (a) $\delta^{13}C_{DIC}$ estimated from authigenic calcite (black), *Helisoma anceps* (blue) and *Pisidium* (red), Suess-corrected $\delta^{13}C_{DIC}$ (applied to years after 1850) is shown in gray; vital effect (VE) corrections used are described in the text; the red star is the mean summer surface water $\delta^{13}C_{DIC}$ (–3.2 ‰), and the green star and circle are the mean spring surface and bottom water $\delta^{13}C_{DIC}$ (–5.2, –5.1 ‰), respectively. (b) $\delta^{18}O_{water}$ estimated from authigenic calcite (black) using temperature record (AD 1850 to present) and adjusted growing season temperatures reconstructed at Marion Lake, Michigan (Bernabo, 1981): 18.7 ℃ (AD 1615-1850), 19 ℃ (AD 1500-1615), 19.2 ℃ (AD 1350-1500), and 19.7 ℃ (AD 1268-1350), *H. anceps* (blue) at constant 17 ℃ and *Pisidium* (red) at constant 15 ℃; the red star and circle are the mean summer surface and bottom water $\delta^{18}O$ (–7.6, –8.2 ‰), respectively, and the green star and circle are the spring surface and bottom water $\delta^{18}O$ (–8.5, –8.4 ‰), respectively; assumptions used for the temperature of carbonate crystallization are described in the text.

5.3.2 Stable Isotopic Compositions of Calcite

Several crystal forms of calcite have been observed in this study (Fig. 4.8), which varied from diamond to needle shapes, suggesting that it is precipitated from lake water. The various sheaths or surfaces to which those calcite grains were attached (Figs. 4.8c, d) likely have an algae and/or cyanobacteria origin and may have served as surface catalysts during the calcite nucleation process (Stabel, 1986).

Other indirect observations support this viewpoint. In modern Barry Lake, specific conductivity measured on July 14th, 2014 shows a gradual increase from lake surface to the bottom (Fig. 4.5c), which may indicate increasing Ca and bicarbonate concentrations with depth in the lake. The ~5 m Secchi depth measured on the same day suggests a euphotic zone in summer Barry Lake with a depth of ~5 m. Supersaturation of Ca and HCO_3^- can lead to precipitation of calcite within the euphotic zone, and algal phototsynthetic uptake of CO_2 and HCO_3^- can increase the pH in the microenvironment, enhancing supersaturation (Stabel, 1986). Here, we refer to this kind of calcite precipitate in Barry Lake as ‘authigenic calcite’; ‘marl’ and ‘whitings’ are other common names for this type of calcite.

Assuming that the calcite in the top 1 cm of sediments from the core BL–G11–01 was precipitated during the last 2 to 4 years (age-depth model yields AD 2010 at 1 cm), the equilibrium $\delta^{13}C_{calcite}$ for precipitation from lake water DIC is –2.2 ‰. This calculation, which is based on Equation 2.10 ($\varepsilon_{calcite\text{-}HCO_3^-}$ = 1.0 ±0.2 ‰), assumes a $\delta^{13}C_{DIC}$ of –3.2 ±0.5 ‰. This $\delta^{13}C_{DIC}$ (–3.2 ±0.5 ‰) is the average of the measured summer surface water $\delta^{13}C_{DIC}$, as authigenic calcite is mainly formed during summer in epilimnetic waters (Strong, 1978). The calculated $\delta^{13}C_{calcite}$ (–2.2 ‰) is 2 ‰ lower than the measured $\delta^{13}C_{calcite}$ (–0.2 ±0.0 ‰), indicating that the precipitation of the calcite did not occur in equilibrium with DIC. Merz (1992) has suggested that a 2 ‰ enrichment in ^{13}C relative to DIC can occur in calcite precipitation driven by cyanobacteria. The optimum growth temperature for cyanobacteria, however, is up to 35 ℃ (e.g. Lürling et al., 2013), which Barry Lake summer water does not reach. As discussed earlier, an algal-mediated origin for this authigenic calcite seems more likely; the optimum growth temperature for algae

varies between 16 and 27 ℃ (Lavens and Sorgeloos, 1996; Cassidy, 2011), which can be easily achieved during summer (~24 ℃ measured in Barry Lake summer surface water). A constant 2 ‰ offset in $\delta^{13}C_{calcite}$ throughout the core has been used to reconstruct the historical lake water $\delta^{13}C_{DIC}$ (Figs. 5.2a, 5.3n; Appendix I), on the assumption that alga- and cyanobacteria-mediated calcite precipitation produce similar effects. Suess effect has been corrected for DIC estimates after AD 1850, following the same processes as described for OM corrections.

Again assuming that calcite in the top 1 cm of core BL–G11–01 precipitated during the last 2 to 4 years prior to its collection, its isotopic compositions can be taken as representative of modern Barry Lake conditions. Solving Equation 2.9 ($T(℃)=13.8 - 4.58\times(\delta c - \delta w)+0.08\times(\delta c - \delta w)^2$) using the $\delta^{18}O_{calcite}$ (–9.3±0.1 ‰ VPDB) and mean summer surface lake water $\delta^{18}O_{water}$ (–7.7±0.2 ‰ VSMOW) yields a crystallization temperature of 21±0 ℃. This temperature (21±0 ℃) is identical to that of mean summer whole lake water (21±4 ℃) and 2 ℃ lower than that of mean euphotic water (0 to 5 m) temperature (23±3 ℃) measured on July 14th, 2014, which supports an inference of calcite precipitation under summer conditions.

Historical temperature records (Environment Canada (EC): http://climate.weather.gc.ca/index_e.html#access) at the Peterborough station (44°13'48"N, 78°21'48"W) and Trent University (44°21'00"N, 78°18'00"W) (the two nearest stations to Barry Lake with data available for 2014) show that the mean monthly air temperatures from June to August are generally the highest on an annual basis: 17.6±0.2, 18.3±0.1 and 17.8±0.2 ℃ for June, July and August 2014, respectively. The mean summer air temperatures (June to August) available from the historical records (stations listed in Table 1.1; Fig. 1.3), combined with the modern air temperature data for the region, can be used to help estimate the historical lake water $\delta^{18}O_{water}$ at Barry Lake. This, of course, requires that the correction for the difference between air and water temperature is known; air temperature around Barry Lake on July 14th, 2014 was 17.8 ℃.

For the purpose of the present study, a difference of 2.2±1.0 ℃ between air and water temperature has been added to air temperatures available from historical records (since

AD 1866) prior to any calculations of $\delta^{18}O_{water}$ at Barry Lake. This temperature difference was obtained using the *R* package "laketemps" (Sharma et al., 2015). Eight lakes (Table 5.3) located in southern Ontario were selected with similar surface area and lake depth to Barry Lake, and their mean summer air and lake water temperatures were measured *in situ* from July to September between AD 1985 and 2009 by Jim Rusak (Appendix L). The water temperatures were measured at 0.1 m below lake surface. The average air temperature between AD 1985 and 2009 in those lakes is 2.2 ±1.0 ℃ higher than that of lake water and this value is considered representative of small lakes in southern Ontario.

For periods beyond EC records, lake water $\delta^{18}O$ has been calculated by using a temperature reference: the growing season temperature (GST) (from May to September) reconstructed at Marion Lake (45.23N 85.25W), Michigan from AD 800 to 1960 (Bernabo, 1981) (Appendix M). Marion Lake is selected because of (1) its similar latitude compared to Barry Lake (44.31N 77.92W) and (2) its similar surface area (0.31 km^2) and water depth at coring site (8 m) compared to Barry Lake (0.16 km^2 surface area and maximum 8 m water depth), which similar climatic conditions and sedimentation rates are expected to have been preserved in sediments at these two lakes.

Table 5.3 Names and coordinates of the eight selected lakes in southern Ontario from the *R* package "laketemps" (Sharma et al., 2015).

Lake name	Latitude (°)	Longitude (°)	Mean depth (m)	Surface area (m^2)	Contributor
Crosson Lake	45.08	–79.03	9.2	0.56	Jim Rusak Jim.Rusak@ ontario.ca
Heney Lake	45.12	–79.10	3.3	0.21	
Dickie Lake	45.15	–79.08	5.0	0.93	
Plastic Lake	45.18	–78.82	7.9	0.32	
Red Chalk Lake (Main)	45.18	–78.94	16.7	0.44	
Blue Chalk Lake	45.19	–78.93	8.5	0.52	
Red Chalk Lake (East)	45.19	–78.94	5.7	0.13	
Harp Lake	45.38	–79.13	13.3	0.71	

5.4 Lake Water Stable Isotopic Compositions

5.4.1 Carbon-isotope Compositions of DIC

The downcore values for Barry Lake $\delta^{13}C_{DIC}$ (Figs. 5.2a, 5.3n) have been calculated using vital effect-corrected $\delta^{13}C$ of *H. anceps* and *Pisidium* and authigenic calcite, and Equations 2.8 and 2.10. Correction for the Suess effect was also made to $\delta^{13}C_{DIC}$ after AD 1850; the corrected results are shown in gray in Figure 5.2. The $\delta^{13}C_{DIC}$ estimated using authigenic calcite from core BL–G11–01 remains constant around –1.0 ‰ between AD 1268 and 1330 before rising to +0.5 ‰ at AD 1350. The $\delta^{13}C_{DIC}$ then decreases to –2.2 ‰ in AD 1370, followed by a sharp increase to +2.1 ‰ in AD 1720 with a negative shift to –0.6 ‰ in AD 1700. The non-Suess corrected $\delta^{13}C_{DIC}$ is relatively constant since AD 1750, having an average of –3.2 ±0.3 ‰ (SD; n=51), similar to that measured for modern summer surface water of Barry Lake, whereas Suess-corrected $\delta^{13}C_{DIC}$ shows an increase from –3.8 to –1.2 ‰ from AD 1850 to 2011 with an average of –2.5 ±0.2 ‰.

The average $\delta^{13}C_{DIC}$ estimated from *H. anceps*, *Pisidium* and authigenic calcite are –2.4 ±1.0 ‰ (SD; n=43), –3.5 ±1.1 ‰ (SD; n=27) and –1.4 ±1.1 ‰ (SD; n=27), respectively. *H. anceps* exhibits a maximum offset to lower $\delta^{13}C_{DIC}$ of ~–3 ‰ compared to authigenic calcite in AD 1350, and $\delta^{13}C_{DIC}$ estimated using *Pisidium* is lower still, by a maximum of ~5 ‰ compared to authigenic calcite in AD 1340. The $\delta^{13}C_{DIC}$ calculated for each species is similar between AD 1400 and 1500.

5.4.2 Oxygen-isotope Compositions

The values of Barry Lake $\delta^{18}O_{water}$ (Figs. 5.2b, 5.3o) can be calculated using the $\delta^{18}O$ of ancient *H.anceps* and *Pisidium* shells and authigenic calcite via Equations 2.6, 2.7 and 2.9, and assuming constant carbonate formation temperatures under equilibrium conditions at 17 ℃ and 15 ℃ for *H. anceps* and *Pisidium*, respectively, as described earlier. For periods with archival temperature records (AD 1866 to 2011, $\delta^{18}O_{water}$ is estimated using adjusted mean summer air temperature, as described earlier. For periods beyond archival records, GST reconstructed at Marion Lake (Bernabo, 1981) (plus 2.2 ℃ to acquire water temperatures) is used for each of the intervals described in more detail later in this study: 16.5 ℃ for AD 1615 to 1850, 16.8 ℃ for AD 1500 to 1615, 17 ℃ for

AD 1350 to 1500, and 17.5 ℃ for AD 1268 to 1350 (Appendices I and M). Overall, $\delta^{18}O_{water}$ estimated using authigenic calcite from core BL-G11-01 increases, reaching two peaks –6.0 ‰ and –5.8 ‰ at AD 1610 and 1360, respectively. The $\delta^{18}O_{water}$ remains relatively constant since AD 1866 with an average of –8.2±0.2 ‰ (SD; n=38) derived from archival temperature records (Fig. 5.2b).

The average $\delta^{18}O_{water}$ estimated from mollusc shells (–7.9±0.7 ‰ (SD; n=43) for *H. anceps*; –7.9±0.8 ‰ (SD; n=34) for *Pisidium*) are identical but lower than those derived from authigenic calcite (–6.2±0.6 ‰ (SD; n=27)) between AD 1268 to 1500 (Fig. 5.2b). There is a ~1 ‰ offset between $\delta^{18}O_{water}$ as calculated using the mollusc shells *versus* the authigenic calcite between AD 1400 and 1500. This offset increases to a maximum of ~3 ‰ between *H. anceps* and authigenic calcite and ~3.5 ‰ between *Pisidium* and authigenic calcite around AD 1350. Several factors can account for these offsets including different temperatures, as is discussed in the next section.

5.5 Environmental/climatic History of Barry Lake

In this section, an environmental/climatic history for Barry Lake since AD 1268 is proposed based on the age-depth model and information gathered from the various proxies described earlier. The history is presented in four time intervals separated based on variations in $\delta^{18}O$ of lake water (Fig. 5.3): (1) *Interval I* (AD 1268 to 1350), during which the Medieval Warm Period (MWP) ends, (2) *Interval II* (AD 1350 to 1615), which is subdivided into two parts: *Interval IIa* (AD 1350 to 1500) and *Interval IIb* (AD 1500 to 1615) based on the presence or absence of mollusc shells, (3) *Interval III* (AD 1615 to 1850), a period when the Little Ice Age (LIA) is widely observed and documented, and (4) *Interval IV* (AD 1850 to 2011), which is the modern Barry Lake period beginning shortly after European settlement.

5.5.1 *Interval I* (AD 1268–1350)

Interval I in core BL–G11–01 spans depths from 41.5 to 37.5 cm and represents AD 1268 to 1350, according to the age-depth model. The MWP (AD 900–1300) is documented widely in the literature (e.g. Crowley and Lowery, 2000; Cronin et al., 2003; Goosse et al., 2006), but its manifestation varied on a regional basis (Broecker, 2001). Warm

conditions have been reported during this period in southeastern and northwestern Ontario, southwestern Quebec and Michigan (Laird et al., 2012; Booth et al., 2012; Paquette and Gajewski, 2013; Lafontaine-Boyer and Gajewski, 2014; Keizer et al., 2015). Temperatures reconstructed from pollen records at Marion Lake in northwestern Michigan indicate a pronounced warm period from AD 1000 to 1200, during which GST is estimated to have reached 17.5 ℃ near the beginning of AD 1200 (Bernabo, 1981). Here, we correlate *Interval I* at Barry Lake with the MWP.

Most proxies analyzed for *Interval I* do not show wide fluctuations (Fig. 5.3), suggesting that climatic and environmental conditions did not vary significantly. One characteristic of *Interval I* is its high calcite abundance (~60 %). This amount of authigenic calcite could be the product of a warm period, during which lake surface water temperature and the supply of Ca and HCO_3^- to the lake increased (Lajewski et al., 2003). These changes would have increased the saturation state of the surface water with respect to calcite and thus drive its precipitation (McFadden et al., 2004). The median grain size in *Interval I* gradually decreases upwards to its lowest value (3.5 μm), which is consistent with authigenic calcite crystallization. The decrease in grain size also suggests a lowered input of coarser material from runoff, as a result of lower amounts of precipitation.

The $\delta^{18}O_{calcite}$ gradually reaches its maximum value at the end of *Interval I* throughout the records. There is an ~1 ‰ upwards increase (from +22.8 to +23.7 ‰) in $\delta^{18}O_{calcite}$ over the MWP (Fig. 5.3l), which could arise from (1) an increase in evaporation, (2) a decrease in the amount of summer rainfall, (3) a ~4 ℃ decrease in surface water temperature, and/or (4) a lower latitude source of water vapor (Rozanski et al., 1993; McFadden et al., 2004). Each possibility is considered next.

GST reconstructions in Marion Lake and Lake Twenty-seven in Michigan show a ~0.5 ℃ increase from AD 1000 to 1200 (Bernabo, 1981; Appendix M), and similar warm conditions could be expected in *Interval I* at Barry Lake. GST at Marion Lake starts to decrease after AD 1200, but there is no evidence showing decreasing temperature during *Interval I* in Barry Lake. Therefore, although the period AD 1000 to 1200 is ~150 years earlier than the beginning of *Interval I* at Barry Lake, the GST is considered

representative of warm conditions during the MWP for the area of southern Ontario and northern Michigan. Assuming there were no major changes in the composition of the source waters, a combination of less input (precipitation (P) ± groundwater) and higher evaporation (E) from the lake surface could account for the positive shift in $\delta^{18}O_{calcite}$ during this time; in other words, P/E ratios decreased. If so, lake level likely also decreased. Assuming the surface water temperature was similar to that of today (21 ℃), the average $\delta^{18}O_{water}$ of water in this period from which calcite precipitated would have a value of –5.9 ±0.3 ‰ (via Equation 2.9), higher than the present-day Barry Lake summer surface waters (–7.7 ±0.1 ‰). Taking the reconstructed GST (17.5 ℃) for the same period from Marion Lake, Michigan and correcting for the difference between air and water temperatures (2.2 ℃), the $\delta^{18}O_{water}$ in *Interval I* would have a value of –6.2 ±0.3 ‰ and provides our best estimate based on current data.

It is most unlikely that the surface water temperature decreased 4 ℃ during this time; all evidence for surrounding areas suggests a warming period, or at least a period of constant temperature. In addition to the GST data for Marion Lake and Lake Twenty-seven (Bernabo, 1981), ground temperatures determined by inversion of geothermal data collected for 120 boreholes in eastern and central Canada suggest a relatively constant period between AD 1000 and 1300 (Beltrami and Mareschal, 1992).

The source of moisture is also unlikely to have changed considerably. Barry Lake is a kettle lake formed during the retreat of the Laurentide Ice Sheet. Its current inflows are mainly from groundwater and precipitation. The contribution from groundwater is unlikely to have been significantly affected by a small change in surface temperature. Modification of precipitation patterns is more difficult to determine. Summer precipitation in southern Ontario is mainly affected by the maritime tropical (mT) air mass from the Gulf of Mexico and the maritime polar (mP) air mass of the Atlantic. Precipitation from the mT would likely carry water vapor more enriched in ^{18}O than the mP. Without further data to suggest the contrary, however, we have assumed that the relative contribution from these sources remained the same and were dominated by the mT.

The $\delta^{13}C_{calcite}$ during this period includes the second highest values throughout the record and increase from +1.8 to +3.5 ‰ during the last 20 years of *Interval I*. This increase also correlates with increasing $\delta^{13}C_{OM}$ from –29.4 to –27.5 ‰ during the last 30 years of *Interval I* (Figs. 5.3d, k). The increasing $\delta^{13}C_{calcite}$ and $\delta^{13}C_{OM}$ together suggest a period of increasing lake productivity, as the formation and sedimentation of algal OM removed ^{12}C from the surface-water DIC pool, leaving the remaining pool enriched in ^{13}C (Meyers, 2003). OM and calcite utilizing this progressively ^{13}C-enriched DIC would accordingly acquire higher $\delta^{13}C$.

From AD 1268 to 1350, a gradual increase occurs in both $\delta^{18}O_{calcite}$ and $\delta^{13}C_{calcite}$ (Figs. 4.14, 5.3k, l). This covariance is a characteristic of closed basin lakes (Talbot, 1990; Li and Ku, 1997); open lakes can show this pattern if the water residence time (less that lost to evaporation) is sufficiently long to allow co-evolution of $\delta^{18}O_{calcite}$ and $\delta^{13}C_{calcite}$ (McKenzie, 1993).

The presence of benthic bivalve *Pisidium* during *Interval I* suggests that Barry Lake bottom waters were well oxygenated. Similar to the authigenic calcite, the $\delta^{18}O$ of *H. anceps* and *Pisidium* show a ~1.5 to 2 ‰ increase by AD 1350 (Fig. 5.3l), which is likely a result of evaporation and overall ^{18}O-enrichment of Barry Lake. The greater ^{18}O-enrichment (by ~1 ‰) of *Pisidium* relative to *H. anceps* was most likely caused by different temperatures of shell formation. *Pisidium* precipitates its shell more or less throughout the year (Apolinarska, 2009), while *H. anceps* precipitate its shells mostly during the spring and summer (von Grafenstein et al., 1999). The average $\delta^{18}O$ of bottom lake water (–7.9±0.6 ‰) collected in spring (May 12th), summer (July 14th) and fall (Nov 3rd) 2014 is identical with the average $\delta^{18}O$ of spring and summer 2014 surface water (–8.0±0.5 ‰), indicating that *Pisidium* and *H. anceps* may precipitate their shells from similar lake water $\delta^{18}O$. The temperatures of shell formation, however, are different for *Pisidium* and *H. anceps*. *Pisidium* is an epifaunal species, living near the bottom of a lake (Apolinarska, 2009) where temperature is generally lower than *H. anceps*'s littoral zone habitat. Therefore, the isotopic fractionation during shell formation for *Pisidium* is larger than that of *H. anceps*, resulting in the measured differences in $\delta^{18}O$.

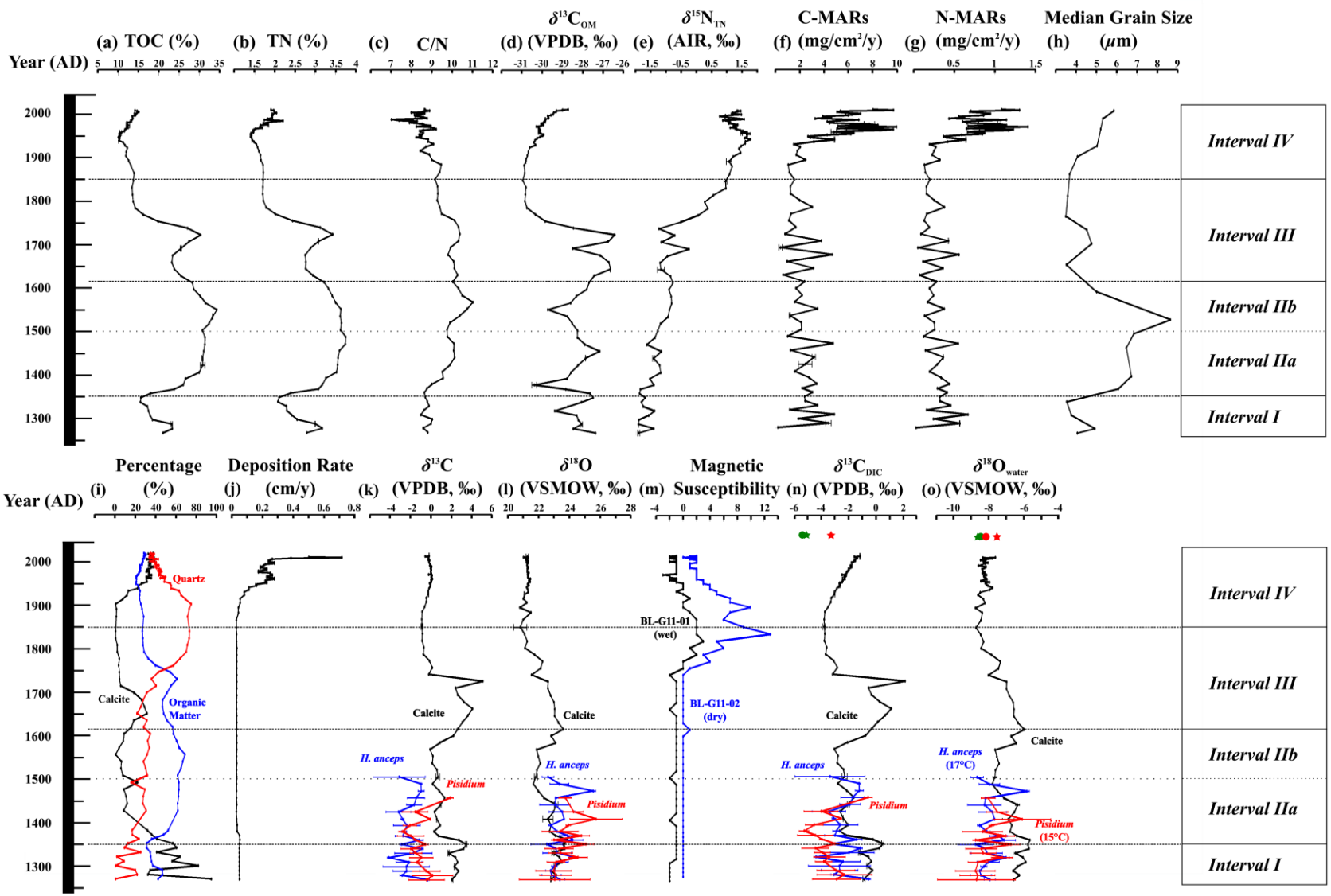
(a) TOC (%)
(b) TN (%)
(c) C/N
(d) δ13COM (VPDB, ‰)
(e) δ15NTN (AIR, ‰)
(f) C-MARs (mg/cm2/y)
(g) N-MARs (mg/cm2/y)
(h) Median Grain Size (μm)
Year (AD)
Interval IV
Interval III
Interval IIb
Interval IIa
Interval I
(i) Percentage (%)
(j) Deposition Rate (cm/y)
(k) δ13C (VPDB, ‰)
(l) δ18O (VSMOW, ‰)
(m) Magnetic Susceptibility
(n) δ13CDIC (VPDB, ‰)
(o) δ18Owater (VSMOW, ‰)
Quartz
Calcite
Organic Matter
H. anceps
Pisidium
BL-G11-01 (wet)
BL-G11-02 (dry)
H. anceps (17°C)
Pisidium (15°C)

Figure 5.3 Summary of data for proxies used in this thesis *versus* time with inferred climatic history: (a) Total organic carbon. (b) Total nitrogen. (c) C/N ratio. (d) δ^{13}C of organic matter (Suess-corrected). (e) δ^{15}N of total nitrogen. (f) Organic carbon mass accumulation rates (C-MARs). (g) Nitrogen-MARs. (h) Median grain size. (i) Authigenic calcite (black), quartz (red) and organic matter (blue) abundance. (j) Sediment deposition rate. (k) δ^{13}C of authigenic calcite (black), *Helisoma anceps* (blue) and *Pisidium* (red). (l) δ^{18}O of authigenic calcite (black) *H. anceps* (blue) and *Pisidium* (red). (m) Magnetic susceptibility (MS) of core BL–G11–01 (analyzed wet) and BL–G11–02 (analyzed dry). (n) Estimated lake water $\delta^{13}C_{DIC}$ from authigenic calcite (black; Suess-corrected), *H. anceps* (blue), *Pisidium* (red); the green star, circle and red star are the mean spring surface, bottom and summer surface water $\delta^{13}C_{DIC}$ (–5.2, –5.1, and –3.2 ‰), respectively. (o) Estimated lake water $\delta^{18}O_{water}$ from *H. anceps* at 17 ℃ (blue), *Pisidium* at 15 ℃ (red), and authigenic calcite (black) using archival temperature records from AD 1866 to 2011 and adjusted growing season temperature (GST) reconstructed by Bernabo (1981) at Marion Lake, Michigan: 19.2 ℃ for AD 1850–present, 18.7 ℃ for AD 1615–1850, 19 ℃ for AD 1500–1615, 19.2 ℃ for AD 1350–1500, 19.7 ℃ for AD 1268–1350; the red star and circle are the mean summer surface and bottom water δ^{18}O (–7.6, –8.2 ‰), respectively; the green star and circle are the mean spring surface and bottom water δ^{18}O (–8.5, –8.4 ‰), respectively.

The maximum ~2.5 ‰ difference among $\delta^{18}O_{calcite}$, $\delta^{18}O_{H.\ anceps}$ and $\delta^{18}O_{Pisidium}$ reflects some combination of: (1) different formation temperatures, (2) different $\delta^{18}O_{water}$ during formation, and (3) different fractionation between water and aragonite *versus* calcite. Calculations for modern *H. anceps* showed that the shell formation temperature (~17 ℃) corresponds more or less to spring water temperature, while the results of such calculations for modern authigenic calcite (~21 ℃) suggest precipitation mainly during summer months. Estimations of *Pisidium* living temperature (~15 ℃) are close to that of modern summer bottom water. During equilibrium precipitation from ambient water, aragonite is enriched in ^{18}O relative to calcite over the temperature range 0 to 40 ℃, and a positive aragonite-calcite fractionation (~0.8 ‰ at 25 ℃) has been reported by Kim et al. (2007). In short, the $\delta^{18}O$ of these coeval carbonates represents three different water situations: $\delta^{18}O_{H.\ anceps}$ represents spring surface water isotopic compositions; $\delta^{18}O_{calcite}$ represents summer surface water isotopic compositions; and $\delta^{18}O_{Pisidium}$ represents average annual bottom water isotopic compositions.

Barry Lake water $\delta^{18}O_{water}$ calculated assuming constant shell formation temperatures: 17 ℃ for *H. anceps* and 15 ℃ for *Pisidium*, are illustrated in Figures 5.2b and 5.3o. These estimates (–8.1 ±0.5 and –8.2 ±0.8 ‰, respectively) are identical within error, and very similar to modern Barry Lake spring surface (–8.5 ±0.1 ‰) and bottom (–8.4 ±0.1 ‰) water. The $\delta^{18}O_{water}$ calculated using the adjusted GST and authigenic calcite is higher (–6.2 ±0.3 ‰), reflecting the summer, shallow water conditions during its formation. .

Concerning $\delta^{13}C_{DIC}$, the lowest $\delta^{13}C_{DIC}$, is obtained for the VE corrected $\delta^{13}C$ of *Pisidium*. Because of its benthic habitat, the $\delta^{13}C_{DIC}$ estimates for *Pisidium* generally reflect bottom water conditions, where respiration and decomposition of OM are most active in returning oxidized ^{12}C to the lake-bottom DIC reservoir. The similar estimates of $\delta^{13}C_{DIC}$ obtained for VE-corrected $\delta^{13}C$ of authigenic calcite and *H. anceps* reflect surface water $\delta^{13}C_{DIC}$, where photosynthesis of algal plants drives upwards the amount of ^{13}C in the residual DIC pool.

The isotopic separation between the estimated lake water and DIC isotopic compositions for the MWP and the modern Barry Lake baseline are: $\Delta^{18}O_{calcite}$= +1.4 ±0.4 ‰, $\Delta^{18}O_{H.}$

$_{anceps}$= +0.4 ±0.6 ‰, and $\Delta^{18}O_{Pisidium}$= +0.2 ±1.0 ‰; $\Delta^{13}C_{calcite}$= +2.8 ±1.0 ‰, $\Delta^{13}C_{H.\ anceps}$ = +2.7 ±1.6 ‰, and $\Delta^{13}C_{Pisidium}$= +1.8 ±1.2 ‰ (Table 5.4, Figs. 5.4, 5.5; $\delta^{13}C$ and $\delta^{18}O$ of calcite are compared with those of modern summer surface water, and $\delta^{13}C$ and $\delta^{18}O$ of *H. anceps* and *Pisidium* are compared with those of modern spring surface and bottom water, respectively). This enrichment in ^{13}C of the MWP over the present time may imply a change in source of DIC, which is likely caused by the different $\delta^{13}C$ of atmospheric CO_2. The $\delta^{13}C$ of atmospheric CO_2 was ~–6.5 ‰ during pre-industrial times (Leuenberger et al., 1992), while it is now ~–8.4 ‰ because of the combustion of fossil fuels (Suess effect). The small variations in the extent of ^{13}C enrichment may reflect the different places in the water column where *H. anceps*, *Pisidium* and authigenic calcite formed and/or some uncertainties in VE-corrections that were used. The $\delta^{18}O_{water}$ estimates for *H. anceps* and *Pisidium* are identical within error and match the range of modern spring Barry Lake $\delta^{18}O$. By comparison, the estimate of $\delta^{18}O_{water}$ using authigenic calcite is 1.4 ‰ higher than that of modern summer surface water, reflecting the warmer and perhaps more highly evaporated nature of the shallower water from which the calcite precipitated during *Interval I*.

Other proxies (magnetic susceptibility, C- and N-MARs, C/N ratio and $\delta^{15}N_{TN}$) during the MWP do not vary significantly except for TOC, TN and $\delta^{13}C_{OM}$ (Figs. 5.3a, b, d). The amounts of TOC and TN show a decrease upwards in the section. Woszczyk et al. (2014) reported that OM decomposition under oxidizing conditions can be enhanced by the lowering of lake level, thus producing a decrease in TOC and TN. In this study, however, this is unlikely the case, as C- and N-MARs remain constant. This suggests instead an increase in allochthonous sedimentation rate caused TOC and TN to be lowered towards the end of the MWP. The near constant C/N of 9 suggests a uniform source for the OM, dominated by aquatic algae (Meyers and Ishtawari, 1993; Meyers and Lallier-Verg ès, 1999). The ~2 ‰ increase in $\delta^{13}C_{OM}$ from AD 1320 to 1350 correlates with an increase in $\delta^{13}C_{calcite}$; both changes may be a sign of increasing lake productivity (Meyers, 2003). As also inferred from the increasing $\delta^{18}O$ of authigenic calcite, *H. anceps* and *Pisidium*, and the GST towards the end of *Interval I*, temperature was likely rising and accompanied by greater evaporation and perhaps diminished precipitation, leading to higher Barry Lake $\delta^{18}O_{water}$. Photosynthetic activities of algal plants would be enhanced under such

conditions, increasing competition for ^{12}C from the surface water DIC pool, and leaving the remaining pool enriched in ^{13}C (Meyers, 2003), as discussed earlier.

Table 5.4 Estimated average of isotopic compositions of Barry Lake for each time period interval and the isotopic separations between carbonates and modern water

	***Interval I* (AD 1268-1350)**			***Interval IIa* (AD 1350-1500)**		
	Calcite[(a)]	***H. anceps*[(b)]**	***Pisidium*[(c)]**	**Calcite[(d)]**	***H. anceps*[(b)]**	***Pisidium*[(c)]**
$\delta^{18}O_{water}$ **(‰ VSMOW)**	–6.2 ±0.3	–8.1 ±0.5	–8.2 ±0.8	–6.9 ±0.6	–7.8 ±0.8	–7.5 ±0.9
$\delta^{13}C_{DIC}$ **(‰ VPDB)**	–0.4 ±0.5	–2.5 ±1.1	–3.3 ±0.7	–2.1 ±0.7	–2.4 ±0.9	–3.6 ±1.6
$\Delta^{18}O$	1.4 ±0.4	0.4 ±0.6	0.2 ±1.0	0.7 ±0.7	0.7 ±0.9	0.9 ±1.2
$\Delta^{13}C$	2.8 ±1.0	2.7 ±1.6	1.8 ±1.2	1.1 ±1.2	2.8 ±1.0	1.5 ±1.6
	***Interval IIb* (AD 1500-1615)**		***Interval III* (AD 1615-1850)**		***Interval IV* (AD 1850-2011)**	
	Calcite[(e)]		**Calcite[(f)]**		**Calcite[(g)]**	
$\delta^{18}O_{water}$ **(‰ VSMOW)**	–7.1 ±0.7		–7.4 ±0.8		–8.2 ±0.2	
$\delta^{13}C_{DIC}$ **(‰ VPDB)**	–2.1 ±1.1		–1.7 ±2.2		–2.5 ±0.2	
$\Delta^{18}O$	0.5 ±0.8		0.2 ±0.9		–0.6 ±0.7	
$\Delta^{13}C$	1.1 ±1.6		1.5 ±2.7		+0.7 ±0.7	

(a) $\delta^{18}O_{water}$ is calculated assuming calcite formation at 19.7 ℃ and compared with modern summer surface water $\delta^{18}O_{water}$ -7.6±0.1 ‰; $\delta^{13}C_{DIC}$ estimated from authigenic calcite is compared with modern summer surface water $\delta^{13}C_{DIC}$ -3.2±0.5 ‰

(b) $\delta^{18}O_{water}$ is calculated assuming *H. anceps* formation at 17.0 ℃ and compared with modern spring surface water $\delta^{18}O_{water}$ -8.5±0.1 ‰; $\delta^{13}C_{DIC}$ estimated from *H. anceps* is compared with modern spring surface water $\delta^{13}C_{DIC}$ -5.2±0.1 ‰

(c) $\delta^{18}O_{water}$ is calculated assuming *Pisidium* formation at 15.0 ℃ and compared with modern spring bottom water $\delta^{18}O_{water}$ -8.4±0.1 ‰; $\delta^{13}C_{DIC}$ estimated from *Pisidium* is compared with modern spring surface water $\delta^{13}C_{DIC}$ -5.1±0.1 ‰

(d) $\delta^{18}O_{water}$ is calculated assuming a calcite formation temperature at 19.2 ℃ and using the same other parameters as listed under (a)

(e) $\delta^{18}O_{water}$ is calculated assuming a calcite formation temperature at 19.0 ℃ and using the same other parameters as listed under (a)

(f) $\delta^{18}O_{water}$ is calculated assuming a calcite formation temperature at 18.7 ℃ and using the same other parameters as listed under (a)

(g) $\delta^{18}O_{water}$ is calculated using the temperature record obtained from seven climatic stations in vicinity of Barry Lake (Fig. 1.3; Table 1.1); $\delta^{13}C_{DIC}$ estimated from authigenic calcite is Suess-corrected and compared with modern summer surface water $\delta^{13}C_{DIC}$ -3.2±0.5 ‰

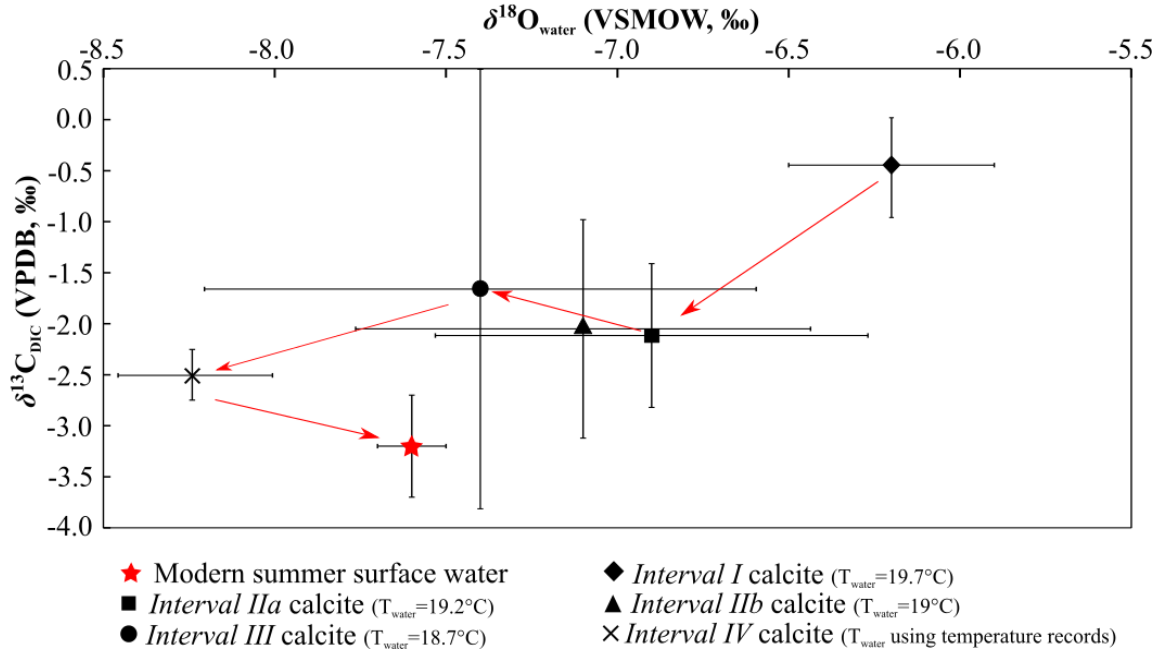

Figure 5.4 Mean estimated Barry Lake water $\delta^{18}O$ and $\delta^{13}C_{DIC}$ from authigenic calcite in each interval compared with modern lake water isotopic composition.

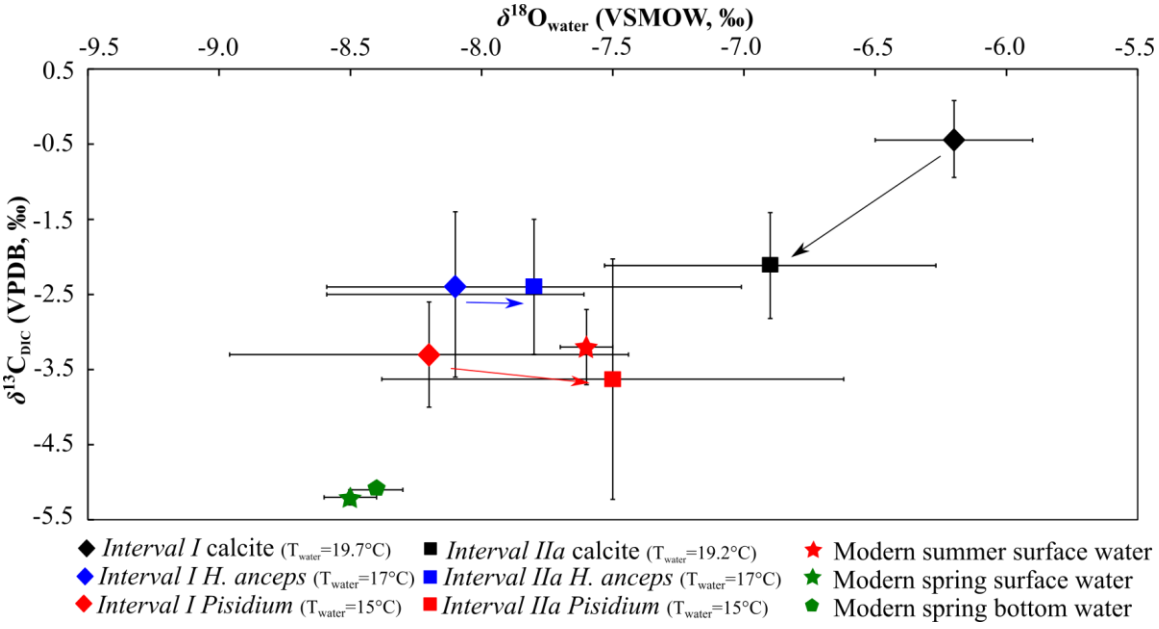

Figure 5.5 Mean estimated Barry Lake water $\delta^{18}O$ and $\delta^{13}C_{DIC}$ from calcite and mollusc shells in *Interval I* and *Interval II* compared with modern lake water isotopic compositions.

5.5.2 *Interval II* (AD 1350–1615)

This interval has been subdivided into *Interval IIa* (AD 1350–1500), which contains mollusc shells and *Interval IIb* (AD 1500–1615), which does not. *Interval IIa* is characterized by a sharp decrease in calcite abundance, a lowering of $\delta^{18}O_{calcite}$ (+23 to +21 ‰) and $\delta^{13}C_{calcite}$ (+3.5 ‰ to 0 ‰), and increases in grain size, TOC, TN, C/N, and $\delta^{15}N_{TN}$ (Figs. 5.3a-c, e, h, i, k, l). The $\delta^{13}C_{OM}$ first decreases from –28 to –30 ‰ from AD 1350 to 1380 and then increases to –28 ‰ in AD 1440 (Fig. 5.3d). Relative to *Interval I*, these features collectively suggest a period of increased precipitation and lower evaporation and temperature. The decrease in the amount of authigenic calcite suggests a lower saturation-state, consistent with lower surface water temperature (McFadden et al., 2004). The decrease in $\delta^{18}O_{calcite}$ could result from (1) a decrease in evaporation, and/or (2) an increase in precipitation. As discussed for *Interval I*, involvement of different water vapour sources (e.g., a higher latitude or transcontinental water vapor source) is difficult to evaluate and not considered further. Likewise, a putative ~9 ℃ increase in water temperature, which could also produce the change in $\delta^{18}O_{calcite}$ is environmentally unrealistic and not considered further.

The GST at Marion Lake during this period shows a decreasing trend, with an average temperature of ~17 ℃ (Bernabo, 1981; Appendix M), 0.5 ℃ lower than that of *Interval I*. Using this summer air temperature plus the 2.2 ℃ air-water temperature difference correction, an average Barry Lake $\delta^{18}O_{water}$ of -6.9 ± 0.6 ‰ can be calculated using $\delta^{18}O_{calcite}$. This $\delta^{18}O_{water}$ is 0.7 ‰ lower than estimated for *Interval I* (Table 5.4; Figs. 5.4, 5.5). The isotopic separation between $\delta^{18}O_{water}$ estimated from authigenic calcite or biogenic carbonates and modern Barry Lake during *Interval IIa* are: $\Delta^{18}O_{calcite} = +0.7 \pm 0.7$ ‰, $\Delta^{18}O_{H.anceps} = +0.7 \pm 0.9$ ‰, and $\Delta^{18}O_{Pisidium} = +0.9 \pm 1.2$ ‰; $\Delta^{13}C_{calcite} = +1.1 \pm 1.2$ ‰, $\Delta^{13}C_{H.anceps} = +2.8 \pm 1.0$ ‰, and $\Delta^{13}C_{Pisidium} = +1.5 \pm 1.6$ ‰ (Table 5.4, Figs. 5.4, 5.5). Mollusc shells of the same species have the same average carbon and oxygen isotopic compositions, within error, during *Intervals I and IIa*, suggesting little difference in environmental conditions during the periods of shell formation. Compared to *Interval I*, however, $\delta^{18}O_{water}$ and $\delta^{13}C_{DIC}$ estimated from authigenic calcite are lower, suggesting a cooler summer period and a more ^{12}C-rich DIC pool. Figure 5.5 further suggests that

while average bottom water isotopic conditions were only moderately enriched in ^{18}O and ^{13}C from modern Barry Lake during *Intervals I and IIa*, surface waters during this time had much higher $\delta^{18}O_{water}$ and $\delta^{13}C_{DIC}$ compared to modern times.

The initial decrease in $\delta^{13}C_{DIC}$ and $\delta^{13}C_{OM}$ from AD 1350 to 1380 likely indicate a decrease in lacustrine production (Figs. 5.3d, n). The small increase in C/N (Fig. 5.3c) may also indicate increased terrestrial input, which is also indicated by appearance of wood fragments and an initial increase in grain size in *Interval IIa* compared to *Interval I* (Fig. 5.3h). The subsequent increase in $\delta^{13}C_{OM}$ after AD 1380 is consistent with increased terrestrial OM contributions, as is the continued rise in C/N; the change in $\delta^{13}C_{OM}$ could also indicate increased lacustrine production. The gradual upward increase in $\delta^{15}N_{TN}$ during *Interval IIa* (Fig. 5.3e), may also reflect increased lacustrine production (Meyers, 2003; Choudhary et al., 2009a,b; Routh et al., 2009), but it could also denote greater terrestrial OM contribution.

The upward increase in $\delta^{13}C_{Pisidium}$ (from –3 to +2 ‰), also beginning at AD ~1380 reaches its maximum as this species disappears from the sediment record (Fig. 5.3k). At its highest value, the associated bottom-water $\delta^{13}C_{DIC}$ for *Pisidium* is similar to that inferred from authigenic calcite and *H. anceps* for higher up in the water column (Fig. 5.3n). This suggests that the supply of low $\delta^{13}C_{DIC}$ from decay of organic matter became limited towards the end of *Interval IIa*, either because of more rapid burial or because bottom waters became dysoxic to anoxic. Such conditions, if they moved upward in the water column and/or the lake became shallower, may have ultimately led to the disappearance of other shelly fauna, such as *H. anceps*, by the end of *Interval IIa*.

The *Interval IIb* is characterized by the disappearance of *H.anceps* and other shelly fauna, an initial sharp decrease in grain size, a continued decrease in $\delta^{13}C_{OM}$ and a gradual increase in C/N (Figs. 5.3c, d, h). This is then followed by a decrease in C/N and grain size and an increase in $\delta^{13}C_{OM}$, $\delta^{13}C_{calcite}$ and $\delta^{18}O_{calcite}$ (and associated $\delta^{13}C_{DIC}$ and $\delta^{18}O_{water}$) towards the end of *Interval IIb* (Figs. 5.3c, d, h, k, l, n, o). Other proxies show similar variations to *Interval IIa* with a slight decrease in TOC, TN, C-MARs and N-MARs (Figs. 5.3a, b, f, g).

The GST at Marion Lake, Michigan suggests an average temperature (16.8 ℃) similar to *Interval IIa*, which based on the average $\delta^{18}O_{calcite}$, produces a calculated average Barry Lake $\delta^{18}O_{water}$ of –7.1 ±0.7 ‰ (Table 5.4; Fig. 5.4), identical within error to *Interval IIa* (–6.9 ±0.6 ‰). Identical average Barry Lake $\delta^{13}C_{DIC}$ for *Interval IIa* (–2.1 ±0.7 ‰) and *IIb* (–2.1 ±1.1 ‰) further support the suggestion that, on average, environmental conditions controlling authigenic calcite precipitation were similar during these two periods, and indeed the amount of authigenic calcite precipitation, on average, is very similar during *Intervals IIa* and *IIb* (Fig. 5.3i). It also follows that the isotopic separation between Barry Lake isotopic compositions inferred from *Interval IIb* calcite and measured for modern summer surface water are virtually the same as for *Interval IIa* $\Delta^{18}O_{calcite}$ =+0.5 ±0.8 ‰, $\Delta^{13}C_{calcite}$ =+1.1 ±1.6 ‰ (Table 5.4, Fig. 5.4).

During the last ~65 years of *Interval IIb* (AD 1550 to 1615), however, C/N peaked, and then started to decline; median grain size continued to decrease; $\delta^{13}C_{OM}$, authigenic calcite abundance, $\delta^{13}C_{calcite}$ and $\delta^{18}O_{calcite}$ began to increase. All of these features are consistent with greater lake production driven by warming conditions towards the end of *Interval IIb*.

The earliest recorded human activity in the Barry Lake area may also have occurred during *Interval II*. Sonnenburg et al. (2013) reported the appearance of Iroquoian people in the Rice Lake area (Fig. 1.1) at about 1 ka BP, and Ekdahl et al. (2007) documented Iroquoian people at Crawford Lake (Fig. 1.1) between AD 1268 and 1468. However, there is no change in sediment magnetic susceptibility during *Interval IIa* (or *Interval IIb*) (Fig. 5.3m), which would have been expected if the onset of human occupation had included agricultural activities that involved land clearance near Barry Lake. Thus it is unlikely that the upward increase in TOC and TN (at constant C-MARs and N-MARs), C/N, $\delta^{13}C_{OM}$, $\delta^{15}N_{TN}$, and median grain size, and overall lower $\delta^{13}C_{calcite}$ and $\delta^{18}O_{calcite}$ compared to *Interval I* (Fig. 5.3) can be attributed to a human environmental impact rather than climate change based on the available proxies.

5.5.3 *Interval III* (AD 1615–1850)

The *Interval III* sediments were deposited during the time period typically associated with the Little Ice Age (LIA), and many proxies show a high degree of variability, consistent with a period of environmental change. On average, this period is characterized by low abundance of authigenic calcite (~5 %), a sharp shift in most proxies around AD 1720 (Fig. 5.3), followed shortly by the beginning of a major increase in MS at AD ~1740 (Fig. 5.3m). The continuous decrease in $\delta^{18}O_{calcite}$ (from +23.3 ‰ to +20.8 ‰) (Fig. 5.3l) is consistent with a cold period, which would reduce precipitation of authigenic calcite (Fig. 5.3i). Colder conditions are also supported by Barry Lake pollen assemblages described by McAndrews (1984). His *Zone 3d* (see Fig. 1.2) represents the period from AD ~1600 to 1820 and indicates rapid decreases in beech and maple (*Fagus*, *Acer*, respectively) and an increase in white pine (*Pinus strobus*). Such changes are characteristics of a cold period (Lafontaine-Boyer and Gajewski, 2014). According to Beltrami and Mareschal (1992), ground temperature histories also indicate a colder period between AD ~1500 and 1800 with a maximum of 2 ℃ drop in mean annual temperature in central and eastern Canada.

The GST reconstructed at Marion Lake, Michigan suggested a minimum of 16.5 ℃ at AD ~1700 (Appendix M). The average Barry Lake $\delta^{18}O_{water}$ of –7.4 ±0.8 ‰, based on this temperature (after the air-water temperature correction) and $\delta^{18}O_{calcite}$ (Table 5.4; Fig. 5.4), is identical to modern Barry Lake summer surface $\delta^{18}O_{water}$ (–7.6 ±0.1 ‰). The isotopic separation between estimated lake water isotopic compositions between authigenic calcite and modern summer surface water isotopic compositions during *Interval III* are $\Delta^{18}O_{calcite}$ =+0.2 ±0.9 ‰, $\Delta^{13}C_{calcite}$ =+1.5 ±2.7 ‰ (Table 5.4; Fig. 5.4).

Increases in TOC, TN, C/N, $\delta^{13}C_{OM}$ and grain size from AD ~1700 to 1720 (Figs. 5.3a-d, h) are consistent with an increased flux of terrestrial OM to Barry Lake. This is then followed by sharp decreases in $\delta^{13}C_{OM}$ (–26 ‰ to ~–31 ‰) and $\delta^{13}C_{calcite}$ (+5 ‰ to ~0 ‰) beginning at AD 1720 (Figs. 5.3d, k). Several possibilities may explain the large changes in $\delta^{13}C_{OM}$ and $\delta^{13}C_{calcite}$: (1) higher input of terrestrial soil-derived OM, which can have low $\delta^{13}C$ depending on its position in the soil column (Hammarlund et al., 1997; Leng

and Marshall, 2004), (2) methanotrophy in water column (Li et al., 2008), (3) wetland plants having low $\delta^{13}C$, and (4) a decrease in biological production (Routh et al., 2009).

Modestly higher allochthonous OM input is supported by the C/N, which remains slightly elevated (~10.5) relative to typical aquatic OM until AD ~1760. The rise in MS beginning at AD ~1740 is also consistent with increased terrestrial input. The median grain size, however, does not show a significant change, which indicates that fine-grained detritus, such as soil clays, must have dominated such additions. Organic matter carried by clays has anomalously low C/N compared to unaltered terrestrial OM, making it hard to distinguish from aquatic OM production using this parameter alone (Hyodo and Longstaffe, 2011; Hladyniuk and Longstaffe, 2015a).

Alternatively, Li et al. (2008) note that methanotrophy (CH_4 oxidation) in the water column can produce mineralized carbon with low $\delta^{13}C$. Such a scenario is possible at Barry Lake during the late LIA; the continued absence of preserved molluscs, especially *Pisidium*, may indicate favourable conditions for methane production from the lake's sediments and bottom waters. Low $\delta^{13}C$ (below –30 ‰) is also characteristic of common terrestrial and wetland plants such as sedge, bulrush and reed (Sensula et al., 2006), which currently populate the shoreline of Barry Lake. However, there is thus far no evidence for a significant change in the abundance of wetland plants at Barry Lake relative to the earlier intervals that have been considered.

A climate-related decrease in lacustrine productivity during this cold period can best explain the lower TOC, TN, $\delta^{13}C_{OM}$ and $\delta^{13}C_{DIC}$, but it remains to explain the steady rise in $\delta^{15}N_{TN}$ (Fig. 5.3e) that occurs at the same time within *Interval III*.

The $\delta^{15}N_{TN}$ shows a sharp increase from –1.5 ‰ to +1 ‰, beginning at AD ~1720 (Fig. 5.3e). Several possibilities can explain the rising $\delta^{15}N_{TN}$: (1) denitrification through microbial decomposition of OM (Talbot, 2001; Woszczyk et al., 2014), (2) a change in nitrogen sources (soil-derived N from arable land and nutrients from agricultural activities can increase $\delta^{15}N_{TN}$) (Ahlgren et al., 1994; Talbot, 2001; Meyers and Teranes, 2001; Routh et al., 2007, 2009), and (3) an increase in lacustrine production (Brenner et al., 1999).

Oxygen deficiency in bottom waters will favor denitrification (Talbot, 2001). On average, the product N_2 is ~20 ‰ lighter than the reactant NO_3^- (Talbot, 2001), which leads to ^{15}N-enrichment of the residual OM. Bratton et al. (2003) have noted that denitrification led to an increase in $\delta^{15}N_{TN}$ of Chesapeake Bay sediments from +5 to +10 ‰ within a few centuries.

There may also have been a change in nitrogen sources that is attribute to human activities during this part of *Interval III*. Ahlgren et al. (1994) and Routh et al. (2009) showed that soil erosion and nutrients from agricultural activities can lead to an increase in $\delta^{15}N_{TN}$. Such activities have also produced enrichment in ^{15}N (~4 ‰) of Lake Ontario sediments over the last century (Hladyniuk and Longstaffe, 2015b).

At Barry Lake, the first indication in the lake sediment record of human activity that modified the environment is interpreted from the increasing magnetic susceptibility (MS) of Barry Lake sediments beginning at AD 1740 (Fig. 5.3m). MS provides an indication of erosion rate, deforestation, afforestation and agricultural changes in the drainage basin (Wetzel, 2001). This change at Barry Lake is attributed, in the first instance, to activities of the Mississauga people. They settled in Rice Lake area (Fig. 1.1) during the late 17th century (Sonnenburg et al., 2013). We suggest that such activities also extended to Barry Lake, causing the increase in $\delta^{15}N_{TN}$. The MS reaches its maximum values around AD 1830 (Fig. 5.3m), which corresponds to subsequent European settlement, deforestation, burning and agricultural activities around Barry Lake, which further enhanced input of terrestrial magnetic materials to the lacustrine system.

An increase in Barry Lake production seems to be the most unlikely explanation for the changes in $\delta^{15}N_{TN}$ during *Interval III*, given the counter indications provided by the other proxies.

5.5.4 *Interval IV* (AD 1850–2011)

The modern period, or *Interval IV* at Barry Lake is characterized by increasing $\delta^{13}C_{OM}$, $\delta^{13}C_{DIC}$ (both Suess-corrected), C- and N-MARs, grain size, authigenic calcite abundance and sediment deposition rates, decreasing C/N and MS, and more or less constant $\delta^{15}N_{TN}$, and $\delta^{13}C_{calcite}$; $\delta^{18}O_{calciate}$ and $\delta^{18}O_{water}$ fluctuate over a narrow range, but a pattern of increase in recent years may be emerging (Fig. 5.3). McAndrew's (1984) pollen assemblages (Fig. 1.2) show a great decrease in maple, hemlock and beech (*Acer*, *Tsuga* and *Fagus*, respectively) during *Interval IV*, likely because of selective logging during clearance (Lafontaine-Boyer and Gajewski, 2014).

Global temperature has been increasing during this period: the average global land and ocean surface temperatures have risen by 0.85 ℃ between AD 1880 and 2012; this change is generally attributed to anthropogenic greenhouse gas emissions (IPCC, 2001, 2014). A warming of 1 to 2 ℃ in eastern and central Canada over the last 150 years has been reported by Beltrami and Mareschal (1992) based on ground temperatures estimated from geothermal borehole measurements.

Regional archival records (Figs. 1.4a, 4.16a; Appendix K) show a maximum of ~5 ℃ increase (from 15 to 20 ℃) in mean summer (June to August) temperatures from AD 1866 to 2011. Using $\delta^{18}O_{calcite}$ and the adjusted mean summer temperatures (June to August) from archival records, the mean summer lake water $\delta^{18}O_{water}$ is –8.2 ±0.2 ‰. The ~1 ‰ increase from –8.8 ‰ to –7.6 ‰ in $\delta^{18}O_{water}$ during *Interval IV* reflects rising summer temperatures, and there is a spike to the highest values in the most recent years (Fig. 5.3o).

Marion Lake, Michigan, also shows a trend of increasing temperature since AD 1800 (Bernabo, 1981; Appendix M); archival records there indicate a measured average GST of 17 ℃ between AD 1930 and 1960 in Marion Lake. This temperature matches very closely to the average measured summer temperature for the vicinity of Barry Lake (16.8 ℃ from AD 1930-1960; 16.7 ℃ from AD 1886-2011). This close comparison provides confidence in the earlier GSTs estimated for Marion Lake in the absence of archival temperature data. The average lake water $\delta^{18}O_{water}$ for *Interval IV*, calculated for

17 ℃ (after correction for the air-lake differential) is –8.2±0.1 ‰, identical to the average obtained using regional archival temperatures (–8.2±0.2 ‰).

The isotopic separations between calculated Barry Lake $\delta^{18}O_{water}$ and modern water isotopic compositions is $\Delta^{18}O_{calcite}$ = –0.6±0.7 ‰, based on archival temperature data (Table 5.4, Fig. 5.4). The lower $\delta^{18}O_{water}$ on average during *Interval IV* than at present reflects the present sharper trend towards increasing summer water temperatures.

The calculated $\delta^{13}C_{DIC}$ (after Suess correction) is more enriched in ^{13}C than today ($\Delta^{13}C_{calcite}$ =+0.7±0.7 ‰; Table 5.4, Fig. 5.4), suggesting the Suess effect has affected modern Barry Lake resulting in low ^{13}C content in DIC pool.

Increases in C-MARs, N-MARs, grain size and sediment deposition rate occur after European settlement (AD ~1820; McAndrews, 1984), particularly after AD ~1950 (Figs. 5.3f-h, j). The progressively lower C/N (9 to 7; Fig. 5.3c) suggests increased in-lake production towards present time (Meyers, 1994, 2003; O'Beirne et al., 2015). This is consistent with higher C- and N-MARs and deposition rates, which enhance burial and preservation of OM in the sediments (Meyers, 2003; O'Beirne et al., 2015). Rising $\delta^{13}C_{OM}$ and $\delta^{13}C_{DIC}$ are also consistent with increased lacustrine production, although some terrestrial contribution cannot be ruled out given the rise in median grain size (Figs. 5.3d, h, n). The flattening of the increase, and even slight lowering of $\delta^{15}N_{TN}$ (Fig. 5.3e) may reflect contributions from inorganic fertilizers on agricultural fields that border Barry Lake.

The MS signal indicates continued but declining perturbation of Barry Lake to at least AD ~1950 (Fig. 5.3m). This behavior is likely the signature of road construction, land clearance, forestry and farmland development around Barry Lake up until the area was developed to its present (apparently stable) level of largely agricultural activity.

Chapter 6

6 Conclusion

This study describes the paleolimnology of Barry Lake, southeastern Ontario, Canada, since AD ~1300, as inferred from several proxies preserved in the top ~41 cm of lake sediments. The physical, chemical and isotopic compositions preserved in the proxy materials are used to investigate paleoclimatic variations, lake productivity changes and impacts from human activities at Barry Lake over the last ~720 years. Proxies employed in this study include mineralogy, magnetic susceptibility (MS), total organic carbon (TOC) content, total nitrogen (TN) content, atomic carbon to nitrogen ratio (C/N), organic carbon and nitrogen mass accumulation rates (C-MARs; N-MARs), grain size, $\delta^{18}O$ and $\delta^{13}C$ of authigenic calcite, $\delta^{18}O$ and $\delta^{13}C$ of mollusc aragonite, and the $\delta^{13}C$ and $\delta^{15}N$ of bulk organic matter (OM). This chapter summarizes the major findings of this study and provides suggestions for future research.

The ^{210}Pb-^{14}C grounded age-depth model for the gravity cores obtained from Barry Lake yields a date of AD 1268 for the bottom of the gravity cores examined. These sediments therefore have recorded changes during the Medieval Warm Period (MWP), the Little Ice Age (LIA), and First Nations and European anthropogenic activity in the Barry Lake region since AD 1268.

Interval I, as defined for these cores, spans AD 1268 to 1350 and includes the latter part of the MWP. This period is characterized by low median grain size (~4 μm), high amounts of authigenic calcite (marl) and a ~1 ‰ increase in Barry Lake $\delta^{18}O_{water}$ calculated using authigenic calcite (–7 to –6 ‰) and shelly fauna, specifically *H. anceps* (–8 to –7 ‰) and *Pisidium* (–8 to –7 ‰). These features collectively support the interpretation of a warmer period during which marl formation was facilitated, and overland inflow was limited, perhaps because of reduced precipitation. This conclusion is supported by diatom assemblages from northwestern Ontario (Laird et al., 2012). Pollen and charcoal records from Michigan also indicate drought conditions during this time period (Booth et al., 2012).

During the last 30 years of *Interval I* at Barry Lake, a ~2 ‰ increase in $\delta^{13}C$ of authigenic calcite (+1.8 to +3.5 ‰) and OM (–29.4 to –27.5 ‰) is interpreted to indicate increased lacustrine production coincident with the end of the MWP. Driven by warmer conditions, photosynthetic activity, and hence greater competition for ^{12}C cause algal plants, residual surface water DIC pool, and associated marl to become enriched in ^{13}C.

Interval II (AD 1350-1615) represents a transition period between the MWP and the LIA. At the start of *Interval IIa* (AD 1350-1500), authigenic calcite deposition declined substantially, which is interpreted to indicate cooler summer surface water temperatures. The $\delta^{18}O_{water}$ calculated using the isotopic composition of authigenic calcite also suggests lower average summer surface water temperatures. Lower $\delta^{13}C_{calcite}$ suggests greater availability of ^{12}C in the near-surface DIC pool, which is interpreted to indicate decreased pelagic productivity. These observations are consistent with the generally cooler conditions previously reported for this time period on the basis of palynology for regions ranging from Maine to Minnesota, including southeastern Ontario and southwestern Quebec (Gajewski, 1988; Paquette and Gajewski, 2013; Keizer et al., 2015).

The $\delta^{18}O_{water}$ and $\delta^{13}C_{DIC}$ calculated for mollusc shells from *Interval IIa*, however, suggest that environmental conditions during spring in the pelagic zone (*H. anceps*) and over the year in the benthic zone (*Pisidium*) remained similar to those of *Interval I*. the disappearance of mollusc shells, first *Pisidium* and then followed by *H. anceps* at the boundary (AD ~1500) between *Intervals IIa* and *IIb* is interpreted to reflect dysoxic to anoxic bottom water conditions. Such interpretation is also supported by an upward rise in $\delta^{13}C_{\textit{Pisidium}}$ before clams disappeared from the record.

The increase in median grain size and C/N during *Interval II* is interpreted to indicate a greater contribution of terrestrial detritus during this period, perhaps reflective of increased overland flow into Barry Lake during cooler and wetter conditions. Two cycles of 3 ‰ variation in $\delta^{13}C_{OM}$ likely indicate changes both in lacustrine production and terrestrial OM input. Many other proxies, however, do not show major variations during *Interval II*, which is interpreted to indicate relative climatic stability.

Most proxies show much larger variations during *Interval III* (AD 1615 to 1850), a time period that includes the LIA. Precipitation of authigenic calcite reaches its lowest levels during this time and Barry Lake $\delta^{18}O_{water}$, as calculated using authigenic calcite, decreases by 3 ‰ (–6 to –9 ‰). Both changes are interpreted to indicate lower summer temperatures. This interpretation matches earlier palynological investigations that indicate lower growing season temperature for Barry Lake (McAndrews, 1984), and more generally, lower (by up to 2 ℃) average annual temperature for this region of North America (Campbell and McAndrews, 1991, 1993; Beltrami and Mareschal, 1992; Keizer et al., 2015).

There is a sharp shift in most proxies beginning at AD ~1720, including a 5 ‰ decrease in $\delta^{13}C_{calcite}$ and $\delta^{13}C_{OM}$, which is interpreted to indicate a climate-related reduction in lacustrine production. The accompanying steady rise in $\delta^{15}N_{TN}$ is best interpreted to indicate a change in nitrogen source related to human modification of the landscape beginning at about this time and continuing through to European settlement initiated at AD ~1830. A significant perturbation in magnetic susceptibility (MS) of the sediments starting at AD ~1740 and peaking at AD ~1830 supports this interpretation.

During *Interval IV* (AD 1850-2011), archival records indicate rising temperature (~1-2 ℃) for the region and even larger increases in average summer temperatures. In response, Barry Lake summer surface $\delta^{18}O_{water}$ has increased by 1 ‰ (–8.8 to –7.6 ‰), as calculated using local temperature records and $\delta^{18}O_{calcite}$.

Increases in C- and N-MARs, median grain size and sediment deposition rates are associated with European settlement, and development of the region. Increasing $\delta^{13}C_{OM}$, $\delta^{13}C_{DIC}$ and decreasing C/N suggest that lacustrine production has increased in Barry Lake in response to these activities. A flattening in the rise of $\delta^{15}N_{TN}$ and then a slight decline after AD ~1950, suggests a change in nitrogen sources to Barry Lake, perhaps the introduction of inorganic fertilizers used in adjacent agriculture. During *Interval IV*, the MS signal indicates decreasing perturbation of the Barry Lake environment, which stabilizes at its current level at AD ~1950. Additional human activity, beyond current agriculture, has had minimal impact on Barry Lake since that time.

We conclude that this paleolimnological study of Barry Lake has provided a unique window into the environmental conditions affecting the area over the last ~720 years. These data are useful in separating climatic from anthropogenic factors affecting the trophic level of Barry Lake, and provide essential baseline information for evaluating environmental change – and its causes – in the future.

There are several avenues for future limnological and paleolimnological investigations at Barry Lake. Chemical, diatom and palynomorph studies of modern Barry Lake, and diatom and palynomorph assemblages in sediments spanning the last ~720 years will provide additional information about human activities and their influences on Barry Lakes trophic state. As part of this work, additional gravity cores should be collected along transect of the lake to characterize spatial and temporal variations that might be related to past changes in lake level and shoreline position. For all cores, a robust age/depth model will be needed to ensure correlation across the lake. Multiply substituted clumped isotopologue measurements on the authigenic calcite and shell aragonite should be undertaken to better constrain the temperatures of their formation. A study of modern calcite precipitation in Barry Lake would also shed light on the chemical, biochemical and physical processes involved in its crystallization, and aid interpretation of ancient marl records.

On a geographically wider scale, gravity cores should be obtained from multiple lakes in southern Ontario. These cores should be used to reconstruct a regional climate history that describes geographical and temporal variations in the impact of the MWP and LIA. Data from these cores should also be used to identify the start and progress of anthropogenic perturbations of these natural lacustrine systems.

Going deeper back in time, a piston core should be obtained from Barry Lake to extend its climatic and environmental history back to the formation of the lake at the end of the last glaciations.

References

Abell, P. I. (1985). Oxygen isotope ratios in modern African gastropod. *Chemical Geology, 58*, 183-193.

Abell, P. I., & Williams, M. A. (1989). Oxygen and carbon isotope ratios in gastropods shells as indicators of paleoenvironments in the Afar region of Ethiopia. *Palaeogeography, Palaeolimnology, Palaeoecology, 74*, 265-278.

Adkins, J., Boyle, E., Curry, W., & Lutringer, A. (2003). Stable isotopes in deep-sea corals and a new mechanism for "vital effects". *Geochimica et Cosmochimica Acta, 67(6)*, 1129-1143.

Ahlgren, I., Soerenson, F., Waara, T., & Vrede, K. (1994). Nitrogen budgets in relation to microbial transformations in lakes. *Ambio (Sweden), 23*, 367-377.

Anderson, T., & Lewis, C. (2012). A new water-level history for Lake Ontario basin: evidence for a climate-driven early Holocene lowstand. *Journal of Paleolimnology, 47(3)*, 513-530.

Apolinarska, K. (2009). δ^{18}O and δ^{13}C isotope investigation of the Late Glacial and early Holocene biogenic carbonates from the Lake Lednica sediments, western Poland. *Acta Geologica Polonica, 59(1)*, 111-121.

Apolinarska, K. (2013). Stable isotope compositions of recent *Dreissena polymorpha* (Pallas) shells: paleoenvironmental implications. *Journal of Paleolimnology, 50(3)*, 353-364.

Apolinarska, K., & Hammarlund, D. (2009). Multi-component stable isotope records from Late Weichselian and early Holocene lake sediments at Imiołki, Poland: palaeoclimatic and methodological implications. *Journal of Quaternary Science, 24(8)*, 948-959.

Appleby, P. (2001). Chronostratigraphic techniques in recent sediments. In *Tracking Environmental Change Using Lake Sediments*, Smol, J., Birks, H. & Last, W. (Eds.), (pp. 171-203). Springer Netherlands.

Appleby, P. (2008). Three decades of dating recent sediments by fallout radionuclides: a review. *The Holocene, 18(1)*, 83-93.

Appleby, P., & Oldfield, F. (1978). The calculation of lead-210 dates assuming a constant rate of supply of unsupported ^{210}Pb to the sediment. *Catena, 5(1)*, 1-8.

Appleby, P., Richardson, N., & Nolan, P. (1991). ^{241}Am dating of lake sediments. In *Environmental History and Palaeolimnology* (pp. 35-42). Springer Netherlands.

Armstrong, D., & Carter, T. (2006). An updated guide to the subsurface Paleozoic stratigraphy of southern Ontario. *Ontario Geological Survey*.

Armstrong, D., & Dodge, J. (2007). Paleozoic geology of southern Ontario. *Ontario Geological Survey, Miscellaneous Release-Data 219*.

Baresić, J., Horvatincic, N., & Roller-Iutz, Z. (2011). Spatial and seasonal variations in the stable C isotope composition of dissolved inorganic carbon and in physico-chemical water parameters in the Plitvice Lakes system. *Isotopes in Environmental and Health Studies, 47(3)*, 316-329.

Barnekow, L., Possnert, G., & Sandgren, P. (1998). AMS ^{14}C chronologies of Holocene lake sediments in the Abisko area, northern Sweden-a comparison between dated bulk sediment and macrofossil samples. *GFF, 120(1)*, 59-67.

Barnett, P. J., Cowan, W. R., & Henry, A. P. (1991). Quaternary geology of Ontario, southern sheet; Ontario Geological Survey, Map 2556, scale 1:100000. pp. 1152-1167.

Beltrami, H., & Mareschal, J. (1992). Ground temperature histories for central and eastern Canada from geothermal measurements: Little Ice Age signature. *Geophysical Research Letters, 19(7)*, 689-692.

Bennett, K., & Willis, K. (2001). Pollen. In *Tracking Environmental Change Using Lake Sediments*, Smol, J., Birks, H. & Last, W. (Eds.), (pp. 5-32). Springer Netherlands.

Benoit, G., & Hemond, H. (1987). A biogeochemical mass balance of ^{210}Po and ^{210}Pb in an oligotrophic lake with seasonally anoxic hypolimnion. *Geochimica et Cosmochimica Acta, 51(6)*, 1445-1456.

Benoit, G., & Rozan, T. (2001). ^{210}Pb and ^{137}Cs dating methods in lakes: a retrospective study. *Journal of Paleolimnology, 25(4)*, 455-465.

Benson, L., & Paillet, F. (2002). HIBAL: a hydrologic-isotopic-balance model for application to paleolake systems. *Quaternary Science Reviews, 21(12)*, 1521-1539.

Benson, L., Meyers, P., & Spencer, R. (1991). Change in the size of Walker Lake during the past 5000 years. *Palaeogeography, Palaeoclimatology, Palaeoecology, 81(3)*, 189-214.

Benson, L., Burdett, J., Kashgarian, M., Lund, S., Phillips, F., & Rye, R. (1996). Climatic and hydrologic oscillations in the Owens Lake basin and adjacent Sierra Nevada, California. *Science, 274*.

Benson, L., May, H., Antweiler, R., Brinton, T., Kashgarian, M., Smoot, J., et al. (1998). Continuous lake-sediment records of glaciation in the Sierra Nevada between 52,600 and 12,500 ^{14}C yr B.P. *Quaternary Research, 50(2)*, 113-127.

Benson, L., Kashgarian, M., Rye, R., Lund, S., Paillet, F., Smoot, J., et al. (2002). Holocene multidecadal and multicentennial droughts affecting Northern California and Nevada. *Quaternary Science Reviews, 21(4)*, 659-682.

Bernabo, J. (1981). Quantitative estimates of temperature changes over the last 2700 years in Michigan based on pollen data. *Quaternary Research, 15(2)*, 143-159.

Bernasconi, S., Barbieri, A., & Simona, M. (1997). Carbon and nitrogen isotope variations in sedimenting organic matter in Lake Lugano. *Limnology and Oceanography, 42(8)*, 1755-1765.

Binford, M., Kahl, J., & Norton, S. (1993). Interpretation of ^{210}Pb profiles and verification of the CRS dating model in PIRLA project lake sediment cores. *Journal of Paleolimnology, 9(3)*, 275-296.

Birks, H. (2002). Plant macrofossils. In *Trachking Environmental Change Using Lake Sediments*, Smol, J., Birks, H. & Last, W. (Eds.), (pp. 49-74). Springer Netherlands.

Björck, S., & Wohlfarth, B. (2001). ^{14}C chronostratigraphic techniques in paleolimnology. In *Tracking environmental change using lake sediments*, Smol, J., Birks, H. & Last, W. (Eds.), (pp. 205-245). Springer Netherlands.

Blaauw, M., & Christén, J. (2011). Flexible paleoclimate age-depth models using an autoregressive gamma process. *Bayesian Analysis, 6(3)*, 457-474.

Blais, J., Kalff, J., Cornett, R., & Evans, R. (1995). Evaluation of ^{210}Pb dating in lake sediments using stable Pb, *Ambrosia* pollen, and ^{137}Cs. *Journal of Paleolimnology, 13(2)*, 169-178.

Böhm, F., Joachimski, M., Dullo, W., Eisenhauer, A., Lehnert, H., Reitner, J., et al. (2000). Oxygen isotope fractionation in marine aragonite of coralline sponges. *Geochimica et Cosmochimica Acta, 64(10)*, 1695-1703.

Bollhöfer, A., Mangini, A., Lenhard, A., Wessels, M., Giovanoli, F., & Schwarz, B. (1994). High-resolution ^{210}Pb dating of Lake Constance sediments: Stable lead in Lake Constance. *Environmental Geology, 24(4)*, 267-274.

Booth, R. K., Jackson, S. T., Sousa, V. A., Sullivan, M. E., Mincklev, T. A., & Clifford, M. J. (2012). Multi-decadal drought and amplified moisture variability drove rapid forest community change in a humid region. *Ecology, 93(2)*, 219-226.

Boyce, J. E., & Eyles, N. (1991). Drumlins carved by deforming till streams below the Laurentide Ice Sheet. *Geology, 19(8)*, 787-790.

Bradley, R., & Jonest, P. (1993). 'Little Ice Age' summer temperature variations: their nature and relevance to recent global warming trends. *The Holocene, 3(4)*, 367-376.

BrattonJ.F., Colman, S., & Seal, R. (2003). Eutrophication and carbon sources in Chesapeake Bay over the last 2700 yr: human impacts in context. *Geochimica et Cosmochimica Acta, 67(18)*, 3385-3402.

Brenner, M., Whitmore, T., Curtis, J., Hodell, D., & Schelske, C. (1999). Stable isotope (δ^{13}C and δ^{15}N) signatures of sedimented organic matter as indicators of historic lake trophic state. *Journal of Paleolimnology, 22(2)*, 205-221.

Briffa, K., Jones, P., & Schweingruber, F. (1992). Tree-ring density reconstructions of summer temperature patterns across western North America since 1600. *Journal of Climate, 5(7)*, 735-754.

Broecker, W. (2001). Paleoclimate: was the Medieval Warm Period global? *Science, 291(5508)*, 1497.

Brunskill, G. (1969). Fayetteville Green Lake, New York. II. Precipitation and sedimentation of calcite in a meromictic lake with laminated sediments. *Limnology and Oceanography, 14(6)*, 830-847.

Buhay, W., & Edwards, T. (1995). Climate in southwestern Ontario, Canada, between AD 1610 and 1885 inferred from oxygen and hydrogen isotopic measurements of wood cellulose from trees in different hydrologic settings. *Quaternary Research, 44(3)*, 438-446.

Burch, J.B. (1982). Freshwater snails (Mollusca: Gastropoda) of North America. Environmental monitoring and support laboratory office of research anad development. US Environmental Protection Agency, Cincinaty, ON.

Campbell, I. D., & McAndrews, J. H. (1991). Cluster analysis of lake Holocene pollen trends in Ontario. *Canadian Journal of Botany*, 1719-1730.

Campbell, I., & McAndrews, J. (1993). Forest disequilibrium caused by rapid Little Ice Age cooling. *Nature, 366(6453)*, 336-338.

Cassidy, K. (2011). Evaluating algal growth at different temperatures. *These and Dissertations-Biosystems and Agricultural Engineering*, Paper 3. http://uknowledge.uky.edu/bae_etds/3

Cespuglio, G., Piccinetti, C., & Longinelli, A. (1999). Oxygen and carbon isotope profiles from *Nassa mutabilis* shells (Gastropoda): accretion rates and biological behaviour. *Marine Biology, 135(4)*, 627-634.

Choudhary, P., Routh, J., & Chakrapani, G. (2009a). An environmental record of changes in sedimentary organic matter from Lake Sattal in Kumaun Himalayas, India. *Science of The Total Environment, 407(8)*, 2783-2795.

Choudhary, P., Routh, J., & Chakrapani, G. (2009b). Comparison of bulk organic matter characteristics in sediments of three Kumaun Himalayan lakes. *Current Science, 97(4)*, 572-575.

Clark, I., & Fritz, P. (1997). *Environmental Isotopes in Hydrogeology*. CRC press.

Cohen, A. S. (2003). *Paleolimnology: the History and Evolution of Lake Systems*. Oxford University Press, USA.

Coniglio, M., & Williams-Jones, A. E. (1992). Diagenesis of Ordovician carbonates from the north-east Michigan Basin, Manitoulin Island area, Ontario: evidence from petrography, stable isotopes and fluid inclusions. *Sedimentology, 39(5)*, 813-836.

Coplen, T. (1994). Reporting of stable hydrogen,carbon, and oxygen isotopic abundances. *Pure and Applied Chemistry, 66*, 273-276.

Coplen, T., Brand, W., Gehre, M., Groning, M., Meijer, H., Toman, B., et al. (2006). New guidelines for δ^{13}C measurements. *Analytical Chemistry, 78(7)*, 2439-2441.

Corti, G., Cocco, S., Basili, M., Cioci, C., Warburton, J., & Agnelli, A. (2012). Soil formation in kettle holes from high altitudes in central Apennines, Italy. *Geoderma, 170*, 280-294.

Covich, A., & Stuiver, M. (1974). Changes in oxygen 18 as a measure of long-term fluctuations in tropical lake levels and molluscan populations. *Limnology and Oceanography, 19(4)*, 682-691.

Craig, H. (1961). Isotopic variations in meteoric waters. *Science, 133(3465)*, 1702-1703.

Cronin, T., Dwyer, G., Kamiya, T., Schwede, S., & Willard, D. (2003). Medieval Warm Period, Little Ice Age and 20th century temperature variability from Chesapeake Bay. *Global and Planetary Change, 36(1)*, 17-29.

Crowley, T., & Lowery, T. (2000). How warm was the Medieval Warm Period? *AMBIO: A Journal of the Human Environment, 29(1)*, 51-54.

Crozier, M. (1975). On the origin of the Peterborough drumlin field: testing the dilatancy theory. *The Canadian Geographer, 19(3)*, 181-195.

Cuntz, M. (2011). Carbon cycle: a dent in carbon's gold standard. *Nature, 477(7366)*, 547-548.

Cwynar, L. (1988). Late Quaternary vegetation history of Kettlehole Pond, southwestern Yukon. *Canadian Journal of Forest Research, 18(10)*, 1270-1279.

Davis, R., Hess, C., Norton, S., Hanson, D., Hoagland, K., & Anderson, D. (1984). ^{137}Cs and ^{210}Pb dating of sediments from soft-water lakes in New England (USA) and Scandinavia, a failure of ^{137}Cs dating. *Chemical Geology, 44(1)*, 151-185.

Dean Jr, W. (1974). Determination of carbonate and organic matter in calcareous sediments and sedimentary rocks by loss on ignition: comparison with other methods. *Journal of Sedimentary Research, 44(1)*.

Dean, W. (1999). The carbon cycle and biogeochemical dynamics in lake sediments. *Journal of Paleolimnology, 21(4)*, 375-393.

Deevey Jr, E., Gross, M., Hutchinson, G., & Kraybill, H. (1954). The natural ^{14}C contents of materials from hard-water lakes. *Proceedings of the National Academy of Sciences of the United States of America, 40(5)*, 285.

Dettman, D., Reische, A., & Lohmann, K. (1999). Controls on the stable isotope composition of seasonal growth bands in aragonitic fresh-water bivalves (Unionidae). *Geochimica et Cosmochimica Acta, 63(7)*, 1049-1057.

Dörr, H., & Münnich, K. (1991). Lead and cesium transport in European forest soils. *Water, Air, and Soil Pollution, 57(1)*, 809-818.

Effler, S. (1984). Carbonate equilibria and the distribution of inorganic carbon in Saginaw Bay. *Jounal of Great Lakes Research, 10(1)*, 3-14.

Effler, S., Field, S., & Quirk, M. (1982). The seasonal cycle of inorganic carbon species in Cazenovia Lake, New York. *Freshwater Biology, 12(2)*, 139-147.

Effler, S., Field, S., & Wilcox, D. (1981). The carbonate chemistry of Green Lake, Jamesville, NY. *Journal of Freshwater Ecology, 1(2)*, 141-153.

Ekdahl, E., Teranes, J., Wittkop, C., Stoermer, E., Reavie, E., & Smol, J. (2007). Diatom assemblage response to Iroquoian and Euro-Canadian eutrophication of Crawford Lake, Ontario, Canada. *Journal of Paleolimnology, 37(2)*, 233-246.

Emrich, K., Ehhalt, D., & Vogel, J. (1970). Carbon isotope fractionation during the precipitation of calcium carbonate. *Earth and Planetary Science Letters, 8(5)*, 363-371.

Environment Canada (2015). *Historical Climate Data*. Retrieved June 2015, from http://climate.weather.gc.ca/index_e.html#access

Epstein, S., & Mayeda, T. (1953). Variation of ^{18}O content of waters from natural sources. *Geochimica et Cosmochimica Acta, 4(5)*, 213-224.

Escobar, J., Curtis, J., Brenner, M., Hodell, D., & Holmes, J. (2010). Isotope measurements of single ostracod valves and gastropod shells for climate reconstruction: evaluation of within-sample variability and determination of optimum sample size. *Journal of Paleolimnology, 43(4)*, 921-938.

Eyles, N., & Westgate, J.A. (1987). Restricted regional extent of the Laurentide Ice Sheet in the Great Lakes basins during early Wisconsin glaciation. *Geology, 15(6)*, 537-540.

Farrand, W., & Miller, B. (1968). Radiocarbon dates on and depositional environment of the Wasaga Beach (Ontario) marl deposit. *The Ohio Journal of Science, 68(4)*, 235-239.

Faure, G., & Mensing, T. (2005). *Isotopes: Principles and Applications.* John Wiley & Sons Inc.

Filion, L., & Begin, Y. (1998). Recent paludification of kettle holes on the central isjands of Lake Bienville, northern Quebec, Canada. *The Holocene, 8(1)*, 91-96.

Filley, T., Freeman, K., Bianchi, T., Baskaran, M., Colarusso, L., & Hatcher, P. (2001). An isotopic biogeochemical assessment of shifts in organic matter input to Holocene sediments from Mud Lake, Florida. *Organic Geochemistry, 32(9)*, 1153-1167.

Fontes, J., & Gonfiantini, R. (1968). Comportement isotopique au cours de l'évaporation de deux bassins sahariens. *Earth and Planetary Science Letters, 3*, 258-266.

Francey, R., Allison, C., Etheridge, D., Trudinger, C., Enting, I., Leuenberger, M., et al. (1999). A 1000-year high precision record of $\delta^{13}C$ in atmospheric CO_2. *Tellus B, 51(2)*, 170-193.

Friedli, H., Lotscher, H., Oeschger, H., Siegenthaler, U., & Stauffer, B. (1986). Ice core record of the $^{13}C/^{12}C$ ratio of atmospheric CO_2 in the past two centuries. *Nature, 324(6094)*, 237-238.

Fritts, H. (1991). *Reconstructing Large-scale Climatic Patterns from Tree-ring Data*. United States: Tucson, University of Arizona Press.

Fritts, H., & Shao, X. (1992). Mapping climate using tree-rings from western North America. In *Climate Since AD 1500*, Bradley, R. & Jones, P. (Eds.), (pp. 269-295). London: Routledge.

Fritz, P., & Poplawski, S. (1974). ^{18}O and ^{13}C in the shells of freshwater molluscs and their environments. *Earth and Planetary Science Letters, 24(1)*, 91-98.

Fritz, P., Anderson, T., & Lewis, C. (1975). Late-Quaternary climatic trends and history of Lake Erie from stable isotope studies. *Science, 190*, 267-269.

Frizzell, R., Cotesta, L., & Usher, S. (2011). Regional geology-southern Ontario. *Nuclear Waste Management Organization Report NWMO DGR-TR-2011-15 R000.* Toronto, Canada.

Fuller, J. (1997). Holocene forest dynamics in southern Ontario, Canada: fine-resolution pollen data. *Canadian Journal of Botany, 75(10)*, 1714-1727.

Fuller, J. (1998). Ecological impact of the mid-Holocene hemlock decline in southern Ontario, Canada. *Ecology, 79(7)*, 2337-2351.

Gajewski, K. (1988). Late Holocene climate changes in eastern North America estimated from pollen data. *Quaternary Research, 29(3)*, 255-262.

Gat, J. (1984). The stable isotope composition of Dead Sea waters. *Earth and Planetary Science Letters, 71(2)*, 361-376.

Gat, J., & Dansgaard, W. (1972). Stable isotope survey of the fresh water occurrences in Israel and the northern Jordan Rift Valley. *Journal of Hydrology, 16(3)*, 177-211.

Gelen, A., Diaz, O., Simon, M., Herrera, E., Soto, J., Gomez, J., et al. (2003). ^{210}Pb dating of sediments from Havana Bay. *Journal of Radioanalytical and Nuclear Chemistry, 256(3)*, 561-564.

GeoGratis. (2015). *GeoGratis*. Retrieved June 2015, from Natural Resources Canada, Government of Canada: http://geogratis.gc.ca/geogratis/search?lang=en

Gibson, J., Edwards, T., Bursey, G., & Prowse, T. (1993). Estimating evaporation using stable isotopes: quantitative results and sensitivity analysis for two catchments in nothern Canada. *Nordic Hydrology, 24*, 79-94.

Glew, J.R., Smol, J.P. & Last, W.M. (2001). Sediment core collection and extrusion. In *Tracking Environmental Change Using Lake Sediments,* vol 1: Basin Analysis, Coring and Chronological Techniques. Last, W & Smol, J. (Eds.), (pp. 73-105). Kluwer Academic Publishers, Dordrecht.

Google Earth (2015). Barry Lake, Trent Hills, Ontario, Canada. Eye altitude 6 km. http://www.google.com/earth/.

Google Map (2015). Regional Map of Lake Ontario and Barry Lake. Retrieved from https://www.google.ca/maps/place/Barry+Lake,+Trent+Hills,+ON+K0L/@44.3075814,77.9212617,16z/data=!4m2!3m1!1s0x89d6009be030ff0f:0x98bdb61926e99b34?hl=en

Goosse, H., Arzel, O., Luterbacher, J., Mann, M., Renssen, H., Riedwyl, N., et al. (2006). The origin of the European "Medieval Warm Period". *Climate of the Past, 2(2)*, 99-113.

Government of Canada and USA. (1995). *The Great Lakes: An Environmental Atlas and Resaource Book*. Great Lakes National Program Office.

Grabau, A. (1920). *A Textbook of Geology - Part 1. General Geology.* Boston, MA: D.C. Heath & Co. Publishers.

Gravenor, C. (1953). The origin of drumlins. *American Journal of Science, 251(9)*, 674-681.

Grimm, E. (2011). High-resolution age model based on AMS radiocarbon ages for Kettle Lake, North Dakota, USA. *Radiocarbon, 53(1)*, 39-53.

Grossman, E. L., & Ku, T. L. (1986). Oxygen and carbon isotope fractionation in biogenic aragonite-temperature effects. *Chemical Geology, 59*, 59-74.

Hakansson, S. (1979). Radiocarbon activity in submerged plants from various South Swedish lakes. In *Radiocarbon Dating-Ninth International Conference* (pp. 433-443).

Hammarlund, D., Aravena, R., Barnekow, L., Buchardt, B., & Possnert, G. (1997). Multi-component carbon isotope evidence of early Holocene environmental change and carbon-flow pathways from a hard-water lake in northern Sweden. *Journal of Paleolimnology, 18(3)*, 219-233.

Harris, D., Horwath, W., & van Kessel, C. (2001). Acid fumigation of soils to remove carbonates prior to total organic carbon or carbon-13 isotopic analysis. *Soil Science Society of America Journal, 65(6)*, 1853-1856.

Hassan, K., Swinehart, J., & Spalding, R. (1997). Evidence for Holocene environmental change from C/N ratios, and $\delta^{13}C$ and $\delta^{15}N$ values in Swan Lake sediments, western Sand Hills, Nebraska. *Journal of Paleolimnology, 18(2)*, 121-130.

Hecky, R., Campbell, P., & Hendzel, L. (1993). The stoichiometry of carbon, nitrogen, and phosphorus in particulate matter of lakes and oceans. *Limnology and Oceanography, 38(4)*, 709-724.

Hladyniuk, R., & Longstaffe, F. (2015a). Paleoproductivity and organic matter sources in Late Quaternary Lake Ontario. *Palaeogeography, Palaeoclimatology, Palaeoecology, 435*, 13-23.

Hladyniuk, R., & Longstaffe, F. (2015b). Anthropocene changes in organic matter accumulation in Lake Ontario. International Association for Great Lakes Research, Burlington, Vermont.

Hollander, D., & MacKenzie, J. (1991). CO_2 control on carbon-isotope fractionation during aqueous photosynthesis: A paleo-pCO_2 barometer. *Geology, 19*, 929-932.

Holopainen, I. (1980). Growth of two *Pisidium* (Bivalvia, Sphaeriidae) species in the laboratory. *Oecologia, 45(1)*, 104-108.

Holopainen, I., & Hanski, I. (1986). Holopainen, I. J., & Hanski, I. (1986). Life history variation in *Pisidium* (Bivalvia: Pisidiidae). *Ecography, 9(2)*, 85-98.

Horita, J. (1988). Hydrogen isotope analysis of natural waters using an H_2-water equilibration method: a special implication to brines. *Chemical Geology: Isotope Geoscience Section, 72(1)*, 89-94.

Hyodo, A., & Longstaffe, F. (2011). The palaeoproductivity of ancient Lake Superior. *Quaternary Science Reviews, 30(21)*, 2988-3000.

Ingraham, N. (1998). Isotopic variations in precipitation. *Isotope Tracers in Catchment Hydrology*, 87-118.

IPCC. (2001). In R. Watson, & T. C. Team (Eds.), *A Contribution of Working Groups I, II, and III to the Third Assessment Report of the.* Cambridge and New York, United Kingdom and USA: Cambridge University Press.

IPCC. (2014). Climate Change 2014: Synthesis Report. In C. W. Team, R. Pachauri, & L. Meyer (Eds.), *Contribution of Working Groups I, II and III to the Fifth Assessment Report of the Intergovernmental Panel on Climate Change*, Geneva, Switzerland. Team, C.W., Pachauri, R. and Meyer, L. (Eds.).

Johnson, T., Halfman, J., & Showers, W. (1991). Paleoclimate of the past 4000 years at Lake Turkana, Kenya, based on the isotopic composition of authigenic calcite. *Palaeogeography, Palaeoclimatology, Palaeoecology, 85(3)*, 189-198.

Johnston, J., Koster, J., Wolfe, B., Hall, R., Edwards, T., Endres, A., et al. (2010). Quantifying Lake Athabasca (Canada) water level during the 'Little Ice Age'highstand from palaeolimnological and geophysical analyses of a transgressive barrier-beach complex. *The Holocene, 20(5)*, 801-811.

Jonsson, C., Leng, M., Rosqvist, G., Seibert, J., & Arrowsmith, C. (2009). Stable oxygen and hydrogen isotopes in sub-Arctic lake waters from northern Sweden. *Journal of Hydrology, 376(1)*, 143-151.

Kalettka, T., & Rudat, C. (2006). Hydrogeomorphic types of glacially created kettle holes in north-east Germany. *Limnologica, 36*, 54-64.

Kantrud, H., Krapu, G., & Swanson, G. (1989). Prairie basin wetlands of the Dakotas: a community profile. *Biological Report 85. US Fish Wildlife Service, Jamestown and Northern Prairie Wildlife Research Centre*.

Kebede, S., Travi, Y., & Rozanski, K. (2009). The $\delta^{18}O$ and $\delta^{2}H$ enrichment of Ethiopian lakes. *Journal of Hydrology, 365(3)*, 173-182.

Keeley, J., & Sandquist, D. (1992). Carbon: freshwater plants. *Plant, Cell & Environment, 15(9)*, 1021-1035.

Keeling, C., Mook, W., & Tans, P. (1979). Recent trends in the $^{13}C/^{12}C$ ratio of atmospheric carbon dioxide. *Nature, 227*, 121-123.

Keeling, C., Piper, S., Bacastow, R., Wahlen, M., Whorf, T., Heimann, M., et al. (2001). Exchanges of atmospheric CO_2 and $^{13}CO_2$ with the terrestrial biosphere and oceans from 1978 to 2000. I. global aspects. *Scripps Institution of Oceanography*, Reference No. 00-21.

Keith, M., & Weber, J. (1964). Carbon and oxygen isotopic composition of selected limestones and fossils. *Geochimica et Cosmochimica Acta, 28(10)*, 1787-1816.

Keizer, P., Gajewski, K., & McLeman, R. (2015). Forest dynamics in relation to multi-decadal late-Holocene climatic. *Review of Palaeobotany and Palynology, 219*, 106-115.

Kilgour, B., & Mackie, G. (1991). Relationships between demographic features of a pill clam (*Pisidium casertanum*) and environmental variables. *Journal of the North American Benthological Society, 10(1)*, 68-80.

Killeen, I., Aldridge, D., Oliver, G., & Council, F. (2004). *Freshwater Bivalves of Britain and Ireland.* Field Studies Council.

Kim, S. T., & O'Neil, J. R. (1997). Equilibrium and nonequilibrium oxygen isotope effects in synthetic carbonates. *Geochimica et Cosmochimica Acta, 61*, 3461-3475.

Kirby, M. E., Poulsen, C. J., Lund, S. P., Patterson, W. P., Reidy, L., & Hammond, D. E. (2004). Late Holocene lake level dynamics inferred from magnetic susceptibility

and stable oxygen isotope data: Lake Elsinore, southern California (USA). *Journal of Paleolimnology, 31*, 275-293.

Kling, G., Hayhoe, K., Johnson, L., Magnuson, J., Ploasky, S., Robinson, S., et al. (2003). Confronting climate change in the Great Lakes. *Union of Concerned Scientists*, 92.

Koener, R. (1977). Devon Island ice cap: core stratigraphy and paleoclimate. *Science, 196(4285)*, 15-18.

Koener, R., & Fisher, D. (1990). A record of Holocene summer climate from a Canadian high-Arctic ice core. *Nature, 343*, 630-631.

Korhola, A., Vasko, K., Toivonen, H., & Olander, H. (2002). Holocene temperature changes in northern Fennoscandia reconstructed from chironomids using Bayesian modelling. *Quaternary Science Reviews, 21(16)*, 1841-1860.

Lafontaine-Boyer, K., & Gajewski, K. (2014). Vegetation dynamics in relation to late Holocene climate variability and disturbance, Outaouais, Quebec, Canada. *The Holocene, 24(11)*, 1515-1526.

Laird, K. R., Haig, H. A., Ma, S., Kingsbury, M. V., Brown, T. A., Lewis, C. M., et al. (2012). Expanded spatial extent of the Medieval Climate Anomaly revealed in lake-sediment records across the boreal region in northwest Ontario. *Global Change Biology, 18*, 2869-2881.

Lajewski, C., Mullins, H., Patterson, W., & Callinan, C. (2003). Historic calcite record from the Finger Lakes, New York: impact of acid rain on a buffered terrane. *Geological Society of America Bulletin, 115(3)*, 373-384.

Lamb, H., Leng, M., Telford, R., Ayenew, T., & Umer, M. (2007). Oxygen and carbon isotope composition of authigenic carbonate from an Ethiopian lake: a climate record of the last 2000 years. *The Holocene, 17(4)*, 517-526.

Langenfelds, R., Francey, R., Park, B., Steele, L., Lloyd, J., Trudinger, C., et al. (2002). Interannual growth rate variations of atmospheric CO_2 and its $\delta^{13}C$, H_2, CH_4, and CO between 1992 and 1999 linked to biomass burning. *Global Biogeochemical Cycles, 16(3)*, 21-1.

Lavens, P., & Sorgeloos, P. (1996). *Manual on the Production and Use of Live Food for Aquaculture* (No. 361). Food and agriculture organization (FAO).

Leng, M. J., & Marshall, J. D. (2004). Paleoclimate interpretation of stable isotope data from lake sediment archives. *Quaternary Science Reviews, 23(7)*, 811-831.

Leng, M., & Henderson, A. (2013). Recent advances in isotopes as palaeolimnological proxies. *Journal of Paleolimnology, 49(3)*, 481-496.

Leng, M., Lamb, A., Lamb, H., & Telford, R. (1999). Palaeoclimatic implications of isotopic data from modern and early Holocene shells of the freshwater snail *Melanoides tuberculata*, from lakes in the Ethiopian Rift Valley. *Journal of Paleolimnology, 21(1)*, 97-106.

Leuenberger, M., Siegenthaler, U., & Langway, C. (1992). Carbon isotope composition of atmospheric CO_2 during the last ice age from an Antarctic ice core. *Nature, 357*, 488-490.

Lewis, C., Cameron, G., Anderson, T., Heil Jr, C., & Gareau, P. (2012). Lake levels in the Erie basin of the Laurentian Great Lakes. *Journal of paleolimnology, 47(3)*, 493-511.

Lewis, C., Moore, T., Rea, D., Dettman, D., Smith, A., & Mayer, L. (1994). Lakes of the Huron basin: their record of runoff from the Laurentide Ice Sheet. *Quaternary Science Reviews, 13(9)*, 891-922.

Li, H., & Ku, T. (1997). $\delta^{13}C$–$\delta^{18}O$ covariance as a paleohydrological indicator for closed-basin lakes. *Palaeogeography, Palaeoclimatology, Palaeoecology, 133(1)*, 69-80.

Li, H., Bischoff, J., Ku, T., Lund, S., & Stott, L. (2000). Climate variability in east-central California during the past 1000 years reflected by high-resolution geochemical and isotopic records from Owens Lake sediments. *Quaternary Research, 54(2)*, 189-197.

Li, L., Yu, Z., Moeller, R., & Bebout, G. (2008). Complex trajectories of aquatic and terrestrial ecosystem shifts caused by multiple human-induced environmental stresses. *Geochimica et Cosmochimica Acta, 72(17)*, 4338-4351.

Libby, W., Anderson, E., & Arnold, J. (1949). Age determination by radiocarbon content: world-wide assay of natural radiocarbon. *Science, 109(2827)*, 227-228.

Liberty. (1969). Paleozoic geology of the Lake Simcoe area, Ontario. *Department of Energy, Mines and Resources*, Geologiacl Survey of Canada.

Lister, G., Kelts, K., Zao, C., Yu, J., & Niessen, F. (1991). Lake Qinghai, China: closed-basin like levels and the oxygen isotope record for ostracoda since the latest Pleistocene. *Palaeogeography, Palaeoclimatology, Palaeoecology, 84(1)*, 141-162.

Lister, G., Kelts, K., Zao, C., Yu, J., & Niessen, F. (1991). Lake Qinghai, China: closed-basin like levels and the oxygen isotope record for ostracoda since the latest Pleistocene. *Palaeogeography, Palaeoclimatology, Palaeoecology, 84(1)*, 141-162.

Longstaffe, F., Ayalon, A., & Skuce, M. (2014). Freshwater oxygen and hydrogen isotope baseline for the Great Lakes region. *AAPG Datapages/Search and Discovery Article #90195*.

Lu, Y., Meyers, P. A., Eadie, B. J., & Robbins, J. A. (2010). Carbon cycling in Lake Erie during cultural eutrophication over the last century inferred from the stable carbon isotope composition of sediments. *Journal of Paleolimnology, 43(2)*, 261-272.

Lürling, M., Eshetu, F., Faassen, E., Kosten, S., & Huszar, V. (2013). Comparison of cyanobacterial and green algal growth rates at different temperatures. *Freshwater Biology, 58(3)*, 552-559.

Macdonald, R. (2012). Late Quaternary histories of Lakes Huron and Michigan: a stable isotope investigation of sediment cores and modern biogenic carbonates. *Electronic Thesis and Dissertation Repository. Paper 457. http://ir.lib.uwo.ca/etd/457*

MacKenzie, A., Hardie, S., Farmer, J., Eades, L., & Pulford, I. (2011). Analytical and sampling constraints in ^{210}Pb dating. *Science of the Total Environment, 409(7)*, 1298-1304.

Maclachlan, J. C., & Eyles, C. H. (2013). Quantitative geomorphological analysis of drumlins in the Peterborough drumlin field, Ontario, Canada. *Geografiska Annaler: Series A, Physical Geography*, 125-144.

Marcenko, E., Srdoc, D., Golubic, S., Pezdic, J., & Head, M. (1989). Carbon uptake in aquatic plants deduced from their natural ^{13}C and ^{14}C content. *Radiocarbon, 31(3)*, 785-794.

Marty, J., & Myrbo, A. (2014). Radiocarbon dating suitability of aquatic plant macrofossils. *Journal of Paleolimnology, 52(4)*, 435-443.

McAndrews, J. H. (1984). Late Quaternary vegetation history of Rice Lake, Ontario, and the McIntyre archaeological site. *The McIntyresite: Archaeology, Subsistence and Environment. Archaeological survey of Canada, Paper, 126*, 161-189.

McAndrews, J., & Boyko-Diakonow, M. (1989). Pollen analysis of varved sediment at Crawford Lake, Ontario: evidence of Indian and European farming. *Quaternary Geology of Canada and Greenland,* Fulton, R.J. ed. *Geological Survey of Canada, Ottawa, Ontario,* 528-530.

McConnaughey, T. (1989a). ^{13}C and ^{18}O isotopic disequilibrium in biological carbonates: I Patterns. *Geochimica et Cosmochimica Acta, 53(1)*, 151-162.

McCommaughey, T. (1989b). ^{13}C and ^{18}O isotopic disequilibrium in biological carbonates: II. In vitro simulation of kinetic isotope effects. *Geochimica et Cosmochimica Acta, 53(1)*, 163-171.

McConnaughey, T., Burdett, J., Whelan, J., & Paull, C. (1997). Carbon isotopes in biological carbonates: respiration and photosynthesis. *Geochimica et Cosmochimica Acta, 61(3)*, 611-622.

McFadden, M. A., Mullins, H. T., Patterson, W. P., & Anderson, W. T. (2004). Paleoproductivity of eastern Lake Ontario over the past 10,000 years. *Limnology and Oceanography, 49(5)*, 1570-1581.

McKenzie, J. (1993). Pluvial conditions in the eastern Sahara following the penultimate degglaciation: implications for changes in atmospheric circulation patterns with global warming. Palaeogeography, Palaeoclimatology, Palaeoecology, 103(1), 95-105.

McKenzie, J., & Hollander, D. (1993). Oxygen-isotope record in recent carbonate sediments from Lake Greifen, Switzerland (1750–1986): application of continental isotopic indicator for evaluation of changes in climate and atmospheric circulation patterns. *Climate Change in Continental Isotopic Records*, 101-111.

Merz, M. (1992). The biology of carbonate precipitation by cyanobacteria. *Facies, 26(1)*, 81-101.

Meyers, P. A. (1994). Preservation of elemental and isotopic source identification of sedimentary organic matter. *Chemical Geology, 114(3)*, 289-302.

Meyers, P. A. (2003). Applications of organic geochemistry to paleolimnological reconstructions: a summary of examples from the Laurentian Great Lakes. *Organic Geochemistry, 34(2)*, 261-289.

Meyers, P. A., & Ishiwatari, R. (1993). Lacustrine organic geochemistry- an overview of indicators of organic matter sources and diagenesis in lake sediments. *Organic Geochemistry, 20(7)*, 867-900.

Meyers, P. A., & Lallier-Vergès, E. (1999). Lacustrine sedimentary organic matter records of Late Quaternary paleoclimates. *Journal of Paleolimnology, 21(3)*, pp. 345-372.

Meyers, P. A., & Teranes, J. L. (2001). Sediment organic matter. In *Tracking Environmental Change Using Lake Sediments*, Smol, J., Birks, H. & Last, W. (Eds.), (pp. 239-269). Springer Netherlands.

Mook, W. G., Bommerson, J. C., & Steverman, W. H. (1974). Carbon isotope fractionation between dissolved bicaronate and gaseous carbon dioxide. *Earth and Planetary Science Letters. 22(2)*, 169-176.

Moore Jr, T., Rea, D., & Godsey, H. (1998). Regional variation in modern radiocarbon ages and the hard-water effects in Lakes Michigan and Huron. *Journal of Paleolimnology, 20(4)*, 347-351.

Norton, S., Hess, C., Blake, G., Morrison, M., & Baron, J. (1985). Excess unsupported ^{210}Pb in lake sediment from Rocky Mountain lakes: a groundwater effect. *Canadian Journal of Fisheries and Aquatic Sciences, 42(7)*, 1249-1254.

O'Beirne, M., Strzok, L., Werne, J., Johnson, T., & Hecky, R. (2015). Anthropogenic influences on the sedimentary geochemical record in western Lake Superior (1800–present). *Journal of Great Lakes Research, 41(1)*, 20-29.

Oldfield, F., & Appleby, P. (1984). Empirical testing of ^{210}Pb-dating models for lake sediments. In *Lake Sediments and Environmental History*, Haworth, E.Y. &Lund, J.G. (Eds.), Leicester University Press: 93-124.

O'Leary, M. (1988). Carbon isotopes in photosynthesis. *Bioscience, 38(5)*, 328-336.

Olsson, I. (1983). Dating non-terrestrial materials. In *Proceedings of the First International Symposium ^{14}C and Archaeology*, Mook, W. & Waterbolk, H. (Eds.), 8, 277-294.

Olsson, I. (2009). Radiocarbon dating history: early days, questions, and problems met. *Radiocarbon, 51(1)*, 1-43.

Ontario Geological Survey (1991). Bedrock geology of Ontario, southern sheet. *Ontario Geological Survey*, Map 2544, scale 1:1,000,000.

O'Reilly, J., Vintro, L., Mitchell, P., Donohue, I., Leira, M., Hobbs, W., et al. (2011). ^{210}Pb-dating of a lake sediment core from Lough Carra (Co. Mayo, western Ireland): use of paleolimnological data for chronology validation below the ^{210}Pb dating horizon. *Journal of Environmental Radioactivity, 102(5)*, 495-499.

Oswald, W., Anderson, P., Brown, T., Brubaker, L., Hu, F., Lozhkin, A., et al. (2005). Effects of sample mass and macrofossil type on radiocarbon dating of arctic and boreal lake sediments. *The Holocene, 15(5)*, 758-767.

Otsuki, A., & Wetzel, R. (1974). Calcium and total alkalinity budges and calcium carbonate precipitation of a small hardwater lake. *Archive fur Hydrogiologie, 73(1)*, 14-30.

PAGES 2k Consortium. (2013). Continental-scale temperature variability during the past two millennia. *Nature Geoscience, 6*, 339-346.

Paquette, N., & Gajewski, K. (2013). Climatic change causes abrupt changes in forest composition, inferred from a high-resolution pollen record, southwestern Quebec, Canada. *Quaternary Science Reviews, 75(1)*, 169-180.

Pennington, W., Tutin, T., Cambray, R., & Fisher, E. (1973). Observations on lake sediments using fallout ^{137}Cs as a tracer. *Nature, 242*, 324-326.

Pennington, W., Cambray, R., Eakins, J., & Harkness, D. (1976). Radionuclide dating of the recent sediments of Blelham Tarn. *Freshwater Biology, 6(4)*, 317-331.

Peterson, B., Howarth, R., & Garritt, R. (1985). Multiple stable isotopes used to trace the flow of organic matter in estuarine food webs. *Science, 227(4692)*, 1361-1363.

Pilbeam, D. (2010). The utilization of nitrogen by plants: a whole plant perspective. *Annual Plant Reviews, 42: Nitrogen metabolism in plants in the Post-Genomic Era*, 305-351.

Qi, H., Coplen, T., Geilmann, H., Brand, W., & Bohlke, J. (2003). Two new organic reference materials for $\delta^{13}C$ and $\delta^{15}N$ measurements and a new value for the $\delta^{13}C$ of NBS 22 oil. *Rapid Communications in Mass Spectrometry, 17(22)*, 2483-2487.

Rea, D., & Colman, S. (1995). Radiocarbon ages of pre-bomb clams and the hard-water effect in Lakes Michigan and Huron. *Journal of Paleolimnology, 14(1)*, 89-91.

Rea, D., Moore Jr, T., Lewis, C., Mayer, L., Dettman, D., Smith, A., et al. (1994). Stratigraphy and paleolimnologic record of lower Holocene sediments in northern Lake Huron and Georgian Bay. *Canadian Journal of Earth Sciences, 31(11)*, 1586-1605.

Reimer, P. J., Bard, E., Bayliss, A., Beck, J. W., Blackwell, P. G. Ramsey, C. B., et al. (2013). IntCal 13 and Marine 13 radiocarbon age calibration curves 0-50,000 years cal BP. *Radiocarbon, 55(4)*, 1869-1887.

Reynolds, C. (1984). *The Ecology of Freshwater Phytoplankton.* Cambridge University Press.

Rickard, D. (1970). The origin of framboids. *Lithos, 3(3)*, 269-293.

Ricketts, R., & Johnson, T. (1996). Climate change in the Turkana basin as deduced from a 4000 year long $\delta^{18}O$ record. *Earth and Planetary Science Letters, 142(1)*, 7-17.

Ritchle, J., McHenry, J., & Gill, A. (1973). Dating recent reservoir sediments. *Limnology and Oceanography, 18(2)*, 254-263.

Romanek, C., Grossman, E., & Morse, J. (1992). Carbon isotopic fractionation in synthetic aragonite and calcite: effects of temperature and precipitation rate. *Geochimica et Cosmochimica Acta, 56(1)*, 419-430.

Routh, J., Choudhary, P., Meyers, P. A., & Kumar, B. (2009). A sediment record of recent nutrient loading and trophic state change in Lake Norrviken, Sweden. *Journal of Paleolimnology, 42(3)*, 325-341.

Routh, J., Meyers, P., Hjorth, T., Baskaran, M., & Hallberg, R. (2007). Sedimentary geochemical record of recent environmental changes around Lake Middle Marviken, Sweden. *Journal of Paleolimnology, 37(4)*, 529-545.

Rozanski, K., Araguas-Araguas, L., & Gonfiantini, R. (1993). Isotopic patterns in modern global precipitation. *Climate Change in Continental Isotopic Records*, 1-36.

Ruiz-Fernández, A., & Hillaire-Marcel, C. (2009). ^{210}Pb-derived ages for the reconstruction of terrestrial contaminant history into the Mexican Pacific coast: potential and limitations. *Marine Pollution Bulletin, 59(4)*, 134-145.

Russell, A., & Knudsen, O. (1999). Controls on the sedimentology of the November 1996 jokulhlaup deposits, Skeioararsandur, Iceland. In *Fluvial Sedimentology VI, Special Publication no. 28, International Association of Sedimentologists*, Smith, N. & Rogers, J. (Eds.), 315-329). Oxford, UK: Blackwell Scientific.

Schelske, C. L., & Hodell, D. A. (1991). Recent changes in productivity and climate of Lake Ontario detected by isotopic analysis of sediments. *Limnology and Oceanography, 49*, 1560-1569.

Schueler, F. W., & Karstad, A. (2012). Introduction to the aquatic "macro" invertebrates of southern, especially eastern Ontario. Bishops Mills Natural History Centre. Retrieved May 2015, from PINICOLA: pinicola.ca/invert_Tay.pdf

Schweingruber, F., Briffa, K., & Jones, P. (1991). Yearly maps of summer temperatures in western Europe from AD 1750 to 1975 and western North America from 1600 to 1982. *Vegetatio, 92(1)*, 5-71.

Scripps CO_2 Program, (2015). *Isotopic Data*. Retrieved June 2015, from http://scrippsco2.ucsd.edu/graphics_gallery/isotopic_data

Seltzer, G., Rodbell, D., & Burns, S. (2000). Isotopic evidence for late Quaternary climatic change in tropical South America. *Geology, 28(1)*, 35-38.

Sensula, B., Bottger, T., Pazdur, A., Piotrowska, N., & Wagner, R. (2006). Carbon and oxygen isotope composition of organic matter and carbonates in recent lacustrine sediments. *Geochronometria, 25*, 77-94.

Shanahan, T., Pigati, J., Dettman, D., & Quade, J. (2005). Isotopic variability in the aragonite shells of freshwater gastropods living in springs with nearly constant temperature and isotopic composition. *Geochimica et Cosmochimica Acta, 69(16)*, 3959-3966.

Sharma, S., Gray, D. K., Read, J. S., O'Reilly, C. M., Schneider, P., Qudrat, A. et al. (2015). A global database of lake surface temperatures collected by in situ and satellite methods from 1985-2009. Scientific data, 2.

Sharp, Z. (2007). *Principles of Stable Isotope Geochemistry.* Upper Saddle River, NJ: Pearson Education.

Sharpe, D. (1987). The stratified nature of drumlins from Victoria Island and southern Ontario, Canada. *Drumlin Symposium*, 185-214. Balkema, Rotterdam.

Shaw, J., & Sharpe, D. (1987). Drumlin formation by subglacial meltwater erosion. *Canadian Journal of Earth Sciences, 24(11)*, 2316-2322.

Sifeddine, A., Meyers, P. A., Cordeiro, R. C., Albuquerque, A. L. S., Bernardem, M., Turcq, B., Abrão, J. J. (2011). Delivery and deposition of organic matter in surfach sediments of Lagoa do Cacó (Brazil). *Journal of Paleolimnology, 45*, 385-396.

Sonnenburg, E., Boyce, J., & Reinhardt, E. (2013). Multi-proxy lake sediment record of prehistoric (Paleoindian–Archaic) archaeological paleoenvironments at Rice Lake, Ontario, Canada. *Quaternary Science Reviews, 73*, 77-92.

St.Jacques, J., Cumming, B., & Smol, J. (2008). A 900-year pollen-inferred temperature and effective moisture record from varved Lake Mina, west-central Minnesota, USA. *Quaternary Science Reviews, 27(7)*, 781-796.

Stabel, H. (1986). Calcite precipitation in Lake Constance: chemical equilibrium sedimentation, and nucleation by algae. *Limnology and Oceanography, 31(3)*, 1081-1093.

Stankowski, W., Muszynski, A., Klimm, K., & Schliestedt, M. (2002). Mineralogy of Morasko meteorite and the structure of the craters. In *Proceedings of the Estonian Academy of Sciences - Geology, 51*, 227-240. Los Angeles, CA: Allen Hancock Foundation.

Strong, A. (1978). Chemical whitings and chlorophyll distributions in the Great Lakes as viewed by Landsat. *Remote Sensing of Environment, 7(1)*, 61-72.

Strong, A., & Eadie, B. (1978). Satellite observations of calcium carbonate precipitations in the Great Lakes. *Limnology and Oceanography, 23(5)*, 877-887.

Szpak, P., White, C., Longstaffe, F., Millaire, J., & Vasquez Sanchez, V. (2013). Carbon and nitrogen isotopic survey of northern Peruvian plants: baselines for paleodietary and paleoecological studies. *PloS one, 8(1)*, e53763.

Talbot, M. (1990). A review of the palaeohydrological interpretation of carbon and oxygen isotopic ratios in primary lacustrine carbonates. *Chemical Geology: Isotope Geoscience Section, 80(4)*, 261-279.

Talbot, M. (2001). Nitrogen isotopes in palaeolimnology. In *Tracking Environmental Change Using Lake Sediments,* Smol, J., Birks, H. & Last, W. (Eds.), (pp. 401-439). Springer Netherlands.

Talbot, M., & Kelts, K. (1986). Primary and diagenetic carbonates in the anoxic sediments of Lake Bosumtwi, Ghana. *Geology, 14(11)*, 912-916.

Talbot, M., & Laerdal, T. (2000). The late Pleistocene-Holocene paleolimnology of Lake Victoriia, east Africa, based upon elemental and isotoipc analyses of sedimentary organic matter. *Journal of Paleolimnology, 23*, 141-164.

Talbot, M., & Livingstone, D. (1989). Hydrogen index and carbon isotopes of lacustrine organic matter as lake level indicators. *Palaeogeography, Palaeoclimatology, Palaeoecology, 70(1)*, 121-137.

Teranes, J., & Bernasconi, S. (2000). The record of nitrate utilization and productivity limitation provided by δ^{15}N values in lake organic matter—a study of sediment trap and core sediments from Baldeggersee, Switzerland. *Limnology and Oceanography, 45(4)*, 801-813.

Terasmae, J. (1979). Radiocarbon dating and palynology of glacial Lake Nipissing deposits at Wasaga Beach, Ontario. *Journal of Great Lakes Research, 5(3)*, 292-300.

Thompson, S., & Eglinton, G. (1978). The fractionation of a recent sediment for organic geochemical analysis. *Geochimica et Cosmochimica Acta, 42(2)*, 199-207.

Tohonen, M. (1984). Differences in pollen and macrophytic remains in sediments from various depths in a small kettle-hole lake in southern Finland. *Boreas, 13*, 403-412.

Torres, I., Inglett, P., Brenner, M., Kenney, W., & Reddy, K. (2012). Stable isotope (δ^{13}C and δ^{15}N) values of sediment organic matter in subtropical lakes of different trophic status. *Journal of paleolimnology, 47(4)*, 693-706.

Turekian, K., Benninger, L., & Dion, E. (1983). ^{7}Be and ^{210}Pb total deposition fluxes at New Haven, Connecticut and at Bermuda. *Journal of Geophysical Research: Oceans (1978–2012), 88(C9)*, 5411-5415.

Verburg, P. (2007). The need to correct for the Suess effect in the application of δ^{13}C in sediment of autotrophic Lake Tanganyika, as a productivity proxy in the Anthropocene. *Journal of Paleolimnology, 37(4)*, 591-602.

Verrecchia, E. P., & Verrecchia, K. E. (1994). Needle-fiber calcite: a critical review and a proposed classification. *Journal of Sedimentary Research, 64(3)*, 650-664.

von Grafenstein, U., Erlernkeuser, H., & Trimborn, P. (1999). Oxygen and carbon isotopes in modern fresh-water ostracod valves: assessing vital offsets and autecological effects of interest for palaeoclimate studies. *Palaeogeography, Palaeoclimatology, Palaeoecology, 148(1)*, 133-152.

Watchorn, M., Hamilton, P., & Patterson, R. (2013). The paleolimnology of Haynes Lake, Oak Ridges Moraine, Ontario, Canada: documenting anthropogenic and climatic disturbances. *Environmental Earth Sciences, 68(7)*, 1823-1834.

Werner, E., Skelly, D., Relyea, R., & Yurewicz, K. (2007). Amphibian species richness across environmental gradients. *Oikos, 116*, 1697-1712.

Wetzel, R. (2001). *Limnology: Lake and River Ecosystems.* Gulf Professional Publishing.

Wolfe, A., Baron, J., & Cornett, R. (2001). Anthropogenic nitrogen deposition induces rapid ecological changes in alpine lakes of the Colorado Front Range (USA). *Journal of Paleolimnology, 25(1)*, 1-7.

Wood, T., Thorp, J., & Covich, A. (2010). *Ecology and Classification of North American Freshwater Invertebrates.* Academic Press.

Woszczyk, M., Grassineau, N., Tylmann, W., Kowalewski, G., Lutynska, M., & Bechtel, A. (2014). Stable C and N isotope record of short term changes in water level in lakes of different morphometry: Lake Anastazewo and Lake Skulskie, central Poland. *Organic Geochemistry*, *76*, 278-287.

Xiao, J., Chang, Z., Si, B., Qin, X., Itoh, S., & Lomtatidze, Z. (2009). Partitioning of the grain-size components of Dali Lake core sediments: evidence for lake-level changes during the Holocene. *Journal of Paleolimnology, 42(2)*, 249-260.

Yakir, D. (2011). The paper trail of the ^{13}C of atmospheric CO_2 since the industrial revolution period. *Environmental Research Letters, 6(3)*, 034007.

Yoneyama, T., Ito, O., & Engelaar, W. (2003). Uptake, metabolism and distribution of nitrogen in crop plants traced by enriched and natural ^{15}N: progress over the last 30 years. *Phytochemistry Reviews, 2(1-2)*, 121-132.

Yoshimura, T., Izumida, H., Nakashima, R., Ishimura, T., Shikazono, N., Kawahata, H., et al. (2015). Stable carbon isotope values in dissolved inorganic carbon of ambient waters and shell carbonate of the freshwater pearl mussel (*Hyriopsis* sp.). *Journal of Paleolimnology, 54(1)*, 37-51.

Yu, S., Berglund, B., Sandgren, P., & Colman, S. (2007). Holocene organic carbon burial rates in the southeastern Swedish Baltic Sea. *The Holocene, 17(5)*, 673-681.

Zhao, Y., Wu, F., Fang, X., & Yang, Y. (2015). Topsoil C/N ratios in the Qilian Mountains area: implications for the use of subaqueous sediment C/N ratios in paleo-environmental reconstructions to indicate organic sources. *Palaeogeography, Palaeoclimatology, Palaeoecology*, *426*, 1-9.

Appendices

Appendix A Results obtained for isotopic and elemental standards

Water

Standards	δ^2H (‰, VSMOW)	Standards	δ^{18}O (‰, VSMOW)	DIC Standards	δ^{13}C (‰, VPDB)	DIC Standards	δ^{13}C (‰, VPDB)
LSD	–157	LSD	–22.6	NBS–19	+1.9	Suprapur	–35.5
LSD	–164	LSD	–22.5	NBS–19	+2.0	Suprapur	–35.6
LSD	–164	HEAVEN	–0.2	NBS–19	+2.0	Suprapur	–35.5
HEAVEN	+91	HEAVEN	–0.3	NBS–19	+1.9	Suprapur	–35.6
HEAVEN	+89	MID	–12.8	NBS–19	+2.0	Suprapur	–35.6
HEAVEN	+86	MID	–13.3	LSVEC	–46.7	WS–1	+0.8
MID	–105	EDT	–7.1	LSVEC	–46.5	WS–1	+0.8
MID	–109	EDT	–7.5	LSVEC	–46.5	WS–1	+0.9
MID	–107	EDT	–7.7	LSVEC	–46.7	WS–1	+0.7
EDT	–54	EDT	–7.5	LSVEC	–46.6	WS–1	+0.8
EDT	–53			NBS–18	–5.2		
EDT	–54			NBS–18	–5.1		
EDT	–56			NBS–18	–5.1		
EDT	–54			NBS–18	–5.1		
EDT	–56			NBS–18	–5.1		

Carbonate

Standards for shell analyses	$\delta^{13}C$ (‰, VPDB)	$\delta^{18}O$ (‰, VSMOW)	Standards for shell analyses	$\delta^{13}C$ (‰, VPDB)	$\delta^{18}O$ (‰, VSMOW)
NBS–19	+1.9	+28.7	NBS–18	–5.1	+7.3
NBS–19	+2.0	+28.7	NBS–18	–5.0	+7.2
NBS–19	+2.0	+28.7	NBS–18	–5.1	+7.1
NBS–19	+1.9	+28.5	NBS–18	–4.9	+7.2
NBS–19	+2.0	+28.7	NBS–18	–5.1	+7.1
NBS–19	+2.0	+28.6	NBS–18	–5.0	+7.3
NBS–19	+2.0	+28.6	NBS–18	–4.9	+7.2
NBS–19	+1.9	+28.7	NBS–18	–5.1	+7.4
NBS–19	+1.9	+28.7	NBS–18	–5.0	+7.3
LSVEC	–46.6	+3.9	WS–1	+0.8	+26.4
LSVEC	–46.6	+4.0	WS–1	+0.7	+26.2
LSVEC	–46.5	+4.1	Suprapur	–35.7	+13.2
LSVEC	–46.7	+4.1	Suprapur	–35.7	+13.1
LSVEC	–46.4	+4.2			
LSVEC	–46.6	+4.1			
LSVEC	–46.6	+4.0			

Standards for authigenic calcite analyses	$\delta^{13}C$ (‰, VPDB)	$\delta^{18}O$ (‰, VSMOW)	Standards for authigenic calcite analyses	$\delta^{13}C$ (‰, VPDB)	$\delta^{18}O$ (‰, VSMOW)
NBS–19	+1.9	+28.7	NBS–18	–5.1	+7.2
NBS–19	+2.0	+28.6	NBS–18	–5.2	+7.4
NBS–19	+2.0	+28.6	NBS–18	–5.0	+7.2
NBS–19	+1.9	+28.5	NBS–18	–5.1	+7.2
NBS–19	+2.0	+28.7	NBS–18	–5.1	+7.2
NBS–19	+2.0	+28.5	NBS–18	–5.0	+7.2
NBS–19	+2.0	+28.6	NBS–18	–5.2	+7.2
NBS–19	+1.9	+28.6	LSVEC	–46.6	+4.0
NBS–19	+1.9	+28.6	LSVEC	–38.1	+3.9
NBS–19	+2.0	+28.6	LSVEC	–46.6	+4.0
NBS–19	+1.9	+28.6	LSVEC	–46.6	+4.1
NBS–19	+2.0	+28.6	LSVEC	–46.5	+4.1
NBS–19	+1.9	+28.6	LSVEC	–46.7	+4.1
NBS–19	+2.0	+28.5	LSVEC	–46.4	+4.1
NBS–19	+2.0	+28.6	LSVEC	–46.6	+4.1
NBS–19	+1.9	+28.6	LSVEC	–46.6	+4.0
NBS–19	+1.9	+28.6	LSVEC	–46.7	+4.0
NBS–19	+1.9	+28.6	LSVEC	–46.6	+4.1
NBS–19	+2.0	+28.6	LSVEC	–46.2	+4.0
NBS–19	+2.0	+28.7	LSVEC	–46.8	+4.0
NBS–19	+1.9	+28.6	LSVEC	–46.4	+4.2
NBS–19	+1.9	+28.5	LSVEC	–46.7	+4.0
NBS–18	–5.1	+7.3	LSVEC	–46.5	+4.1
NBS–18	–5.0	+7.2	LSVEC	–46.8	+3.9
NBS–18	–5.1	+7.1	Suprapur	–35.7	+13.2
NBS–18	–4.9	+7.2	Suprapur	–35.7	+13.0
NBS–18	–5.1	+7.1	Suprapur	–35.7	+13.1
NBS–18	–5.0	+7.3	Suprapur	–35.5	+13.2
NBS–18	–4.9	+7.2	Suprapur	–35.7	+13.2
NBS–18	–5.1	+7.2	Suprapur	–35.6	+13.2
NBS–18	–5.0	+7.3	WS–1	+0.8	+26.3
NBS–18	–5.1	+7.1	WS 1	+0.7	+26.1
NBS–18	–5.1	+7.2	WS–1	+0.8	+26.2
NBS–18	–5.0	+7.1	WS–1	+0.8	+26.3
NBS–18	–5.1	+7.1			

Bulk organic matter

Total Nitrogen analyses

Standards	TN (%)	Standards	TN (%)
HighOrg	0.46	LowOrg	0.15
HighOrg	0.45	LowOrg	0.15
HighOrg	0.45	LowOrg	0.13
HighOrg	0.47	LowOrg	0.13
HighOrg	0.47	LowOrg	0.13
HighOrg	0.47	LowOrg	0.13
HighOrg	0.46	LowOrg	0.13
HighOrg	0.48	LowOrg	0.13
HighOrg	0.45	LowOrg	0.13
HighOrg	0.46	LowOrg	0.13
HighOrg	0.46	LowOrg	0.13
HighOrg	0.46	LowOrg	0.13
HighOrg	0.46	LowOrg	0.13
HighOrg	0.46	Peach leaf	2.90
HighOrg	0.46	Peach leaf	2.94
HighOrg	0.46	Peach leaf	2.90
HighOrg	0.46	Peach leaf	2.90
HighOrg	0.45	Peach leaf	2.92
HighOrg	0.46	Peach leaf	2.97
HighOrg	0.46	Peach leaf	2.91
HighOrg	0.46	Peach leaf	2.91
HighOrg	0.46	Peach leaf	2.93
HighOrg	0.46		
HighOrg	0.46		

Total Organic Carbon analyses

Standards	TOC (%)	Standards	TOC (%)
HighOrg (untreated)	6.06	HighOrg (untreated)	6.17
HighOrg (untreated)	6.11	HighOrg (untreated)	6.00
HighOrg (untreated)	6.11	HighOrg (untreated)	6.34
HighOrg (untreated)	6.10	HighOrg (untreated)	6.14
HighOrg (untreated)	6.39	HighOrg (untreated)	6.17
HighOrg (untreated)	6.12	HighOrg (untreated)	6.15
HighOrg (untreated)	6.06	HighOrg (untreated)	6.05
HighOrg (untreated)	6.13	HighOrg (untreated)	5.95
HighOrg (untreated)	5.99	HighOrg (untreated)	5.95
HighOrg (untreated)	5.91	Peach leaf (untreated)	46.37
HighOrg (untreated)	6.08	Peach leaf (untreated)	46.24
HighOrg (untreated)	6.12	Peach leaf (untreated)	46.52
HighOrg (untreated)	6.06	Peach leaf (untreated)	46.23
HighOrg (untreated)	6.08	Peach leaf (untreated)	46.01

*Low Org= Low Organic Content Soil, percent total organic carbon (TOC) and total nitrogen (TN) are defined by calibration curve.
*High Org= High Organic Content Soil, percent total organic carbon (TOC) and total nitrogen (TN) are defined by calibration curve.
*Peach leaf total organic carbon (TOC) and total nitrogen (TN) contents are defined independently from calibration curve.

Bulk Organic matter isotopic analyses

Standards	δ^{13}C (‰, VPDB)	Standards	δ^{13}C (‰, VPDB)	Standards	δ^{15}N (‰, AIR)	Standards	δ^{15}N (‰, AIR)
Keratin	–24.0	USGS 40	–26.4	Keratin	+6.3	USGS–41	+47.7
Keratin	–24.0	USGS–40	–26.4	Keratin	+6.3	USGS–41	+47.5
Keratin	–24.1	USGS–40	–26.4	Keratin	+6.3	USGS–41	+47.7
Keratin	–24.1	USGS 40	–26.4	Keratin	+6.3	USGS 41	+47.4
Keratin	–24.1	USGS 40	–26.4	Keratin	+6.5	USGS 41	+47.6
Keratin	–24.0	USGS 40	–26.4	Keratin	+6.6	USGS 41	+47.6
Keratin	–24.1	USGS 40	–26.4	Keratin	+6.4	USGS 41	+47.5
Keratin	–24.1	USGS 40	–26.4	Keratin	+6.4	USGS 41	+47.6
Keratin	–24.0	USGS–41	+37.6	Keratin	+6.5	USGS 41	+47.4
Keratin	–24.0	USGS–41	+37.8	Keratin	+6.4	USGS 41	+47.8
Keratin	–23.9	USGS–41	+37.5	Keratin	+6.4	USGS 41	+47.6
Keratin	–24.0	USGS–41	+37.6	Keratin	+6.3	USGS–40	–4.5
Keratin	–24.0	USGS–41	+37.7	Keratin	+6.4	USGS–40	–4.5
Keratin	–24.0	USGS 41	+37.6	Keratin	+6.4	USGS–40	–4.5
Keratin	–24.1	USGS 41	+37.5	Keratin	+6.4	USGS–40	–4.6
USGS–40	–26.4	USGS 41	+37.6	Keratin	+6.5	USGS 40	–4.5
USGS–40	–26.4	USGS 41	+37.6	Keratin	+6.3	USGS–40	–4.5
USGS–40	–26.4	USGS 41	+37.8	Keratin	+6.3	USGS 40	–4.5
				Keratin	+6.4	USGS 40	–4.5
				Keratin	+6.4	USGS 40	–4.6
				Keratin	+6.2	USGS 40	–4.4
				Keratin	+6.5	USGS 40	–4.6
				Keratin	+6.3	USGS 40	–4.7
				Keratin	+6.4	USGS 40	–4.3
				USGS–41	+47.5	USGS 40	–4.6
				USGS–41	+47.7	USGS 40	–4.4

Appendix B Mineral percentages of sediments in core BL–G11–01 as determined by powder X–ray diffraction (pXRD) and by isotopic analysis (for calcite)

Depth (cm)	Year (AD)	Weighted peak height (%)		Measured during isotope analyses	OM (%)*	Quartz (%)**
		Quartz by pXRD (%)	Calcite by pXRD(%)	Calcite (%)		
0.5	2011	21	79	N/A	N/A	N/A
1	2010	18	82	N/A	N/A	N/A
1.5	2009	18	82	37	28	35
2	2008	16	84	32	29	38
2.5	2006	18	82	36	30	34
3	2004	18	82	34	29	36
3.5	2002	19	81	35	28	37
4	2000	18	82	38	29	33
4.5	1998	18	82	37	28	35
5	1996	18	82	31	27	42
6	1992	17	83	39	27	34
6.5	1989	22	78	33	27	40
7	1986	17	83	35	26	39
7.5	1984	26	74	34	26	40
8	1982	23	77	33	24	43
8.5	1979	23	78	38	24	38
9	1976	25	75	35	25	41
9.5	1974	24	76	33	24	44
10	1972	23	77	31	24	45
10.5	1970	26	74	33	25	42
11	1968	25	75	30	24	46
11.5	1966	26	74	33	23	43
12	1964	27	73	33	23	44
12.5	1962	27	73	33	23	44
13	1960	25	75	36	22	43
13.5	1958	27	73	33	21	46
14	1956	30	70	30	20	49
14.5	1953	25	75	35	20	44
15	1951	25	75	31	21	49
15.5	1948	24	76	N/A	N/A	N/A
16	1945	31	69	31	21	48
16.5	1940	43	57	26	20	54
17	1936	34	66	23	22	55
17.5	1930	43	57	22	23	55
18	1924	48	52	13	24	63
18.5	1914	50	50	11	24	65
19	1905	62	38	7	24	69
19.5	1894	66	34	0	25	75
20	1882	75	25	1	26	73
20.5	1865	75	25	1	28	72
21	1849	73	27	N/A	N/A	N/A

Mineral percentages continued

21.5	1832	75	25	0	27	73
22	1816	71	29	0	27	73
22.5	1801	73	27	2	27	71
23	1785	70	30	2	28	70
23.5	1770	61	39	4	32	64
24	1755	49	51	3	40	57
24.5	1739	62	38	4	54	42
25	1723	35	65	4	61	36
25.5	1708	22	78	5	55	40
26	1692	21	79	18	51	31
26.5	1676	15	85	26	47	27
27	1660	10	90	29	46	25
27.5	1645	12	88	31	48	21
28	1629	16	84	18	51	31
28.5	1614	22	78	16	57	28
29	1598	25	75	8	57	34
29.5	1582	29	71	8	61	32
30	1567	34	66	4	63	33
30.5	1551	24	76	0	69	31
31	1535	24	76	6	67	28
31.5	1519	21	79	5	65	30
32	1504	13	80***	7	62	31
32.5	1488	13	78***	22	63	15
33	1472	14	86	8	63	29
33.5	1456	17	75***	10	62	27
34	1440	14	76***	11	62	27
34.5	1423	9	84***	8	62	30
35	1407	9	91	N/A	N/A	N/A
35.5	1393	8	84***	N/A	N/A	N/A
36	1378	10	80***	32	52	16
36.5	1368	5	87	36	48	17
37	1359	0	96***	41	36	23
37.5	1349	0	98***	57	31	12
38	1339	0	98***	61	31	9
38.5	1329	0	96***	41	34	25
39	1319	3	97	64	35	1
39.5	1308	0	94***	56	36	8
40	1298	0	93***	63	37	0
40.5	1288	0	93***	34	46	19
41	1278	4	89***	32	47	21
41.5	1268	0	93***	58	42	0

* %OM=2*%TOC (OM=organic matter; TOC=total organic carbon

** Calculated by 100%–%calcite–%OM

*** The remaining phase is aragonite

Appendix C Grain size measurements of core BL–G11–01.

Depth (cm)	Year (AD)	Median grain size (μm)*
1.5	2009	5.85
6	1992	5.30
11	1968	5.20
17.5	1930	5.02
19	1905	4.05
20.5	1865	3.65
22	1816	3.56
23.5	1770	3.46
24.5	1739	4.51
25.5	1708	4.75
27	1660	3.49
29	1598	5.00
31	1535	8.66
32	1504	6.85
33	1472	6.48
35	1407	6.72
36	1378	6.08
37.5	1349	3.51
39	1319	3.74
40.5	1288	4.91
41	1278	4.03

* median grain size is the midpoint of grain size distribution: 50% of the sediment is coarser than the size and 50% is finer than this size

Appendix D Magnetic susceptibility measurements of core BL–G11–01.

Depth (cm)	Year (AD)	Magnetic susceptibility	
		BL–G11–01 (wet)	BL–G11–02 (dry)
0.5	2011	–1	+2
1	2010	–2	+1
1.5	2009	–2	+2
2	2008	–1	+0
2.5	2006	–2	+2
3	2004	–1	+1
3.5	2002	–1	+2
4	2000	–1	+2
4.5	1998	–2	+2
5	1996	–1	+2
5.5	1994	–1	+1
6	1992	–1	+1
6.5	1989	–1	+1
7	1986	–1	+1
7.5	1984	–1	+1
8	1982	–1	+2
8.5	1979	–1	+2
9	1976	–1	+2
9.5	1974	–1	+2
10	1972	–1	+2
10.5	1970	–1	+2
11	1968	–3	+2
11.5	1966	–2	+2
12	1964	–2	+2
12.5	1962	–2	+2
13	1960	–1	+2
13.5	1958	–1	+2
14	1956	–2	+3
14.5	1953	–1	+3
15	1951	–1	+3
15.5	1948	+0	+3
16	1945	+0	+4
16.5	1940	+0	+4
17	1936	+0	+4
17.5	1930	–1	+5
18	1924	+0	+5
18.5	1914	+1	+7
19	1905	+0	+7
19.5	1894	+0	+10
20	1882	+1	+7
20.5	1865	+2	+6
21	1849	+2	+9

Magnetic susceptibility measurements continued

21.5	1832	+2	+13
22	1816	+3	+5
22.5	1801	+1	+6
23	1785	+2	+3
23.5	1770	+0	+4
24	1755	+0	+1
24.5	1739	–2	+0
25	1723	–1	+0
25.5	1708	–1	+0
26	1692	–1	+0
26.5	1676	–1	+0
27	1660	–2	+0
27.5	1645	–1	+0
28	1629	–1	+0
28.5	1614	–1	+1
29	1598	–1	+0
29.5	1582	–1	+0
30	1567	–1	+0
30.5	1551	–1	+0
31	1535	–1	+0
31.5	1519	–1	+0
32	1504	–2	+0
32.5	1488	–1	+0
33	1472	–1	+0
33.5	1456	–1	+0
34	1440	–1	+0
34.5	1423	–1	+0
35	1407	–2	+0
35.5	1393	–1	+0
36	1378	–1	+0
36.5	1368	–1	+0
37	1359	–1	+0
37.5	1349	–1	+0
38	1339	–1	+0
38.5	1329	–1	+0
39	1319	–1	+0
39.5	1308	–2	+0
40	1298	–2	+0
40.5	1288	–2	+0
41	1278	–2	+0
41.5	1268	–2	N/A

Appendix E Chemical and physical properties of modern Barry Lake water as measured on samples collected in field trips.

Field trip on May 12, 2014

Station 1 (N44 18.585 W77 55.321)

Time	1410HRS	**Secchi depth (m)**		Infinite
Depth (m)	1.3	**Top water temperature (℃)**		20
Water Depth (cm)	**Temperature (℃)**	**Specific Conductivity (*μ*S)**	**pH**	**Dissolved Oxygen (mg/L)**
50	17.5	258.3	8.2	10.51

Station 2 (N44 18.427 W77 55.264)

Time	1440HRS	**Secchi depth (m)**		3.75
Depth (m)	7.6	**Top water temperature (℃)**		18
Water Depth (cm)	**Temperature (℃)**	**Specific Conductivity (*μ*S)**	**pH**	**Dissolved Oxygen (mg/L)**
50	15.3	242.3	8.1	10.28
100	15.3	242.3	8.1	10.12
150	15.3	242.3	8.1	10.25
200	15.2	242.1	8.1	10.08
250	15.2	241.9	8.1	10.03
300	13.1	229.0	8.1	10.75
350	11.2	218.8	8.0	11.09
400	10.5	213.6	8.1	11.96
450	10.0	209.8	8.2	12.75
500	9.6	205.4	8.4	14.40
550	9.3	206.4	8.2	12.14
600	8.9	209.7	7.6	4.57
650	8.8	211.0	7.5	3.34
700	8.7	216.2	7.4	1.69
750	7.3	220.2	7.3	1.10

Field trip on May 12, 2014 continued

Station 3 (N44 18.502 W77 55.301)

Time	1535HRS	**Secchi depth (m)**		3.75
Depth (m)	7.5	**Top water temperature (℃)**		17
Water Depth (cm)	**Temperature (℃)**	**Specific Conductivity (*μ*S)**	**pH**	**Dissolved Oxygen (mg/L)**
50	15.3	242.1	8.1	10.22
100	15.3	241.8	8.1	10.12
150	15.3	242.0	8.1	10.20
200	15.3	242.0	8.1	10.03
250	15.3	241.9	8.1	10.26
300	15.3	242.0	8.1	9.81
350	11.0	216.4	8.1	11.64
400	10.1	209.5	8.2	13.25
450	9.6	205.6	8.4	14.08
500	9.3	205.6	8.2	12.82
550	9.1	207.1	7.9	9.42
600	8.8	211.0	7.6	5.06
650	8.8	212.4	7.5	3.59
700	8.7	213.1	7.4	2.62
750	8.6	214.7	7.4	1.15

Station 4 (N44 18.552 W77 55.318)

Time	1607HRS	**Secchi depth (m)**		3.75
Depth (m)	6.2	**Top water temperature (℃)**		18
Water Depth (cm)	**Temperature (℃)**	**Specific Conductivity (*μ*S)**	**pH**	**Dissolved Oxygen (mg/L)**
50	15.3	242.6	8.1	11.64
100	15.3	242.5	8.1	9.92
150	15.3	242.5	8.1	10.20
200	15.3	242.6	8.1	10.19
250	15.3	242.5	8.1	10.10
300	15.3	242.5	8.1	10.02
350	12.0	226.5	8.1	12.15
400	10.2	210.9	8.2	13.01
450	9.5	207.9	8.1	11.64
500	9.2	206.8	7.9	10.37
550	9.0	208.9	7.7	5.41
600	9.0	212.0	7.6	4.20
650	9.0	215.0	7.4	2.15

Field trip on July 14, 2014

Station 1 (N44 18.580 W77 55.316)

Time	1345HRS	**Secchi depth (m)**	Infinite
Depth (m)	N/A	**Top water temperature (℃)**	23
Water Depth (cm)	**Temperature (℃)**	**Specific Conductivity (*μ*S/cm)**	**Dissolved Oxygen (mg/L)**
50	24.6	245	8.35

Station 2 (N44 18.470 W77 55.284)

Time	1403HRS	**Secchi depth (m)**	4.65
Depth (m)	7.3	**Top water temperature (℃)**	23
Water Depth (cm)	**Temperature (℃)**	**Specific Conductivity (*μ*S/cm)**	**Dissolved Oxygen (mg/L)**
50	23.8	251.8	7.52
100	23.7	251.7	7.69
150	23.6	251.2	7.49
200	23.6	251	7.62
250	23.6	250.9	7.44
300	23.6	251.2	7.28
350	23.6	252.2	7.05
400	22.2	258.9	2.36
450	20.5	267.3	0.65
500	17.9	266.6	0.63
550	16	262.7	0.66
600	15.1	266.5	0.61
650	13.9	269.9	0.59
700	13.9	279.1	0.58

Field trip on July 14, 2014 continued

Station 3 (N44 18.502 W77 55.297)

Time	1435HRS	**Secchi depth (m)**	4.65
Depth (m)	7.3	**Top water temperature (℃)**	24
Water Depth (cm)	**Temperature (℃)**	**Specific Conductivity (*μ*S/cm)**	**Dissolved Oxygen (mg/L)**
50	23.8	252.6	7.82
100	23.8	252.3	7.43
150	23.8	251.9	7.27
200	23.6	251.4	7.54
250	23.6	251.3	7.27
300	23.5	251.2	7.37
350	23.5	252.1	7.2
400	22.2	258.1	2.75
450	20.5	266.5	0.59
500	18.1	268.7	0.59
550	15.8	262	0.66
600	13.9	264.8	0.6
650	13.2	270.7	0.6
700	13.1	280.9	0.6

Station 4 (N44 18.546 W77 55.311)

Time	1503HRS	**Secchi depth (m)**	4.65
Depth (m)	6.5	**Top water temperature (℃)**	23
Water Depth (cm)	**Temperature (℃)**	**Specific Conductivity (*μ*S/cm)**	**Dissolved Oxygen (mg/L)**
50	24	253.9	7.71
100	23.9	253.3	7.59
150	23.8	252.7	7.34
200	23.6	251.7	7.81
250	23.5	251.3	7.41
300	23.5	251.5	7.39
350	23.1	255.7	5.06
400	22	257.8	3.74
450	19.3	269.1	0.63
500	17.4	268.1	0.65
550	14.9	263.5	0.58
600	14.2	270.8	0.59
650	14.2	270.8	0.54

Field trip on November, 3, 2014

Station 1 (N44 18.581 W77 55.321)

Time	1426HRS	**Secchi depth (m)**		Infinite
Depth (m)	0.7	**Top water temperature (℃)**		8.0
Water Depth (cm)	**Temperature (℃)**	**Specific Conductivity (*μ*S/cm)**	**pH**	**Dissolved Oxygen (mg/L)**
50	9.5	189.6	8.3	12.3

Station 2 (N44 18.459 W77 55.262)

Time	**1245HRS**	**Secchi depth (m)**		**5.5**
Depth (m)	**8.1**	**Top water temperature (℃)**		**9.0**
Water Depth (cm)	**Temperature (℃)**	**Specific Conductivity (*μ*S/cm)**	**pH**	**Dissolved Oxygen (mg/L)**
50	9.0	183.8	8.0	10.2
100	9.0	183.9	8.1	10.2
150	9.0	183.9	8.1	10.2
200	9.0	183.8	8.1	10.2
250	9.0	183.8	8.1	10.1
300	9.0	183.8	8.0	10.2
350	9.0	183.8	8.0	10.2
400	9.0	183.8	8.0	10.1
450	9.0	183.8	8.0	10.3
500	9.0	183.8	8.0	10.1
550	9.0	183.8	8.0	10.2
600	9.0	183.8	8.0	10.2
650	9.1	184.7	8.0	9.7
700	9.4	190.6	7.8	1.7
750	9.6	193.2	7.6	1.4

Field trip on November 3, 2014 continued

Station 3 (N44 18.500 W77 55.302)

Time	1325HRS	**Secchi depth (m)**		4.5
Depth (m)	7.8	**Top water temperature (℃)**		8.0
Water Depth (cm)	**Temperature (℃)**	**Specific Conductivity (*μ*S/cm)**	**pH**	**Dissolved Oxygen (mg/L)**
50	9.1	184.1	8.0	11.3
100	9.1	184	8.0	10.8
150	9.1	184.1	7.9	10.5
200	9.1	184	8.0	10.1
250	9.1	184	8.0	10.0
300	9.1	183.9	8.0	10.1
350	9.1	184	8.0	10.1
400	9.1	184	8.0	10.0
450	9.1	183.9	8.0	9.7
500	9.1	184	8.0	9.7
550	9.1	183.9	8.0	9.9
600	9.1	184	8.0	9.9
650	9.7	192.3	7.4	0.9
700	9.7	193.5	7.4	0.9
750	9.7	194.3	7.4	0.8

Station 4 (N44 18.533 W77 55.308)

Time	1355HRS	**Secchi depth (m)**		5.3
Depth (m)	7	**Top water temperature (℃)**		8.0
Water Depth (cm)	**Temperature (℃)**	**Specific Conductivity (*μ*S/cm)**	**pH**	**Dissolved Oxygen (mg/L)**
50	9.1	184.1	8.0	10.8
100	9.1	184.2	8.0	10.3
150	9.1	184.2	8.0	10.2
200	9.1	184.1	8.0	9.9
250	9.1	184	8.0	10.0
300	9.1	183.9	8.0	9.9
350	9.1	184	8.0	9.9
400	9.1	183.9	8.0	9.8
450	9.1	184	8.0	9.8
500	9.1	183.9	8.0	9.9
550	9.1	183.9	8.0	9.9
600	9.2	184.3	8.0	9.5
650	9.4	189.3	7.6	0.9

Field trip on November 6, 2011

Water Depth (cm)	Temperature (℃)	Specific Conductivity (μS/cm)	Salinity (ppt)
0	8.9	276.6	0.1
100	8.9	276.6	0.1
200	8.9	276.5	0.1
300	8.9	276.4	0.1
400	8.9	276.3	0.1
500	8.9	276.3	0.1
600	8.9	276.2	0.1
700	9.1	290.6	0.1
750	9.1	292.2	0.1

Appendix F Modern lake water isotopic compositions.

Sample ID	$\delta^{18}O$ (‰, VSMOW)	$\delta^{2}H$ (‰, VSMOW)	$\delta^{13}C_{DIC}$ (‰, VPDB)
1–1–T	–8.6	–62	–5.3
1–2–T	–8.4	–62	–5.2
1–2–M	–8.4	–64	–5.2
1–2–B	–8.4	–61	–4.9
1–2–T	N/A	N/A	–5.1
1–3–M	–8.3	–63	–5.1
1–3–B	–8.4	–60	–5.0
1–4–T	–8.5	–61	–5.2
1–4–M	–8.5	–63	–5.1
1–4–B	–8.3	–62	–5.2
2–1–T	–7.8	–57	–2.4
2–2–T	–7.6	–61	–3.4
2–2–M	–7.7	–62	–3.6
2–2–B	–8.3	–63	–6.6
2–3–T	–7.6	–58	–3.5
2–3–M	–7.4	–60	–3.6
2–3–B	–8.2	–65	–3.4
2–4–T	–7.6	–60	–3.5
2–4–M	–7.8	–59	–3.7
2–4–B	–8.0	–60	–6.3
3–1–T	–7.1	–57	–4.6
3–1–M	–7.0	–56	–4.6
3–1–B	–7.1	–55	–4.5
3–2–T	–7.1	–57	–4.6
3–2–M	–7.1	–56	–4.6
3–2–B	–7.1	–55	–4.6
3–3–T	–7.2	–53	–4.6
3–3–M	–7.0	–54	–4.6
3–3–B	–6.9	–55	–4.5
3–4–T	–7.8	–56	–4.0

T: samples collected at surface (0.5 m)

M: samples collected at 3–3.5 m

B: samples collected at 6–7 m

Appendix G Modern mollusc shell oxygen– and carbon–isotopic compositions and estimated shell formation temperatures and lake water $\delta^{13}C_{DIC}$.

Modern shell oxygen isotopic compositions and shell formation temperatures

Sample	$\delta^{18}O$ (‰, VSMOW)	$\delta^{18}O$ (‰, VPDB)	Calculated O–isotope $\alpha_{aragonite–water}$ [(a)]	Calculated growth temperature (℃)[(b)]	Calculated O–isotope $\alpha_{aragonite–water}$ [(c)]	Calculated growth temperature (℃)[(d)]	Average growth temperature (℃)[(e)]	Average growth temperature for each species (℃)
Helisoma anceps dark shell[(f)]	+23.4	–7.3	1.0312	18.4	1.0323	13.9	16.2	17.4 ±2.6
	+23.6	–7.1	1.0314	17.7	1.0324	13.2	15.4	
	+23.7	–7.0	1.0315	17.3	1.0325	12.8	15.0	
H. anceps light shell[(g)]	+22.5	–8.2	1.0303	22.7	1.0313	18.0	20.4	
	+22.6	–8.1	1.0304	22.3	1.0314	17.6	20.0	
Planorbella campanulatum light shell[(g)]	+23.8	–6.9	1.0316	16.8	1.0327	12.3	14.5	14.3 ±1.2
	+23.6	–7.1	1.0314	17.8	1.0324	13.2	15.5	
P. campanulatum dark shell[(f)]	+24.2	–6.5	1.0321	14.9	1.0331	10.4	12.6	
	+23.8	–6.9	1.0316	16.7	1.0327	12.2	14.4	
Lymnaea stagnalis fragments	+22.3	–8.3	1.0301	23.5	1.0312	18.7	21.1	20.4 ±0.4
	+22.5	–8.2	1.0303	22.6	1.0314	17.9	20.2	
	+22.5	–8.2	1.0303	22.6	1.0314	17.9	20.2	
L. stagnalis	+22.5	–8.2	1.0303	22.6	1.0314	17.9	20.3	
	+22.5	–8.2	1.0303	22.7	1.0313	18.0	20.3	

(a) $\delta^{18}O$ value of –7.6‰ of summer lake surface water has been assumed in the calculations
(b) calculated using Equation 2.6 and α obtained in (a)
(c) $\delta^{18}O$ value of –8.6‰ of spring lake surface water has been used in the calculations
(d) calculated using Equation 2.6 and α obtained in (c)
(e) average the values calculated in (b) and (d)
(f) dark shell means the colour of the shell overall is dark
(g) light shell means the colour of the shell overall is light

Modern shell carbon isotopic compositions and lake water $\delta^{13}C_{DIC}$

Sample	$\delta^{13}C$ (‰, VPDB)	Estimated lake water $\delta^{13}C_{DIC}$ (‰, VPDB)[a]	Average estimated lake water $\delta^{13}C_{DIC}$ (‰, VPDB)
Helisoma anceps dark shell[b]	–3.0	–3.3	–3.8 ±0.5
	–3.8	–4.1	
	–3.6	–3.8	
H. anceps light shell[c]	–4.2	–4.5	
	–3.1	–3.4	
Planorbella campanulatum light shell[c]	–3.8	–3.3	–3.8 ±0.6
	–3.8	–3.3	
P. campanulatum dark shell[b]	–4.9	–4.4	
	–4.8	–4.3	
Lymnaea stagnalis fragments	–3.5	–2.6	–3.8 ±0.9
	–3.9	–3.0	
L. stagnalis	–5.2	–4.3	
	–5.4	–4.5	
	–5.6	–4.7	

(a) calculated with using Equation 2.8 plus +2.4‰, +3.2‰ and +3.6‰ vital effect corrections for *H. anceps*, *P. campanulatum* and *L. stagnalis*, respectively

(b) dark shell means the colour of the shell overall is dark

(c) light shell means the colour of the shell overall is light

Appendix H Isotopic compositions of ancient mollusc shells including estimations of lake water $\delta^{18}O$ and $\delta^{13}C_{DIC}$.

Helisoma anceps

Depth (cm)	Year (AD)	$\delta^{13}C$ (‰, VPDB)	$\delta^{18}O$ (‰, VSMOW)	$\delta^{18}O$ (‰, VPDB)	Estimated lake water $\delta^{18}O$ (‰, VSMOW) at 17 ℃*	Estimated lake water DIC $\delta^{13}C_{DIC}$ (‰, VPDB)**
32.0	1504	–4.9	+22.4	–8.3	–8.9	–5.2
32.0		–1.3	+22.9	–7.8	–8.4	–1.6
32.5	1488	–1.1	+23.8	–6.9	–7.5	–1.4
32.5		–0.9	+22.9	–7.7	–8.4	–1.2
33.0	1472	–0.7	+25.7	–5.1	–5.7	–1.0
33.0		–1.2	+25.4	–5.3	–6.0	–1.4
33.5	1456	–0.8	+23.1	–7.6	–8.2	–1.1
33.5		–2.0	+23.2	–7.5	–8.2	–2.3
34.0	1440	–2.2	+22.4	–8.3	–8.9	–2.5
34.0		–1.1	+23.8	–6.9	–7.6	–1.4
34.5	1423	–4.0	+22.9	–7.7	–8.4	–4.3
34.5		–2.3	+24.1	–6.6	–7.2	–2.6
35.0	1407	–2.9	+23.7	–7.0	–7.7	–3.2
35.0		–2.7	+23.6	–7.1	–7.7	–3.0
35.5	1393	–3.3	+22.9	–7.8	–8.5	–3.6
35.5		–1.4	+22.7	–8.0	–8.6	–1.7
36.0	1378	–2.4	+23.1	–7.6	–8.3	–2.7
36.0		–2.8	+23.3	–7.3	–8.0	–3.1
36.5	1368	–2.2	+24.3	–6.5	–7.1	–2.5
36.5		–3.3	+23.5	–7.2	–7.8	–3.5
37.0	1359	–1.6	+23.4	–7.3	–7.9	–1.9
37.0		–0.9	+24.5	–6.3	–6.9	–1.2
37.0		–0.9	+24.7	–6.0	–6.6	–1.2
37.5	1349	–3.0	+21.8	–8.8	–9.5	–3.3
37.5		–2.7	+23.3	–7.4	–8.0	–3.0
38.0	1339	–0.8	+23.1	–7.6	–8.2	–1.1
38.0		–1.0	+23.1	–7.5	–8.2	–1.3
38.5	1329	–0.3	+24.1	–6.6	–7.3	–0.6
38.5		–1.1	+23.3	–7.4	–8.1	–1.4
38.5		–3.8	+22.2	–8.4	–9.0	–4.1
39.0	1319	–4.0	+24.2	–6.5	–7.2	–4.3
39.0		–4.2	+24.5	–6.3	–6.9	–4.5
39.5	1308	–3.0	+22.8	–7.8	–8.5	–3.3
39.5		–1.2	+23.7	–7.0	–7.6	–1.5
40.0	1298	–0.8	+23.2	–7.5	–8.2	–1.1
40.0		–4.0	+22.9	–7.8	–8.4	–4.3
40.5	1288	–2.8	+22.9	–7.8	–8.4	–3.1
40.5		–0.9	+23.0	–7.7	–8.3	–1.2
40.5		–3.4	+22.4	–8.2	–8.9	–3.7
41.0	1278	–3.0	+23.3	–7.4	–8.0	–3.2
41.0		–2.7	+22.4	–8.2	–8.9	–2.9
41.5	1268	–0.4	+23.6	–7.1	–7.7	–0.7
41.5		–0.2	+23.1	–7.5	–8.2	–0.5

* calculated assuming a constant shell formation temperature using Equation 2.6

** calculated using Equation 2.8 and +2.4‰ vital effect corrections

Pisidium

Depth (cm)	Year (AD)	$\delta^{13}C$ (‰, VPDB)	$\delta^{18}O$ (‰, VSMOW)	$\delta^{18}O$ (‰, VPDB)	Estimated lake water $\delta^{18}O$ (‰, VSMOW) at 15 ℃*	Estimated lake water DIC $\delta^{13}C_{DIC}$ (‰, VPDB)**
33.5	1456	+2.1	+23.5	–7.2	–8.3	–0.4
33.5		+1.5	+24.2	–6.5	–7.6	–1.0
33.5		+2.1	+23.5	–7.2	–8.3	–0.4
34.5	1423	–2.4	+23.8	–6.9	–8.0	–4.9
34.5		–0.6	+24.7	–6.0	–7.1	–3.1
35.0	1407	–0.0	+26.9	–3.9	–4.9	–2.5
35.0		–0.1	+24.5	–6.2	–7.3	–2.6
35.5	1393	–1.6	+23.8	–6.9	–7.9	–4.1
35.5		–2.5	+24.0	–6.7	–7.7	–5.0
36.0	1378	–2.5	+24.2	–6.5	–7.5	–5.0
36.0		–3.0	+22.6	–8.1	–9.2	–5.5
36.5	1368	–2.9	+24.9	–5.8	–6.9	–5.3
36.5		–0.5	+25.2	–5.5	–6.6	–3.0
36.5		–2.6	+24.2	–6.5	–7.6	–5.0
37.0	1359	–1.6	+23.1	–7.6	–8.6	–4.1
37.0		–1.3	+22.9	–7.8	–8.9	–3.8
37.5		–0.7	+24.7	–6.0	–7.1	–3.2
37.5	1349	–0.3	+25.4	–5.3	–6.4	–2.8
38.0		–2.7	+24.0	–6.7	–7.8	–5.1
38.0	1339	–1.3	+22.7	–8.0	–9.1	–3.7
38.5		–1.5	+22.6	–8.1	–9.2	–4.0
38.5	1329	–2.0	+24.1	–6.6	–7.7	–4.5
38.5		–0.8	+23.6	–7.1	–8.1	–3.3
39.0		–1.7	+24.1	–6.6	–7.7	–4.2
39.0	1319	–0.1	+25.0	–5.7	–6.8	–2.6
39.5		–1.8	+22.5	–8.2	–9.3	–4.3
39.5	1308	–0.7	+23.4	–7.3	–8.4	–3.1
39.5		–1.6	+23.6	–7.1	–8.2	–4.1
40.5	1288	–1.4	+22.2	–8.5	–9.6	–3.9
40.5		+0.5	+23.8	–6.9	–8.0	–2.0
41.0	1278	–1.2	+22.4	–8.3	–9.3	–3.7
41.0		+1.6	+23.8	–6.9	–7.9	–0.9
41.5	1268	–1.6	+21.4	–9.2	–10.3	–4.1
41.5		+0.8	+24.7	–6.1	–7.1	–1.7

* calculated using a constnatn shell formation temperature 15 ℃ using Equation 2.6

** calculated using Equation 2.8 and –0.2‰ vital effect corrections

Appendix I Stable isotopic compositions of calcite.

Depth (cm)	Year (AD)	$\delta^{13}C$ (‰, VPDB)	$\delta^{18}O$ (‰, VSMOW)	$\delta^{18}O$ (‰, VPDB)	Estimated lake water $\delta^{18}O$ (‰, VSMOW) using GST*	Estimated lake water DIC $\delta^{13}C_{DIC}$ (‰, VPDB)**	Calcite formation temperature (℃)***
1	2010	-0.2	+21.3	-9.3	-7.6	-1.2	21.9
1.5	2009	-0.5	+21.0	-9.6	-8.3	-1.6	19.6
2	2008	-0.3	+21.3	-9.3	-7.8	-1.4	20.8
2.5	2006	-0.2	+21.3	-9.3	-8.2	-1.4	19.4
3	2004	-0.2	+21.2	-9.4	-8.5	-1.5	18.3
3.5	2002	-0.3	+21.2	-9.4	-8.2	-1.6	19.3
4	2000	-0.1	+21.3	-9.3	-8.3	-1.5	18.4
4.5	1998	-0.2	+21.2	-9.4	-8.0	-1.7	20.1
5	1996	-0.2	+21.3	-9.3	-8.2	-1.8	18.9
6	1992	-0.1	+21.3	-9.4	-8.6	-1.8	17.3
6.5	1989	-0.1	+21.3	-9.3	-8.2	-1.9	19.3
7	1986	+0.1	+21.3	-9.3	-8.2	-1.8	18.6
7.5	1984	+0.0	+21.3	-9.3	-8.4	-1.9	18.3
8	1982	-0.0	+21.3	-9.3	-8.4	-2.0	18.4
8.5	1979	+0.0	+21.3	-9.3	-8.4	-2.0	18.4
9	1976	+0.0	+21.3	-9.3	-8.2	-2.1	19.0
9.5	1974	-0.0	+21.4	-9.2	-8.4	-2.2	17.9
10	1972	+0.0	+21.4	-9.3	-8.2	-2.2	18.7
10.5	1970	+0.0	+21.3	-9.3	-8.1	-2.2	19.4
11	1968	-0.2	+21.3	-9.3	-8.3	-2.5	18.5
11.5	1966	+0.1	+21.4	-9.3	-8.3	-2.2	18.4
12	1964	+0.1	+21.3	-9.3	-8.2	-2.3	18.9
12.5	1962	+0.0	+21.4	-9.3	-8.2	-2.4	19.0
13	1960	+0.1	+21.5	-9.1	-8.1	-2.3	18.6
13.5	1958	+0.2	+21.4	-9.2	-8.3	-2.3	18.0
14	1956	+0.0	+21.4	-9.2	-8.5	-2.5	17.4
14.5	1953	+0.1	+21.5	-9.2	-8.0	-2.5	19.4

Calcite isotopic data continued

15	1951	+0.0	+21.4	-9.3	-8.2	-2.5	18.7
15.5	1948	-0.1	+21.3	-9.3	-8.1	-2.7	19.3
16	1945	-0.0	+21.4	-9.2	-8.1	-2.7	19.3
16.5	1940	-0.1	+21.2	-9.4	-7.8	-2.8	21.2
17	1936	-0.2	+21.3	-9.3	-8.0	-2.9	20.2
17.5	1930	-0.3	+21.3	-9.3	-8.5	-3.0	17.5
18	1924	-0.2	+21.1	-9.5	-8.6	-3.1	18.0
18.5	1914	-0.4	+21.0	-9.6	-8.3	-3.3	19.7
19	1905	-0.4	+21.2	-9.4	-8.2	-3.3	19.2
19.5	1894	-0.6	+20.8	-9.8	-8.8	-3.5	18.7
20	1882	-0.8	+21.5	-9.1	-8.4	-3.8	17.2
20.5	1865	-0.9	+21.0	-9.6	-8.5	-3.8	
21	1849	-0.9	+20.8	-9.8	-8.7	-3.8	
21.5	1832	-0.8	+21.1	-9.5	-8.5	-3.8	
22	1816	-0.9	+21.3	-9.4	-8.3	-3.8	
22.5	1801	-0.7	+21.1	-9.5	-8.4	-3.7	
23	1785	-0.7	+21.7	-8.9	-7.8	-3.7	
23.5	1770	-0.1	+22.3	-8.4	-7.3	-3.1	
24	1755	+0.1	+22.1	-8.5	-7.5	-2.9	18.7
24.5	1739	-0.2	+21.5	-9.1	-8.0	-3.2	
25	1723	+5.1	+22.6	-8.0	-7.0	2.1	
25.5	1708	+2.4	+22.6	-8.1	-7.0	-0.6	
26	1692	+2.6	+22.8	-7.9	-6.8	-0.4	
26.5	1676	+3.2	+23.0	-7.7	-6.6	0.2	
27	1660	+4.1	+23.0	-7.6	-6.6	1.1	
27.5	1645	+3.6	+23.0	-7.6	-6.6	0.6	
28	1629	+3.1	+23.3	-7.4	-6.3	0.1	
28.5	1614	+2.7	+23.6	-7.1	-6.0	-0.3	
29	1598	+2.2	+22.8	-7.8	-6.7	-0.8	19
29.5	1582	+0.9	+23.1	-7.6	-6.5	-2.1	

Calcite isotopic data continued

30	1567	-0.1	+21.9	-8.8	-7.6	-3.1	
30.5	1551	+0.2	+22.0	-8.7	-7.5	-2.8	
31	1535	+0.1	+22.1	-8.5	-7.4	-2.9	
31.5	1519	+0.6	+21.9	-8.7	-7.6	-2.4	
32	1504	+0.7	+21.8	-8.8	-7.7	-2.3	
32.5	1488	+0.2	+21.7	-9.0	-7.8	-2.8	
33	1472	+0.8	+22.0	-8.7	-7.5	-2.2	
33.5	1456	+1.4	+22.3	-8.3	-7.1	-1.6	
34	1440	+1.0	+23.1	-7.5	-6.4	-2.0	
34.5	1423	+0.4	+23.0	-7.7	-6.5	-2.6	
35	1407	+0.6	+22.6	-8.0	-6.9	-2.4	19.2
35.5	1393	+0.9	+22.8	-7.9	-6.7	-2.1	
36	1378	+0.3	+22.7	-7.9	-6.8	-2.7	
36.5	1368	+0.8	+23.1	-7.6	-6.4	-2.2	
37	1359	+2.8	+23.9	-6.8	-5.7	-0.2	
37.5	1349	+3.5	+23.7	-7.0	-5.8	0.5	
38	1339	+3.2	+23.7	-7.0	-5.7	0.2	
38.5	1329	+1.8	+22.9	-7.7	-6.5	-1.2	
39	1319	+2.4	+23.4	-7.3	-6.1	-0.6	
39.5	1308	+2.6	+23.5	-7.2	-5.9	-0.4	19.7
40	1298	+2.3	+23.0	-7.6	-6.4	-0.7	
40.5	1288	+2.7	+22.8	-7.9	-6.6	-0.3	
41	1278	+2.4	+23.1	-7.5	-6.3	-0.6	
41.5	1268	+2.1	+22.8	-7.8	-6.6	-0.9	

* GST=growing season temperature reconstructed at Marion Lake, Michigan (Bernabo, 1981); 16.5 ℃ for AD 1615–1850, 16.8 ℃ for AD 1500–1615, 17 ℃ for AD 1350–1500, 17.5 ℃ for AD 1268–1350

** calculated using Equation 2.10 and corrected for +2 ‰ enrichment in ^{13}C; $\delta^{13}C_{DIC}$ after 1850 has been corrected for Suess effect

*** a +2.2 ℃ correction for air temperature has been applied to archival temperature data (1866-2011) and GST listed in *

Appendix J Bulk organic matter carbon and nitrogen elemental and isotopic compositions including calculated molar carbon to nitrogen ratios.

Depth (cm)	Year (AD)	TOC (%)	TN (%)	C/N	$\delta^{13}C_{OM}$ (‰ VPDB)	$\delta^{15}N_{TN}$ (‰ AIR)	C–MAR (mg/cm^2/yr)	N–MAR (mg/cm^2/yr)
0.5	2011	N/A	N/A	N/A	–28.7	–1.4	N/A	N/A
1	2010	N/A	N/A	N/A	–29.0	–1.5	N/A	N/A
1.5	2009	14.1	1.9	8.6	–29.0	–1.4	8.0	1.1
2	2008	14.6	2.0	8.7	–29.3	–1.3	9.7	1.3
2.5	2006	15.0	2.0	8.9	–29.4	–1.2	5.3	0.7
3	2004	14.6	2.0	8.6	–29.5	–1.2	5.1	0.7
3.5	2002	13.9	2.0	8.0	–29.5	–1.5	5.8	0.8
4	2000	14.3	1.9	8.6	–29.5	–1.0	7.0	0.9
4.5	1998	14.1	1.9	8.4	–29.6	–0.8	6.3	0.9
5	1996	13.3	1.9	8.1	–29.8	–1.0	6.0	0.9
5.5	1994	N/A	N/A	N/A	N/A	N/A	3.9	0.6
6	1992	13.6	1.9	8.2	–29.7	–1.6	4.6	0.6
6.5	1989	13.3	1.8	8.6	–29.9	–0.9	3.2	0.4
7	1986	13.0	1.7	8.8	–29.9	–1.1	6.8	1.1
7.5	1984	13.2	2.2	7.0	–29.9	–1.1	5.0	0.8
8	1982	12.1	1.9	7.4	–30.0	–1.1	4.2	0.6
8.5	1979	12.1	1.7	8.3	–30.1	–1.4	4.4	0.7
9	1976	12.3	1.8	7.9	–30.0	–1.2	7.7	1.1
9.5	1974	12.0	1.6	8.5	–30.1	–1.3	8.4	1.1
10	1972	12.0	1.6	8.6	–30.3	–1.1	5.1	0.7
10.5	1970	12.4	1.6	8.9	–30.2	–1.3	10.0	1.4
11	1968	11.9	1.7	8.2	–30.2	–1.3	6.4	0.8
11.5	1966	11.6	1.5	8.9	–30.2	–1.5	5.1	0.6
12	1964	11.5	1.5	9.1	–30.1	–1.5	9.7	1.2
12.5	1962	11.4	1.4	9.2	–30.2	–1.7	8.6	1.2
13	1960	10.8	1.5	8.6	–30.2	–1.5	5.8	0.8
13.5	1958	10.5	1.5	8.4	–30.2	–1.8	4.8	0.7

Bulk organic matter data continued

14	1956	10.1	1.4	8.4	–30.1	–1.7	6.4	0.9
14.5	1953	10.2	1.4	8.6	–30.0	–1.7	6.2	0.8
15	1951	10.4	1.4	8.5	–30.0	–1.7	4.2	0.6
15.5	1948	9.9	1.4	8.4	–30.2	–1.6	2.6	0.4
16	1945	10.3	1.4	8.5	–30.3	–1.8	2.8	0.4
16.5	1940	10.1	1.4	8.2	–30.4	–1.6	4.9	0.6
17	1936	11.2	1.5	8.8	–30.5	–1.6	3.1	0.4
17.5	1930	11.6	1.5	8.8	–30.4	–1.5	1.5	0.2
18	1924	12.2	1.6	9.1	–30.7	–1.4	2.0	0.3
18.5	1914	11.9	1.6	8.7	–30.7	–1.5	1.8	0.2
19	1905	11.8	1.6	8.4	–30.8	–1.2	1.7	0.2
19.5	1894	12.5	1.6	8.9	–30.9	–1.1	2.5	0.3
20	1882	13.1	1.7	9.0	–31.0	–1.2	1.0	0.1
20.5	1865	13.9	1.7	9.4	–30.9	–1.1	1.1	0.1
21	1849	13.7	1.7	9.4	–31.0	–1.0	1.5	0.2
21.5	1832	13.3	1.7	9.1	–30.9	–1.0	1.2	0.2
22	1816	13.5	1.7	9.3	–30.9	–0.6	1.2	0.2
22.5	1801	13.6	1.7	9.3	–30.9	–0.3	2.0	0.2
23	1785	14.1	1.8	9.3	–30.8	–0.4	3.0	0.4
23.5	1770	16.2	2.0	9.4	–30.4	–0.1	1.2	0.2
24	1755	19.8	2.4	9.5	–29.9	+0.5	1.1	0.1
24.5	1739	27.1	3.1	10.1	–28.5	+1.2	1.6	0.2
25	1723	30.4	3.4	10.3	–26.4	+0.7	0.7	0.1
25.5	1708	27.4	3.1	10.4	–26.7	+1.2	3.7	0.4
26	1692	25.5	2.9	10.3	–28.5	+0.3	0.4	0.0
26.5	1676	23.4	2.8	9.9	–27.1	+1.0	4.7	0.6
27	1660	23.2	2.8	9.8	–26.7	+1.2	0.9	0.1
27.5	1645	23.8	2.8	10.1	–26.6	+1.2	3.1	0.4
28	1629	25.5	2.9	10.1	–27.5	+0.9	0.6	0.1
28.5	1614	28.3	3.2	10.3	–27.7	+0.8	2.4	0.3

Bulk organic matter data continued

29	1598	28.7	3.3	10.0	–27.8	+0.9	1.7	0.2
29.5	1582	30.3	3.4	10.3	–28.3	+0.8	2.2	0.2
30	1567	31.6	3.5	10.5	–28.6	+0.8	1.6	0.2
30.5	1551	34.4	3.6	11.0	–29.8	+0.9	3.4	0.4
31	1535	33.3	3.6	10.7	–28.8	+0.9	1.1	0.1
31.5	1519	32.5	3.7	10.4	–28.6	+1.2	2.1	0.2
32	1504	30.8	3.6	9.9	–28.3	+1.3	2.1	0.3
32.5	1488	31.4	3.8	9.7	–28.3	+1.4	1.0	0.1
33	1472	31.4	3.8	9.8	–27.9	+1.6	4.7	0.5
33.5	1456	31.1	3.6	10.1	–27.2	+1.2	1.2	0.1
34	1440	30.8	3.6	10.1	–27.9	+1.4	3.1	0.4
34.5	1423	30.8	3.6	10.1	–28.3	+1.2	2.4	0.3
35	1407	30.0	3.5	9.9	–28.6	+1.2	1.6	0.2
35.5	1393	26.6	3.3	9.5	–28.8	+1.5	2.7	0.3
36	1378	26.0	3.2	9.5	–30.4	+1.4	3.4	0.4
36.5	1368	23.8	3.1	9.0	–28.9	+1.9	2.2	0.3
37	1359	17.9	2.4	8.7	–27.7	+1.9	3.0	0.4
37.5	1349	15.5	2.1	8.6	–27.5	+1.7	2.4	0.3
38	1339	15.4	2.1	8.7	–28.1	+1.8	2.4	0.3
38.5	1329	17.1	2.3	8.8	–28.8	+1.8	3.4	0.5
39	1319	17.4	2.3	8.8	–29.4	+1.4	1.1	0.2
39.5	1308	17.8	2.4	8.6	–28.3	+1.6	4.8	0.7
40	1298	18.5	2.5	8.4	–28.2	+1.9	1.8	0.2
40.5	1288	23.2	3.0	9.0	–28.1	+1.9	4.3	0.6
41	1278	23.3	3.2	8.6	–28.5	+1.4	0.2	0.0
41.5	1268	21.0	2.8	8.8	–27.4	+1.9	N/A	N/A

Appendix K Historical climate data

Summer data (June to August)

Peterborough Station (44 °17'00"N 78 °19'00"W)			Peterborough Station (44 °17'00"N 78 °19'00"W)			Peterborough airport Station (44 °14'00"N 78 °22'00"W)		
Year (AD)	Summer Precipitation (mm)	Mean summer temperature (℃)	Year (AD)	Summer Precipitation (mm)	Mean summer temperature (℃)	Year (AD)	Summer Precipitation (mm)	Mean summer temperature (℃)
1866	206.00	18.23	1921	224.30	20.77	1969	230.20	18.20
1867	176.80	19.37	1922	198.60	19.07	1970	155.70	19.03
1868	214.60	20.37	1923	181.10	19.50	1971	154.60	17.77
1869	165.60	16.53	1924	205.80	18.13	1972	261.10	17.60
1870	205.20	19.03	1925	222.20	19.30	1973	183.30	19.63
1871	166.60	17.10	1926	212.10	17.43	1974	242.10	18.17
1872	140.90	21.60	1927	248.70	17.50	1975	220.50	19.03
1873	135.40	19.87	1928	222.50	18.87	1976	183.90	18.37
1877	108.10	18.85	1929	165.60	18.03	1977	292.10	17.63
1878	197.60	18.15	1930	195.30	19.33	1978	162.10	17.83
1879	220.30	18.70	1931	200.40	20.00	1979	165.30	17.90
1880	259.00	19.30	1932	202.00	18.80	1980	342.10	17.90
1881	107.30	18.75	1933	172.50	20.03	1981	274.30	18.37
1882	179.80	18.57	1934	166.30	18.45	1982	264.10	16.70
1883	132.60	18.73	1935	274.00	20.53	1983	236.80	19.20
1884	264.20	19.27	1936	160.80	20.27	1984	238.50	18.20
1885	217.70	18.70	1937	223.50	21.77	1985	250.20	16.63
1886	178.60	18.40	1938	357.40	20.63	1986	252.90	17.37
1887	144.80	21.13	1939	167.90	20.93	1987	201.60	19.03
1891	210.20	18.40	1940	154.60	19.53	1988	130.00	19.07
1892	289.10	20.80	1941	268.20	20.23	1989	177.40	18.63
1893	241.30	20.13	1942	153.40	19.57	1990	259.20	18.53
1894	150.40	19.70	1943	210.60	19.40	1991	85.40	18.90
1895	140.00	19.40	1944	178.60	19.63	1992	249.60	15.93

Peterborough and Peterborough airport summer data continued

1896	163.50	20.43	1945	197.20	18.27	1993	227.80	18.10
1897	268.50	18.90	1946	127.20	18.13	1994	153.60	18.30
1898	170.40	20.30	1947	236.20	19.90	1995	265.00	19.07
1899	213.10	19.47	1948	166.60	19.20	1996	277.40	18.07
1900	219.20	20.67	1949	147.30	19.77	1997	203.20	17.67
1901	198.60	20.47	1950	185.70	18.30	1998	283.00	18.37
1902	319.50	17.43	1951	270.00	18.17	1999	221.20	18.57
1903	241.30	17.63	1952	113.60	19.33	2000	337.20	17.37
1904	303.50	17.80	1953	170.40	19.20	2001	115.60	18.67
1905	199.40	18.60	1954	189.20	18.53	2002	250.60	19.33
1906	321.80	19.87	1955	129.60	21.27	2003	209.80	18.60
1907	149.00	18.10	1956	189.00	18.07	2004	412.60	17.23
1908	167.10	19.03	1957	187.70	18.37	2005	156.60	20.97
1909	177.60	18.83	1958	135.10	17.60	2006	180.40	19.67
1910	235.70	18.73	1959	182.90	20.07			
1911	241.00	19.67	1960	207.00	17.00			
1912	213.40	17.57	1961	89.10	18.63			
1913	180.10	19.00	1962	117.90	18.37			
1914	162.10	18.87	1963	N/A	18.37			
1915	328.90	17.83	1964	N/A	18.80			
1916	186.20	19.93	1965	271.00	18.07			
1917	189.00	18.57	1966	210.60	20.37			
1918	283.80	18.77	1967	360.40	18.90			
1919	185.60	20.73	1968	216.70	18.67			
1920	267.90	18.87	1969	219.70	18.97			
			1970	146.50	19.30			

Peterborough Dobbin TS (44°19'00"N 78°24'00"W)			Peterborough STP (44°17'00"N 78°19'00"W)			Stirling (44°18'00"N 78°38'00"W)		
Year (AD)	Summer Precipitation (mm)	Mean summer temperature (°C)	Year (AD)	Summer Precipitation (mm)	Mean summer temperature (°C)	Year (AD)	Summer Precipitation (mm)	Mean summer temperature (°C)
1965	133.60	17.25	1965	250.90	N/A	1940	131.80	18.53
1966	214.10	19.30	1966	205.50	N/A	1941	264.90	19.60
1967	330.50	18.83	1967	345.70	N/A	1942	116.80	18.77
1968	218.50	18.17	1968	197.10	N/A	1943	193.80	19.60
1969	185.40	18.27	1969	213.90	N/A	1944	157.80	20.17
1970	182.70	18.77	1970	139.20	19.50	1945	264.70	18.43
1971	190.00	18.30	1971	101.10	18.95	1946	149.90	18.30
1972	319.30	17.60	1972	307.10	18.17	1947	406.20	19.70
1973	203.70	19.93	1973	158.70	20.60	1948	155.20	19.13
1974	244.60	18.27	1974	271.80	19.10	1949	127.90	21.10
1975	194.50	19.57	1975	218.90	20.33	1950	202.20	18.37
1976	192.30	18.87	1976	186.50	19.33	1951	317.50	18.13
1977	300.90	18.33	1977	289.80	18.97	1952	169.90	20.00
1978	172.40	18.70	1978	163.80	19.40	1953	168.60	19.53
1979	171.90	17.45	1979	181.40	19.33	1954	146.60	18.70
1980	351.10	18.20	1980	304.20	18.90	1955	234.50	21.07
1981	244.30	18.63	1981	270.80	19.43	1956	189.50	18.13
1982	348.40	17.23	1982	315.10	18.00	1957	181.90	18.43
1983	216.90	19.47	1983	279.10	20.33	1958	152.00	18.03
1984	225.00	18.90	1984	214.60	19.97	1959	158.20	20.80
1985	246.30	16.90	1985	171.50	18.23	1960	210.50	18.37
1986	285.70	17.70	1986	136.50	19.30	1961	204.50	18.60
1987	188.60	19.53	1987	210.80	20.30	1962	130.90	18.40
1988	119.50	19.97	1988	135.80	20.47	1963	190.50	18.60
1989	205.80	19.23	1989	307.20	19.90	1964	198.90	18.00
1990	235.10	19.07	1990	216.90	19.90	1965	211.60	17.03
1991	147.70	19.87	1991	117.50	20.87	1966	147.30	19.03
1992	190.70	16.25	1992	230.00	17.50	1967	254.30	18.63
1993	258.50	19.20	1993	249.70	19.87	1968	237.10	18.00
1994	145.80	18.70						

Trent University (44°22'00"N 78°18'00"W)			Campbellford (44°18'00''N 78°48'00'' W)		
Year (AD)	**Summer Precipitation (mm)**	**Mean summer temperature (°C)**	**Year (AD)**	**Summer Precipitation (mm)**	**Mean summer temperature (°C)**
1968	242.90	18.53	1915	286.00	N/A
1969	190.60	18.57	1916	251.20	N/A
1970	197.90	19.23	1917	134.40	N/A
1971	188.50	18.67	1918	230.10	N/A
1972	312.80	18.03	1919	208.00	N/A
1973	210.60	20.20	1920	146.50	N/A
1974	228.40	18.43	1921	217.70	N/A
1975	162.60	19.67	1922	178.00	N/A
1976	213.60	18.70	1923	173.40	N/A
1977	275.60	18.33	1924	170.50	N/A
1978	182.80	18.73	1925	184.90	N/A
1979	201.30	18.53	1926	215.40	N/A
1980	313.00	18.17	1927	207.50	N/A
1981	263.50	18.33	1928	334.60	N/A
1982	280.40	17.77	1929	148.30	N/A
1983	237.90	20.07	1930	187.90	N/A
1984	302.50	19.40	1931	186.70	N/A
1985	260.90	17.77	1932	240.30	N/A
1986	260.30	18.23	1933	183.70	N/A
1987	211.20	20.07	1934	158.50	N/A
1988	127.70	20.43	1935	252.80	N/A
1989	294.40	19.63	1936	161.30	N/A
1990	157.70	19.60	1937	168.10	N/A
1991	118.80	20.50	1938	263.90	N/A
1992	250.80	17.00	1939	136.40	N/A
1993	240.50	19.37	1940	131.30	N/A
1994	148.70	19.20	1943	107.10	N/A

Trent University and Campbellford summer data continued

1995	275.80	21.00
1996	360.80	19.67
1997	213.70	19.67
1998	344.00	20.00
1999	166.20	20.33
2000	314.60	18.50
2001	166.20	19.83
2002	232.80	19.70
2003	137.20	19.33
2004	541.90	17.57
2005	158.60	21.13
2006	216.10	19.53
2007	92.30	18.75
2008	305.80	18.57
2009	237.90	17.37
2010	256.10	19.70
2011	229.20	19.63

1944	428.20	N/A
1945	159.50	N/A
1946	135.20	N/A
1947	186.70	N/A
1948	330.00	N/A
1949	165.30	N/A
1950	156.00	N/A
1951	168.50	N/A
1952	271.30	N/A
1953	200.10	N/A
1954	209.30	N/A
1955	153.50	N/A
1956	129.90	N/A
1957	193.10	N/A
1958	192.00	N/A
1959	124.90	N/A
1960	181.90	N/A
1961	242.30	N/A
1962	243.10	N/A
1963	230.60	N/A
1964	212.40	N/A
1965	271.70	N/A
1966	149.80	N/A
1967	200.00	N/A
1968	341.10	N/A
1969	111.40	N/A
1970	189.00	N/A
1971	174.20	N/A
1972	155.70	N/A

Campbellford summer data continued

1973	238.70	N/A
1974	144.10	N/A
1975	140.70	N/A
1976	226.70	N/A
1977	215.40	N/A
1978	255.00	N/A
1979	237.00	N/A
1980	285.90	N/A
1981	205.00	N/A
1982	204.50	N/A
1983	229.60	N/A
1984	132.00	N/A
1985	252.20	N/A
1986	193.00	18.80
1987	116.30	20.50
1988	263.10	21.07
1989	258.60	20.13
1990	199.20	20.00
1991	189.10	20.70
1992	236.20	17.17
1993	86.20	19.90
1994	59.20	20.40
1995	66.40	21.17
1996	63.03	19.90
1997	78.73	20.03

Annual historical data

Peterborough Station (44°17'00"N 78°19'00"W)			Peterborough Station (44°17'00"N 78°19'00"W)			Peterborough airport Station (44°14'00"N 78°22'00"W)		
Year (AD)	**Annual Precipitation (mm)**	**Mean annual temperature (°C)**	**Year (AD)**	**Annual Precipitation (mm)**	**Mean annual temperature (°C)**	**Year (AD)**	**Annual Precipitation (mm)**	**Mean annual temperature (°C)**
1867	735.30	5.25	1922	684.40	7.18	1969	669.70	7.37
1868	768.30	4.91	1923	775.40	6.09	1970	695.70	6.05
1869	788.10	4.50	1924	799.60	5.61	1971	703.30	6.03
1870	896.10	5.38	1925	911.10	6.28	1972	915.20	4.95
1871	749.60	N/A	1926	904.50	4.69	1973	837.80	6.92
1872	565.60	7.22	1927	847.20	6.79	1974	769.60	5.65
1873	710.60	5.33	1928	906.80	6.57	1975	788.00	6.54
1877	554.90	6.42	1929	923.50	6.12	1976	750.10	5.23
1878	953.70	N/A	1930	743.20	6.99	1977	902.00	5.96
1879	674.70	5.04	1931	723.30	8.17	1978	770.60	4.79
1880	831.70	N/A	1932	902.40	7.08	1979	766.70	5.80
1881	617.90	5.91	1933	674.40	6.88	1980	944.30	5.27
1882	746.00	6.37	1934	740.10	4.38	1981	881.80	5.98
1883	514.50	6.68	1935	714.50	8.56	1982	897.10	5.38
1884	829.40	6.33	1936	865.70	6.62	1983	894.50	6.48
1885	786.40	5.05	1937	846.60	8.03	1984	811.20	5.82
1886	837.80	5.65	1938	902.50	7.80	1985	967.00	5.60
1887	577.20	4.90	1939	706.90	7.08	1986	897.00	6.16
1891	754.80	N/A	1940	895.80	6.17	1987	731.90	6.93
1892	838.40	7.97	1941	811.50	7.51	1988	687.00	6.24
1893	1126.50	5.27	1942	900.50	6.97	1989	773.60	5.34
1894	792.00	6.98	1943	777.20	5.08	1990	1006.00	6.98
1895	648.80	7.07	1944	605.10	6.61	1991	720.80	6.80

Peterborough and Peterborough airport annual data continued

1896	692.00	8.20	1945	844.00	6.03	1992	909.00	5.14
1897	913.90	6.34	1946	689.40	6.41	1993	781.30	5.27
1898	847.30	6.41	1947	736.80	5.80	1994	693.40	5.37
1899	880.90	6.34	1948	673.90	6.38	1995	1065.20	5.76
1900	908.10	6.96	1949	648.50	6.77	1996	952.10	5.61
1901	816.40	6.24	1950	652.60	5.79	1997	727.10	5.45
1902	956.20	6.10	1951	858.50	6.59	1998	806.20	7.78
1903	712.40	6.09	1952	710.20	7.23	1999	828.70	6.98
1904	889.20	3.90	1953	624.10	7.73	2000	897.00	5.87
1905	753.70	4.20	1954	N/A	6.47	2001	708.40	7.13
1906	922.40	5.85	1955	646.80	7.21	2002	869.10	7.21
1907	750.80	4.82	1956	658.30	5.83	2003	886.70	5.52
1908	707.30	5.88	1957	675.10	6.22	2004	844.30	7.39
1909	846.00	6.03	1958	564.00	5.78	2005	709.00	8.58
1910	790.60	6.08	1959	763.10	6.02	2006	950.90	7.93
1911	792.40	6.87	1960	776.50	5.26			
1912	1017.60	5.44	1961	528.20	6.63			
1913	614.00	7.23	1962	N/A	5.97			
1914	614.70	5.67	1963	N/A	5.65			
1915	739.70	6.55	1964	N/A	7.27			
1916	811.50	6.50	1965	776.50	6.85			
1917	745.90	4.58	1966	704.90	7.10			
1918	934.50	6.05	1967	990.60	6.40			
1919	737.30	7.43	1968	735.10	6.37			
1920	785.70	6.23	1969	662.40	6.80			
1921	760.60	8.46	1970	663.70	6.29			

Peterborough Dobbin TS (44°19'00"N 78°24'00"W)			Peterborough STP (44°17'00"N 78°19'00"W)			Stirling (44°18'00"N 78°38'00"W)		
Year (AD)	Annual precipitation (mm)	Mean annual temperature (°C)	Year (AD)	Annual Precipitation (mm)	Mean annual temperature (°C)	Year (AD)	Annual Precipitation (mm)	Mean annual temperature (°C)
1966	749.30	5.90	1966	855.00	N/A	1940	694.80	8.40
1967	955.80	5.63	1967	750.00	N/A	1941	801.60	6.89
1968	798.60	5.52	1968	970.00	N/A	1942	812.90	6.70
1969	749.90	5.89	1969	732.40	N/A	1943	803.20	5.73
1970	736.20	5.45	1970	716.10	N/A	1944	716.00	6.81
1971	739.40	5.90	1971	672.00	8.15	1945	962.40	6.22
1972	971.10	4.39	1972	614.60	5.55	1946	678.70	7.07
1973	786.40	9.80	1973	959.40	5.53	1947	1033.60	6.55
1974	804.70	5.52	1974	797.70	7.53	1948	699.70	6.73
1975	771.80	6.58	1975	829.00	6.37	1949	705.50	7.72
1976	873.00	5.21	1976	790.00	7.39	1950	770.30	6.05
1977	979.90	6.13	1977	803.00	6.00	1951	981.90	6.58
1978	808.50	5.78	1978	949.90	7.06	1952	709.20	7.70
1979	885.30	4.65	1979	793.70	6.10	1953	754.00	8.18
1980	948.90	5.77	1980	822.00	6.94	1954	784.80	6.75
1981	858.60	6.11	1981	942.60	6.28	1955	942.90	7.05
1982	1090.50	5.63	1982	892.10	6.99	1956	762.10	5.96
1983	895.60	6.36	1983	1012.20	6.62	1957	775.60	6.74
1984	924.50	6.06	1984	884.00	7.38	1958	623.60	6.11
1985	1042.10	5.59	1985	810.20	7.15	1959	737.20	6.91
1986	975.20	6.33	1986	884.20	6.79	1960	789.20	6.45
1987	812.50	7.13	1987	750.80	6.15	1961	724.90	6.78
1988	719.10	6.58	1988	745.20	8.23	1962	666.60	6.23
1989	800.20	5.53	1989	756.50	7.38	1963	672.50	5.78
1990	1002.90	7.23	1990	879.20	6.42	1964	652.80	6.48
1991	854.80	7.18	1991	923.30	7.97	1965	815.40	5.72
1992	968.70	4.19	1992	745.70	8.33	1966	720.40	6.15
1993	935.80	5.71	1993	900.10	6.34	1967	905.90	5.81
1994	747.30	5.50				1968	738.40	6.97

Trent University (44°22'00"N 78°18'00"W)			Campbellford (44°18'00"N 78°48'00" W)		
Year (AD)	**Annual Precipitation (mm)**	**Mean annual temperature (°C)**	**Year (AD)**	**Annual Precipitation (mm)**	**Mean annual temperature (°C)**
1968	714.80	5.51	1916	922.90	N/A
1969	724.50	6.40	1917	777.90	N/A
1970	722.10	6.25	1918	859.20	N/A
1971	739.30	6.63	1919	773.40	N/A
1972	998.80	5.48	1920	650.40	N/A
1973	895.70	7.41	1921	772.40	N/A
1974	824.00	5.99	1922	550.40	N/A
1975	705.10	6.87	1923	608.70	N/A
1976	861.20	5.48	1924	688.20	N/A
1977	917.50	6.49	1925	798.10	N/A
1978	706.10	5.38	1926	806.90	N/A
1979	795.60	6.32	1927	699.50	N/A
1980	895.40	5.59	1928	934.50	N/A
1981	864.90	6.09	1929	860.90	N/A
1982	952.20	6.13	1930	711.20	N/A
1983	911.30	6.96	1931	763.10	N/A
1984	972.20	6.56	1932	965.80	N/A
1985	1003.80	6.41	1933	720.60	N/A
1986	889.10	6.86	1934	682.60	N/A
1987	766.50	7.58	1935	745.10	N/A
1988	707.30	7.02	1936	895.30	N/A
1989	920.60	5.91	1937	838.30	N/A
1990	878.40	7.70	1938	813.10	N/A
1991	787.10	7.84	1939	667.80	N/A
1992	935.50	5.88	1940	659.00	N/A
1993	798.90	6.15	1944	727.90	N/A
1994	698.90	6.00	1945	1083.90	N/A
1995	995.90	6.98	1946	703.00	N/A
1996	1204.20	6.82	1947	1065.40	N/A
1997	788.90	6.76	1948	887.20	N/A
1998	756.00	8.89	1949	720.20	N/A
1999	731.00	8.17	1950	839.10	N/A
2000	852.10	6.88	1951	1132.30	N/A
2001	763.40	8.16	1952	745.50	N/A
2002	784.00	7.49	1953	780.70	N/A
2003	808.70	6.08	1954	836.40	N/A
2004	1191.10	6.23	1955	959.90	N/A

Trent University and Campbellford annual data continued

2005	730.10	7.18
2007	579.70	4.17
2008	1061.50	6.02
2009	905.40	5.92
2010	705.30	7.69
2011	869.80	7.16

1956	799.10	N/A
1957	834.20	N/A
1958	631.20	N/A
1959	639.20	N/A
1960	690.70	N/A
1961	649.10	N/A
1963	617.70	N/A
1964	574.80	N/A
1965	776.80	N/A
1966	722.60	N/A
1967	899.40	N/A
1968	829.20	N/A
1969	836.20	N/A
1970	759.70	N/A
1971	775.90	N/A
1972	1031.00	N/A
1973	763.40	N/A
1974	789.20	N/A
1975	829.80	N/A
1976	748.00	N/A
1977	910.30	N/A
1978	699.10	N/A
1979	747.90	N/A
1980	859.00	N/A
1981	837.10	N/A
1982	920.80	N/A
1983	970.60	N/A
1984	999.80	N/A
1985	972.10	N/A
1986	785.10	N/A
1987	839.10	8.26
1988	737.80	7.64
1989	869.90	6.60
1990	927.50	8.26
1991	778.00	8.26
1992	964.70	5.83

Appendix L Eight lakes selected in *R* package 'laketemps' for air – water temperature difference estimations

Crosson Lake (45.08 °, -79.03 °)				Red Chalk Lake (main) (45.18 °, -78.94 °)			
Year (AD)	**Water Temperature (℃)**	**Air Temperature (℃)**	**Temperature Difference (℃)**	**Year (AD)**	**Water Temperature (℃)**	**Air Temperature (℃)**	**Temperature Difference (℃)**
1985	21.0	18.2	2.9	1985	20.6	18.2	2.4
1986	20.9	18.1	2.8	1986	20.7	18.1	2.7
1987	21.4	19.9	1.5	1987	21.8	19.9	1.9
1988	21.9	20.3	1.6	1988	21.9	20.3	1.6
1989	21.1	19.8	1.4	1990	19.3	19.5	-0.2
1990	20.1	19.5	0.6	1991	20.7	20.5	0.2
1991	21.3	20.5	0.8	1992	20.1	17.3	2.8
1992	20.0	17.3	2.7	1994	21.0	19.2	1.8
1994	20.5	19.2	1.3	1995	21.7	20.9	0.9
1996	21.0	19.2	1.8	1996	21.4	19.2	2.2
1997	20.0	18.6	1.4	1997	20.4	18.6	1.8
1998	21.1	19.3	1.9	1998	21.6	19.3	2.3
1999	20.5	20.1	0.4	1999	21.5	20.1	1.4
2000	19.8	17.6	2.3	2000	20.4	17.6	2.8
2001	22.2	19.3	2.8	2001	22.4	19.3	3.1
2002	21.4	19.3	2.2	2002	23.1	19.3	3.8
2003	21.4	18.4	3.0	2003	21.7	18.4	3.3
2004	21.0	17.2	3.8	2004	20.9	17.2	3.7
2005	23.4	20.8	2.7	2005	23.2	20.8	2.4
2006	21.5	19.5	2.0	2006	21.5	19.5	2.0
2007	21.4	19.6	1.8	2007	20.1	19.6	0.5
2008	20.3	18.3	2.0	2008	20.4	18.3	2.2
2009	21.6	17.4	4.2	2009	21.0	17.4	3.6

Red Chalk Lake (East) (45.19 °, -78.94 °)				Blue Chalk Lake (45.19 °, -78.93 °)			
Year (AD)	**Water Temperature (℃)**	**Air Temperature (℃)**	**Temperature Difference (℃)**	**Year (AD)**	**Water Temperature (℃)**	**Air Temperature (℃)**	**Temperature Difference (℃)**
1985	20.6	18.2	2.4	1985	20.4	18.2	2.2
1986	21.3	18.1	3.2	1986	20.4	18.1	2.3
1987	22.0	19.9	2.1	1987	21.2	19.9	1.3
1988	22.2	20.3	1.9	1988	22.6	20.3	2.3
1990	20.2	19.5	0.7	1990	20.7	19.5	1.2
1991	21.7	20.5	1.2	1991	21.9	20.5	1.4
1992	20.1	17.3	2.8	1992	19.7	17.3	2.4
1994	20.7	19.2	1.6	1994	20.9	19.2	1.7
1995	21.6	20.9	0.7	1995	21.7	20.9	0.8
1996	21.2	19.2	2.0	1996	21.0	19.2	1.8
1997	20.3	18.6	1.7	1997	20.0	18.6	1.4
1998	21.7	19.3	2.4	1998	21.3	19.3	2.1
1999	21.5	20.1	1.5	1999	21.3	20.1	1.2
2000	20.4	17.6	2.8	2000	20.2	17.6	2.6
2001	22.4	19.3	3.1	2001	22.2	19.3	2.9
2002	23.2	19.3	4.0	2002	22.4	19.3	3.2
2003	21.4	18.4	3.0	2003	21.6	18.4	3.2
2004	20.8	17.2	3.6	2004	20.5	17.2	3.3
2005	23.3	20.8	2.5	2005	23.3	20.8	2.6
2006	21.5	19.5	2.0	2006	21.8	19.5	2.3
2007	19.8	19.6	0.2	2007	20.7	19.6	1.0
2008	20.2	18.3	2.0	2008	20.9	18.3	2.6
2009	21.0	17.4	3.6	2009	21.3	17.4	3.9

Henry Lake (45.12°, -79.10°)				Plastic Lake (45.18°, -78.82°)			
Year (AD)	**Water Temperature (°C)**	**Air Temperature (°C)**	**Temperature Difference (°C)**	**Year (AD)**	**Water Temperature (°C)**	**Air Temperature (°C)**	**Temperature Difference (°C)**
1985	20.8	18.2	2.7	1985	20.3	18.2	2.2
1986	21.4	18.1	3.3	1986	20.9	18.1	2.8
1987	21.9	19.9	1.9	1987	21.9	19.9	2.0
1988	22.8	20.3	2.5	1988	22.5	20.3	2.2
1989	20.4	19.8	0.6	1989	21.9	19.8	2.2
1990	20.8	19.5	1.3	1990	20.6	19.5	1.1
1991	21.9	20.5	1.4	1991	21.2	20.5	0.7
1992	21.0	17.3	3.7	1992	19.8	17.3	2.5
1994	20.9	19.2	1.8	1994	20.1	19.2	0.9
1995	21.7	20.9	0.8	1995	21.6	20.9	0.8
1996	20.6	19.2	1.4	1996	20.8	19.2	1.6
1997	20.3	18.6	1.7	1997	19.8	18.6	1.2
1998	22.7	19.3	3.4	1998	21.8	19.3	2.5
1999	20.8	20.1	0.7	1999	22.1	20.1	2.0
2000	21.7	17.6	4.1	2000	21.0	17.6	3.4
2001	22.5	19.3	3.2	2001	21.5	19.3	2.1
2002	23.0	19.3	3.7	2002	21.9	19.3	2.6
2003	21.3	18.4	3.0	2003	21.7	18.4	3.3
2004	22.3	17.2	5.1	2004	21.2	17.2	3.9
2005	23.1	20.8	2.4	2005	22.2	20.8	1.4
2006	21.6	19.5	2.1	2006	21.2	19.5	1.7
2007	21.0	19.6	1.3	2007	21.7	19.6	2.1
2008	21.2	18.3	2.9	2008	21.2	18.3	2.9
2009	21.3	17.4	3.9	2009	20.9	17.4	3.5

Dickie Lake (45.15 °, -79.08 °)				Harp Lake (45.38 °, -79.13 °)			
Year (AD)	**Water Temperature (°C)**	**Air Temperature (°C)**	**Temperature Difference (°C)**	**Year (AD)**	**Water Temperature (°C)**	**Air Temperature (°C)**	**Temperature Difference (°C)**
1985	20.3	18.2	2.2	1985	20.1	18.2	1.9
1986	21.2	18.1	3.1	1986	20.2	18.1	2.2
1987	21.6	19.9	1.7	1987	21.1	19.9	1.2
1988	21.0	20.3	0.7	1988	22.1	20.3	1.9
1989	21.9	19.8	2.1	1989	21.5	19.8	1.7
1990	19.8	19.5	0.3	1990	20.6	19.5	1.1
1991	21.4	20.5	0.9	1991	21.4	20.5	0.9
1992	20.6	17.3	3.3	1992	20.0	17.3	2.7
1994	20.6	19.2	1.4	1994	20.7	19.2	1.5
1995	20.9	20.9	0.1	1995	21.2	20.9	0.3
1996	20.2	19.2	1.0	1996	20.8	19.2	1.6
1997	19.5	18.6	0.9	1997	20.0	18.6	1.4
1998	22.4	19.3	3.2	1998	21.3	19.3	2.0
1999	21.4	20.1	1.3	1999	22.0	20.1	1.9
2000	21.0	17.6	3.4	2000	21.0	17.6	3.5
2001	21.8	19.3	2.4	2001	21.8	19.3	2.5
2002	22.4	19.3	3.1	2002	22.1	19.3	2.9
2003	21.2	18.4	2.8	2003	21.2	18.4	2.8
2004	20.1	17.2	2.9	2004	20.5	17.2	3.3
2005	23.3	20.8	2.5	2005	21.7	20.8	1.0
2006	21.6	19.5	2.1	2006	20.9	19.5	1.4
2007	21.9	19.6	2.2	2007	21.6	19.6	2.0
2008	22.1	18.3	3.9	2008	21.5	18.3	3.3
2009	21.5	17.4	4.1	2009	20.7	17.4	3.2

Appendix M Temperature reference by Bernabo (1981)

Periods in this study	Calcite formation temperature obtained from growing season temperature reconstructed at Marion Lake, Michigan
Interval IV (1850-2011)	17
Interval III (1615-1850)	16.5
Interval IIb (1500-1615)	16.8
Interval IIa (1350-1500)	17
Interval I (1268-1350)	17.5

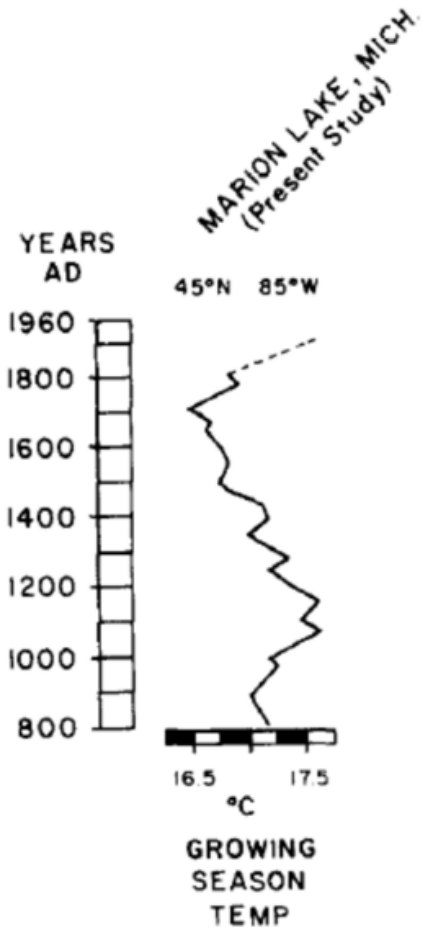

Figure M.1 Growing season temperature reconstructed at Marion Lake, Michigan from AD 800 to 1960. Dashed section shows difference between estimated temperatures at AD 1860 and the mean measured temperature during 1930-1960 (Bernabo, 1981).

Curriculum Vitae

Name:	Zijun Liu
Post–secondary Education and Degrees:	The University of Western Ontario London, Ontario, Canada 2013–2015 M.S. University of Waterloo Waterloo, Ontario, Canada 2011–2013 B.S. China University of Geoscience (Beijing) Beijing, China 2009–2011 B.S.
Honours and Awards:	Faculty of Science-Chinese Universities Program Award 2011-2012
Related Work Experience	Teaching assistant and Research assistant The University of Western Ontario 2013–2015 Laboratory Assistant University of Waterloo 2011–2012
Publication:	Liu, Z., Lin, S., and Duguet, M. (2013). Late dextral strike-slip event in the northern Mazinaw domain, Central Metasedimentary Belt, Grenville Province; in Summary of Field Work and Other Activities 2013, Ontario Geological Survey, Open File Report 6290, p.17-1 to 17-9.